Soil Interpretation in Groningen

Verification and improvement of CPT-based correlations

Claudio Guglielmelli

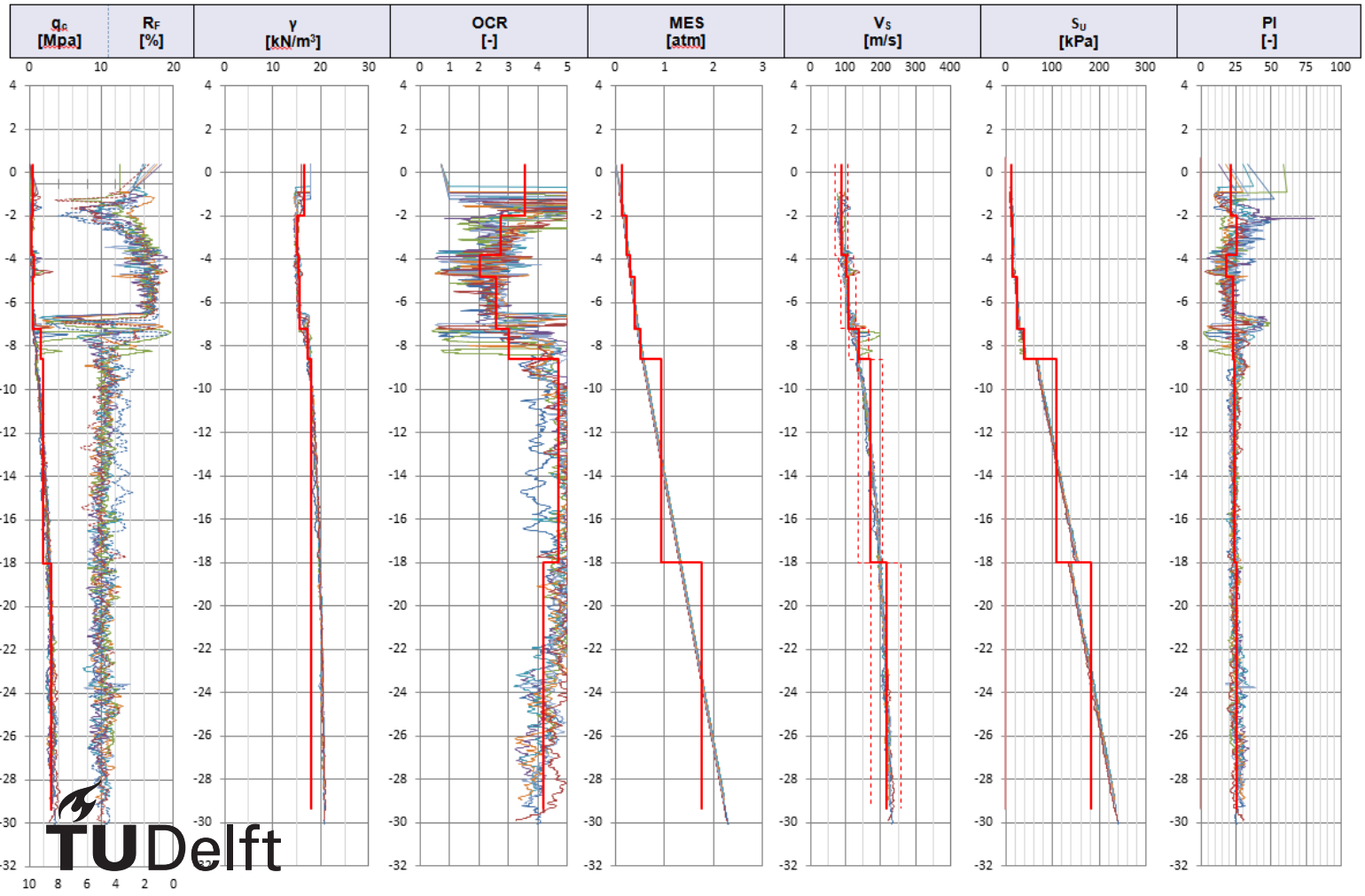

Soil Interpretation in Groningen

Verification and improvement of CPT-based correlations

by

Claudio Guglielmelli

in partial fulfillment of the requirements for the degree of

Master of Science
in Civil Engineering

at the Delft University of Technology,

to be defended publicly on Wednesday, 11th of April, 2018 at 11:00.

Student number:	4520742	
Thesis committee:	Prof. Dr. Hicks M.A.,	TU Delft, chairman
	Prof. Dr. Bertotti G.,	TU Delft, external supervisor
	Dr. Vardon P.J.,	TU Delft, daily university supervisor
	Ir. de Gast T.,	TU Delft, university supervisor
	Dr. Sigarán Loría C.,	Royal Haskoning DHV, daily company supervisor
	Ir. Verweij A.,	Arcadis, company supervisor

An electronic version of this thesis is available at `http://repository.tudelft.nl/`.

TU Delft

Royal HaskoningDHV
Enhancing Society Together

ARCADIS Design & Consultancy for natural and built assets

Abstract

In the northern part of the Netherlands, the exploitation of gas fields has been inducing small earthquakes, causing damage to existing buildings.
With the aim of preventing consequences to people and structures, the VIIA Groningen project deals with CC2 and CC3 buildings retrofit and provides reinforcement measures when necessary.
As part of the structural response assessment, after the NPR 9998 (2015), and eventual special cases from the latest NPR 9998 (2017), non-linear time history analyses (NLTH) are executed, comprising seismic ground response analysis (SRA).
The propagation of seismic waves through a 1D soil column is highly dependent on the characteristics of the materials constituting the soil deposits. Hence, it is essential to correctly interpret the soil properties, in order to achieve realistic representations of the in-situ conditions.

To interpret the soil layering at a particular site, the Cone Penetration Test (CPT) is commonly used in Groningen. It offers a quick, economical and reliable measurement of ground conditions. However, the CPT-based correlations used to estimate soil properties can constitute a source of uncertainty if not coupled with full scale testing and laboratory measurements.
The present thesis, thus, deals with the verification and the improvement of two CPT-based correlations used for soil interpretation in Gronigen specifically. The research study focuses on the mathematical models related to the plasticity index (PI) and the undrained shear strength (Su) of soft soils present in Groningen.

A comprehensive database of factual data was compiled in order to group various test types and provide a best-estimate of soil properties for different soil types using geotechnical and stratigraphic considerations. Secondly, a statistical characterisation of data-sets was performed to obtain insight on the correlations performance in relation to the in-situ and laboratory measurements. Based on the outcomes of the statistical comparison, analytical and regression analyses were carried out with the scope of improving the correlation that was deemed to be inadequate. Additionally, a sensitivity analysis was executed to investigate the influence of three relevant soil properties on the seismic ground response from a typical soil profile from Groningen. The parameters assessed are: plasticity index (PI), undrained shear strength (Su), and shear wave velocity (Vs).

Results indicate that, among the considered CPT-based correlations, the equation for PI from Cetin and Ozan (2009) is adequate in some cases. The geotechnical units sandy Clay and Loam show good correspondence with the factual data. On the other hand, the PI predicted with such relation tends to be lower than the laboratory measurements for the remaining soil units (e.g. clean Clay, silty Clay, OC Clay). Conversely, the PI behind the models implemented in the NPR 9998 (Bommer et al., 2017a) are in closer agreement to the factual data, however, the PI from some soil units can be further improved with the findings from the present research.
For the interpretation of Su the SHANSEP model from Ladd and Foott (1974) is frequently used. The available factual data showed a poor correspondence with the predicted Su values. Therefore, the SHANSEP model was further studied to calibrate its parameters for different soil types. From the available triaxial consolidated undrained laboratory tests, best-estimate of SHANSEP coefficients were obtained for the main soil types (clean, sandy, and silty Clay). New Su values were validated with the in-situ and laboratory measurements. In this context, it is confirmed that the dependency of Su on the overconsolidation ratio (OCR) is crucial. Moreover, the estimation of OCR from CPT measurements (following the Mayne, 2014, procedure) is found to be partially inaccurate within the SHANSEP framework, and needs to be studied in more detail.

Engineering aspects related to the topics of the research are discussed and considerations regarding the applicability of the new correlations are provided. Furthermore, the present study gives indications about the usefulness of a number of test types, suggesting direction for future soil investigations. In addition, look-up tables for PI and Su, based on the outcomes of the present research, are provided as part of the recommendations for implementation in the soil parameter interpretation for the Groningen region.

Acknowledgements

In everyone's life, there is a limited number of situations where the world is sending you a message, which normally contains an opportunity. If you grab it, you get lucky. The Netherlands and TU Delft have been my luck, as they opened the door to the world. After almost three years, this special adventure comes to an end. My luggage is now full of experiences, knowledge, and new people that I came across.

First of all, I would like to express my gratitude to my graduation committee.
My first and biggest thanks go to my supervisor from Royal Haskoning DHV, Dr. Carolina Sigarán Loría, for introducing me to the research topic and providing guidance and support during this whole process. Thanks to Dr. Phil J. Vardon for contributing with feedback throughout the study and guiding me toward a deeper understanding of the theoretical background of my research. A special thanks goes to Ir. Tom de Gast for sharing his contagious enthusiasm for scientific research, helping me to overcome the challenges encountered during this experience. I am grateful to Ir. Ad Verweij to share interest in my thesis and for his valuable comments. I am also grateful to Prof. Dr. Michael A. Hicks, chair of my committee, for being an inspirational icon, and to Prof. Dr. Giovanni Bertotti for participating as the external member of my committee.

Secondly, I would like thank my parents and my brother for literally make this journey possible, and for their continuous support and encouragement. I will be always grateful to them for placing enormous amount of trust in me, teaching me the sense of duty and to never surrender.

My next thanks go to my friends from my hometown, Napoli, for having being always present in my life even from far away. Distance does not make true friendship fade away. I will always keep you all in my mind, "In Generale Nella Vita".
Thanks to my "Socio" Peppo for being "my light in the dark moments". I am sure that our paths, soon or later, will cross again.
Thanks to "big" Jeroen for always offering his help and being such a generous person.
A special thanks goes to the friends I met in Delft, for giving me so many unforgettable experiences. In particular, thanks to Omar, Pascale, Alex, Andrei, Saurabh, Giorgos, and Kamesh for becoming my new family and making me a better person.

Last but not least, I would like to express my immense gratitude to Chiara, for have been sharing with me the tough and happy moments of this adventure, providing me with the trust and the enthusiasm that made this journey successful and pleasant. If I am who I am now, huge merit goes to her.

Claudio Guglielmelli
Delft, April 2018

Contents

Nomenclature

Abbreviations

α, β	Empirical parameters for undrained shear strength equations from Bommer et al., 2017
Δ_u	Relative movement between the two walls of the fault
μ	Mean value
σ	Standard deviation
$\sum$	Summation
A	Seismic Wave amplitude
A_0	Calibration factor for seismic wave amplitude
C	Viscous damping matrix
f_i	Predicted value
f_{max}	Cut-off frequency
f_c	Corner frequency
I	Unit vector
K	Stiffness matrix
M	Mass matrix
M_0	Seismic moment
M_L	Richter magnitude
M_w	Moment magnitude
SS	Sum of squares
V_L	Love-wave velocity
V_P	P-wave velocity
V_R	Reyleigh-wave velocity
V_S	S-wave velocity
y_i	Observed value
$\bar{y}$	Mean of the observed values

AAOP	Anthropogenic Formation
BE	Best estimate
BX	Boxtel Formation
C&O	Cetin & Ozan (2009)
CC2	Consequence class 2
CC3	Consequence class 3
CG/H	Generalised quadratic/hyperbolic model
COV	Coefficient of variation
CPT	Cone penetration test
CU	Triaxial consolidated undrained test
DB	Database
DR	Drente Formation
DS-NL4	Non-linear time-domain model
DSS	Direct simple shear test
EQL	Equivalent linear analysis
GI	Ground investigation
GMPE	Ground motion prediction equation
GRA	Ground response analysis
GWT	Ground water table
HPGA	Horizontal peak ground acceleration
ID	Identity
KNMI	Koninklijk Nederlands Meteorologisch Institut

lab	Laboratory
LB	Lower boundary
MRDF	Pressure-dependent hyperbolic model with non-Masing rule
MRS	Modal spectral response
N	Number
NA	Naaldwijk Formation
NAM	Nederlandse Aardolie Maarschappij
NAP	Normaal amsterdams peil
NC	Normally consolidated
NI	Nieuwkoop Formation
NIBA	Nieuwkoop Holland Formation
NIHO	Nieuwkoop Basal Formation
NL	Non-linear analysis
NLTH	Non-linear time history analysis
NS_B	Lower North Sea Supergroup Formation
NU_B	Upper North Sea Supergroup Formation
OC	Overconsolidated
PE	Peelo Formation
PGA	Peak ground acceleration
PSA	Peak spectral acceleration
PSHA	Probabilistic seismic hazard assessment
Q	Quartile
SA	Spectral acceleration
SCPT	Seismic cone penetration test
SDOF	Single-degree-of-freedom system
SH	Horizontal S-wave
SHANSEP	Stress history and normalised soil engineering properties
SodM	Staatstoezicht op de Mijnen (Ministerie van Economische Zaken and Klimaat)
SPT	Standard penetration test
SRA	Site response analysis
SU	Geotechnical soil unit
SU1	Soil unit: Clay
SU1_A	Soil unit: Clay, clean, soft
SU1_A1	Soil unit: Clay, clean, moderately stiff
SU1_A2	Soil unit: Clay, clean, stiff
SU1_B	Soil unit: Clay, slightly sandy
SU1_B2	Soil unit: Clay, moderately sandy
SU1_B3	Soil unit: Clay, highly sandy
SU1_C	Soil unit: Clay, sandy/silty + organic
SU1_D	Soil unit: Clay, organic
SU1_E	Soil unit: Clay, slightly silty
SU1_E2	Soil unit: Clay, moderately silty
SU1_E3	Soil unit: Clay, highly silty
SU2	Soil unit: Overconsolidated Clay
SU3	Soil unit: Sand
SU3_A	Soil unit: Sand, clean, loose/dense
SU3_B	Soil unit: Sand, slightly silty, clayey
SU3_C	Soil unit: Sand, highly silty, clayey
SU4	Soil unit: Peat, not preloaded
SU4_A	Soil unit: Peat, moderately preloaded
SU5	Soil unit: Loam, slightly sandy
SU5_A	Soil unit: Loam, highly sandy
SV	Vertical S-wave

tan	Tangent
UB	Upper boundary
UU	Triaxial unconsolidated undrained test
V	Version
V4	V4 Ground motion model (Bommer et al., 2017)
VIIA	VIIA Groningen project
VPGA	Vertical peak ground acceleration
X	Object identity code
Y	Object identity code

Soil parameters

α'	[◦]	Effective internal angle of friction angle in $t-s'$ space
$\dot{u}$	$[m/s]$	Velocity
$\ddot{u}$	$[m/s^2]$	Acceleration
$\ddot{u}_g$	$[m/s^2]$	Acceleration at the base of SDOF
Δu	$[kN/m^2]$	Excess pore water pressure
γ	$[KN/m^3]$	Soil unit weight
γ_s, γ_c	$[-]$	Shear strain, peak shear strain
ϕ, ϕ'	[◦]	Total, effective internal angle of friction in $\tau-\sigma, \sigma'$ space
ρ	$[kg/m^3]$	Material density
σ, σ'	$[kN/m^2]$	Total, effective stress
σu	$[kN/m^2]$	Pore water pressure
τ	$[kN/m^2]$	Shear stress
c	$[-]$	Power law exponent for cone tip resistance normalisation
D or ξ or λ	$[-]$	Damping ratio
$F(t)$	$[kN]$	Excitation function
F_R or R_f	[%]	Friction ratio
f_s	$[kN/m^2]$	Sleeve friction
G	$[kN/m^2]$	Shear modulus
G_{max}/G_0	$[-]$	Modulus reduction curve
$I_{c,def}$	[%]	Soil behaviour type index
k_0	$[-]$	Earth pressure at rest
m	$[-]$	Power law exponent for overconsolidation ratio
MSS	$[-]$	Maximum shear strain
N_{kt}	$[-]$	Empirical cone factor
OCR	$[-]$	Overconsolidation ratio
p, p'	$[kN/m^2]$	Total, effective mean stress
P_a	$[atm]$	Atmospheric pressure
PI	[%]	Plasticity index
q or t	$[kN/m^2]$	Deviatoric stress
$q_{t,1,net}$	$[-]$	Normalised net cone tip resistance
q_c	$[kN/m^2]$	Cone tip resistance
q_t	$[-]$	Normalised cone tip resistance
R	$[-]$	Factor for cone tip resistance normalisation
S	$[-]$	Normalised undrained shear strength for normally consolidated clay
Su	$[kN/m^2]$	Undrained shear strength
T	$[s]$	Period
u	$[m]$	Displacement
V_s	$[m/s]$	Shear wave velocity
V_{S30}	$[m/s]$	Shear wave velocity of the uppermost 30 m of soil

Subscripts

$0, i$	initial
avr	average
c	confinement
def	definition
dry	unsaturated
f	final
ff or max	maximum
p	pre-consolidation
pm	maximum mean
res	residual
s	shear
sec	secant
tot	total
u	undrained
v, h	vertical, horizontal
wet or sat	saturated

List of Figures

List of Tables

1

General Introduction

In the late 1950's, the Nederlandse Aardolie Maatschappij BV (NAM) initiated the exploitation of natural gas fields in the northern part of the Netherlands. The production of natural gas has been inducing small earthquakes which are projected to become more severe in the future (van der Voort and Vanclay, 2015), causing failure and damage to existing buildings.
Aiming to prevent severe consequences to people and structures, the VIIA Groningen project was developed as a partnership between Royal Haskoning DHV and Visser & Smit Bouw responsible for CC2 and CC3 buildings' retrofit. This consists of investigating and assessing the risk related to seismic events in the buildings from the Groningen area, providing reinforcement measures when necessary.

1.1. Background

In order to introduce this research, it is useful to emphasise the purpose of the VIIA Groningen project and the role that Royal Haskoning DHV plays in it. All the information related to the VIIA project is strictly confidential and, therefore, only the main concepts are going to be presented in this report.
Since the beginning of the project, in 2014, the geotechnical department and the structural section have been working together, evaluating the current condition of important buildings and eventually assessing the consequences and the impact of seismic events.
In earthquake engineering, the risk of an event is defined as the product of the probability of occurrence and the vulnerability of the object(s), where the vulnerability is the probability of death for exposed people per calendar year. Therefore, it is crucial to take care primarily of sensitive buildings, defined as CC2 and CC3 after NPR 9998 (2015), which are populated on a daily basis by large numbers of people (i.e. schools, hospitals, etc.).

Consequences Class	Description	Examples of buildings and civil engineering works
CC3	High consequence for loss of human life, or economic, social or environmental consequences very great	Grandstands, bridges, public buildings where consequences of failure are high (e.g. a concert hall)
CC2	Medium consequence for loss of human life, economic, social or environmental consequences considerable	Residential and office buildings, public buildings where consequences of failure are medium (e.g. an office building)
CC1	Low consequence for loss of human life, and economic, social or environmental consequences small or negligible	Agricultural buildings where people do not normally enter (e.g. for storage), greenhouses

Figure 1.1: Definition of CC1 to CC2 consequence classes (source: NPR 9998, 2015).

The main purpose of the VIIA project is to perform Modal Spectral Response (MRS) and Non-linear Time History Analysis (NLTH), in order to predict the response of a structure and the associated stresses and deformations (Figure 1.2).
The "Near Collapse" situation is the principal concern of the VIIA research. The primary goal is to avoid collapse and, only in few cases, to perform damage limitation.
When modelling an object in a NLTH analysis, three effects have to be considered:

- Site response
- Soil-structure interaction - Local
- Soil-structure interaction - Global

The first two effects can be decoupled from the actual NLTH DIANA-model, and modelled separately with different tools, such as 1D models in Excel, DEEPSOIL or Plaxis. Effect 3 is ignored in principle, since only the ultimate limit state (Near Collapse) is analysed. The effect 3 is indicative of the global impact that seismic loads can have on a structure (during and post an earthquake). For instance, the local failure or plastic deformation of a foundation element does not necessarily mean that the Near Collapse limit is exceeded. However, for the time that follows an earthquake, there should still be several calculation steps to check whether the structure and the foundation are still able to fully perform their function (He et al., 2016).

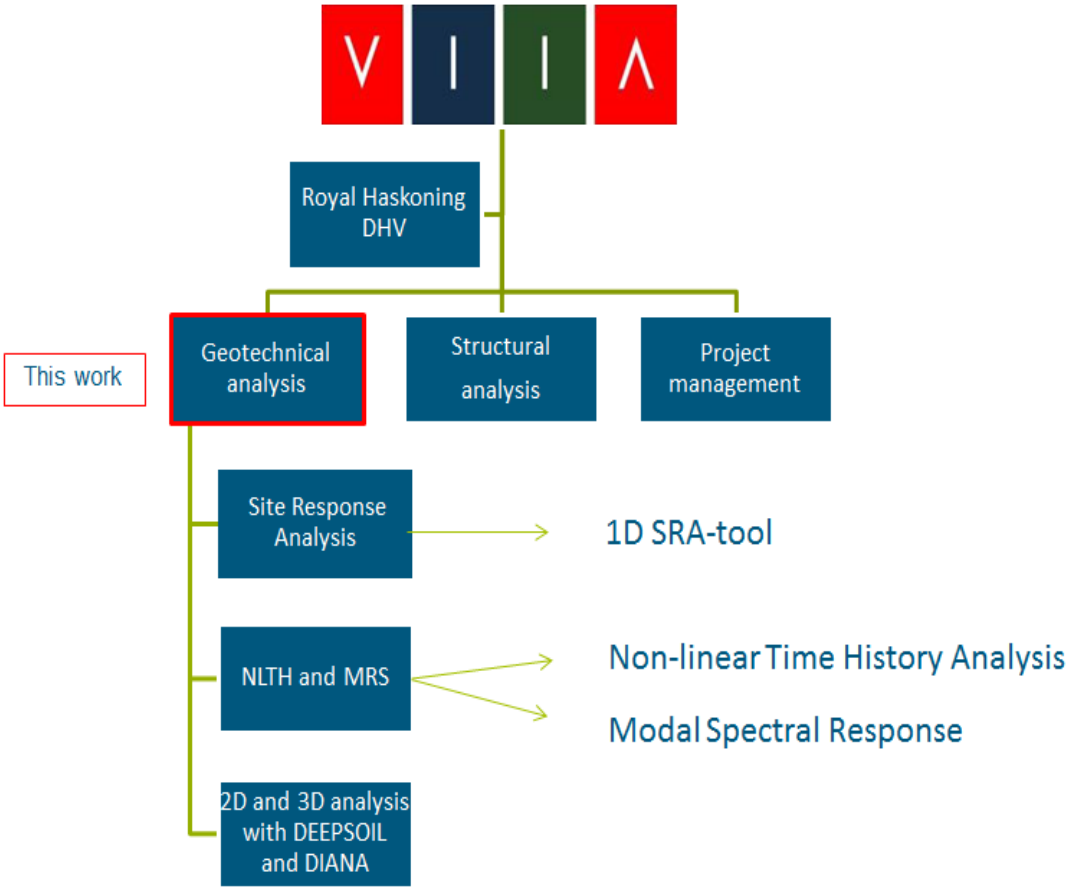

Figure 1.2: Schematic representation of the VIIA Groningen project work-flow until 2017 (after NPR 9998, 2015).

1.2. Problem Statement

In order to assess the structural response to earthquakes, propagation of seismic waves is modelled numerically, using a 1D soil column analysis, also known as Site Response Analysis (SRA).
The propagation of seismic waves through a 1D soil column is highly dependent on the composition and the behaviour of the materials constituting the soil deposits. Hence, it is crucial to correctly predict the soil properties, leading to a realistic representation of the in-situ conditions.
For this purpose, it is well known that Cone Penetration Test (CPT) offers a quick, economical and reliable way of conducting site investigations for exploring and profiling the subsurface soil layering at a particular site. In general practice, soil properties are obtained indirectly from CPT measurements, allowing quick, preliminary conclusions for design.
However, without proper calibration, using full-scale load testing coupled with soil borings and laboratory testing, the CPT results may lead to a large amount of uncertainty and to unrealistic soil properties estimates.

1.3. Aim of the Thesis

In lieu of the lack of factual data from the local soils and large uncertainties in the soil parameters used, there exists a strong need to assess and, when necessary, improve the CPT-based correlations used in practice, in order to verify and/or improve the accuracy of the ongoing seismic studies in the region.
Hence, the main goals of this research project are:

- Verify the approach used by practitioners to interpret plasticity index and undrained shear strength of soft soils, towards SRA and NLTH analyses.
- Develop new site-specific relations for Groningen.

Secondary goals are:

- Compile a detailed ground investigation database containing all the information available for the study objects.
- Deliver look-up table for PI and Su which can be used in practical engineering applications.

1.4. Research Questions

Several studies have incorporated statistical and regression analyses to study and improve CPT-based correlations. In particular, many authors have investigated the adequacy of multiple mathematical models (e.g. the SHANSEP model, after Ladd and Foott, 1974) used to evaluate the soil properties for a variety of soft soils, reporting the effect of different soil conditions and soil types (e.g. Jamiolkowski et al., 1985 and Mayne, 1980). However, only a few have focused their attention on the performance of such equations with respect to the soil conditions typical of the Groningen region. For this Groningen-specific framework, the following primary and secondary research questions are identified:

1. How accurately do the plasticity index and undrained shear strength correlations describe the actual soil properties?
    - Do the PI and Su estimations match the factual in-situ and laboratory data?
    - What is their adequacy with respect to the different soil type and units present in Groningen?
    - Are the individuated soil units in agreement with the stratigraphic units proposed by Bommer et al. (2017a)?
2. How precise can the PI and Su predictions be, based on cone penetration tests?
    - Which are the main parameters affecting the correlations performance?
3. Is the current factual data-set of adequate quality to carry out statistical and regression analyses to calibrate the models' parameters?
    - Which test type is more reliable? Why?
4. Does the adjusted SHANSEP model (calibration per soil type) yield Su predictions in better agreement with the in-situ data?
    - What are the limitations?
5. What is the influences of the parameters PI, Su, and Vs on seismic ground response?
    - Is there any clear depth trend?

1.5. Methodology

To answer the research questions of this thesis, the approach to be followed is described next:

I. **GI Database compilation** - Investigating the applicability and the correctness of the CPT-based correlations, it is important to create a database in which all the available information is contained. Traceability is guaranteed by specifying the geotechnical survey report number and the ID of each CPT and borehole used in the analysis.

II. **Estimation of PI and Su with CPT-based correlations** - This step is addressed to compute best-estimate soil properties predictions for specific soil types.

III. **Post-processing of laboratory and in-situ data** - Laboratory and in-situ data are checked first with respect to the "Overzicht laboratoriumderzoek 12-12-2016" file (written comm. R. Jeltes, 24/01/2017). Once ascertained the availability and traceability of the factual data, these are included in the GI Database.

IV. **Detailed study of regional geology and soil classification** - In order to gain insight on the typical Groningen soil stratigraphy, the Dutch database, so-called DINOloket, is used to check the quality of the CPT measurements. Next, the available data is grouped together per geotechnical unit, according to the laboratory soil classification and engineering judgement. This process allows an easier evaluation of the models' performance and helps to interpret the results.

V. **Sensitivity analysis** - To identify the influence of different soil properties on the outcomes of SRA simulations in DEEPSOIL, a sensitivity analysis is executed. This includes the investigation of the sensitivity of PGA, PSA and MSS to changes in mean values (PI, Su, and Vs means).

VI. **Statistical characterisation** - With the purpose of obtaining a valuable and significant indication of the correlations' performance, a first statistical characterisation of various soil units is executed. This consists of creating scatter plots in which predicted and measured PI and Su values are compared over the depth. Secondly, scatter plots with equality lines are created in order to evaluate the divergence between the predicted and the measured values. Consequently, box-plots are generated to have a better visual representation of the correlations' performance.

VII. **Correlation Improvement and Validation** - In lieu of the poor correspondence existing between Su predicted values and in-situ measurements, the predictive models are evaluated for potential improvements. Therefore, an analytical approach and a regression analysis are performed to calibrate the correlations parameters (e.g. S and m for the SHANSEP model) based on different soil types.

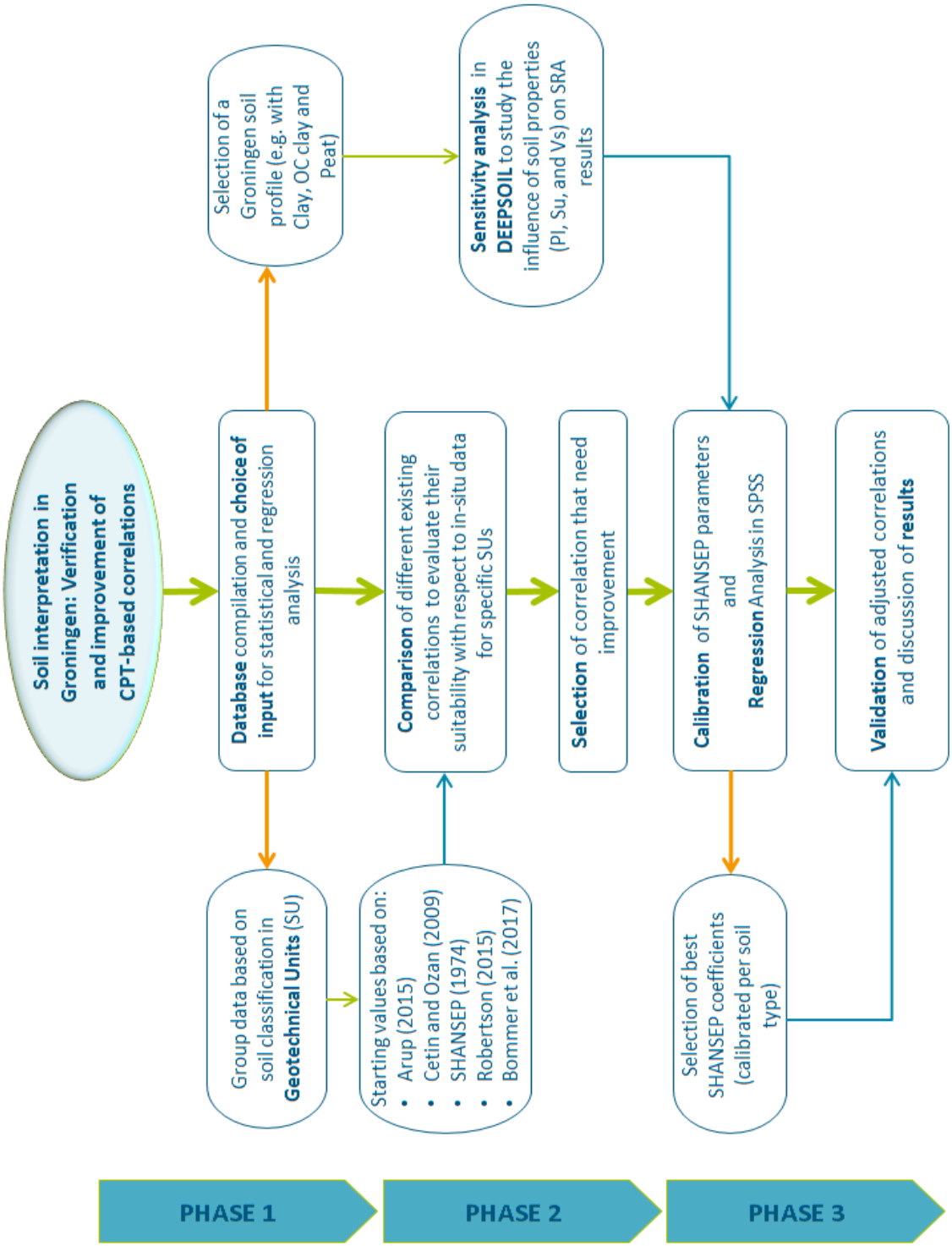

Figure 1.3: Flow chart of the thesis methodology.

1.6. Outline of the Report

The report investigates the suitability of a number of CPT-based correlations used for the soil interpretation in the Groningen region. It is structured into several parts, which are listed and explained below:

Literature Review
A literature review (Chapters 2 and 3) is meant to introduce the reader to the VIIA project, which is the framework of the present research. It comprehends an extensive study of man-induced earthquakes, the principles and the main correlations used in site response analysis.

Sensitivity Analysis
Chapter 4 contains a sensitivity analysis performed for three soil properties, in order to investigate their influence on SRA results.

Statistical Characterisation
In Chapter 5, exploratory statistical analysis is carried out to examine the suitability of a number of CPT-based mathematical equations in relation to the factual data.

Correlation Improvement and Validation
Based on the outcomes of the statistical analysis, Chapter 6 focuses on the improvement and the validation of one of the CPT-based correlations used to estimate the undrained shear strength of soft clays: the SHANSEP model (Ladd and Foott, 1974) with single calibration (after Arup, 2015).

Discussion, Conclusion and Recommendation
In Chapter 7 the results obtained from the previous chapters are summarised and discussed, giving an answer to the research questions. The study concludes with recommendations regarding future research, discussed in Section 7.2.

Moreover, there are a number of appendices which are listed and explained below:

- Appendix A comprehends a literature review on the tectonic earthquakes, giving insight on the factors that generate natural seismic phenomena, the main parameters and the fundamental terminology used to measure and describe them.
- Appendix B explains the criteria based on which the available ground investigation data is post-processed and compiled into a GI database, describing its main parts.
- Appendix C reports the results from statistical analysis for the soil units SU1_D, SU2, SU3, SU4, and SU5.
- Appendix D contains the additional analytical and regression analyses carried out for the improvement of the SHANSEP model, as a part of Chapter 6,
- Appendix E includes the look-up table for Su, displaying the average values of the soil properties obtained from the in-situ and laboratory tests and from the CPT-based correlations considered in this work.

2

Literature review

2.1. Introduction

This Chapter provides the first part of the literature study of the present report. The Chapter begins with a general introduction concerning earthquakes, briefly mentioning the difference between tectonic and induced earthquakes. The second part focuses on Ground Response Analysis, giving a short overview of the existing methods and the most important parameters used to model the non-linear soil behaviour due to propagation of seismic waves. The Chapter concludes investigating the influence of a number of soil properties (e.g. PI, Su, OCR) on the the dynamic behaviour of soft soil.
A general outlook on the main features and terminology related to natural tectonic earthquakes, and the mechanisms that lead to generation and propagation of seismic waves, will be covered in the Appendix A.

2.2. Earthquakes

During the last few centuries, earthquakes have been the object of a growing interest that led to a significant amount of studies being carried out worldwide. For instance, in China and in Japan the first written earthquake records date back to almost 3000 and 1200 years ago, respectively (Kramer, 1996). However, the human knowledge and experience with respect to earthquakes and seismology covers an interval of the earth's history that is insignificantly short.
Currently, earthquakes represent a global phenomenon that affects hundreds of millions of people around the world. Many people who live in seismic areas are direct victims of earthquakes, having their lives and possessions continuously at risk. Many others, although do not strictly live in seismic areas, may be damaged by earthquakes induced by man's activity, e.g. Groningen in the Netherlands.
Scientists and researchers affirm that earthquakes will continue to exist, and the idea that they cannot be prevented from occurring is, nowadays, largely diffused and accepted. However, with the modern technology and knowledge, it has become possible to mitigate and reduce the effects of strong ground shaking (Kramer, 1996). In other words, when it is not feasible to completely impede damage to structures, there still exist a possibility to reduce loss of life, injures and failure of buildings.

2.3. Induced Earthquakes

Earthquakes are generally the consequence of tectonic movements and fault mechanisms that occur in an entirely natural way, due to the brittle behaviour of rocks (refer to Appendix A). Nevertheless, there exist seismic events, defined *induced earthquakes*, that are purely triggered by the effect of human activity (Bommer et al., 2015a). The earthquakes caused by anthropogenic activity create, generally, a smaller strain energy release compared to those events triggered by crust movements, however, they can equally produce a considerable amount of damage (Foulger et al., 2016).
It is largely accepted that shear slip on fault planes represents probably the most crucial cause of earthquakes occurrence (see Appendix A, Section A.2.1). The opening of new faults, or the initiation of failing mechanisms in existing faults may be caused by several industrial activities such as: injection of fluid into a fault zone, which can cause a change in the fluid pressure in the fault; influx of ground water (e.g. suspension of groundwater extraction in mines), leading to an increase in pore water pressure; alteration of cohesion or

shear stress acting on the fault plane (e.g. stress redistribution from surrounding earthquakes); rapid temperature alteration; and forced change in vertical and/or horizontal stress (e.g. gaining or loosing overburden weight); etc.
Induced earthquakes result from a stress change in the sub-surface, and their magnitude can be often comparable to natural earthquakes (Figure 2.1). However, they differ from the tectonic ones in three major ways: (1) the depth at which they take place is around ($\backsim$ 3 km and $\backsim$ 15 – 700 km, respectively); (2) their duration is generally shorter, leading to less damage potential with respect to buildings and structures; (3) the soil configuration at a relatively shallow depth is mostly composed of soft soil deposits with a lower wave speed ($\backsim$ 50 – 300 m/s), compared to the majority of hard materials such as rocks and stones with a wave speed up to 1500 m/s (van Elk et al., 2013).
Given that the seismic events that have been occurring in Groningen are ascertained to be man-induced earthquakes, in Chapter 3 particular attention will be given to earthquakes triggered by the extraction of gas.

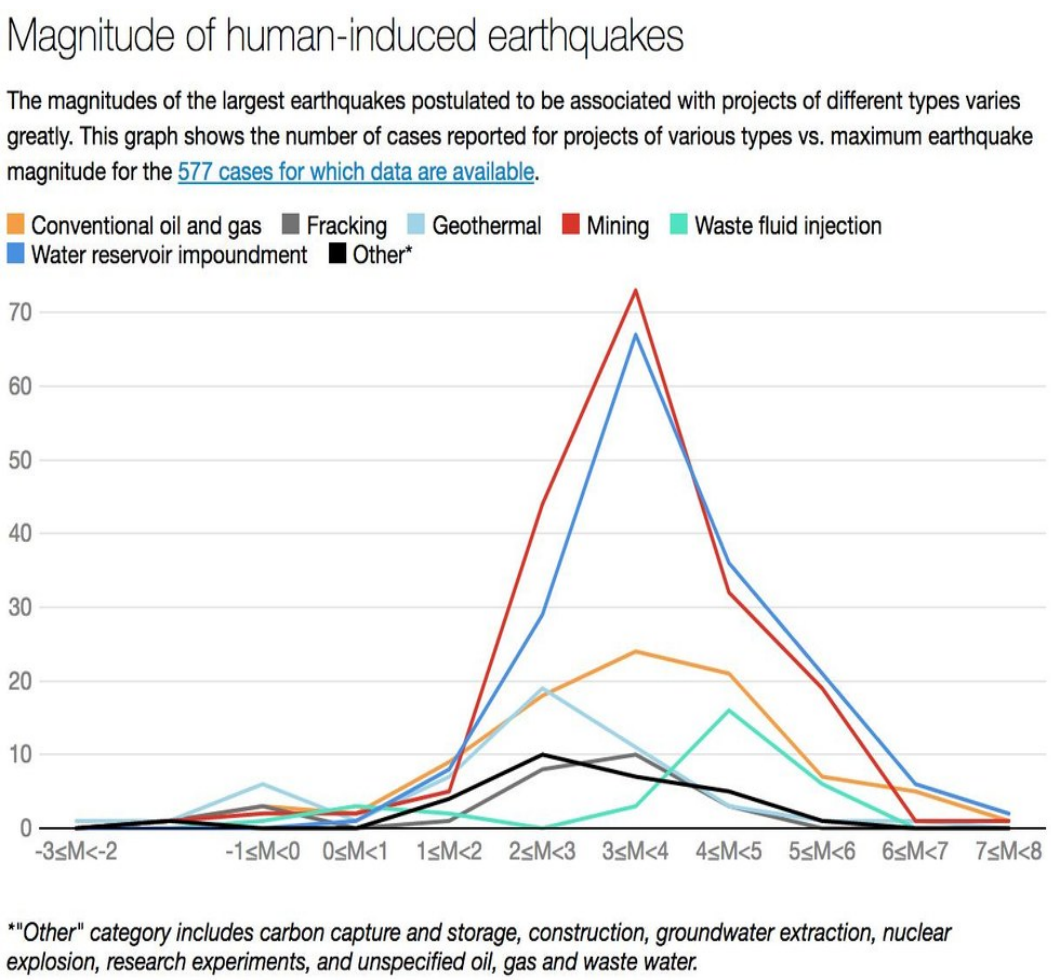

Figure 2.1: Analysis of the Magnitude distribution for 577 induced earthquakes occurred all over the world. On the x-axis are shown the magnitude (M) ranges, while on the y-axis is displayed the frequency of the seismic events. Coloured lines indicates earthquakes due to different human activities (source: Foulger et al., 2015).

2.4. Ground Response Analysis

The following Section of the literature review focuses on Ground Response Analysis (GRA or SRA). Herein, it is briefly presented the theoretical background knowledge regarding ground response and some of its applications from a geotechnical point of view, including the soil properties that play a crucial role in dynamic calculations.
The reader is asked to refer to Appendix A for more information about the typology and characteristics of seismic waves (Section A.2.3).

2.4.1. Ground Response Background

It is commonly accepted that structures such as buildings, bridges, houses, etc. which are exposed to earthquake loading may be subjected to damage and/or failure. The local structural behaviour of different structures is dependent not only on their own specific period of vibrations (eigenfrequencies) and on the seismic event features, such as magnitude, distance, etc. (more details in Appendix A), but also on the soil response (van Elk et al., 2013).
With the aim of modelling the influence of soil conditions on ground motions and performing retrofit of buildings, several numerical methods, constitutive models, and computer programs are readily available to perform site response analysis, including 1-, 2-, and 3-D analysis (e.g. DEEPSOIL, DIANA, PLAXIS, ABAQUS, LS-DYNA).
Propagation of seismic waves in the subsurface is a highly complex mechanism which involves considerations of geological and geotechnical variability that may influence the behaviour of the soil column in analysis. For instance, weak geological units and morphological irregularities can have a significant impact on the amplification of the seismic signal and, therefore, on the development of the peak ground acceleration (PGA). Given that amplification and de-amplification of seismic waves due to soil variability seem to be the dominant factors in damage distribution (Kramer, 1996), it is crucial to use models that account for such effects.

2.4.2. Modelling Seismic Waves

For ground modelling purposes, in a 1D analysis it is common practice to simplify the soil as a continuous linear visco-elastic system in which geological units of materials are assumed to be uniform and homogeneous. In order to model the visco-elastic wave propagation, it is convenient to use a Kelvin-Voigt solid that represents those materials which resist to shearing deformation with the contribution of two components: an elastic and a viscous part. In this way, the soil behaviour is modelled with a linear elastic shear modulus and viscous damping (Kumar et al., 2015).
The contacts (boundaries) between the geological units represent the interfaces where wave mechanisms such as reflection, refraction and transmission occur (Kramer, 1996). Such a large direction and length variety in wave paths induces the motion to be spread out in time by a scatter effect, leading to rather complicated mechanisms between stress waves and boundaries (see Section A.2.3).
Another important aspect of the interaction between soil deposits and wave propagation is the damping effect. In general, damping is defined as the mechanism responsible of energy dissipation within a soil system subjected to cyclic loading. This may alter the amplitude of the waves travelling through the subsurface (i.e. attenuation of the input motion). Two factors are considered to be essential in explaining this phenomenon (Brinkgreve, 2015): (1) *viscous damping*, as a consequence of the direct absorption of energy by the materials encountered within the travel path, and (2) *radiation damping*, based on the geometry of the wave propagation, in terms of volume of material over which the wave energy is radiated.
Generally speaking, because of the highly complicated soil characteristics at relatively shallow depth, traditional intensity scales, e.g. Richter scale (see Sections A.4.4 and A.4.5), are not commonly used for damage estimation (Elnashai and Di Sarno, 2008). In order to characterise seismic hazard, attempting to quantify the impact of ground shaking on the built environment, it is more convenient to use parameters that describe the maximum amplitude on the acceleration time series, such as the peak ground acceleration (see Section A.4.1). In this way, by collecting ground motions records, geological information and other variables (e.g. magnitude and site-to-source distance), it is possible to develop empirical relationships, so-called ground motion prediction equation or GMPE (more details in Section 3.4) that can be used for a more accurate estimation of PGA and the related site response (Bommer et al., 2015b, van Elk et al., 2013).

2.4.3. One Dimensional Site Response Analysis Techniques

According to Kramer (1996) and Matasovic and Hashash (2012), there exist Linear, Equivalent Linear and Non-linear analyses, which require similar sets of input, including: (1) ground motion time histories, (2) specification of subsurface characteristics (e.g. geometry, stratigraphy, and bedrock level), (3) definition of material properties such as shear wave velocity, unit weight, shear strength, plasticity index, shear modulus and damping. In more advanced models, it is often required information about hydraulic conductivity (for saturated conditions), hysteretic and viscous damping model parameters, and curve-fitting model parameters (Matasovic and Hashash, 2012).

Linear Analysis

Benz et al. (2009) demonstrated that the linear-elastic behaviour of soils is limited to a certain strain range, called *very small strains*, at which the soil is able to fully recover the strains generated during the loading phase (shear strain γ_s between 0 and 10^{-6}%). At this strain level, in fact, any small damping is the result of intrinsic viscous behaviours.
As described further by Kramer (1996), there exist several linear models which presume the use of a number of transfer functions needed to describe ground surface response parameters, such as displacement, velocity, acceleration, shear stress and strain, with respect to an input bedrock motion (generally the peak acceleration at ground surface is lower than the PGA at bedrock level).
Linear models transform acceleration time series (at bedrock level) in time domain into frequency domain, using a Fast Fourier Transform algorithm. This determine the amplitude of harmonic waves at many different frequencies, whose summation represents the acceleration time series. The resulting Fourier series is subsequently multiplied by the transfer functions which establish the amplification or de-amplification of the input motion (Carlton, 2014).
As already mentioned, such linear approach can be applied only to linear systems, which are characterised by linear-elastic properties and a medium range of strain, approximately below the level of 10^{-3}% (Ishihara, 1996). A simple schematisation of a linear system is a linear-elastic soil deposit of a certain thickness underlain by a rigid bedrock. The governing soil properties are shear modulus and damping ratio (explained in more details in Section 2.4.4), which are assumed to be strain-independent and constant for each geotechnical unit. In reality, however, ground configurations are usually far more complex than the above simplified case, and involve layered soil deposits with varying stiffness and damping features, and with boundaries responsible of refection and/or transmission of elastic wave energy. Modelling a multi-layered linear system involves that each layer is described with constant and strain-independent properties, with the only difference that the transfer function will result considerably more complex than the one obtained for a single-layered system.

Equivalent Linear Analysis

When ground motions are caused by large vibrations (such as design level earthquakes with strain levels $> 10^{-3}$%) dynamic soil properties can be extremely non-linear. As a result, the change in shear modulus and material damping ratio with respect to shearing strain amplitude must be accounted for in ground response analysis (Carlton, 2014, Ishihara, 1996, Kramer, 1996, Seed et al., 1986, etc.). One approach to tackle non-linear soil behaviour is to perform site response analyses with so-called equivalent linear properties, such as secant shear modulus and equivalent linear damping ratio. according to Schnabel et al. (1972) (in Carlton, 2014), these are iterated until the difference between stiffness and the damping properties in two consecutive iterations are contained with a certain tolerance level. Such iterative approach, based on the frequency domain, is called equivalent linear analysis (EQL).
The frequency domain analysis relies on the consideration that the damping properties are constant and independent on the strain level, assuming the soil as a linear visco-elastic system. In this domain, after having obtained the small strain stiffness and damping as for the linear method, shear strain histories for each layer can be estimated (Carlton, 2014). Subsequently, for each layer, the effective shear strain is computed (as a fraction of the maximum shear strain, usually 0.65), giving a prediction of stiffness and damping at the selected effective shear strain level (Kumar et al., 2015).
Nevertheless, EQL analysis does not account for cyclic behaviour of soil (i.e. strain-dependent modulus degradation due to a number of loading cycles), residual strain of soil (i.e. the strain will always return to zero after cyclic loading, meaning that failure cannot occur in linear material), and excess pore water pressure generation (Kumar et al., 2015). Moreover, the application of constant values of stiffness and damping properties, leads to the overestimation of the damping and to the underestimation of stiffness in case the shear

strain level is larger than the shear strains at other time intervals, and to the opposite trend when the shear strain does not vary with time (Carlton, 2014). Likewise, being stiffness and damping properties constant with time, EQL analyses may estimate high levels of resonance (amplification of the motion) in correspondence with the natural frequency of the soil, which are in poor agreement with real observations.

Non Linear Analysis

To properly model the non-linear behaviour of soils, it has been found that the dynamic equation of motion should be integrated in small time steps in the time domain (Kumar et al., 2015). This is called non-linear analysis of ground response (NL). In general, a one-dimensional NL analysis involves the implementation of a vertical soil column schematised either as a continuous medium organised in finite elements with their own mass or as a multi-degree-of-freedom lumped mass system (Carlton, 2014). In both cases, the equation of motion is solved in time domain (differently from linear and equivalent linear analyses which are based on frequency domain) in order to follow the stress-path of the soil for the entire duration of the ground shaking. In a lumped mass system, for instance, each soil layer is represented by a single non-linear spring, a dashpot, and its own mass. This requires assembling appropriate mass, stiffness, and (viscous) damping matrices (Stewart et al., 2014), as well as the definition of a global equation of motion (2.1) in which the dynamic equations of motion for each node are combined together.

$$M \cdot \ddot{u} + C \cdot \dot{u} + K \cdot u = -F(t) \tag{2.1}$$

where M is the mass matrix, C is the viscous damping matrix, K is the stiffness matrix, $\ddot{u}, \dot{u}$ and u are the vectors of nodal relative acceleration, velocity, and displacement, respectively. The excitation function, F(t), can be expressed as $M \cdot I \cdot \ddot{u_g}$, where I is the unit vector, and $\ddot{u_g}$ is the acceleration at the base of the system (input time series) (Hashash et al., 2016).
According to Kramer (1996), starting from the input acceleration time series, the motion at the base of the soil column is computed. Next, moving upwards, the motion and the displacements at each layer boundary (nodes) are determined and, consequently, the shear strain and the shear stress in each layer are computed using constitutive models.
In such analysis, the constitutive model involves a backbone curve, which in combination with unload-reload rules, determines the shape of the cyclic loops. These, in turn, control the level of soil damping for a given strain level. Precisely, the unloading reloading characteristic of soils are governed by the extend Masing rule (after Masing, 1926 and Pyke, 1979, in Carlton, 2014) which presumes that:

1. For initial loading, the stress-strain curve follows the backbone curve.
2. The hysteresis loop for unloading and reloading can be determined by scaling the backbone curve by a factor of two.
3. After the initial loading phase, the scaled curve is flipped on the horizontal and vertical axes, respectively, and the origin shifted at the end of the backbone curve in order to represent the unloading path. Next, to capture the reloading behaviour, the curve is placed at the end of the unloading path.
4. As the unloading and reloading is continued, the path of the previous cycle is followed by the updated stress-strain curve.

2.4.4. Modelling Non-linearity

Already at *small strain* levels (between approximately 10^{-5} and 10^{-3}%) the soil behaviour is mainly non-linear, and permanent slippage occurs between particles relatively to each other (Brinkgreve, 2015). After several cycles, the soil response starts to be significantly "softer" and "weaker", leading to degradation of both shear stiffness and shear stress. The soil behaviour turns into a non-linear (plastic) regime, i.e. stress-strain loops evolve implicating energy dissipation. Non-linearity should always be considered as the governing behaviour of many geotechnical materials such as clays, silts gravels, and rocks, under static and dynamic loading (Benz et al., 2009).

2.4.5. Non-linear Dynamic Properties

In earthquake engineering, cyclic loading effects play a very important role. In this case, not only hysteresis and damping, but, more importantly, the accumulation of strains and the generation of excess pore pressure should be considered (e.g. special attention should be paid to particular sites where soil liquefaction, lateral

spreading and slope stability may represent possible events following an earthquake), according to Seed et al. (1986).
In ground response analysis, thus, it is essential to input dynamic parameters that specify the soil characteristics in terms of soil damping (or backbone) and modulus reduction curves, whether an equivalent-linear or non-linear analysis is being performed (Matasovic and Hashash, 2012). These two "quantities" are generally related to each other, being representative of the same concept: stress and strain-dependent stiffness (Brinkgreve, 2015).
The "loop" that is formed by the unloading-reloading cycle is named *hysteresis* (Figure 2.2) and can be described in two ways according to Kramer (1996), namely by the path of the loop itself or by its shape. The shape of an hysteresis loop is characterised by its inclination and its breadth. The former, which is essentially the slope of the relationship between shear stress and shearing strain (Darendeli, 2001), depends on the stiffness of the soil (indicated with the *shear modulus*, G, or with the *secant shear modulus*, G_{sec}), given that the shear modulus changes with strain amplitude during cyclic loading. The latter is related to the area within the hysteresis loop which represents the dissipated energy in a load cycle, conveniently described by the damping ratio (Stewart et al., 2014), D or ξ.
In other words, the material damping ratio indicates the amount of dissipated energy with respect to the retained strain energy (at each cycle) at a given strain level. As shown in figure 2.2, the maximum retained energy is depicted by the triangle that connects the axes origin with peak shear stress, τ_{ff}, and peak shear strain, γ_c. While the total dissipated energy over a loading cycle is represented by the area enclosed in the hysteresis loop. The larger the area enclosed in the hysteresis cycle, the more is the dissipated energy.
Figure 2.2 shows the backbone curve, which is the curve corresponding to the tips of the hysteresis loop at different shear strain levels. The backbone curve approaches the maximum shear strength (τ_{ff}) at large strains, and the slope of the curve at smalls strains is the small strain shear modulus (G_{max}).
The backbone curve can be defined by three types of parameters (Stewart et al., 2014):

- The initial (or maximum) shear modulus, G_{max} or G_0, that is calculated either as the tangent to the stress-strain curve in the origin of the diagram or directly from shear wave velocity measurements, V_s, being:
$$G_{max} = \rho\,(V_s)^2 \tag{2.2}$$
- The variation of normalised secant shear modulus, G_{sec}, depending on the specific applied cyclic shear strain level (γ_c), typically referred to the modulus reduction curve
- The maximum value of shear stress, τ_{ff}, which is indicative of the shear strength at large strains

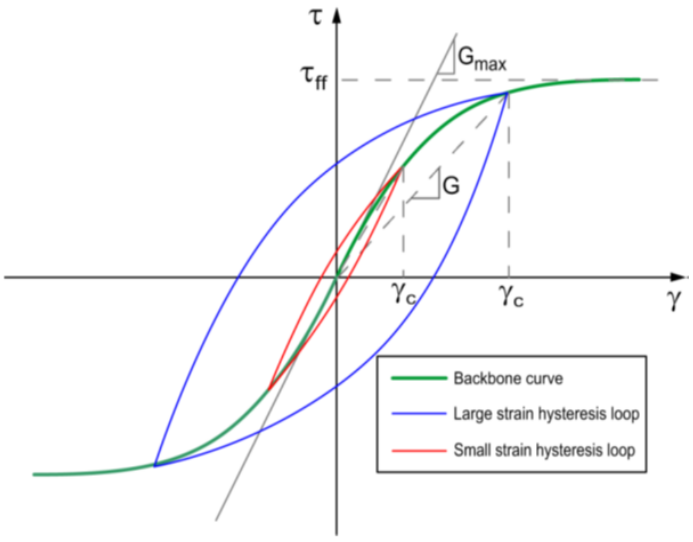

Figure 2.2: Schematic illustration of backbone curve and small strain and large strain hysteresis loops. G_{max} is the maximum (small strain) shear modulus, G is the secant shear modulus for a given strain level, and τ_{ff} is the shear stress at failure (source: Stewart et al., 2014).

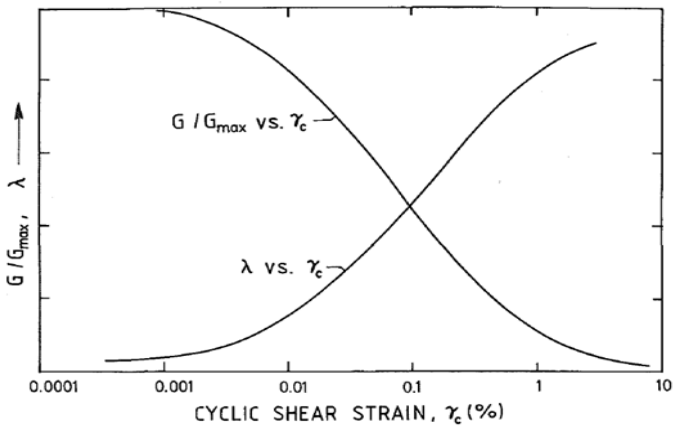

Figure 2.3: Illustration of the variation of Cyclic Parameters with Cyclic Shear Strain. G/G_0 vs γ_c represents the modulus reduction curve and λ vs γ_c the damping ratio curve (source: Vucetic and Dobry, 1991).

The relationship between shear modulus and shear strain is represented by a (normalised) modulus reduction curve (G/G_0 vs γ_c in figure 2.3) (Darendeli, 2001). At zero cyclic strain amplitude, or at strains smaller than the linear cyclic threshold shear strain, the shear modulus is the largest (G_{max}) and the soil exhibits linear elastic behaviour. Conversely, when the threshold shear strain is exceeded, the shear modulus decreases with increasing strain amplitudes (Figure 2.3).
The relationship between damping and shear strain is illustrated in figure 2.3, where the damping (λ, according to Vucetic and Dobry, 1991) is plotted against the peak shearing strain, γ_c. At small strain the material damping is a constant minimum value (D_{min}), which for cohesive soils range between 0.5 % and 5 %. Whereas, at shear strain larger than the linear cyclic threshold strain, the damping increases, as the soils exhibit non-linear elastic behaviour (Figure 2.3).

2.5. Influence of Soil Properties on Dynamic Response

Ascertained that soil stiffness and soil damping represent the dominant aspects of site response analysis (Kramer, 1996), many researchers have been investigating the influence of soil parameters on damping shear reduction curves of both sands and cohesive soils (e.g. Carlton, 2014, Darendeli, 2001, Stewart et al., 2014, Vucetic and Dobry, 1991, etc.).
In the present Section, the main characteristics of soil properties commonly used in SRA (i.e. Plasticity Index, PI, Undrained Shear Strength, Su, Shear Wave Velocity, V_s, Over Consolidation Ratio, OCR) and their effect on dynamic response (in terms of G and D) are briefly described.
Furthermore, in Chapter 4, it will be given a practical example which investigates the effect of the soil properties PI, Su, and V_s on the seismic ground response.

2.5.1. Plasticity Index

The measured values for the liquid and the plastic limits of soils, as recommended by Atterberg in 1991 (Gutierrez, 2006), are widely used as index parameters, which can be empirically correlated against many soil properties in geotechnical practice.
The plasticity index represents an assessment of the brittle and (or) ductile transition of a material, as the PI is equal to the difference between the liquid limit and the plastic limit of a soil sample. In other words, the PI represents the amount of water required to transform a remoulded soil from a semisolid to a liquid state.
Many researchers (e.g. Vucetic and Dobry, 1991 and Darendeli, 2001) have investigated and established that this index has a considerable influence on cyclic stress-strain parameters of soils, affecting the modulus reduction and the damping ratio curves (Figure 2.3). This is also a very convenient conclusion from a practical point of view, since the PI is a common soil index property, determined practically in every project. The Atterberg limits, required to obtain the PI, are among the simplest, most inexpensive, and well-established geotechnical tests.
Dobry and Vucetic (1987) investigated extensively the influence of the plasticity index on all the parameters

and aspects of the cyclic behaviour. They discovered that the PI correlates well with G_{max}, G/G_0 versus γ_c, λ versus γ_c, and the degradation of G with the number of cycles, N. The most important conclusions reported in their study are summarised as follow (Vucetic and Dobry, 1991):

- G_{max} increases with PI, and increases faster with OCR and with geologic age.
- The modulus reduction curve rises with increasing PI.
- The damping ratio curve decreases with increasing PI.
- The shear modulus, G, degrades less after N cycles at a given γ_c.

For strains smaller than about 0.005%, D increases as PI increases, whereas for strains larger than about 0.005%, D and PI are inversely correlated (Carlton, 2014). The reason of this switch was explained experimentally by Darendeli (2001), who found that the type of damping occurring in the soil is a crucial factor. At small strains, the soil behaves more linearly, and the effect of the viscosity of the soil skeleton (also known as creep) is predominant. Differently, at medium and large strains, the non-linearity is more dominant and the area of the hysteresis loop becomes larger, leading to greater damping. However, with higher PI the non-linearity decreases and, consequently, the damping decreases.
Moreover, the soil is more linear and its stiffness degrades less at a given γ_c when the PI is higher. As the soil plasticity increases, the level of cyclic shear strain γ_c, needed to induce a significant non-linear stress-strain response and stiffness reduction, increases as well (Figure 2.4a). Somehow, a soil with high plasticity index subjected to a higher strains tends to develop a microstructure that behaves more linearly than a soil with a lower PI. In fact, soils with very high plasticity index (e.g. PI=100-200) are composed of considerably small particles that have a relatively high surface area per unit weight, and the electrical and chemical bonds and repulsion forces between particles are larger compared to the weight of the particles themselves. As a result, these bonds and repulsion forces dominate the behaviour of the soil under cyclic load (Mitchell, 1976).
The importance of PI in seismic response analysis is to be found in particular for high-plasticity soils, for which the maximum dynamic shear force applied by an earthquake could be amplified (Vucetic and Dobry, 1991). This conclusion has been demonstrated through the analysis of the recorded motions and site response calculations, obtained during the Mexico City earthquake in 1985. A soil with high values of G/G_0 and low damping ratio, like the Mexico City clay, was found to behave linearly at relatively high levels of cyclic shear strain. Thus, less energy was dissipated during ground shaking and higher peak spectral accelerations of the ground response spectra were generated. This resulted in a large amplification of the earthquake motions.
On the other hand, low plasticity clays exhibited a higher degree of non-linearity and, ultimately, a tendency for less ground motion amplification (Dobry and Vucetic, 1987).
Figures 2.4a and 2.4b confirm the influence of the plasticity index on dynamic properties.

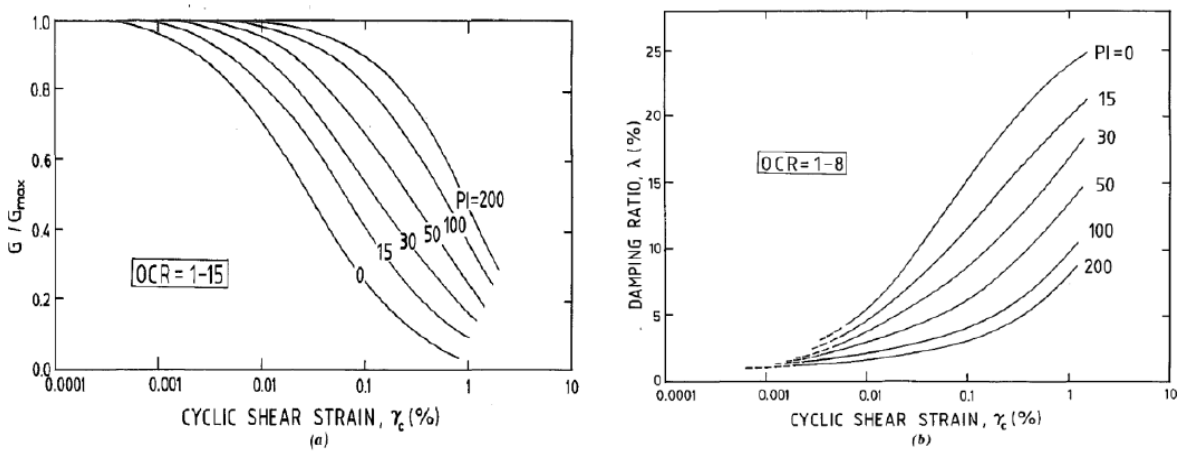

Figure 2.4: Relations between a) G/G_{max} versus γ_c, and b) λ vs γ_c curves for varying PI (0-200 %) and varying OCR (1-15 in left figure, 1-8 in right figure)(source: Vucetic and Dobry, 1991).

2.5.2. Undrained Shear Strength

Soil strength is one of the fundamental soil properties used to assess the capability of a soil material of bearing load (Brinkgreve, 2015).
In earthquake engineering, the analysis of shear strength needs to account for cyclic strength degradation due to pore pressure development. This concept is of particular importance for soils below the ground water table. In this regard, the undrained shear strength is the measurement used the most in seismic analysis (for all soils with degrees of saturation larger than 90 %).
For the understanding of the change in effective stress due to an increase or decrease in total stress, consider a fully saturated cohesive material that undergoes a rapid raise of vertical stress with zero lateral strain. The volume change, which should follow the vertical deformation, leads the solid particles to rearrange themselves, occupying part of the inter-particles voids previously filled with pore water (under static pore water pressure conditions). Since the water is incompressible and cannot instantaneously escape, a pore pressure rise takes place. The generation of excess pore pressure induces, in turn, the reduction of effective stresses which can lead to important phenomena such as liquefaction of loose sands and softening of clays.
Carlton (2014) is one of the researchers who studied, among the other parameters, the importance of shear strength on site response analysis. One of the conclusion is that the shear strength is particularly significant for large level of shear strains, at which also a sand can exhibit undrained conditions. A slight underestimation or overestimation of the soil strength can yield results that may not match the actual soil behaviour under cyclic loading. Underestimation of shear strength, for instance, could generate a ground motion intensity at the surface way lower than in reality, leading to an unconservative design, whilst overestimation of τ_{ff} may induce unrealistic predictions of shear stress (Carlton, 2014).
Furthermore, it was found that the undrained shear strength is positively correlated to the maximum shear modulus (e.g. Hardin and Black, 1969). Nonetheless, almost all of the data in the literature suggest a significant reduction of the initial elastic modulus after cyclic loading. This aspect may be crucial when the soil undergoes sustained shear stresses during which excessive deformations are generated. These in combinations to strain softening may eventually lead to failure (Ansal and Erken, 1989).
Undrained shear strength measured in laboratory, generally, reach failure at 20-30 minutes. However, during an earthquake the strain rate is much faster than that applied in a conventional laboratory test. Thus, considering that the shear strength of clayey soils is rate-dependent, corrector factors (in the order of 1.2-1.4) should be used to account for rate effects on shear strength (Stewart et al., 2014). Nevertheless, in case of soils affected by cyclic softening effects related to cyclic degradation, thus, when softening (or liquefaction) is expected, correction factors should not be applied.

In seismic analysis, the undrained shear strength is normally used for soils below the groundwater table. On the other hand, for cohesionless soils, Stewart et al. (2014) recommend to calculate the shear strength based on the friction angle and zero cohesion, using the Mohr Coulomb failure criteria:

$$\tau_{ff} = \sigma'_v \cdot tan(\phi) \tag{2.3}$$

where ϕ is defined as the internal angle of friction, which can be estimated with different relations from in-situ measurements (e.g. Peck et al., 1974), and σ'_v is the effective vertical stress.

2.5.3. Confining Pressure and Over Consolidation Ratio

It has been demonstrated by a number of studies that there exist other parameters that influence the ground response to a larger extent: the overconsolidation ratio and the pre-consolidation pressure (i.e. Darendeli, 2001, Stokoe et al., 1999, etc.). These properties are related to the stress history of a material, giving information about the degree of stiffness of the soil.
Darendeli (2001) stated that the relationship between the development of pore water pressure and the disposition of the particles (e.g. loosely or densely packed) may have a drastic influence on the seismic response of a soil, when a certain strain threshold is exceeded (i.e. small to large strain level).
The first observation is that the shear modulus becomes higher with an increasing confining pressure. Precisely, the shear modulus increases after having reached the maximum mean effective stress, $log(\sigma'_{pm})$, which the soil specimen has ever experienced throughout its stress history. The main effect caused by confining pressure on dynamic properties is a sort of stress memory, leading the material to show a bi-linear relationship between G_{max} and $log(\sigma'_0)$.
The second finding concerns the confining pressure which was found to be inversely correlated to the damping ratio D (Darendeli, 2001).

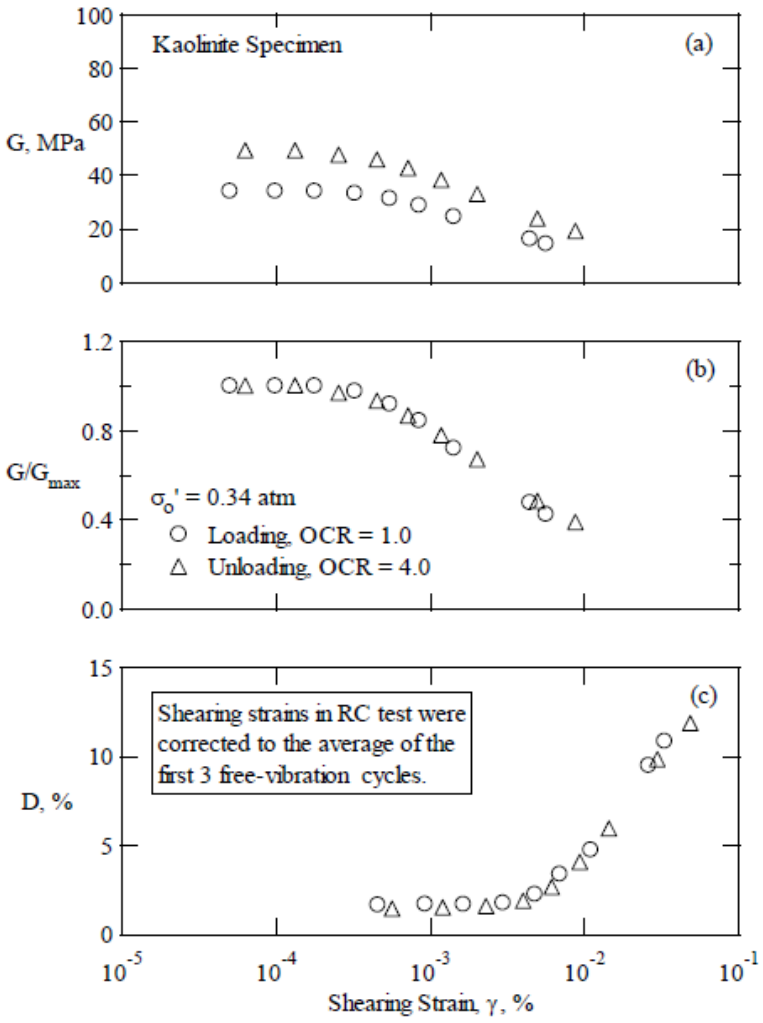

Figure 2.5: Comparison of a normally consolidated (OCR=1) and a over consolidated (OCR=4) kaolinite specimen response in loading and unloading regions. The plots show the effect of OCR on a) shear modulus, b) normalised shear modulus, and c) material damping ratio with respect to shearing strain amplitude (source: Darendeli, 2001).

These behaviours are observed in both normally consolidated and overconsolidated materials. With respect to both D and G_{max}, normally consolidated soils exhibit higher slopes than the latter materials (Carlton, 2014).

Figure 2.5 depicts the effect of OCR on dynamic properties and the difference in non-linear behaviour of a specimen of kaolinite that has been consolidated at 0.34 atm and has been tested first at increasing consolidation pressure (from 0.09 to 1.36 atm) and then unloaded to 0.34 atm and tested again in a torsional resonant column (Darendeli, 2001). Figure 2.5a illustrates that the normally consolidated sample has a smaller shear modulus, compared to the "unloading" specimen with $OCR = 4.0$. On the other hand, the normalised shear modulus curves (Figure 2.5b) and the damping curves (Figure 2.5c) of the two specimens seem to be in good agreement.

From these plots it is clear that, in general, overconsolidated materials are characterised by greater G_{max} and slightly smaller D.

2.5.4. Shear Wave Velocity

One of the main features of ground shaking is the upward propagation of body waves generated by an earthquake (Day, 2002). As discussed in Section A.2.3, the body waves (P-, and S-waves) produce at ground level compressional stress and shear stress, respectively. Compressional waves induce almost only compressional

stress with a deviatoric stress nearly equal to zero, meaning that there is no change in effective stress, since the water carries the compressional load entirely. On the other hand, S-waves generate horizontal shear stress which cannot be carried by the pore water creating, therefore, horizontal displacement (which is of great importance in earthquake engineering).
Elnashai and Di Sarno (2008) showed that the shear velocity is function of the soil stiffness, the depth of the soil formations, and the frequency of the perturbation. In other words, it represents the stiffness of the geological material in the small strain range, and the time needed by the wave to travel a certain distance (e.g the time needed by a wave to travel from a transmitter to a receiver). Such distance is itself a function of the damping which occurs during the migration of waves through a soil deposit (Pitilakis, 2007).
Shear wave velocity is inversely correlated to some dynamic properties: with a decreasing Vs an increase of maximum shear strain, shear stress ratio, and PGA is observed (Carlton, 2014). Contrarily, for high intensity input motions and soft soil layers (i.e. low shear wave velocity) shear wave velocity and PGA are positively correlated.

2.6. Summary and Conclusions

In this Chapter, the first part of the literature review of the the present research has been presented and discussed. The principal aim of the literature review is to outline the ground response theory, the current knowledge on induced earthquakes, and the main soil properties used to analyse the ground response through a 1D analysis (whether linear, equivalent linear or non-linear).
To summarise, the main points of discussion are:

2.6.1. Induced Earthquakes

- The causes of induced earthquakes may be highly variable and may depend on anthropogenic activity, such as fluid extraction (i.e. gas) and injection (waste-water), mining, hydraulic fracturing, etc. Induced earthquakes are usually shallower and smaller in magnitude than tectonics ones, nevertheless, the amount of damage that they can provoke, in some cases, is comparable to tectonic earthquakes.

2.6.2. Ground Response

- Several methods may be applied to model the seismic waves, depending on what is the desired outcome. GRA, for instance, is a 1D analysis of a ground column specifically performed to investigate the propagation of waves and the influence of soil characteristics on ground motion.

- Modelling the propagation of waves through a soil column presumes considerations about the non-linearity of soil properties. As well as, the strain-dependency of the main dynamic properties (shear modulus and damping ratio) needs to be taken into account, as it considerably influences the GRA results.

- Within GRA, there exist linear, equivalent linear, and non-linear analyses. The linear analysis considers dynamic properties to be constant (for each geotechnical unit) and strain independent. In the EQL analysis, these properties are consistently iterated with the effective strain level, however they remain still strain independent. With non-linear analysis, the dynamic equations of motions are integrated in small time steps in the time domain, and strain dependency is introduced.

- Modelling the propagation of waves, the soil characteristics and its behaviour is currently dominated by empirical approaches in engineering practice. It is generally considered that an analytic approach often dismisses the complexity of the problem, including imprecision of ground investigation equipment and operations, as well as inhomogeneity of ground conditions.

2.6.3. Influence of Soil Parameters on Dynamic Response

- Plasticity Index is particularly important since highly plastic soils can amplify considerably the shear force generated by an earthquake (with factor of $\backsim$ 3 to 4). Furthermore, increasing PI induces a reduction of the damping ratio, an increase of maximum shear modulus, and a rise of the the modulus reduction curve.

- Undrained Shear Strength is found to be remarkably relevant at relatively large strain level, at which also sands can exhibit an undrained behaviour (that can possibly lead to liquefaction). In general, underestimation of shear strength, for instance, could generate a ground motion intensity at the surface way lower than in reality, leading to an unconservative design, whilst overestimation of τ_{ff} may induce unrealistic predictions of shear stress.

- Over Consolidation Ratio gives indications about the stress memory of a specific material. Soils which have experienced a larger load than the current one, generally, show higher values of shear modulus and smaller damping ratio.

- Shear Wave Velocity is dependent on soil characteristics, depth, and frequency of the perturbation. V_s is a good indicator of the stiffness of the soil deposits: a stiffer material commonly possesses a higher V_s.
  This parameter influences other dynamic properties such as maximum shear strain, shear stress ratio: a decrease in V_s produces an increase in these properties. PGA, instead, is both positively and negatively correlated with V_s, depending on the ground motion intensity and the soil stiffness: the PGA tends to increase as shear wave velocity decreases, but for soft soil layers (i.e. low shear wave velocity),

undergoing high intensity input ground motions, the PGA decreases due to the higher levels of shear strain and the greater soil damping.

3

Seismic Studies in Groningen

3.1. Introduction

The present chapter introduces the current state of knowledge regarding ground response in the province of Groningen, and describes the most relevant aspects which constitutes the basis of numerical modelling of ground shaking due to induced earthquakes.
First, an introduction to the man-induced earthquakes in Groningen is given, presenting the triggering mechanism (gas extraction) of such phenomena. Following, some information is given about the Winnigsplan (developed by NAM) and the existing risk models for Probabilistic Seismic Hazard Analysis, including PGA maps and GMPEs (Section 3.4). Section 3.4 describes as well the different methods to model ground response are investigated, with focus on site response analysis as performed within VIIA. Following, in section 3.6, the empirical and semi-empirical correlations, applied to predict soil properties within VIIA, together with a number of other CPT-based correlations published by various authors are analysed in detail, explaining their different components and parameters. Furthermore, an insight of the regional geology of the Gronigen area is given, highlighting the predominant formations and seismic microzonation (Section 3.7). Finally, to link the theoretical approach to real engineering practice it is highlighted the necessity of a new ground investigation database, specifically for Groningen, which structure will be fully explained in Appendix B.

3.2. Groningen Seismicity

The extraction of natural gas, initiated more then half a century ago (1959), has constituted in the last few decades a leading business for the Dutch economy (Kamp, 2013). According to the Minister of economy in 2013, Kamp (2013), the extraction of natural gas in the Netherlands produces an income of €12 to 14 billion per year, of which approximately €10 billion are generated directly from the province of Groningen (with a rate of extraction of about 50 billion m^3 per year).
Nonetheless, the exploitation of gas fields presents several disadvantages affecting in different ways both the petroleum company, Nederlandse Aardolie Maatschappij (NAM), and Groningen's inhabitants (Koster and van Ommeren, 2015).
The gas is extracted from deep porous sandstone layers of the Upper-Rotliegend formation (approximately 200 m thick at varying depths ranging from 3.15 to 2.6 km) subjected to large soil stresses, representing the weight of the overlying soil layers and water. Removal of gas has caused a volume reduction that has generated, in turn, a poro-elastic stress change (pore pressure/stress coupling, according to van Wees et al., 2014) in the soil underneath the uppermost layers, and higher vertical stresses on the sandstone, which started to compact (van Eck et al., 2006, van Wees et al., 2014).
Geomechanical models demonstrate that the exploitation of gas fields, in the long term, may provoke land subsidence and in-situ stress changes, leading to initiation of new cracks in and/or around the exploited gas fields, and the possible re-activation of major existing faults (e.g. Geertsma, 1973, Fokker and Orlic, 2006, Segall and Fitzgerald, 1998, in van Wees et al., 2014).
In Gronigen, stress measurements prior to induced seismic events show that most faults are generally far from critically stressed prior to gas depletion. Therefore, differential compaction in areas localised on pre-existing fault structures is likely to be the main cause of energy release due to earthquakes (DvhN, 2013, van Wees et al., 2014).

Since 1986, several hundred small-magnitude seismic events have been recorded in the provinces of Groningen, Drente, North-Holland, and northern Germany (Foulger et al., 2016), at depths between 2.5 km and 4 km. In the past, the magnitude of these earthquakes was relatively small and, in fact, no major damage has been recorded. From the early '90s, however, the intensity and the frequency of earthquakes' occurrence increased drastically, leading the Dutch Government to begin a multidisciplinary research which, in 1993, stated that the origin of the seismicity was not connected to natural events, but to human activity such as gas withdrawal. Consequently, it was highlighted the need of a comprehensive plan to reduce uncertainties and mitigate risk and damage to people and structures (NAM, 2016).

Figure 3.1 shows the induced seismic activity from 1991 to 2017. It is clear that the occurrence of such events has drastically increased during the years, starting with less than 5 events per year (with magnitude between 2.0 and 3.0 on the Richter scale) in 1991, and reaching a peak in 2011 and 2013, with almost 30 events of magnitude not greater than $M_L = 3.5$ per year. Over the years 2014 and 2015, the rate of earthquakes levelled off at a relatively stable amount of 20 and 25 events per year of $M_L > 1.5$, respectively, and it finally decreased (due to a reduction in gas production) over the years 2016 and 2017 up to an average of 10 events per year of $M_L > 2.5$.
For the following five years, earthquakes with a maximum magnitude of 4.5 should be considered for the assessment and retrofit of important structures such as dikes, dams, power pylons and pipelines (Bommer et al., 2017a and Spetzler and Dost, 2017). According to Kamp (2013), currently the majority of these structures are not in serious danger of failure, nevertheless, special attention should be given to those structures located in highly built-up areas and to important civilian buildings, such as schools and hospital.

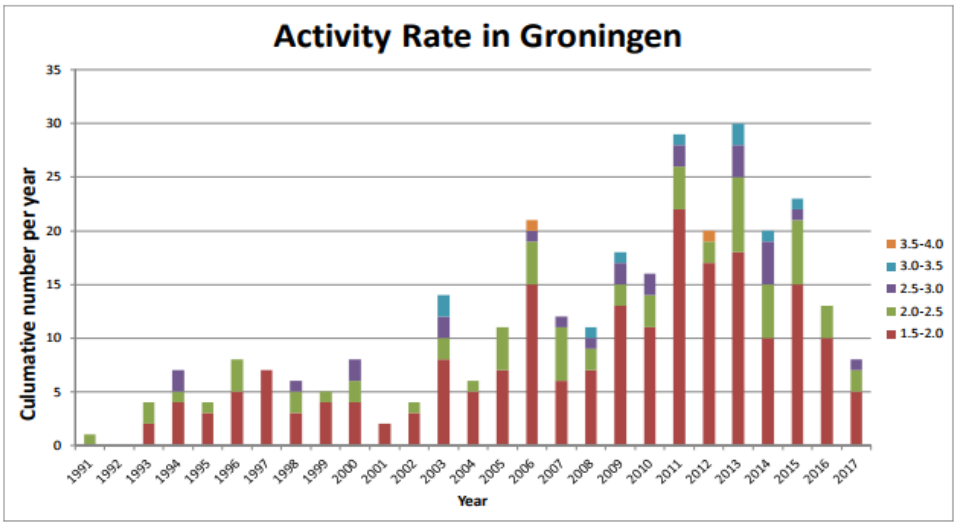

Figure 3.1: Activity rate of observed induced earthquakes in Groningen from 1991 to 2017. With different colours are indicated the varying magnitudes shown in the legend. Only events with a magnitude greater than 1.5 on the Richter scale are considered in this catalogue (source: Spetzler and Dost, 2017).

3.3. NAM Winningsplan

The effects of many years of gas withdrawal from the natural gas reservoirs in Groningen have become increasingly explicit over the past years. The citizen of the region, especially those who live in the Loppersum area, started to seriously worry about the safety of their lives and possessions after the Huizinge earthquake ($M_L = 3.6$), occurred in August 2012 (Spetzler and Dost, 2016).
Following the Huizinge earthquake, several new studies have been carried out, e.g. Arup (2015), Bommer et al. (2015a, 2017a, 2015b, 2017b), Kruiver et al. (2015, 2017), NAM (2003, 2016), Spetzler and Dost (2016), Vasileiadis (2015), etc. to further study such seismic phenomena. According to KNMI, SodM and NAM studies, the uncertainty associated to the earthquakes hazard in Groningen is far greater than the uncertainty considered at previous stages. Thus, in the following years, NAM begun performing seismic hazard assessment, introducing a multi-year plan with the purpose of collecting and analysing data from the region.
The Winningsplan 2016 (NAM, 2016) contains a description of the data acquisition plan from 2013 to 2016. The main objectives of this plan are shown schematically in figure 3.2, where it is shown a causal chain starting from gas extraction and ending to risk/safety assessment stage. As part of the data acquisition plan, the installation of a new digital monitoring systems, meant to improve the control of different phenomena (e.g. compaction, subsidence, and seismic activity), has been initiated in order to perform risk and hazard assessment based on specific factual data for Groningen.

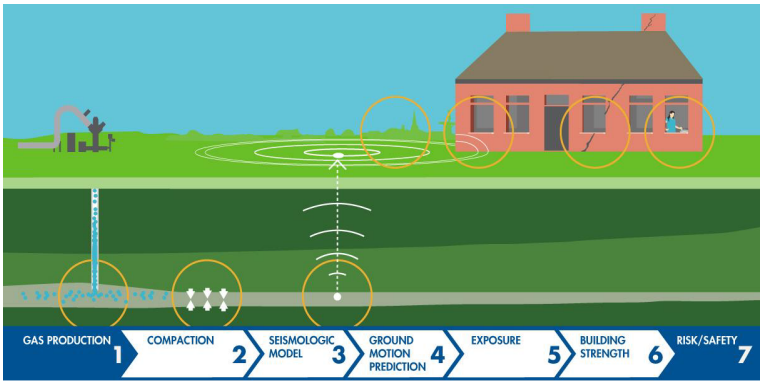

Figure 3.2: Schematic representation of the causal chain from gas extraction to risk/safety assessment for people. Note that the vertical scale of the figure is exaggeratedly reduced for illustrative purposes (source: NAM, 2016).

3.4. Seismic Hazard

The purpose of the Winnigsplan was to develop a seismic hazard and risk model specifically for Groningen, aimed to estimate seismic actions to be taken in the design of new construction and/or retrofit of existing buildings (e.g. Bommer et al., 2015a). The first Probabilistic Seismic Hazard Assessment (PSHA) developed for Gronigen was released in 2014 (named Version 0, or V0). The main differences between this and the new models have to be found mainly in the Ground Motions Prediction Equations (GMPEs). As recommended by the Dutch building design guideline (NPR 9998, 2015), in the long term, the seismic risk model will lead to an iterative modelling that can estimate suitable strengthening thresholds for existing buildings, involving the creation of GMPEs for the risk calculation and PSHA. Using the words of the Pacific Earthquake Engineering Research Center (PEER) (Stewart et al., 2014):

> *GMPEs, or attenuation relationships, are employed in both probabilistic and deterministic seismic hazard analyses to predict the level of ground shaking and related uncertainty, accounting for earthquake magnitude, source-to-site distance, local soil conditions, fault mechanism, etc.*

The first model used GMPEs derived from tectonic earthquakes to match local recordings in the small-magnitude range, the V0 GMPEs were based on tectonic earthquakes, generally larger in magnitude (Bourne et al., 2014). Despite the fact that these equations introduced valuable considerations about site amplification terms and

non-linearity of soil response (although not yet calibrated specifically for Groningen conditions), they were developed for the estimation of PGA and PGV, and were based on large sigma (standard deviation) resulting from a regression analysis performed using a database containing information from Europe and Middle East (after Akkar et al., 2014a, in Bommer et al., 2017a). Moreover, a constant value of shear wave velocity was assigned to the uppermost 30 m of soil (V_{S30}) equal to 200 m/s, meaning that any spatial variability within the uppermost ground layers was not taken into account (Bommer et al., 2015b, Kruiver et al., 2017).
The V0 model was updated one year later (2015) by the Version 1 (V1). In 2015 Version 2 was published (Bommer et al., 2015b), and in the same year it was replaced by Version 3 (Bommer et al., 2016). Nowadays, the latest version available is the Version 4 (Bommer et al., 2017c) that basically constitutes an update of the V2 hazard model (which was the base of the Winnigsplan 2016).
Already with the use of V1 GMPEs and V2 GMPEs, several limitations in the V0 relations were eliminated. First of all, the creation of a Groningen database (with data-set comprehending from 85 to 146 records) allowed the extrapolation of models able to capture epistemic uncertainty (which increases for larger magnitude events) (Spetzler and Dost, 2017). However, according to Bommer et al. (2017a), one shortcoming of this approach is that it assumes that the sampling of the dynamic characteristics at the recording station locations is a reasonable approximation to the average amplification functions across the entire field. To some extent, this is likely to be a conservative assumption since most of the records were obtained by instruments located in the north of the gas field where softer soils are encountered than in the south. The model, thus, was considered to be limited in reflecting the spatial variation of ground conditions and their effect on the surface motions. The most serious deficiency in the model, however, is the failure to account for non-linear site response. Given the weak levels of motion recorded to date, it is likely that the inferred amplification function is a reasonable estimate of the average linear site response term across the recording network. However, when extrapolated to larger magnitudes, the soils would be expected to respond non-linearly to the higher amplitudes of acceleration propagating upwards from the underlying rock, leading to reduced surface accelerations. Consequently, it can be assumed with confidence that the V1 GMM is potentially conservative when applied for larger magnitudes and short distances.
With V2 GMPEs, field-specific non-linear site amplification functions were introduced and the possibility to create predictive equations for a significantly wider range of response periods was achieved (Bommer et al., 2015b). A reference horizon was selected at a depth of 350 m (Upper North Sea Supergroup Formation, NU_B) and the soil, up to this depth, was divided in 167 microzones (based on amplification factors) with different site response characteristics (Spetzler and Dost, 2016).
To accommodate the use of the V2 GMPEs, which consider spatial variability induced by geologic processes in the uppermost soil layers (up to -350 m), the hazard model, used in the Probabilistic Seismic Hazard Analysis (following Cornell, 1968), was modified according to the Bazzurro and Cornell (2004) approach (Spetzler and Dost, 2016), including an amplification factor for the shallow part of ground columns. In this way, the hazard curve at a certain depth was obtained considering the contribution of different seismic events (i.e. induced earthquakes) over the zonations, with varying magnitude. Furthermore, the hazard curve is corrected accounting for both the probability density function of the spectral acceleration and the probability distribution of the amplification factor (convolution method). This approach leads to the realisation of seismic hazard assessment of a certain surface ground motion level, based on the contribution of different reference ground motion levels.
According to Bommer et al. (2017a,c), the V3 model share many aspects in common with the V4 model and the framework of the ground motion model is essentially the same. The most significant change from the V2 to the V3 model was to consider a deeper reference rock horizon (from the Upper North Sea Supergroup Formation, NU_B, to the base of the North Sea Supergroup Formation, NS_B), allowing for a clearer and pronounced impedance contrast. Additionally, V4 GMPEs incorporate rupture effects, based on extended source ruptures rather than points (hypocentres), especially for larger magnitude earthquakes (beyond $M_L = 6.5$), and introduce a model for a more accurate PGV prediction. Thanks to the new detailed ground motion database and the use of three different definition of horizontal components of motions, namely the geometric mean of the two horizontal components, the larger of the two horizontal components and the maximum component identified by rotation of the recorded traces, it was possible to create new empirical PGV equations. PGV values, obtained using these three different models, result to progressively increase. The equations include coefficients for the prediction of the median values of PGV and also the standard deviations to allow values to be estimated at other exceedance values. Furthermore, in order to obtain the top of the elastic half-space to be coincident with the most marked impedance contrast, the target horizon is assumed at the base of the North Sea Supergroup Formation (as in the V3 model), and the reference rock elevation is fixed at a depth of

-800 m.
The final result of the application of the PSHA in Groningen, calculated in terms of a 10 % probability of exceedance in 50 years, equivalent to a return period of 475 years, is represented in Figures 3.3, 3.4, and 3.5 where the probabilistic seismic hazard map for Groningen is illustrated, with indication PGA distribution across the entire region. Probably, the most significant achievement obtained by the use of the the V2 GMPEs is an overall reduction of the maximum PGA from 0.36 g (Figure 3.5) to 0.22 g in Spetzler and Dost, 2016. On the other hand, in Figure 3.3 it is clear that, employing V4 GMPEs, the PGA distribution remains almost identical to the previous one (Figure 3.4), with the only difference that the max PGA is, in the latter case, 0.24 g.
The PGA map represents the distribution of Spectral Acceleration (SA) at bedrock level at a period of 0.01 seconds. Equivalently, it is possible to plot SA versus the period (1/frequency), as represented in Figure 3.6. In the latter case, a site analysis for two locations (one in the city of Groningen and another in Loppersum) has been carried out by Spetzler and Dost (2016), showing a maximum peak in the spectra about 0.3 s in both curves.

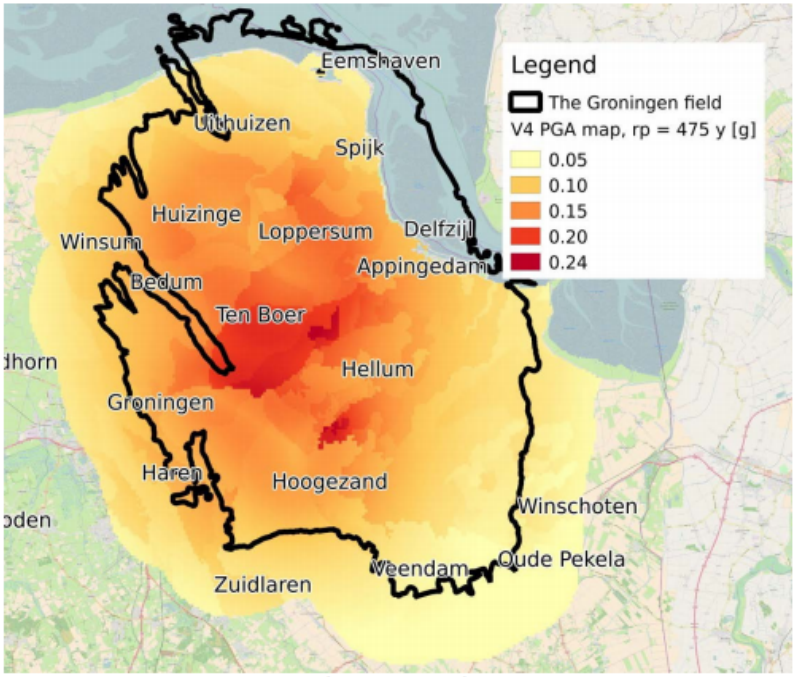

Figure 3.3: Probabilistic seismic hazard map for Groningen using GMM V4, for a return period of 475 years and a period of T=0.01 s. With varying colours are indicated PGA zones (max PGA is 0.24 g near Loppersum). The black line define the contours of the gas field (source: Spetzler and Dost, 2017).

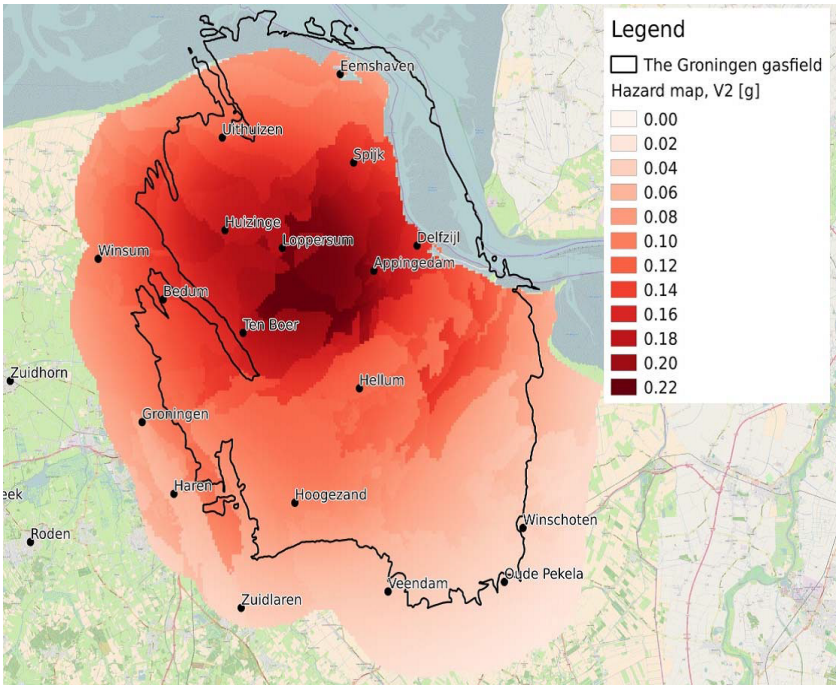

Figure 3.4: Probabilistic seismic hazard map for Groningen using V2 GMPEs, for a return period of 475 years (according to Eurocode 8) and a period of T=0.01 s. With varying colours are indicated PGA zones (max PGA is 0.22 g near Loppersum). The black line define the shape the gas field (source: Spetzler and Dost, 2016).

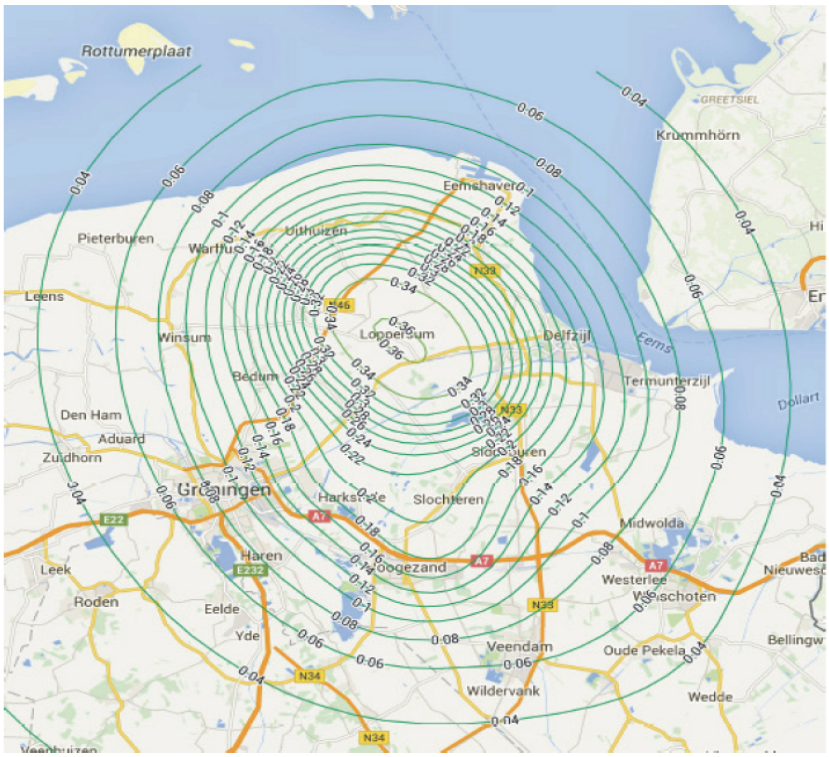

Figure 3.5: Probabilistic seismic hazard map for Groningen using V0 GMPEs, for a return period of 475 years and a period of T=0.01 s. The contour lines indicate the PGA zones (max PGA is 0.36 g near Loppersum) (source: Spetzler and Dost, 2016 in NPR 9998, 2015).

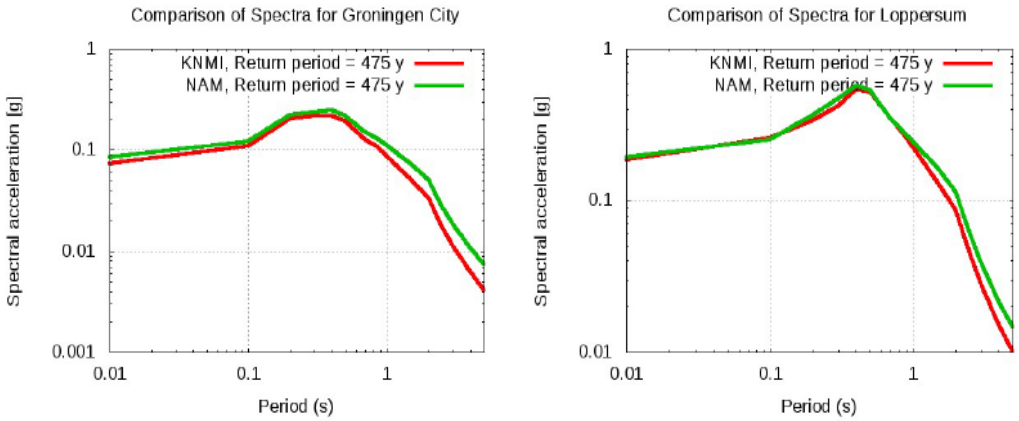

Figure 3.6: Comparison of spectral acceleration prection by KNMI and NAM for a site in Groningen city and Loppersum. The model is calibrated to a return period of 475 years. In red and green are presented results from KNMI and NAM, respectively (source: Spetzler and Dost, 2016).

3.5. Site Response Analysis in Groningen

The present section illustrates the basic concepts of SRA as it is performed in Groningen by Bommer et al. (2017a). Figure 3.7 shows a schematic illustration of a 1D soil column analysis. The motions recorded at the site where the bedrock is exposed may considerably differ from those which reach the surface, after having travelled through soft soil deposits (*free surface motion*). The specification of a bedrock and selection of input rock motions is, thus, essential for properly modelling the propagation of shear waves and site response effects, such as resonance and amplification or attenuation of ground motions (Kramer, 1996).
However, since the absence of such an outcropping rock in Groningen, an "engineering bedrock" (or reference rock) near 800 m depth is being used for dynamic calculations. This depth coincides with the base of the Upper North Sea Supergroup Formation, under which the lateral spatial variability is considered to be negligible (NAM, 2016) (see Sections 3.4 and 3.7).
Currently, SRAs in Groningen, following NPR 9998 (2015), have been performing using a 1D model able to capture the non-linear soil behaviour under cyclic loading, which presumes the input soil parameters needed to set a 1D SRA in DEEPSOIL or DIANA, necessary to characterise the backbone curve of non-linear models (e.g. damping ratio and modulus reduction curve). In practice, to capture the characteristics of the uppermost layers, giving information about the soil profile, including stratigraphy, water table depth, shear wave velocity, and dynamic soil properties, a combination of in-situ measurements and correlations based on cone penetration tests resistance is employed.

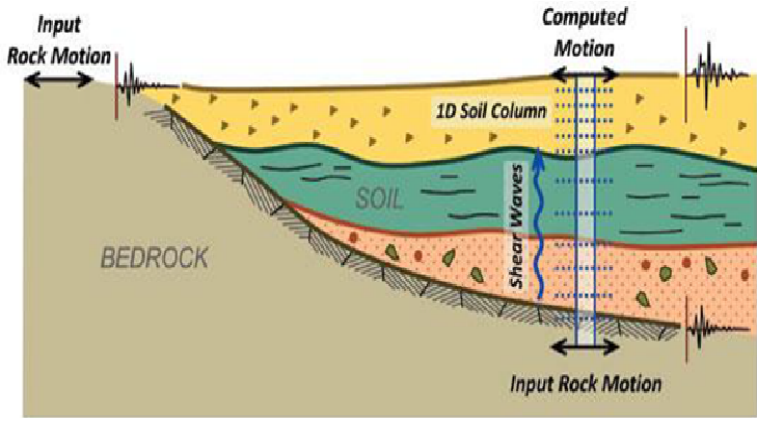

Figure 3.7: Schematic representation of a 1D soil column analysis in which it is represented the computed ground motion at surface according to the shear waves that propagate from a bedrock (from which the motion is input) through a layered soil column (source: Nikolaou et al., 2012, in Carlton, 2014).

3.5.1. State of Knowledge

Table 3.1 presents a summary of different approaches used for estimating soil properties for site response in Groningen. Widely used CPT-based relations from the literature are employed for the prediction of several soil properties (i.e. γ, PI, Su, and OCR, Table 3.1). For the shear wave velocity a site-specific CPT-based correlation is available after the study conducted by Vasileiadis (2015) (Table 3.1).

Table 3.1: CPT-based correlations used in SRA to predict soil properties in Groningen (i.e. soil unit weight, plasticity index, undrained shear strength, over consolidation ratio, and shear wave velocity) by three different parties, namely Arup (2015), Bommer et al. (2015b), and Bommer et al. (2017a).

	ARUP (2015)	**Bommer et. al (2015) V2 model**	**Bommer et. al (2017) V4 model**
Soil Property	**Reference**		
Soil Unit Weight, γ	Robertson & Cabal, 2010	Lunne et al., 1997	Lunne et al., 1997, and $21 kN/m^3$ for deeper layers
Plasticity Index, PI	Cetin & Ozan, 2009	Skempton & Henkel, 1953	Representative values from Sorensen & Okkels, 2013
Undrained Shear Strength, Su	Ladd and Foott, 1974, SHANSEP	Lunne et al., 1997	Lunne et al., 1997 and Bommer et al. 2017with N_{kt} as recommended by Robertson, 2009
Over Consolidation Ratio, OCR	Kulhawy and Mayne, 1990, and Robertson, 2009	Lunne et. al, 1997	Kulhawy and Mayne, 1990, in Robertson & Cabal, 2015
Shear Wave Velocity, V_s	Site-specific $CPT - Vs$ correlation (ARUP, 2015)	Bommer et al., 2015	Bommer et al., 2017

3.6. CPT-based Correlations to Derive PI and Su

The present study is going to focus on the relations used to estimate plasticity index and undrained shear strength, which have not been developed specifically for the Groningen region. In the following sections, a number of CPT-based correlations for PI and Su from various authors are presented and discussed.

3.6.1. Plasticity Index

Several CPT-PI correlations have been proposed in literature, starting from more the half century ago (e.g. Terzaghi and Peck, 1948 , Skempton and Henkel, 1953, Mayne and Peuchen, 2012, etc., in Cetin and Ozan, 2009). In particular, correlations between soil properties and the Atterberg limits have been shown to be reasonably convenient given that the measurement of such soil indices requires very simple techniques, low costs and short time. In this section, only the correlations presented in table 3.1 are analysed. These are:

1. Equation 3.1, after Skempton & Henkel, 1953
2. Equation 3.8, after Cetin & Ozan, 2009
3. Equation 3.9, 3.11, and 3.12, after Sorensen & Okkels, 2013

1. The equation 3.1, developed by Skempton & Henkel in 1953, can be adopted to back calculate the plasticity index from values of undrained shear strength, obtained using equation 3.18 with $N_{kt} = 15$. This relationship can be expressed in the form of a linear function:

$$\frac{Su}{\sigma'_{v0}} = 0.11 + 0.0037\left(\frac{PI}{100}\right) \tag{3.1}$$

2. The Cetin and Ozan (2009) correlation is the result of a semi-probabilistic methodology that accounts for uncertainty and spatial variability deriving from the lack of soil sampling during conventional cone penetration testing (Cetin and Ozan, 2009). This new methodology involves the composition of a detailed database with 484 CPT/standard penetration test (SPT) data pairs formed by corrected cone tip resistance (q_t), sleeve friction (f_s), fines content (FC), liquid limit (LL), plasticity index (PI), and soil type based on the Unified Soil Classification System ($USCS$). The CPT logs, as well as the SPT data have been obtained from seven different databases from all over the world, and associated to boreholes realised mainly within 2 m from the CPT (Cetin and Ozan, 2009). In this formula, the measured tip resistance (q_c) has been first corrected and then normalised with respect to a vertical effective stress σ'_v, following the Cetin & Isik (2007) scheme, as shown in the following equations (Equations 3.2 to 3.8) :

Corrected cone tip resistance

$$q_t = q_c + u \cdot (1 - a) \tag{3.2}$$

Normalised net cone tip resistance

$$q_{t,1,net} = \frac{q_t - \sigma_v}{\left(\frac{\sigma'_v}{P_a}\right)^c} \tag{3.3}$$

In Equations 3.2 and 3.3, a represents the area ratio,u the pore pressure measured behind the cone shoulder, P_a the atmospheric pressure (expressed in the unit of σ'_v) and c is the power law that can be calculated as:

$$c = \frac{R - 272.38}{275.19 - 272.38} \pm 0.085 \tag{3.4}$$

in which

$$272.38 < R < 275.19 \tag{3.5}$$

that is computed as:

$$R = \sqrt{[log(F_R) + 243.91]^2 + \left[log\left(\frac{q_{t,1,net}}{Pa}\right) - 126.24\right]^2} \tag{3.6}$$

Similarly, the sleeve friction is also normalised:

$$F_R = \frac{f_s}{q_t - \sigma_v} \cdot 100 \tag{3.7}$$

Next, these quantities are implemented into Equation 3.8, obtained from a semi-probabilistic approach involving the Bayesian model assessment approach (Cetin and Ozan, 2009):

$$PI = 10^{\frac{2.37 + 1.33 \cdot log\,(F_R) - log\,(q_{t,1,net})}{2.25}} \tag{3.8}$$

in which F_R is the percentile ratio of the sleeve friction normalised to an effective stress $\sigma'_{v0} = 1atm$, and $q_{t,1,net}$ is the corrected con tip resistance normalised to the same effective stress $\sigma'_{v0} = 1\ atm$.

3. The correlation developed by Sorensen and Okkels (2013) expresses the relationship between the effective internal peak friction angle, ϕ'_{NC} and PI for normal consolidated clays. The best estimate and the cautious low boundary (LB, corresponding roughly to the 5 % fractile) relationships, obtained from data collected from literature (233 measurements) are, respectively:

$$\phi'_{NC} = 43 - 10 \cdot logPI \tag{3.9}$$

$$\phi'_{NC} = 39 - 11 \cdot logPI \tag{3.10}$$

where ϕ'_{NC} is expressed in degrees and PI in %.
Similarly, for over consolidated clays two correlations based on two PI ranges are proposed:

$$4 < PI < 50 \qquad \phi'_{OC} = 45 - 14 \cdot logPI \tag{3.11}$$

$$50 \leq PI < 150 \qquad \phi'_{OC} = 26 - 3 \cdot logPI \tag{3.12}$$

and their cautious LB estimate:

$$4 < PI < 50 \qquad \phi'_{OC} = 44 - 14 \cdot logPI \tag{3.13}$$

$$50 \leq PI < 150 \qquad \phi'_{OC} = 30 - 6 \cdot logPI \tag{3.14}$$

The authors suggests to apply the above correlations (Equations 3.11 and 3.12) to most overconsolidated clays with clay-size fraction below 80 % (Sorensen and Okkels, 2013). For soils with larger clay-size fractions, the above relations should be used with caution until their validity is confirmed by additional tests.

3.6.2. Undrained Shear Strength

Determination of undrained shear strength is a highly complex task, given that does not exist a unique value of Su in reality. It is well known that for cohesive soils the undrained shear strength depends on a vast number of factors, such as stress history, soil heterogeneity (i.e. anisotropy), and strain rate.
For clayey materials, there exist several in-situ and laboratory techniques that can measure this soil property with a good approximation of real conditions. In-situ vane shear testing, for example, is widely used in Groningen for a quick representative estimation of undrained shear strength of shallow soils, even though the resulting undrained shear strength values should be cautiously post-processed, taking into account several limiting factors (e.g. stress history, loading direction, partial saturation). Likewise, soil sampling and undrained triaxial tests in laboratory can describe the soil strength with an acceptable accuracy and precision. However, triaxial tests involve a wide range of problems (e.g. sample disturbance, determination of in-situ overburden pressure). Furthermore, laboratory testing may be considered too expensive for certain clients especially in small projects, resulting in a strong need of alternative solutions such as the application of empirical and semi-empirical correlations on CPT measurements.
In this context, many authors have been trying to develop strength models based on CPT/CPTU results, which are nowadays easily available, practical, and relatively cheap. The existing correlations are thought to be representative of actual soil conditions, attempting to account for as many factors as possible. The correlations considered in this study are:

1. Equation 3.15, after Ladd & Foott, 1974
2. Equation 3.18, after Lunne et al., 1997
3. Equation 3.19, after Robertson & Cabal, 2015
4. Equation 3.20, after Robertson & Cabal, 2015
5. Equation 3.21, after Bommer et al., 2017

1. A procedure that is widely used to estimate Su values for a large variety of clays is the SHANSEP (Stress History and Normalised Soil Engineering Properties) framework, developed by Ladd and Foott in 1974. According to this procedure in order to estimate the shear strength of a saturated clay it is important to account for the effects of sample disturbance, anisotropy and (to lesser degrees) strain rate effects. Based on in-situ measurements and experimental observations, it is convenient to "normalise" the undrained stress-strain-strength behaviour of most "ordinary" clays with respect to the stress history. The SHANSEP model claims that there is a unique value representing the ratio of undrained shear strength and effective vertical soil pressure for a normal consolidated (NC) clay. Based on this assumption, the undrained shear strength of any over consolidated (OC) clay, normalised to the effective soil stress, can be calculated as a function of the OCR, the normalised undrained shear strength ratio of NC clay, S, and an empirical parameter, m, which governs the shape of the $Su = f(OCR)$ function. (more details in Chapter 6).
   The SHANSEP relation can be expressed as follows:

$$\left(\frac{Su}{\sigma'_v}\right) = S \cdot OCR^m \tag{3.15}$$

   where σ'_{v0} is the effective soil stress, OCR is the over consolidation ratio, $S = \left(\frac{Su}{\sigma'_v}\right)_{OCR=1}$ is the undrained shear strength ratio for normally consolidated soils and m is an dimensionless parameter, also know as the critical-state pore pressure parameter (Mayne, 1980), that varies depending on the material and whether the shear is active, passive or direct (D'Ignazio, 2016).
   The exponent m was observed to range between 0.75 and 0.95 (Jamiolkowski et al. 1985) indicating that the relations between Su/σ'_v and OCR is generally non-linear. Moreover, m can be calculated as a function of the soil behaviour type index, $I_{c;def}$ (after Robertson and Wride, 1998, in Robertson and Cabal, 2015) according to the following relation (Mayne, 2014):

$$m = 1 - \frac{0.28}{1 + (I_{c;def}/2.65)^{25}} \tag{3.16}$$

In general, values of m for clays and silts should theoretically lie within the range $0 \leq m \geq 1$ (Mayne, 1980).
On the other hand, the undrained shear strength ratio of NC clay, S, has been further studied by Robertson and Cabal (2015) in relation to the friction angle (ϕ'). From direct simple shear tests, it was found that for a normally consolidated clay, with an average ϕ of 26°, S resulted to be approximately 0.22. The range of S can be relatively large, depending on the test type, water content, plasticity index and sample disturbance (e.g. $S = 0.08$ to 0.35 for Norwegian clays, according to Karlsrud & Hernandez-Martinez (2013), in D'Ignazio, 2016).
For NC to low OC clays with low to moderate plasticity index, Jamiolkowski et al. (1985) suggests the relation:

$$S = (0.23 \pm 0.04) \tag{3.17}$$

For Groningen, Arup recommends a value of S equal to 0.25, which produces results in good agreement with those obtained from the Lunne et al. (1997) correlation (with N_{kt} varying from 14 to 18, see Equation 3.18).

2. As presented by Lunne et al. (1997), Su can be calculated considering the total *in-situ* vertical stress, the measured cone tip resistance (q_c) and the empirical cone factor (N_{kt}), through the following formula:

$$Su = \frac{(q_c - \sigma_{v0})}{N_{kt}} \tag{3.18}$$

The empirical factor N_{kt} tries to catch the soil anisotropy, varying from 14 to 18 (Robertson and Cabal, 2015). However, the use of such empirical factor, may influence the results and, therefore, depending on the entity of the project more conservative approaches can be considered, selecting, for instance, the upper limit of the N_{kt} range slightly different from the one previously mentioned (e.g. 15 to 20).

3. An improvement of the above relation was found by Lunne (in Robertson and Cabal, 2015) using CPTU data (2nd category). The cone resistance was modified accounting for pore pressure influence ($q_t = q_c - \sigma u$), yielding the following equation:

$$Su = \frac{(q_t - \sigma_{v0})}{N_{kt}} \tag{3.19}$$

Several studies have been conducted with the aim of obtaining suitable cone factor values (e.g. Nash and Duffin, 1982; Lunne and Kleven, 1981; Aas et Al., 1986; Lunne et al., 1986; La Rochelle et al., 1988; Lee, 1997; Chang et al., 2001; Chung et al., 2003; Park et al., 2007, as reported by Shin and Kim, 2011), given that N_{kt} is probably the most significant quantity affecting the undrained shear strength predictions. Lunne et al. (1997) affirmed that N_{kt} is also affected by the plasticity index and other localised soil features.

4. In very soft soils, Su can be computed accounting for the excess pore water pressure measured in CPTUs. The relation, available in Robertson and Cabal (2015), is expressed as:

$$Su = \frac{\Delta u}{N_{\Delta u}} \tag{3.20}$$

where Δu represents the excess pore pressure and $N_{\Delta u}$ is a cone factor similar N_{kt} that varies from 4 to 10.
As recommended by Robertson and Cabal (2015), for complicated projects, involving high risk, it is advisable to compute Su by developing site-specific correlations, and coupling estimations with laboratory data.

5. Based on the linearity observed the undrained shear strength and the effective vertical soil stress, Bommer et al. (2017a) suggest a number of linear relations for the different stratigraphic units encountered in Groningen. The empirical parameters α and β for the units analysed in this research are summarised in table 3.2. The recommended equations for organic materials (i.e. peat) are not reported in this section, given that the present study focuses mainly on Holocene clays. The equations proposed by Bommer et al. (2017a) are in the form of:

$$Su = \alpha \cdot \sigma'_{v0} + \beta \tag{3.21}$$

where σ'_{v0} is the effective vertical stress, expressed in kPa.

Table 3.2: Empirical parameters for undrained shear strength equations proposed by Bommer et al. (2017a).

Stratigraphic Unit	**Soil Type**	**Unit weight**	α	β
[-]	[-]	[kN/m^3]	[-]	[-]
Naaldwijk	Clay	12,9	0,38	12
	Sandy clay and clayey sand	16,2	0,49	44
Drente	Clay	14,7	1,15	1
	Sandy clay and clayey sand	16,7	0,97	30
Boxtel	Clay	14,1 - 14,4	1,15	1
	Sandy clay and clayey sand	16,9	0,97	30
Nieuwkoop	Clay	14,1 - 17	0,38	12
	Sandy clay and clayey sand	16 - 17	0,49	44
Peelo	Clay	17,6	0,88	26
	Sandy clay and clayey sand	18,1	0,60	55
Anthropogenic	Clay	13,9	0,60	55
	Sandy clay and clayey sand	16,8	0,97	30

3.7. Geology of Groningen

Modelling of the ground motion in Groningen requires a deep understanding of the geological characteristics of the materials belonging to the shallow subsurface of the North of the Netherlands.
As NAM asserted (van Elk et al., 2013), the *Slochteren* sandstone layer (at a depth of approximately 3000 m), containing natural gas, is underlying different soil deposits formed during the Mesozoic and Cenozoic Era (Figure 3.8). Above the sandstone, the subsurface comprehends all soil materials developed during the last one million years. For instance, a typical stratigraphy of the region (Figure 3.9) shows the presence of deposits which have formed during the Quaternary period, composed by the Holocene and late Pleistocene Ephocs (Kruiver et al., 2015).
The upper 800 m of the entire region show a thick layer of unconsolidated deposits, characterised by a considerable heterogeneity. Within this layers, it is possible to encounter Cretaceous limestones, belonging to the Chalk Group at large depths (Mulder et al., 2003, Vos, 2015), underlying formations consisting of a sequence of marine grey sands, sandstones, and clays dating back to the Late Paleocene to Middle Eocene age, also known as the *Lower North Sea Group* (Kruiver et al., 2017). The bottom edge of such formation is approximately 840 m deep, on top of which, between 450 and 350 m deep, Oligocene clay constitutes the *Middle North Sea Group*. This, in turn, is located underneath the *Upper North Sea Group* which is mainly formed of marine sediments (e.g. marine clays, sandy clays and loam), so called *Breda Formation*. According to TNO (2016), these three groups are called the *North Sea Supergroup*, and they constitute the base of the younger formations, described in more details in Section 3.7.1.
On the other hand, the upper 200 meters were formed during the second half of the Pleistocene period and were subjected to several climatic changes which have influenced the soil composition (i.e. ice ages and sea level fluctuations). Precisely, around 450,000 and 150,000 years ago, respectively, the Netherlands was almost completely covered by ice. The first glaciation, called *Elsterian* glaciation, generated deep subglacial formations (also know as *tunnel valleys*), which have been filled with sands and clays during a later glaciation: the *Peelo Formation*. The second important glaciation, so-called *Drente Substage* of the *Saalian* glaciation, produced till sheets which constitute the Drente plateau, also known as *Dtrenthe Formation*. Differently, during the last glaciation (between 25,000 and 14,000 years ago), the Pleistocene deposits were covered by a shallow superficial blanket of eolian sand, rather than by ice sheets. Eventually, the region turned out to be a coastal plain, subjected to a number of sea level rises occurred during the inter-glacial periods. Consequently, it is common to encounter an alternation of shallow marine inter-tidal deposits such as Naaldwijk and Niuewkoop Formations (more details in Section 3.7.1). Moreover, the sea level rises have produced the formation of peat beds, clay beds (edges of the basin), and sand channels (in the central part of the tidal basin). In addition to glacial and eolian activities, rivers and floods have spread out the periglacial sands all over the region (Kruiver et al., 2015), modifying the characteristics of the shallow subsurface.
It is clear that the subsurface of the Groningen region is highly heterogeneous. Indeed, it is a complicate task to combine all available geological and geomechanical data into a single model representing this complex spatial variability. Figure 3.8 attempts to give an illustration of the coexistence of such variable formations, including sand channels and clay deposits in under-tidal basins.

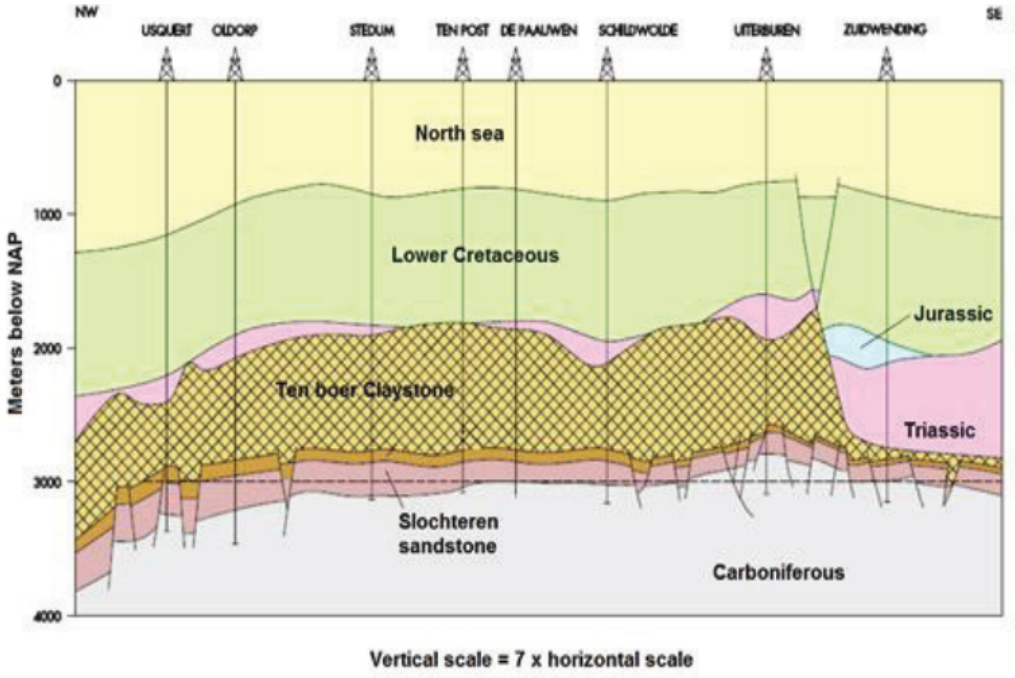

Figure 3.8: Deep geological cross-section of the province of Groningen (up to 4km deep) representing the position of the wells (in 2003) and the main stratigraphic intervals, e.g. Carboniferous, Cretaceous, etc. (source: NAM, 2003).

3.7.1. Groningen Stratigraphic Units

The regional geology of the province of Groningen was studied mainly using DINOloket, which provides access to the largest databank of records (descriptions) from CPT's and boreholes performed at shallow depth (less than 500 m deep) all over the Netherlands. This databank comprises borehole data, groundwater data, cone penetration test data, vertical electrical soundings, the results of geological, chemical and mechanical sample analyses, borehole log, and seismic data (TNO, 2016).
The principal geological formations individuated in the northern part of the Netherlands are:

- ***Naaldwijk Formation***
  The formation of Naaldwijk, dating back to the Holocene sea level rise, comprises soils formed in marine, lagoon, and beach environments. The lithology comprehends a strong variation from fine to coarse sands, silts, and clays. It is quite common to find very fine to medium sands (105 – 210 micron) and slightly to highly silty clays with frequent shell fragments and calcareous formations. The clay deposits are often laminated with thin sand layers and, at the same time, sands with clay laminae or pockets are frequently encountered. The layers' thickness is variable, i.e. from less than a meter to 75 m (i.e. in tidal channels).

- ***Nieuwkoop Formation***
  This formation consists mainly of peat and clay. The peat, formed during the Holocene sea level rise, can be slightly to highly clayey and it is generally poor in minerals (mainly dark brown in colour). It is common to find silty and sandy layers locally reach in carbonates. The thickness of the layers can oscillate from 0.1 to 0.8 m but it stays, most of the times, between 0.5 and 4 m.

- ***Boxtel Formation***
  The Boxtel formation, dating back to periglacial phases of the Saalian and Weichselian glacial eras, is composed primarily of Aeolian sands and local coarser fluvial sediments. The lithology is frequently composed of very fine to medium sand (105 – 300 micron), slightly to strongly silty, and loam (slightly to highly sandy). Isolated peat layers can be encountered as well. The thickness may change from less than a meter up to 30 m (i.e. in glacial basins).

- ***Peelo Formation***
  Among the dominant formations of the Groningen region, it is ordinary to find the Peelo formation,

generated during the Elsterin glaciation. The maximum extension of the ice sheet that reached the northern part of the Netherlands, led to the formation of deep subglacial valleys. These are characterised by slightly to highly silty lacustrine and glacial clays, and very fine to coarse sands transported by the ice movements. The clay is generally particularly dense (*OC Clay* or *Potklei*) and may contain sand and gravel. The valleys' thickness can go up to 400 m, whereas the layers' thickness varies between 10 to 30 m.

- ***Drente Formation***
  The Drente formation consists principally of clay soil deposits, generated during the Saalian glaciation. These soils, formed as a basal till, are nowadays called *boulder clay*. In most cases, the lithology consists of clays and loam that can be highly sandy and/or highly silty, and may contain gravel and rare boulders and blocks. The layers' thickness ranges from less than 1 m up to 10 m.

To summarise, the typical shallow subsurface of Groningen is composed of mainly clays and sands, along with peat and organic materials in the northern part of the region. Particular formations, such as *potklei* and *boulder loam*, are also quite common. The groundwater level is generally enough close to the surface (between -0.5 to -2 m), thus, it is regular practice to assume the soils completely saturated.

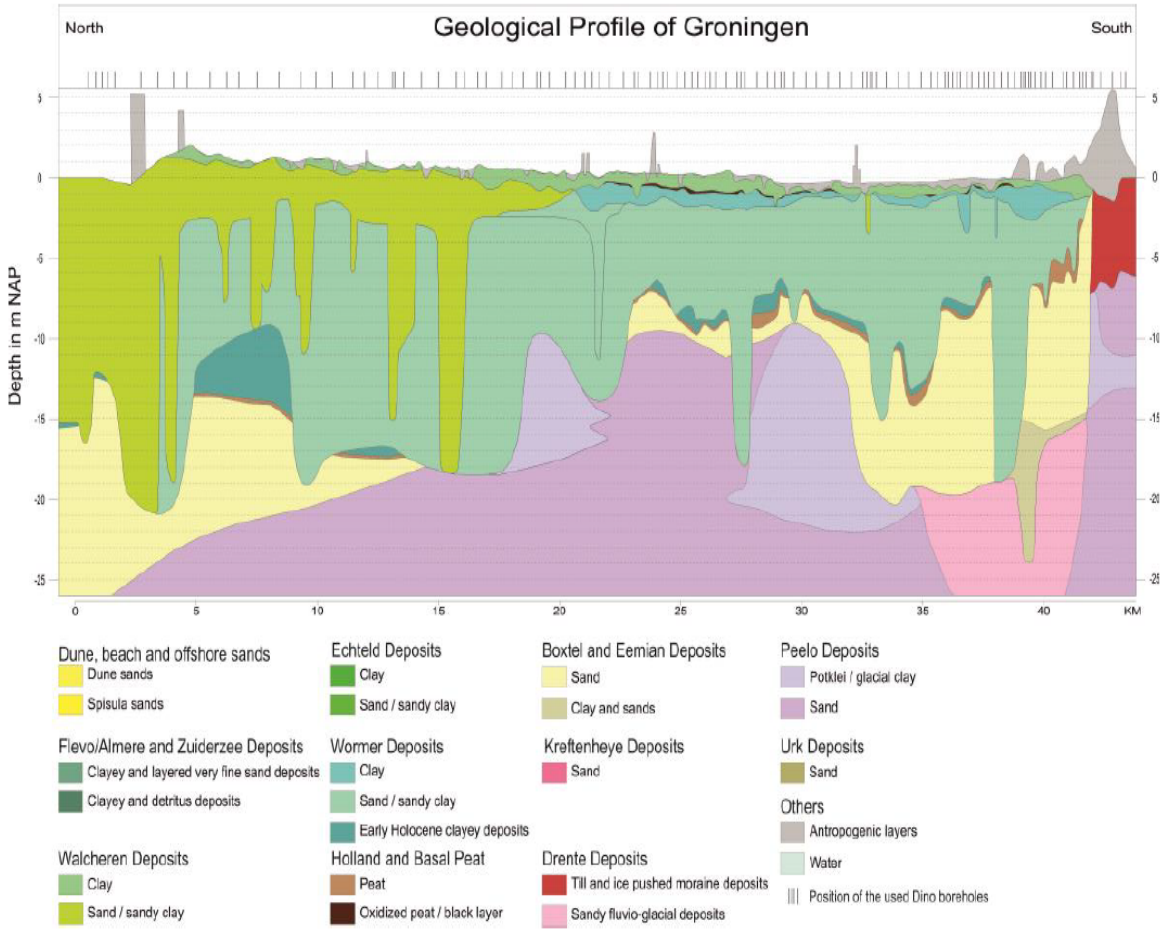

Figure 3.9: Geological cross-section from North to South showing the complex coexistence of Holocene and Pleistocene coastal deposits. Description of the formation type and origin is given in the legend (source: Kruiver et al., 2015).

3.8. Summary and Conclusions

In the present chapter it was presented the current state of knowledge from the seismic hazard in Groningen and the approaches used in practice to execute seismic ground response, applying CPT-based correlations to estimate soil properties.
The main points of discussion are:

- Earthquakes in Groningen are ascertained to be caused by gas withdrawal. The magnitude of those seismic events is relatively low compared to natural tectonic earthquakes. The maximum magnitude (M = 3.6 on the Richter scale) registered so far was the Huizinge earthquake in 2012. Nevertheless, the damage produced by these events led several Dutch companies to study such phenomena in order to develop specific models for risk analysis and mitigation.

- Probabilistic seismic Hazard Analysis in Groningen is, nowadays, executed with detailed risk models and specific Ground Motions Prediction Equations, realised exclusively for the Groningen region, able to estimate values of PGA, PGV, PSA, etc. The production of new PGA maps, for instance, constitutes one of the great accomplishments of the recent studies, and create the basis for more accurate dynamic calculations. Precisely, first the V2 GMPEs (developed by Bommer et al. in 2015b), and then the updated V4 GMPEs, included in the so called V4 Ground Motion Model (Bommer et al., 2017a), achieved the reduction of the maximum PGA from 0.36 g (as in 2015) to 0.24 g.

- Site Response Analysis presumes the determination of a set of input, which characterises the soil conditions at the specific site. When a detailed laboratory soil classification is not available, soil properties are estimated by means of CPT-based correlations. In Groningen, and specifically within the VIIA project, values of soil unit weight, over consolidation ratio, plasticity index, shear strength, etc. are computed employing existing correlations available in literature. Only the shear wave velocity is, up to date, determined with a site-specific correlation developed by Vasileiadis in 2015.

- In this context, a number of correlation equations, used for the prediction of plasticity index and undrained shear strength, are presented and discussed in more detail, as these soil properties are the focus of this research.

- Finally, the typical geology of the Groningen region is presented, giving an brief overview of the geological history and climatic conditions that have determined the characteristics of the soil deposits. The upper 200 meters of the entire region date back to the Plesistocene period, during which several glaciations occurred. In addition, due to the effect of sea level rises and river activity, the shallow subsurface of Groningen consists mainly of soft soils such as sand and clay of different composition and consolidation states, belonging to the Naaldwijk, Boxtel and Nieuwkoop Formations. Peat (from the Nieuwkoop Formation) is also a material frequently encountered in the region, in combination with Loam and boulder clay materials, belonging to the Drente Formation.

4

Sensitivity of PI, Su, and Vs effect on Site Response Analysis

4.1. Introduction

The present chapter reports a sensitivity analysis focused on the influence of the following soil properties on Site Response Analysis:

- Plasticity index
- Undrained shear strength
- Shear wave velocity

For the sensitivity analysis, individual parameters (e.g. PI, Su or Vs) are modified while keeping all other input constant. The effect on the results is then assessed.
In literature, there is already a vast knowledge on the effect of soil properties on the propagation of ground motions (e.g. Bazzurro and Cornell, 2004, Carlton, 2014, Darendeli, 2001, Senthamilkumar and Muthukkumaran, 2017, Stewart et al., 2014).
With the aim of gaining a more detailed insight into Groningen's typical soil materials, SRA simulations are carried out taking an existing soil column profile, namely the object XX in Delfzijl, as a reference.

4.2. Site Response Analysis Procedure

The non-linear time-domain model (version DS-NL4) is used in DEEPSOIL for the SRA. The main features needed to build the DS-NL4 model are:

- Non-linear analysis
- Generalised Quadratic/Hyperbolic (GQ/H) model
- Non-Masing behaviour
- Input ground motion

4.2.1. Non-linear Analysis

For a non-linear analysis (explained more in detail in Section 2.4.3, Chapter 2), DEEPSOIL solves the equation of motion in time-domain according to the Newmark β method. This procedure allows the estimation of the response for single-degree-of-freedom systems and, thus, to compute the response spectra (Woodward and Griffiths, 1996).
The Newmark β method suggests to use numerical integration to solve differential equations. For instance, the nodal relative velocity can be expressed as:

$$\dot{u}_{i+1} = \dot{u}_i + \Delta t \ddot{u}_\gamma \tag{4.1}$$

where the nodal relative acceleration is:

$$\ddot{u}_\gamma = (1-\gamma)\,\ddot{u}_i + \gamma\,\ddot{u}_{i+1} \quad 0 \le \gamma \le 1 \tag{4.2}$$

hence

$$\dot{u}_{i+1} = \dot{u}_i + (1-\gamma)\Delta t\,\ddot{u}_i + \gamma\Delta t\,\ddot{u}_{i+1} \tag{4.3}$$

While the nodal relative displacement can be expressed as:

$$u_{i+1} = u_i + (\Delta t)\,\dot{u}_i + [(0.5-\beta)(\Delta t)^2]\,\ddot{u}_i + [\beta(\Delta t)^2]\,\ddot{u}_{i+1} \tag{4.4}$$

in which the parameters β and γ determine the assumption that the acceleration varies over a time step (Δt), and evaluate the stability and accuracy of the integration process. These are usually assumed as: $\beta = 0.5$ and $\gamma = 0.25$, in order to insure no numerical damping and an unconditionally stable integration for every Δt (Hashash et al., 2016).

4.2.2. Generalised Quadratic/Hyperbolic (GQ/H) Model

In order to capture the small-strain and large-strain behaviour of soils, it is necessary to know the initial shear stiffness and the shear strength at failure, which represent the boundaries of stress-strain behaviour in stress-strain space. To produce a continuous curve in which the two lines join together (given that these two linear boundaries, namely G_{max} and τ_{max}, are known to intersect at a certain shear strain), it is convenient to use a quadratic equation, that can be simplified to a general hyperbolic equation.
Hyperbolic models were introduced in the past to couple the monotonic stress-strain curve with the unloading-reloading behaviour of soft soils (e.g. Duncan and Chang, 1970, Al-Shayea, 2002, in Brinkgreve, 2015). Such models allow the estimation of the non-linear cyclic response of soils under dynamic loading and the definition of the initial stress-strain curve, as well as the unloading-reloading behaviour and the generation of pore water pressure. These curves were then corrected with respect to reference curves of normalised shear modulus and damping values as a function of the shear strain. However, such strength correction procedure, implemented manually, increased the possibility of employing unrealistic shear strength values, resulting in a time-consuming procedure. The Generalised Quadratic/Hyperbolic model (GQ/H) was developed by Groholski and Hashash (2015) for the optimisation of the large-strain strength correction procedure, defining the shear strength at failure while maintaining the characteristics of typical of a small-strain soil behaviour. The backbone curve in this model is in the form of a general quadratic-hyperbolic model (Groholski and Hashash, 2015), thus GQ/H.

4.2.3. Non-Masing Rules

With the goal of establishing the model parameters which best represent the actual soil properties, the DS-NL4 model in DEEPSOIL uses the non-Masing rule, so-called MRDF pressure-dependent hyperbolic model (after Phillips and Hashash, 2009, in Hashash et al., 2016). This approach introduces the use of a reduction factor into the hyperbolic model (function of the max strain, γ_{max}), overcoming, according to Stewart et al. (2014), a well know problem encountered with Masing rule (i.e. underestimation of damping at small strain levels, approaching zero, and damping values too large at moderate and large strains, which can lead to under-predict both the strain level and, potentially, the intensity of motion at the surface).
The non-Masing rule is able to achieve the best fit for the modulus reduction curve, however, it may create a potential mismatch of the damping curve (Darendeli, 2001) (more details about the extended Masing rule can be found in section 2.4.3 of chapter 2).

4.2.4. Input Ground Motions

Site response analysis in DEEPSOIL requires acceleration time histories to be uploaded through the selected soil column. Figure 4.1 presents a number of plots that depict the ground motion used in the analysis. On the left-hand side of the figure, from top to bottom, are plotted versus time (expressed in seconds): peak ground acceleration, peak ground velocity, peak ground displacement, and Arias intensity time histories, where the Arias intensity is the square of the acceleration integrated over the duration of the motion, and PGA, PGV, and peak ground displacement are explained in Appendix A (Section A.4.1). In the same picture (Figure 4.1), on the right-hand side, it is displayed the damped spectral acceleration versus the period in logarithmic scale (top-right), and the Fourier amplitude plotted against the frequency, also in logarithmic

scale (bottom-right). The former indicates the 5% damped spectral acceleration for the used accelerogram, whilst the latter depicts the frequency content of the ground motion, showing the distribution of its amplitude across different frequency levels (Hashash et al., 2016).

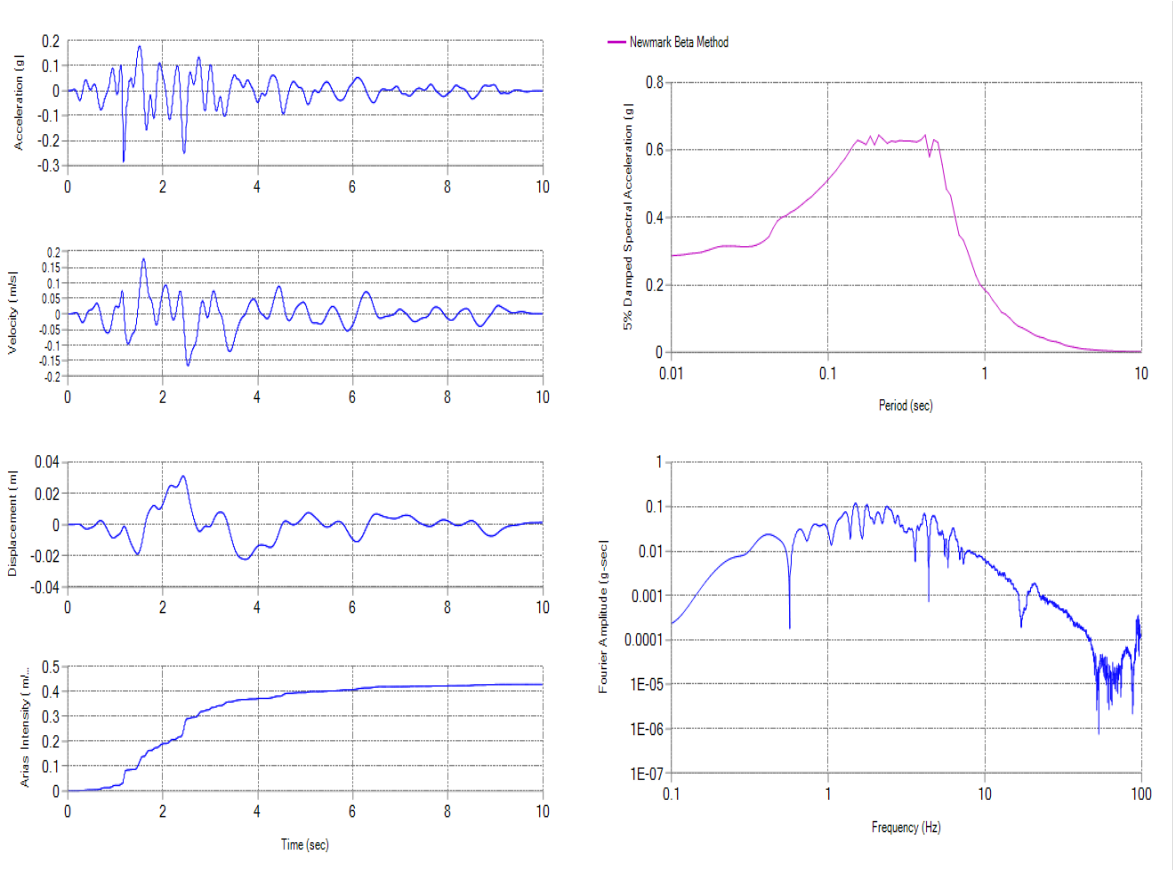

Figure 4.1: Ground motion overview. Left-hand side from top to bottom: acceleration, velocity, displacement and Arias intensity time histories. Right-hand side from top to bottom: 5% damped spectral acceleration versus period and Fourier amplitude (source: Hashash et al., 2016.

4.3. Sensitivity Analysis

For Groningen, input ground motions consist of a minimum of 7 or preferably 11 generated triaxial time histories, 11 in each direction, provided by NEN. In this study, a total of 14 time histories are used in the analysis (7 in the x-direction and 7 in the y-direction).

The considered acceleration time histories are scaled to the PGA_{ref}-contour line equal to -0.29 g, obtained from the NPR 9998 (2017) for the Delfzijl area. According to Stewart et al. (2014), the scaling procedure consists of a simple multiplication of the time series by a constant (time-invariant) factor, which will increase its PSA by the same amount.

The mean profiles of PGA, maximum shear strain (MSS), and spectral acceleration (PSA) are computed for each simulation (e.g. Figures 4.2a, 4.2b, and 4.2c), using a PYTHON script (written comm. S. Tan, Royal Haskoning DHV, 2017).

The entire sensitivity analysis (i.e. creation of best estimate, upper and lower boundaries, and comparison of properties influence) is performed based on the calculated means (e.g. Figures 4.2a, 4.2b, and 4.2c, respectively), in agreement with the procedure recommended by Stewart et al. (2014).

Figure 4.3a depicts the cone tip resistance (continuous lines) and friction ratio (dashed lines) profiles for the object XX in Delfzijl, as a result of three CPTs used in input (presented in the figure with three different colours: red, green, and blue, respectively). On the other hand, the thick red line represents the mean value of q_c for each individuated layer (10 in total). The top and the bottom level of the soil layers are represented

Figure 4.2: Illustrative example of PGA, maximum shear strain, and response spectra profiles. The solid red line indicates the mean value, obtained from the 14 records (in grey). The dashed black lines represent the mean ± the standard deviation, respectively.

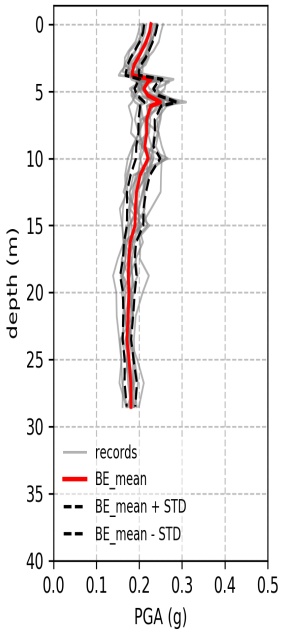

(a) PGA profiles (expressed in g) versus depth (in m NAP).

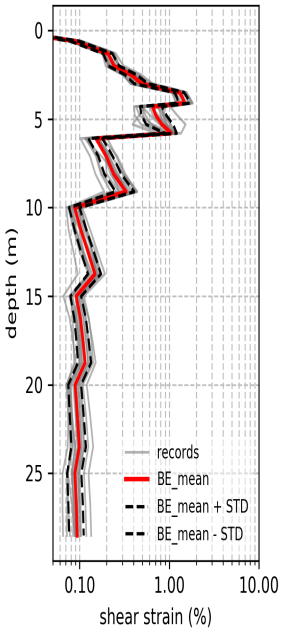

(b) Maximum Strain profiles in logarithmic scale (expressed in %) versus depth (in m NAP).

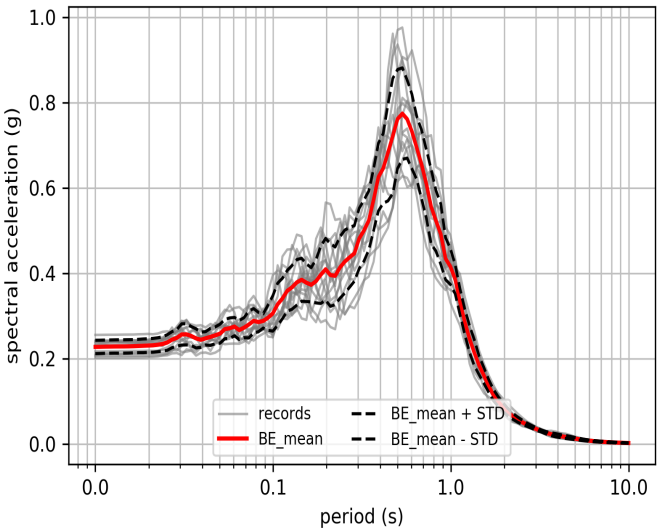

(c) Spectral Acceleration profiles (PSA in g) versus period in logarithmic scale (expressed in seconds).

in figure 4.3a by the thick horizontal black lines.
Following, this soil column is implemented in DEEPSOIL, as shown in figure 4.3b. Each layer is divided in a number of thinner layers, in order to ensure the maximum frequency (expressed in Hertz, Hz) to be at least 30 Hz. Next, soil properties, obtained using CPT-based correlations are assigned to every layer.
In table 4.1 a description of the soil type, the layer thickness, and mean values of PI, Su, and Vs for the 10 individuated layers is given. Following, table 4.2 contains a summary of input parameters used for each individual analysis for the uppermost layer (klei matig). In red are represented the altered parameters, and in black all the parameters used in the "best estimate" simulation. Note that when altering one parameter (e.g. PI, Su or Vs) the damping ratio values changes accordingly, together with a number of coefficients (i.e. Theta 1 to 5, A and P1, which are not shown in this table) needed for the fitting procedure in DEEPSOIL.
In a first moment, soil properties were being modified only in the uppermost layer of the soil profile. This affected, only to a small extent, the PGA at the surface and the maximum strain in the first 5m of soil. Successively, it was decided to apply the same (mean) variation scheme to the entire soil column (e.g. red values in table 4.2). In this way, for each simulation, the influence of one single changing soil property, modified consistently for the 10 layers, on the SRA outcomes is assessed. The results illustrated in the following sections refer to the latter procedure, according to which one parameter is modified for the entire soil column while the others are kept at their baseline values.

Table 4.1: Best estimate parameters set for the entire 430V soil column. Values of PI, Su, and Vs are the mean values obtained from CPTs post-processing

Soil column description					
Layer #	**Soil type**	**Thickness** [m]	**PI** [%]	**Su** [kPa]	**Vs** [m/s]
1	Clay, silty, soft	1.99	20	18	84
2	Clay, organic, soft	1.50	28	19	86
3	Peat, slightly preloaded	0.80	29	22	42
4	Clay, silty, soft	1.50	22	20	95
5	Peat, moderately preloaded	0.30	25	30	49
6	OC Clay	3.90	21	39	131
7	OC Clay	5.00	22	92	169
8	OC Clay	5.00	25	147	193
9	OC Clay	5.00	25	185	213
10	OC Clay	5.00	25	201	224

Figure 4.3: Soil profile for the object XX in Delfzijl implemented in DEEPSOIL.

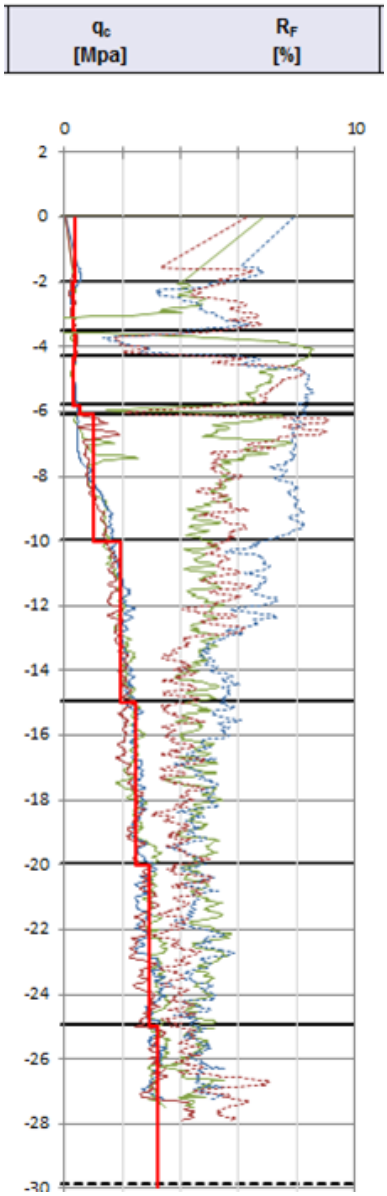

(a) Soil profile for the object XX in Delfzijl using 3 CPTs in input. The continuous red, green, and blue lines on the left-hand side of the plot represent the cone tip resistance (MPa) profiles of the different CPTs; the dashed red, green, and blue lines on the right-hand side represent the friction ratio (%) profiles of the different CPTs; the thick red line represents the mean q_c value (MPa) calculated for each layer.

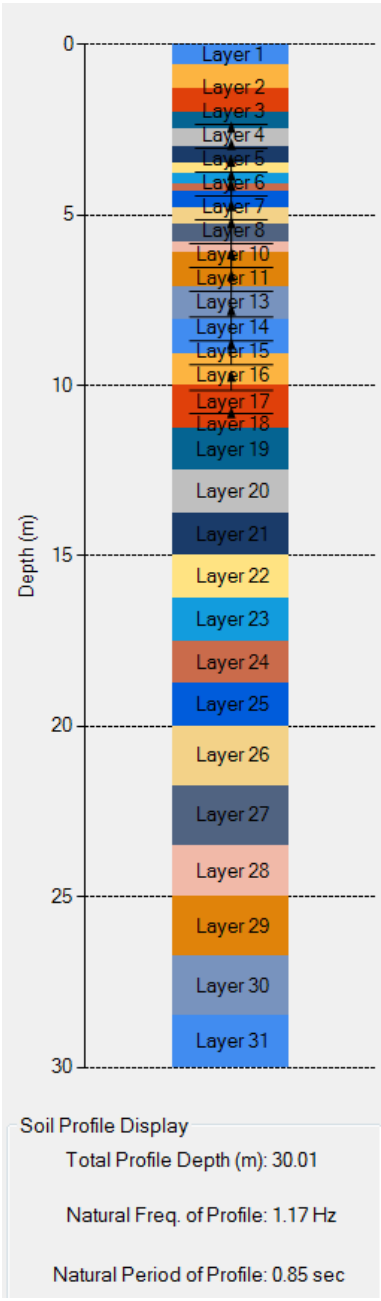

(b) Schematic representation of the soil column for the object XX in Delfzijl implemented in DEEPSOIL.

Table 4.2: First layer's parameters set for each sensitivity analysis (red indicates the altered parameters for each analysis)

Sensitivity Analysis	PI [%]	Su [kPa]	Vs [m/s]	Layer thickness [m]	Unit Weight [kN/m3̂]	Damping ratio [%]	σ'_v [kPa]	OCR [-]	k_o [-]
1) LB1 of PI	$\mu - \sigma_{PI;C\&O}$	18	84	1.99	15.1	2.389011	1.6	4.09	0.9583
2) UB1 of PI	$\mu + \sigma_{PI;C\&O}$	18	84	1.99	15.1	2.389011	1.6	4.09	0.9583
3) LB2 of PI	$\mu - 2\sigma_{PI;C\&O}$	18	84	1.99	15.1	2.389011	1.6	4.09	0.9583
4) UB2 of PI	$\mu + 2\sigma_{PI;C\&O}$	18	84	1.99	15.1	2.389011	1.6	4.09	0.9583
5) LB1 of Su	20	0.8μ	84	1.99	15.1	2.389011	1.6	4.09	0.9583
6) UB1 of Su	20	1.2μ	84	1.99	15.1	2.389011	1.6	4.09	0.9583
7) LB2 of Su	20	0.7μ	84	1.99	15.1	2.389011	1.6	4.09	0.9583
8) UB2 of Su	20	1.3μ	84	1.99	15.1	2.389011	1.6	4.09	0.9583
9) LB3 of Su	20	0.3μ	84	1.99	15.1	2.389011	1.6	4.09	0.9583
10) UB3 of Su	20	1.7μ	84	1.99	15.1	2.389011	1.6	4.09	0.9583
11) LB of Vs	20	18	0.8μ	1.99	15.1	2.389011	1.6	4.09	0.9583
12) UB of Vs	20	18	1.2μ	1.99	15.1	2.389011	1.6	4.09	0.9583

4.4. Sensitivity from PI on SRA

Figures 4.4a, 4.4b and 4.4c are the outcomes for the sensitivity of peak ground acceleration (g), maximum strain (%), and spectral acceleration (g) to change in the mean of PI. For each figure, the light blue line indicates the results for the initial set of means (best estimate, BE), the red and orange lines depict results of the two upper boundaries, UB1 and UB2 ($\mu+\sigma_{PI;C\&O}$ and $\mu+2\sigma_{PI;C\&O}$, respectively), while the green and purple lines show results of the two lower boundaries, LB1 and LB2 ($\mu-\sigma_{PI;C\&O}$ and $\mu-2\sigma_{PI;C\&O}$, respectively). The y-axes in the first two plots show the depth (expressed in meters NAP), while the x-axes the PGA and maximum shear strain, respectively. Whereas in the third plot the y-axis represents the spectral acceleration (PSA), and the x-axis the time period (s).

As expected, an increase in soil plasticity is positively correlated with PGA, confirming that soils with low plasticity generally tend to amplify the earthquake motions (Vucetic and Dobry, 1991).

Examining figure 4.4a, in particular at a depth between -4 and -10 m NAP, the PGA appears to be slightly more sensitive to a decrease of PI mean values rather than to their increase (e.g at -9 m NAP the PGA for the LB2 is around 0.19 g and for the UB2 it is around 0.23 g, while the best estimate PGA is about 0.215 g). However, from approximately -17.5 m NAP downward, all the profiles result to be almost equal to the BE, except for the LB2 which deviates slightly at a depth of around -22 m NAP. As well as toward surface, PGA results to be more sensitive to a decrease of PI rather than its increase.

A change in PI affects, on a smaller degree, the surface spectral acceleration as well. The lower is the soil plasticity the lower becomes the spectral acceleration measured at the surface. This is visible in figure 4.4c, especially on the medium and short period parts of the response spectrum (e.g. from 0.1 to 0.3 seconds). For instance, the peak visible in the BE profile at 0.15 s (around 0.4 g) seems to almost disappear when the soil column is modelled with low plasticity (LB2). Similarly, the maximum PSA, measured between 0.4 and 0.5 s, is visibly reduced in the LB2 profile.

Furthermore, an increase in soil plasticity induces a gradual, slight decrease in maximum shear strain (e.g. in the area between -6.5 and -10 m NAP) in the soil with high stiffness and low plasticity (Potklei), whilst it induce the opposite effect on the softest, highly plastic layer (Peat) between -3.5 and -4.5 m NAP.

Overall, the maximum strain (Figure 4.4b) seems to be less sensitive to changes in the mean of PI. Therefore, the shear strain sensitivity to PI changes is less important than the effect of PI reduction on PGA and SA.

Figure 4.4: Sensitivity of SRA results to change in PI mean for the entire soil column.

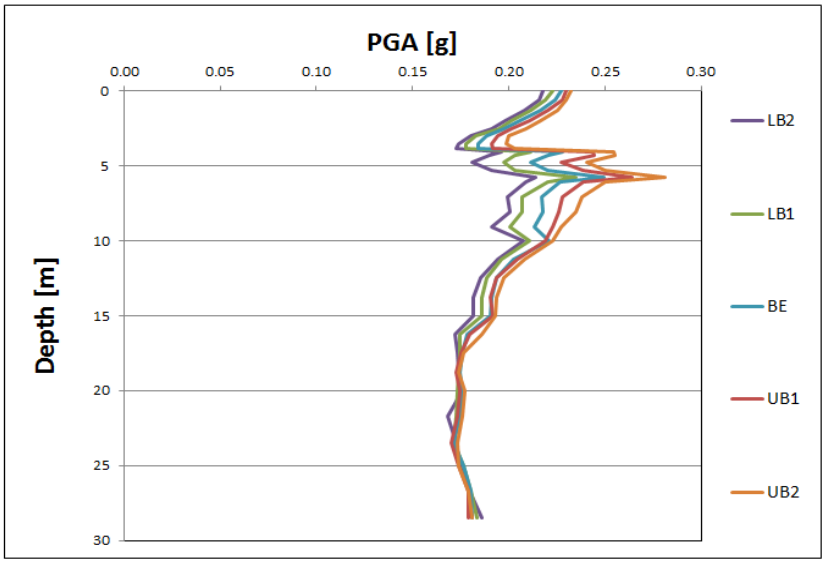

(a) PGA profiles

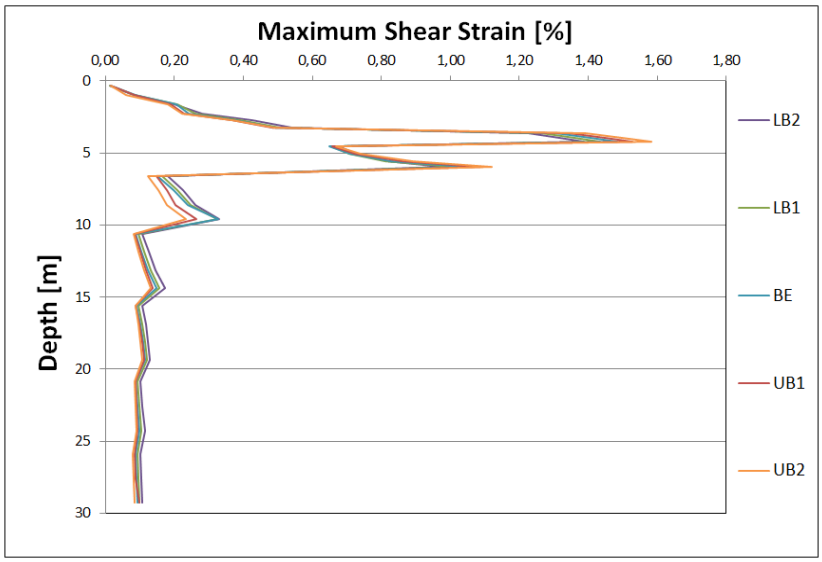

(b) Maximum Strain profiles

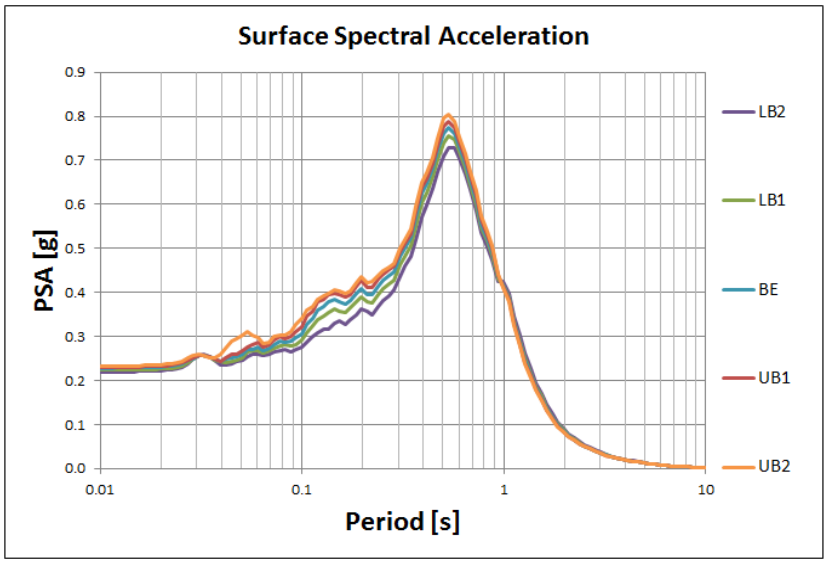

(c) Spectral Acceleration profiles

4.5. Sensitivity from Su on SRA

Figures 4.5a, 4.5b and 4.5c are the outcomes for the sensitivity of peak ground acceleration (g), maximum strain (%), and spectral acceleration (g) to change in the mean undrained shear strength. In this case the analysis is performed six times: three simulations consider Su values lower than the reference set of means, and three simulations account for an increase of Su mean.

For each figure, the light blue line indicates the results for the initial set of means (best estimate, BE); the red, orange, and pink lines depict the results of three upper boundaries: UB1, UB2, and UB3 ($\mu + 20\%$, $\mu + 30\%$, and $\mu + 70\%$, respectively); while the green, purple, and dark blue lines show the three lower boundaries: LB1, LB2, and LB3 ($\mu - 20\%$, $\mu - 30\%$, and $\mu - 70\%$, respectively).

Figure 4.5a, shows that the PGA at the surface increases gradually with increasing Su values. It is interesting to see that at very low values of Su (e.g. LB3) the PGA at the surface results to be significantly lower than both the BE_PGA (precisely, LB3_PGA = 0.13 g, and BE_PGA = 0.23 g), as well as than the LB2_PGA (LB2_PGA = 0.185 g), confirming that SRA results are very sensitive to extremely low values of Su (i.e. Su_LB3 of the uppermost layer is equal to 5.4 kPa). Such low shear strength values induce the soil to behave as very soft soil, absorbing a consistent part of the motions (as can be seen in figure 4.5b, those extremely high strain peaks indicate that some soil layers are failing).

Within deeper layers (i.e. from -10 to -25 m NAP) the LB3_PGA is predicted to be higher than the best estimate PGA, yielding values even higher than the upper boundaries profiles (being, for example, at -20 m NAP LB3_PGA around 0.219 g and BE_PGA, LB2_PGA, LB1_PGA, UB3_PGA, UB2_PGA, and UB1_PGA around 0.17 g). In the LB3 SRA, the deep layers, consisting mainly of Potklei, are modelled with an extremely low strength (i.e. at -20 m NAP Su is equal to 44 kPa), although they should be characterised by relatively high values of Su, due to the high vertical soil pressure and the nature of the material. Such low shear strengths (typical of extremely soft or even softened soils) induce the soil to absorb a considerable part of the motions, limiting, thus, the propagation of shear waves to surface. This phenomenon may explain the low PGA value at the surface for the LB3 profile.

Contrarily, examining the LB2, LB1 and the upper boundaries profiles, the observed general trend is that the higher is the Su the higher becomes the PGA at the surface, as expected.

Using shear strength values 70 % higher than the means, as for the UB3 profile, the PGA at the surface is predicted to be well above the BE (precisely, UB3_PGA = 0.30 g, and BE_PGA = 0.23 g), meaning that also an increase of Su can create large effects on the peak ground acceleration development in soft soils.

Furthermore, also the surface response spectrum appears to be positively correlated to the Su. The spectral acceleration increases accordingly with Su (Figure 4.5c), while its maximum peak moves gradually leftward. Overall, the response spectrum results to be more sensitive to a large reduction of shear strength (LB3) than its increase (UB3), both on short and medium periods. Precisely, the difference between the peaks of the best estimate and the most extreme lower and upper boundaries profiles is about 50 and 15 %, respectively, being the best estimate PSA peak about 0.8 g, while the LB3 is less than 0.4 g, and the UB3 is around 1.0 g.

On the other hand, figure 4.5b, illustrates a negative correlation between Su and maximum shear strain. Indeed, the higher is the Su the smaller are the generated maximum strains. The sensitivity of MSS to the reduction of Su is particularly evident in the softer layers (e.g. Peat), confirming the expectation that the softer is the material the larger is the strain development.

Figure 4.5: Sensitivity of SRA results to change in Su mean for the entire soil column.

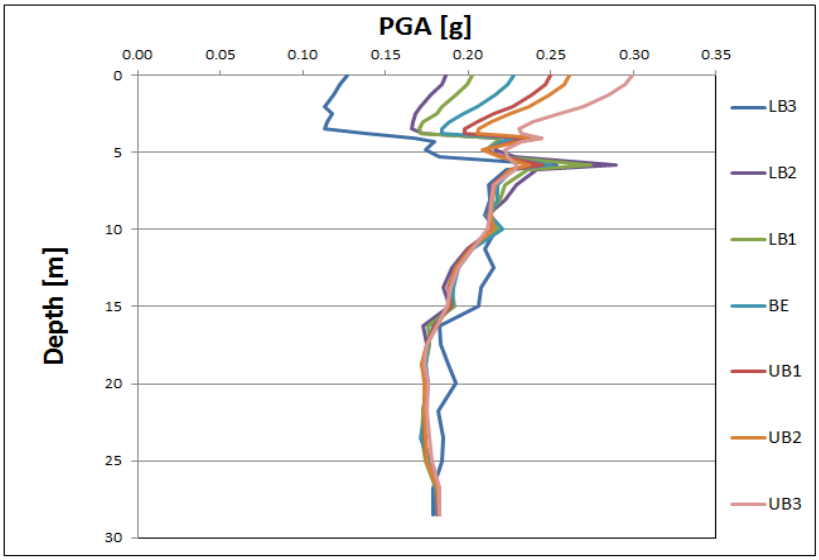

(a) PGA profiles

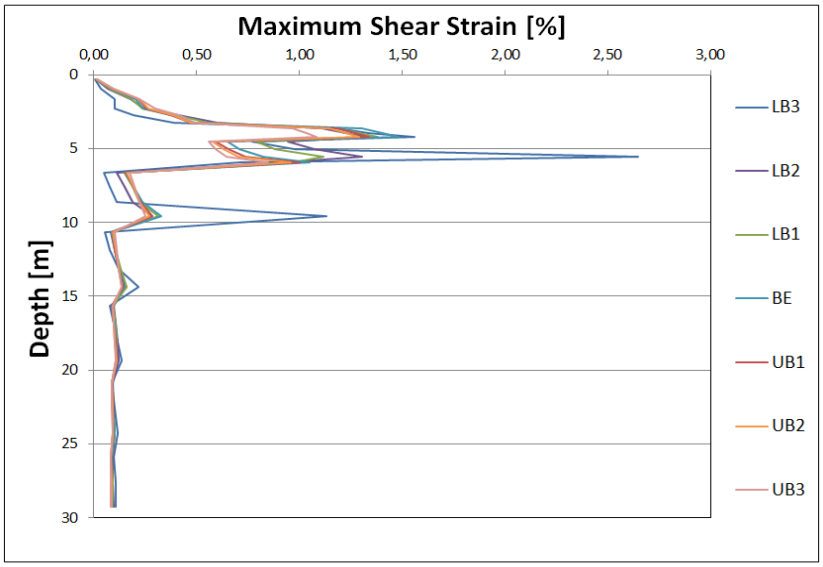

(b) Maximum Strain profiles

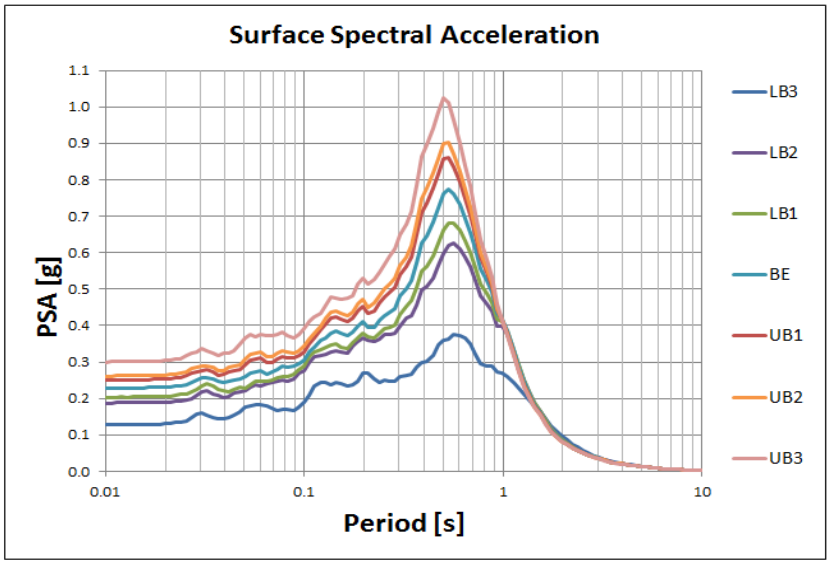

(c) Spectral Acceleration profiles

4.6. Sensitivity from Vs on SRA

Figures 4.6a, 4.6b and 4.6c depict the influence of varying shear velocity mean values on the SRA outcomes. The profiles in those figures indicate: the light blue line the initial set of mean values (best estimate, BE), the red line the upper boundary, calculated as $\mu + 20\%$, and the green line the lower boundary of the mean, fixed at $\mu - 20\%$.

The choice of performing only two analyses (i.e. LB and UB) derives from the recommendations given by Robertson (2009) (in Vasileiadis, 2015). Robertson observed that in the majority of the cases examined, using a region-specific correlation, the interpreted Vs profiles lie reasonably close to the SCPT interpreted Vs, with an error smaller than ±20%.

From the examination of figure 4.6a, it can be observed that the influence of changes in Vs mean on PGA is relatively significant. The peak ground acceleration is positively correlated to the shear wave velocity, meaning that when Vs decreases also PGA decreases gradually, and vice versa, consistently with the results presented in other studies (e.g. Junfeng, C. and Weidong, F. and Fanyue, M. and Shuanglin, D., 2014). This reponse, however, can be observed from surface until a certain depth (approximately -19 m NAP), below which an opposite trend takes place. In the latter case, although the Vs is reduced of -20 %, leading to the accumulation of more strain, more damping and less amplification, the PGA of deeper soil layers decreases when the shear wave velocity increases. This indicates that the effect of the natural large stiffness of the deepest layers (Potklei) is dominant and, thus, motions are amplified, in agreement with Carlton (2014) and Rathje et al. (2010).

The effect of the increase of Vs is larger than its decrease on the surface peak ground acceleration (i.e. Vs_LB = 0.22 g and Vs_UB = 0.23 g, while Vs_BE = 0.226 g). However, from -6 m NAP downwards, the influence of decreasing Vs values appears to be significantly larger than Vs accretion, being the green line consistently more distant than the red line from the BE profile.

The same positive correlation can be observed in the spectral acceleration plot (Figure 4.6c). Nevertheless, the sensitivity of PSA to small Vs values is less evident. In fact, comparing the distance of the red line (UB) and the green line (LB) with respect to the BE profile, both the UB and LB lines appear to be comparably close to light blue profile. In particular, on the short and medium period of the response spectrum is where the most significant effects of Vs variation occur (e.g. between periods of 0.01 and 0.2 s, and 0.9 and 3 s, UB, LB, and BE spectral acceleration profile have clearly different shapes, while they become more similar between 0.5 and 0.9 s).

Likewise, the maximum strain generated with 20% higher Vs is relatively similar to the best estimate profile from -10 m NAP downwards and lower at shallower depths. Oppositely, with 20 % lower Vs values the difference between LB and BE profiles is comparably larger over the entire profile, confirming the fact that SRA outcomes are more sensitive to a shear wave velocity decrease than its increase.

Generally, an increase in shear velocity, which means an increase in soil stiffness, induce the shear strain for a given ground motion to decrease, together with the damping ratio. However, a decrease in damping ratio induces less energy to be released, which can cause an increase in shear strain (as it can be seen in figure 4.6b from approximately -4 to -7 m NAP). This trend is consistent with Carlton (2014) studies.

Figure 4.6: Sensitivity of SRA results to change in Vs mean for the entire soil column.

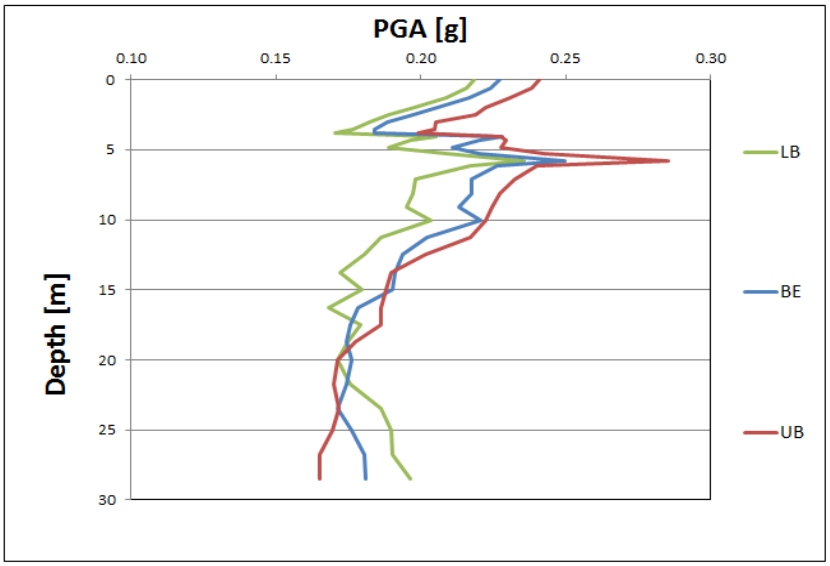

(a) PGA profiles

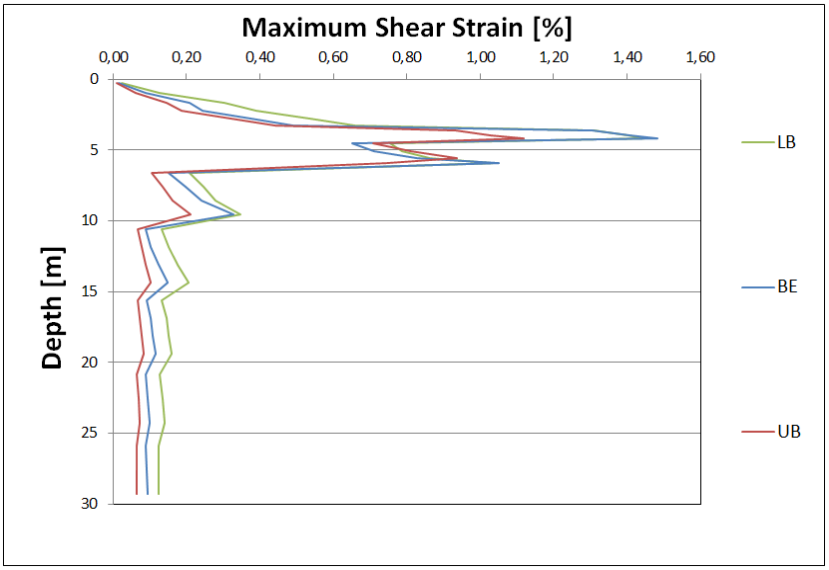

(b) Maximum Strain profiles

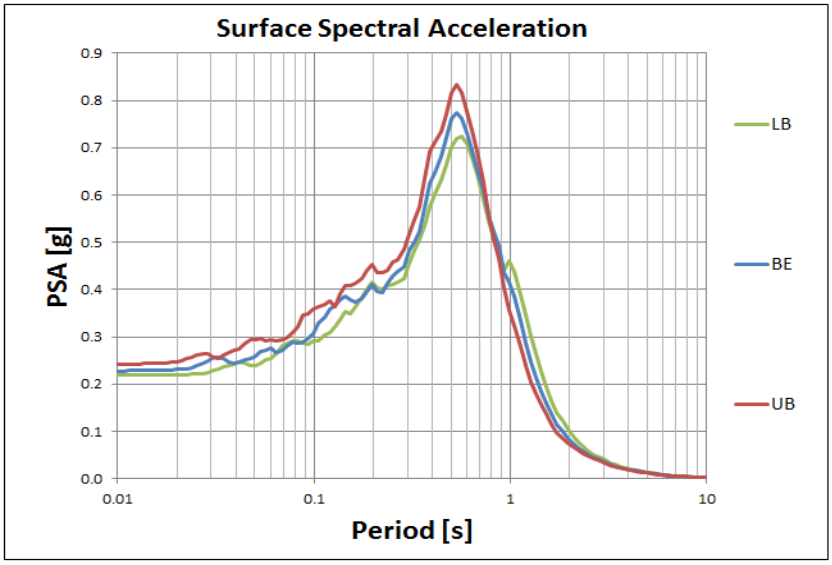

(c) Spectral Acceleration profiles

4.7. Multi-variate Sensitivity from PI, Su, and Vs on SRA

In order to establish which one is the soil property that influences the most the SRA outcomes, figures 4.7a, 4.7b, 4.8a, 4.8b, 4.9a, and 4.9b illustrate a comparison of the peak ground acceleration, maximum shear strength, and spectral acceleration profiles of PI, Su, and Vs, obtained from the three different sensitivity analyses, performed for both lower and upper boundaries, with respect to the best estimate profile (described in section 4.4 to 4.6. Precisely, for the PI and Su, only the PI_LB1, PI_UB1, Su_LB1, and Su_UB1 are considered in the comparison.

4.7.1. PGA

From the comparison of lower boundaries and best estimate PGA profiles (Figure 4.7a) it can be said that, overall, shear wave velocity has a larger influence on PGA. However, toward the surface, the predominant parameter is clearly the undrained shear strength. At 0 m NAP, in fact, the BE PGA is around 0.23 g, the Su_LB PGA results to be around 0.20 g, whilst Vs_LB and PI_LB are around 0.22 g.
The Vs effect is particularly significant at a certain depth (from approximately -5 m downwards). Especially below -20 m NAP, the PGA measured is notably higher than the best estimate profile, reaching a peak of about 0.20 g at -28 m NAP, whilst the BE, the Su_LB, and PI_LB values at that depth are about 0.18 g. Contrarily, at shallower depths, low values of shear wave velocity produce low values of peak ground acceleration, consistently with Carlton (2014) (see Chapter 3, Section 2.5.4). For instance, at a depth of -7.5 m NAP the Vs_LB PGA results to be less than 0.20 g, while the best estimate PGA is around 0.22 g (similar to the Su_LB), and the PI_LB is around 0.21 g.
The large influence of shear wave velocity on peak ground acceleration is also visible from the comparison of upper boundaries and best estimate PGA profiles, shown in figure 4.7b. The Vs_UB profile, indeed, is the one that diverges the most from the best estimate profile. Although, this trend does not occur at the surface (i.e. Vs_UB PGA is around 0.24 g, while BE is almost 0.23 g), where the Su results to be once again the dominant soil factor, it is clearly visible within deeper layers (e.g. at -8 m NAP, Vs_UB PGA is about 0.23 g and BE is 0.215 g). On the other hand, at larger depths, the undrained shear strength profile appears to barely deviate from the best estimate PGA profile in both upper and lower boundaries comparisons.
Conversely, it emerges that changes in PI have little or negligible effect on PGA. In figure 4.7b, the PI upper boundary profile appears to barely deviate from the best estimate PGA profile. The only visible effects occur between -6 and -10 m NAP for the UB comparison, and between -6 and -15 m NAP for the LB comparison. In general, PGA seems to be more sensitive to a reduction in PI mean than its increase. This can be seen in particular at the surface, where the PI_LB PGA is 0.23 g, while the BE PGA is slightly higher, namely 0.23 g, and between -6 and -15 m NAP, where the PI_LB PGA considerably lower than the best estimate PGA.

Figure 4.7: Sensitivity of Peak Ground Acceleration to change in PI, Su, and Vs mean (lower and upper boundaries) for the entire soil column

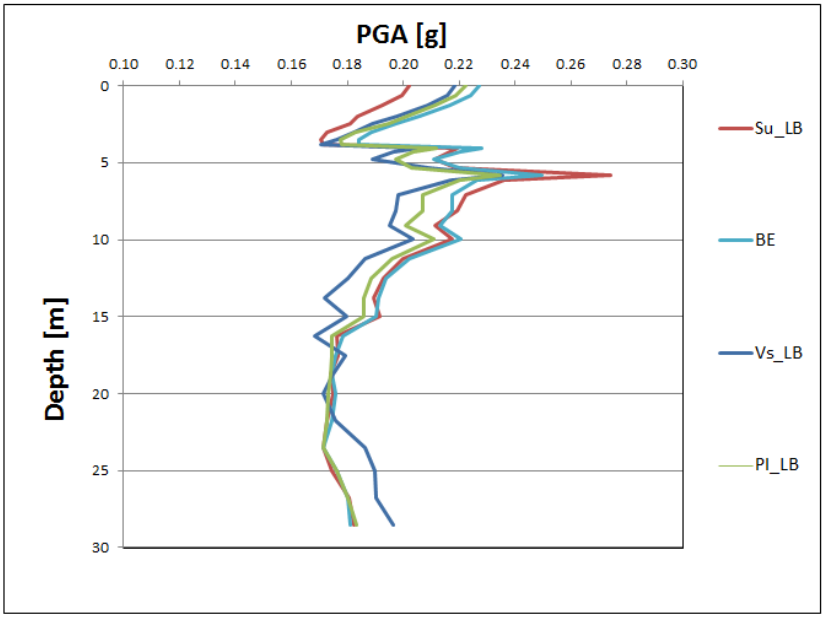

(a) In red, dark blue, and green are represented the lower boundaries for the three soil properties in analysis (namely, PI mean -9.83%, Su mean - 20%, Vs mean -20%), and in light blue is indicated the best estimate PGA profile

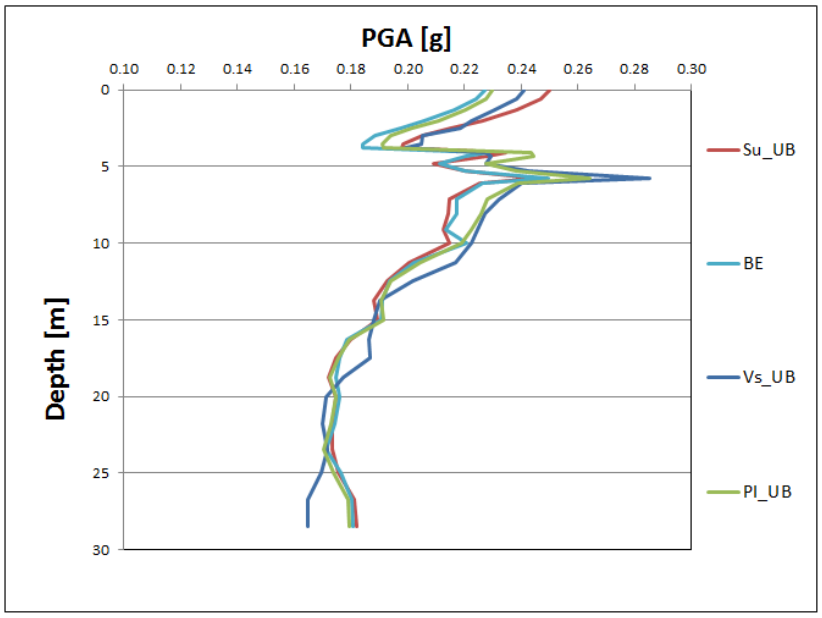

(b) In red, dark blue, and green are represented the upper boundaries for the three soil properties in analysis (namely, PI mean +9.83%, Su mean +20%, Vs mean +20%), and in light blue is indicated the best estimate PGA profile

4.7.2. Maximum Shear Strain

When examining figures 4.8a and 4.8b, the maximum shear strain results to be more sensitive to shear wave velocity (both decrease and increase) than undrained shear strength and plasticity index changes. This conclusion can be drawn looking at the divergence existing between the Vs_LB profile and the other profiles, which is particularly evident in the depth ranges from approximately -1.5 to -3.2 m NAP, and from -7 m NAP downwards (Figure 4.8a).
A reduction of undrained shear strength also affects, to a smaller extent, the generation of shear strains (e.g. between -4.5 and -7 m NAP, in figure 4.8a). However, it is observable that, in general, its influence is less important than the effect induced by shear wave velocity variations.
In contrast, a decrease in PI creates overall a negligible effect on the shear strain development (Figure 4.8a).
The same conclusions can be drawn when considering figure 4.8b. Also in this case, the maximum shear strain is more sensitive to an increase in Vs, then to Su, and finally to PI changes.

Figure 4.8: Sensitivity of Maximum Shear Strain results to change in PI, Su, and Vs mean (lower and upper boundaries) for the entire soil column

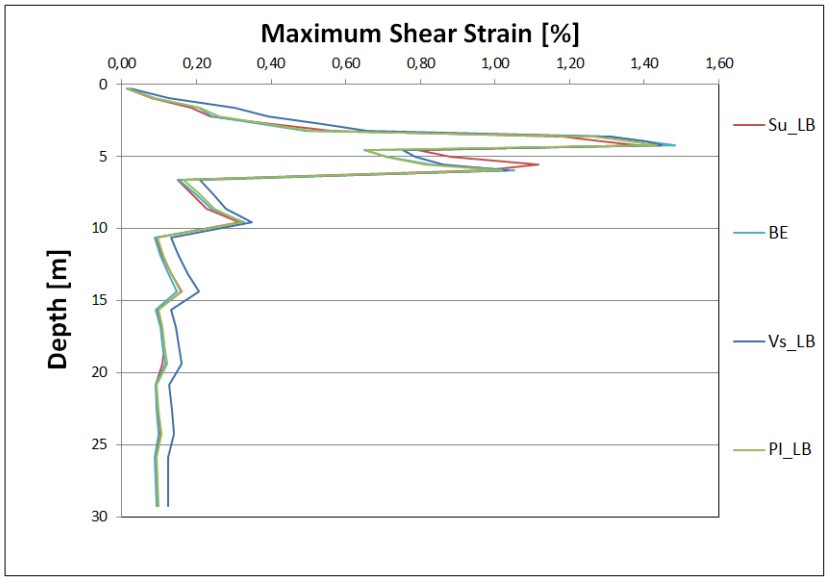

(a) In red, dark blue, and green are represented the lower boundaries for the three soil properties in analysis (namely, PI mean -9.83%, Su mean - 20%, Vs mean -20%), and in light blue is indicated the best estimate maximum shear strain profile

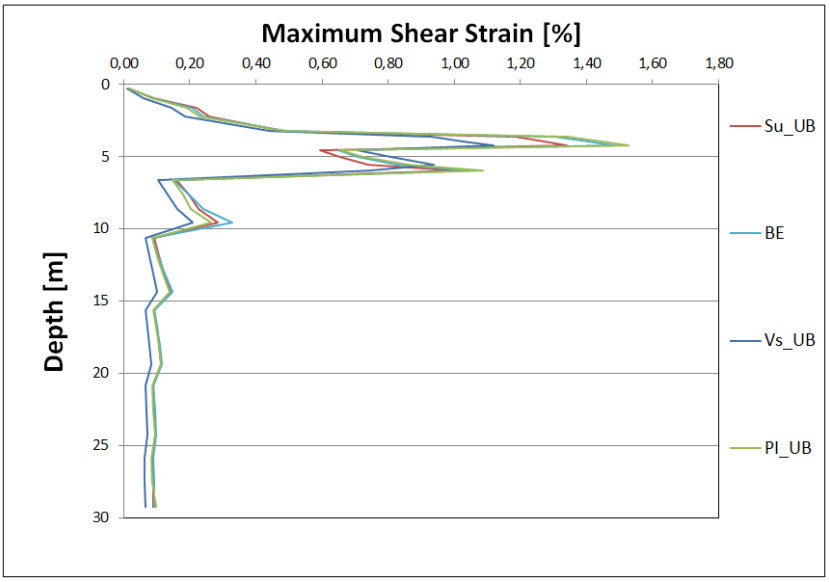

(b) In red, dark blue, and green are represented the upper boundaries for the three soil properties in analysis (namely, PI mean +9.83%, Su mean +20%, Vs mean +20%), and in light blue is indicated the best estimate maximum shear strain profile

4.7.3. Response Spectrum

Finally, the influence of soil properties alteration on the response spectrum is hereby presented. Figures 4.9a and 4.9b show that, particularly for the short and medium period of the response spectrum, the spectral acceleration is almost equally sensitive to changes in Vs, Su, and PI. From the LB comparison (Figure 4.9a), it appears that the Su profile is the one the diverges the most from the BE line, confirming that Su is the dominant property at the surface. In this graph, the large spectral peaks predicted by the BE profile (namely, 0.39 g between 0.1 and 0.2 seconds, and 0.53 to 0.62 g between 0.2 and 0.4 seconds) are almost absent in the other spectra, indicating that the motions, causing this estimated peaks, are almost completely absorbed by soils with low values of Vs and PI. A similar trend is visible when comparing the Su_LB spectra to the BE spectra. Softer (or less strong) soils, characterised by values of undrained shear strength 20% lower than the mean, usually lead motions to be absorbed more rapidly (consistently with (Stewart et al., 2014)).
In general, the surface spectral acceleration is slightly more sensitive to the decrease of these soil properties means than their decrease. In figure 4.9b, the divergence between best estimate and Vs, Su, and PI upper boundaries profiles is very small. Only at periods between 0.05 and 0.1, and 0.1 and 0.3 s, Vs, PI, and Su profiles diverge quite notably from the BE spectrum.

Figure 4.9: Sensitivity of Spectral Acceleration to change in PI, Su, and Vs mean (lower and upper boundaries) for the entire soil column

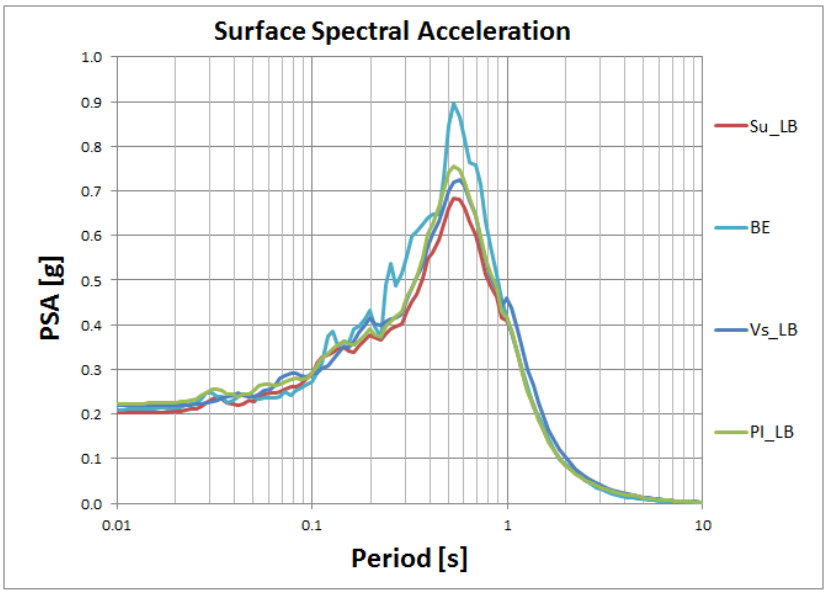

(a) In red, dark blue, and green are represented the lower boundaries for the three soil properties in analysis (namely, PI mean -9.83%, Su mean - 20%, Vs mean -20%), and in light blue is indicated the best estimate spectral acceleration profile

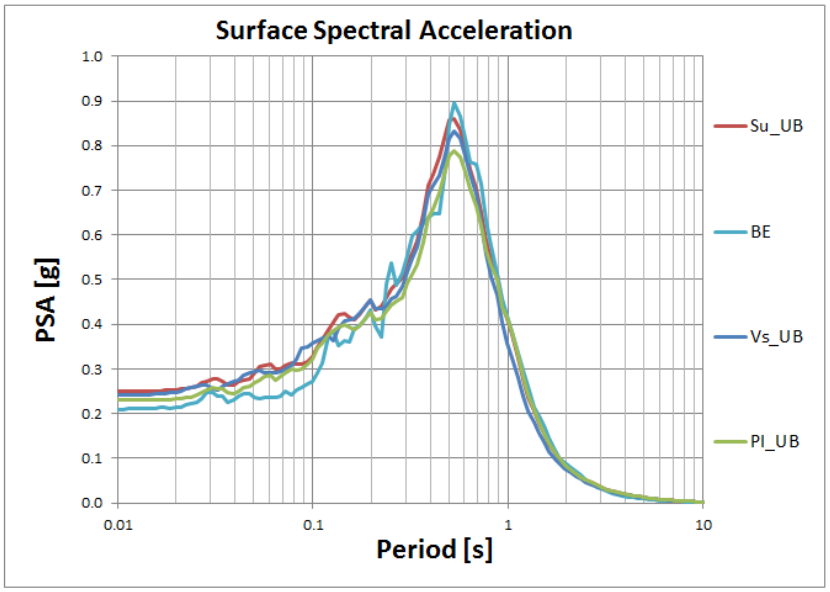

(b) In red, dark blue, and green are represented the upper boundaries for the three soil properties in analysis (namely, PI mean +9.83%, Su mean +20%, Vs mean +20%), and in light blue is indicated the best estimate spectral acceleration profile

4.8. Summary and Conclusions

A sensitivity analysis was performed to evaluate the influence of different soil properties (e.g. PI, Su and Vs) on the outcome of the Site Response Analysis performed in DEEPSOIL. The sensitivity on the ground response, measured in terms of peak ground acceleration, maximum shear strain, and spectral acceleration to changes in PI, Su, and Vs, was hence investigated.
The most important topics discussed are summarised as follows:

- The model used to carry out Site Response Analyses in DEEPSOIL was the DS-NL4, which performs non-linear analysis in time domain, following the Newmark β integration method. In this model, the shear strength control procedure is executed using the Generalised Quadratic/Hyperbolic (GQ/H) model, and the fitting process consists of non-Masing Unload-Reload Rules, which introduce a reduction factor for the best fit of the modulus reduction curve.

- The input signals used in the analyses consisted of 14 acceleration time histories scaled to a peak ground acceleration of -0.29 g. The results of the ground response from all the signals were then averaged out in order to perform subsequent comparisons using only the mean profiles.

- The soil profile (in Delfzijl) and the soil properties, implemented in DEEPSOIL, were obtained from CPT-based correlations on three CPTs. The soil stratigraphy was characterised by the presence of soft clean Clay, slightly organic Clay, and moderately soft silty Clay in combination with thin Peat layers in the uppermost 6 m, and over consolidated Clay from -6 to -28 m NAP.

- The sensitivity analysis was carried out altering the mean values of PI, Su, and Vs while keeping the other parameters constant. Precisely, for the PI two lower boundaries and two upper boundaries were created (namely PI mean -9.83%, PI mean -19.66%, PI mean +9.83%, and PI mean +19.66%). For the Su, three lower and three upper boundaries were considered (Su mean -20%, Su mean -30%, Su mean -70%, Su mean +20%, Su mean +30%, Su mean +70%, respectively). For the Vs, only one lower and one upper boundaries were modelled (Vs mean -20% and Vs mean +20%). In addition, the best estimate simulation, using the parameters obtained directly from CPT-based correlations, was carried out in order to make subsequent comparisons.

The main findings resulting from the sensitivity analysis are:

- By modifying the plasticity index of the entire soil column, it was found that an increase in PI led to an overall increase in PGA and PSA and, oppositely, to a reduction in maximum shear strain. Both PGA and PSA were almost similarly sensitive to reduction and increase of the PI mean. The impact of PI on MSS varied in depth per soil type. The stiffer soils showed a reduction of strains at higher PI while the soft soils towards surface showed larger MSS.

- The results of the undrained shear strength analysis revealed that while PGA and PSA are positively correlated with the Su mean, there exists a negative correlation between the maximum shear strain and Su. The lower Su resulted on larger MSS, especially within the softer soils (peat), but lower PGA towards surface and larger PGA within stiffer soils in depth. On the other hand, the larger Su resulted on overall larger PGA and spectral accelerations. In general, it can be concluded that the sensitivity of the SRA outcomes was more enhanced for reduction of Su mean values than its increase.

- From the shear wave velocity sensitivity analysis it was observed that varying only ±20% the Vs mean, the influence on the SRA results were significant.
  The lower Vs resulted on larger MSS, but smaller PGA (especially at relatively large depths, from -5 to -28 m NAP) and PSA. On the other hand, the larger Vs resulted on overall smaller MSS, in particular at shallow depth between 0 and -5 m, and larger PGA and PSA.
  The PGA was observed to be very sensitive to both reduction and accretion of Vs mean values. In contrast, the maximum shear strain appeared to be more sensitive to Vs reduction (particularly from -11 to -28 m NAP), whilst the response spectrum was similarly affected by Vs reduction and increase.

- Comparing all together the profiles resulting from the previous analyses, it can be concluded that the shear wave velocity was the parameter the influenced SRA results the most at great depths. Towards surface, the most crucial property was found to be the undrained shear strength. Finally, the plasticity index produced a smaller (or negligible) effect. Although there were differences among PGA, PSA and

MSS (e.g. MSS;UB were largely decreased and UB;PGA increased notably towards surface), the sensitivity analysis outcomes revealed that, in general, PGA, PSA and maximum shear strain were more sensitive to the reduction of these soil properties means rather than their increase.

5

Statistical Characterisation

5.1. Introduction

The present chapter aims to provide exploratory statistical analysis, carried out on the data compiled in the GI database (see Appendix B). The available data were grouped per geotechnical unit in order to investigate the variability of data-sets (PI and Su measured and calculated values) and gain insight on the adequacy of the employed CPT-based correlations (e.g. Cetin and Ozan, 2009 and Ladd and Foott, 1974).
The chapter contains the first section focusing on the plasticity index, and second one concerning the undrained shear strength. Each section contains an overview table of the soil units in the analysis (with a description of soil types and amount of measurements and data pairs per soil unit) and a number of histograms showing the frequency distribution of the measurements.
The predominant soil units (clean Clay, sandy Clay, and silty Clay) are analysed in detail, presenting several plots and tables containing descriptive statistics for each unit.
The results of this statistical characterisation and the limitations encountered during the analysis constitute the conclusions of the present chapter and serve as the basis for the next phase of the research: correlations improvement and/or development of alternative predictive models (Chapter 6).
Table 5.1 illustrates an overview of the eight soil units considered in this study (SU1_A, SU2, etc.) in correspondence with the stratigraphic units, the recommended soil properties values (soil unit weight and plasticity index) and the empirical correlations (for the estimation of the undrained shear strength) after the V4 GeoTOP model (Bommer et al., 2017a).

Table 5.1: Soil units used in this research in relation to the stratigraphic units from the GeoTOP model, with indication of γ_{wet} and PI, for clays, and empirical correlations used to determine Su (after Bommer et al., 2017a) (see Tables E.2 and E.1 for soil and stratigraphic units codes).

Soil Unit	Stratigraphic Unit	Stratigraphic Unit Symbol	Soil Type	Average Unit weight wet	Plasticity Index	PI Source	Average Su	Su Source
[SU]	[-]	[-]	[-]	[kN/m^3]	[%]	[-]	[kPa]	[-]
SU1_A	Naaldwijk	NA	clay	12,9	30	Skempton (1953) and expert judgement	0,38*σ'_{v0}+12	For all NA
	Drente	DR	clay	14,7	15	Sorensen & Okkels (2013)	1,15*σ'_{v0}	-
	Boxtel	BX	clay	14,4	50	Sorensen & Okkels (2013) and expert judgement	1,15*σ'_{v0}	-
SU1_B	Naaldwijk	NA	sandy clay or clayey sand	16.2	30	Skempton (1953) and expert judgement	0,49*σ'_{v0}+44	For all NA
	Nieuwkoop	NI	sandy clay or clayey sand	17,0	50	Based on NA	0,49*σ'_{v0}+44	From NA
	Drente	DR	sandy clay or clayey sand	16,7	10	Based on NA	0,97*σ'_{v0}+30	-
	Peelo	PE	sandy clay or clayey sand	18.1	30	Skempton (1953) and expert judgement	0,60*σ'_{v0}+55	-
SU1_D	Nieuwkoop	NI	clay	14,1	50	Based on NA	0,38*σ'_{v0}+12	From NA
			sandy clay or clayey sand	17,0	50		0,49*σ'_{v0}+44	
	Drente	DR	clay	14,7	15	Sorensen & Okkels (2013)	1,15*σ'_{v0}	-
			sandy clay or clayey sand	16,7	10		0,97*σ'_{v0}+30	
SU1_E	Naaldwijk	NA	sandy clay or clayey sand	16.2	30	Skempton (1953) and expert judgement	0,49*σ'_{v0}+44	For all NA
	Nieuwkoop	NI	sandy clay or clayey sand	17,0	50	Based on NA	0,49*σ'_{v0}+44	From NA
	Drente	DR	sandy clay or clayey sand	16,7	15	Based on NA	0,97*σ'_{v0}+30	-
	Anthropogenic	AAOP	sandy clay or clayey sand	16,8	50	Based on NA	55	-
SU2	Peelo	PE	clay	17,6	50	Sorensen & Okkels (2013) and TNO data	0,88*σ'_{v0}+26	-
			sandy clay or clayey sand	18,1	30		0,60*σ'_{v0}+55	
SU3	Naaldwijk	NA	sandy clay or clayey sand	16.2	30	Skempton (1953) and expert judgement	0,49*σ'_{v0}+44	For all NA
	Boxtel	BX	sandy clay or clayey sand	16,9	50	Sorensen & Okkels (2013) and expert judgement	0,97*σ'_{v0}+30	-
	Anthropogenic	AAOP	sandy clay or clayey sand	16,8	50	Based on NA	55	-
SU4	Nieuwkoop	NIHO, NIBA	clay	14,1	50*	Based on NA	12,5	From NIHO for peat
SU5	Peelo	PE	sandy clay or clayey sand	18.1	30	Skempton (1953) and expert judgement	0,60*σ'_{v0}+55	-

* Bommer et al. (2017b), in the V5 ground motion model, prescribes PI=100 % to be used in the damping curves for Peat.

5.2. Plasticity Index Data Analysis

There are 413 PI measurements in total from the Groningen region compiled in the database.
Figure 5.1 depicts the data frequency distribution based on PI measurements. Out of the 413, a consistent part of the measurements is contained within the bins ranging from 12 to 20 % (80 measurements), 20 to 30 % (81 measurements), and 35 to 45 % (132 measurements). The latter is the bin containing the most PI data. The remaining values are distributed with a descending trend within the bins ranging from 45 to 173 %, and 1 value is contained in the bin with PI smaller than 12 % (non-plastic soils).

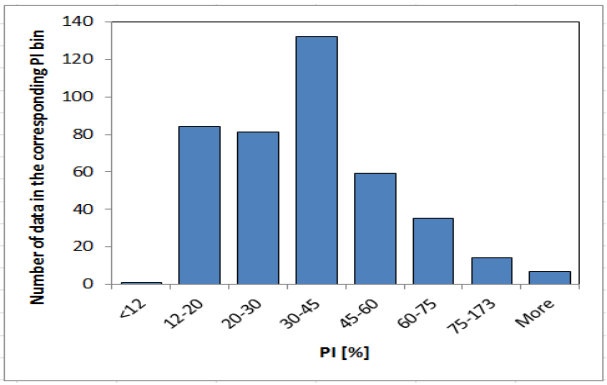

Figure 5.1: Data frequency of PI measurements.

Out of the 413 PI measurements present in the database, according to the laboratory description reports and engineering judgement (see Section B.2, Appendix B), 376 measurements are classified as Clay and the remaining 37 as Sand (20 measurements), Peat (11 measurements), overconsolidated Clay (4 measurements), and Loam (2 measurements) (Table 5.2).
Out of the 413 measurements, only for 378 it was possible to find a suitable CPT to compare with (5.2).
The amounts of samples are grouped per soil type (based on the criteria shown in table B.1, Section B.2). As shown in table 5.2 and figure 5.2, among the clay samples, the most recurrent soil type is the Sandy Clay (SU1_B) with 208 samples (of which only 202 are paired with calculated PI values), followed by the Silty Clay (SU1_E) with 110 samples and 98 data pairs, soft clean Clay with 32 samples and 30 data pairs, and organic clay with 26 samples and 15 data pairs (Table 5.2).
20 samples are classified as Sand, silty and/or clayey Sand. Their plastic behaviour (generally below 25 %) is likely be connected to the presence of some clay and/or silty material within the specimens.

Table 5.2: Summary of Soil Unit codes, primary and secondary soil type definition (in Dutch and English), amount of measured PI values and data pairs for every geotechnical unit, and stratigraphic units (according to table 5.1) (see Tables E.2 and E.1 for soil and stratigraphic units codes).

Soil Unit [SU]	**Soil Type** Primary	**Soil Type** Secondary	**Soil Type** English	**Amount of Samples** [-]	**Amount of Data Pairs** [-]	**Stratigraphic Unit** [-]
SU1_A	Klei	Schoon, slap	Clay, clean, soft	32	30	NA, DR, BX
SU1_B	Klei	Zandig	Clay, sandy	208	202	NA, NI, DR
SU1_D	Klei	Organisch	Clay, organic	26	15	NI, DR
SU1_E	Klei	Siltig	Clay, silty	110	98	NA, NI, DR, AAOP
SU2	Potklei	Potklei	overconsolidated Clay	4	4	PE
SU3	Zand	Kleig/siltig	clayey/silty Sand	20	20	NA, BX, AAOP
SU4	Veen	Niet voorbelast	Peat, not preloaded	11	7	NI
SU5	Leem	Zandig	Loam, sandy	2	2	PE

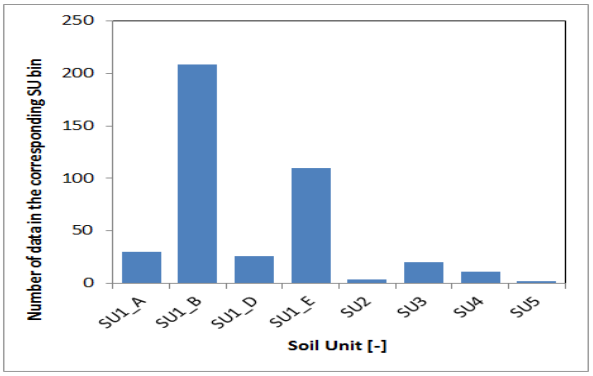

Figure 5.2: Data frequency of PI measurements organised in soil units.

5.2.1. Data and Approach

In the following sections are reported only the results and conclusions from the soft, clean Clay. The soil units sandy Clay, silty Clay, organic Clay, overconsolidated Clay, Sand, Peat, and Loam are reported in Appendix C. The models used for the comparison with PI measures are listed below (more details in Chapter 3, Section 3.6.1):

- Cetin & Ozan, 2009
- Bommer et al., 2017 (after Sorensen & Okkels, 2013)
- Arup, 2015

The descriptive statistics from the remaining units are shown in Appendix C (Section C.2.3, Table C.5).
The statistical parameters are:

1. N: amount of data pairs
2. *Min*: lowest value
3. *Max*: highest value
4. μ: mean value, calculated as:
$$\mu = \frac{x_1 + x_2 + \cdots + x_N}{N} \tag{5.1}$$
5. σ: standard deviation, calculated as:
$$\sigma = \sqrt{\frac{\sum_{i=1}^{N}(x_i - \mu)^2}{N-1}} \tag{5.2}$$
where x_i are the observed values of the data-set items, $\bar{x}$ is the mean value of these observations and N is the number of observations in the data-set
6. *COV*: coefficient of variation, calculated as:
$$\sigma / \mu \tag{5.3}$$
7. *Median*: median value

Successively, the data-sets are divided into sample classes (i.e. classes 1, 2, and 3, described in Section B.4.3, Table B.3) to account for depth mismatch between laboratory PI values and CPT measurements and exploratory statistics are given for the three classes.
The statistical characterisation presented in the next sections consists of:

1. Scatter plots (PI versus depth, stratigraphic units versus depth, and PI measured versus PI calculated).
2. Data exploration with histograms, underlying distributions (probability density function, PDF), and Box-plots for linear and logarithmic data-sets prior re-classification in sample classes, and for linear data-sets post re-classification.
3. Summary tables with descriptive statistical parameters from the different data-sets.

5.2.2. Soil Unit: Soft, Clean Clay (SU1_A)

The soft clean Clay soil unit contains 32 laboratory measurements, of which 30 are paired with Cetin and Ozan (2009) calculated values (Table 5.2). The geological units used by Bommer et al. (2017a), which the samples of this data-set belong to, are the Naaldwijk, Drente, and Boxtel formations (hereafter indicated as NA, DR, and BX, as in Tables 5.1 and 5.2).

PI versus Depth

The plot in figure 5.3 depicts the distribution of the PI data pairs over depth and PI values recommended by Bommer et al. (2017a) as a generalised range to cover all the stratigraphic units implied.
The points in red represent the measured values (PI;measured), and the vertical red line represents the mean value of the data-set (27.7%). The blue points (crosses) indicate the calculated values (using the Cetin and Ozan, 2009 correlation) and the vertical blue line their mean value ($PI_{C\&O}$ mean = 22.2%). The dashed red and blue lines display the PI mean ± 1 time the standard deviation ($\sigma_{PI;measured} = \pm 15.4\%$ and $\sigma_{PI;C\&O} = \pm 9.8\%$), for measured and calculated PI, respectively. The solid green line represents the PI as suggested by Arup (2015) ($PI_{Arup} = 25\%$ for all clays), whilst the coloured area (in yellow) defines the range of PI values recommended by Bommer et al. (2017a), hereafter PI_{V4}. The lower boundary of this area represents the average PI value for Drente clean clays ($PI_{DR;clays} = 15$ %), and the upper boundary depicts the PI suggested for Boxtel clean clays ($PI_{BX;clays} = 50$ %), while the PI for Naaldwijk clean clays lies almost in the middle of the range, being $PI_{NA;clays} = 30$ %.
As shown in figure 5.3, most of the samples (24 out of 30 data pairs) were collected at shallow depths (from 0.4 to -4 m NAP), and only 6 samples from deeper layers (e.g. from about -4 up to -11.97 m NAP).
The mean PI calculated with Cetin and Ozan (2009) is similar to the mean PI measured at the laboratory (22.2 and 27.7 %, respectively), meaning that the Cetin and Ozan (2009) correlation is well-predicting PI values (or slightly under-predicting). The measured and calculated values do not deviate significantly from each other at shallow depths, showing better correlation than at greater depth.
Furthermore, the majority of the $PI_{C\&O}$ values falls within the PI_{V4} range considering the different stratigraphic units.
Figure 5.4 shows the correspondence between measured and calculated PI from the SU1_A unit in a scatter plot with the equality line (x=y). The closer the points fall to the equality line (i.e. line where measured and predicted are perfectly equal), the more accurate the fit.

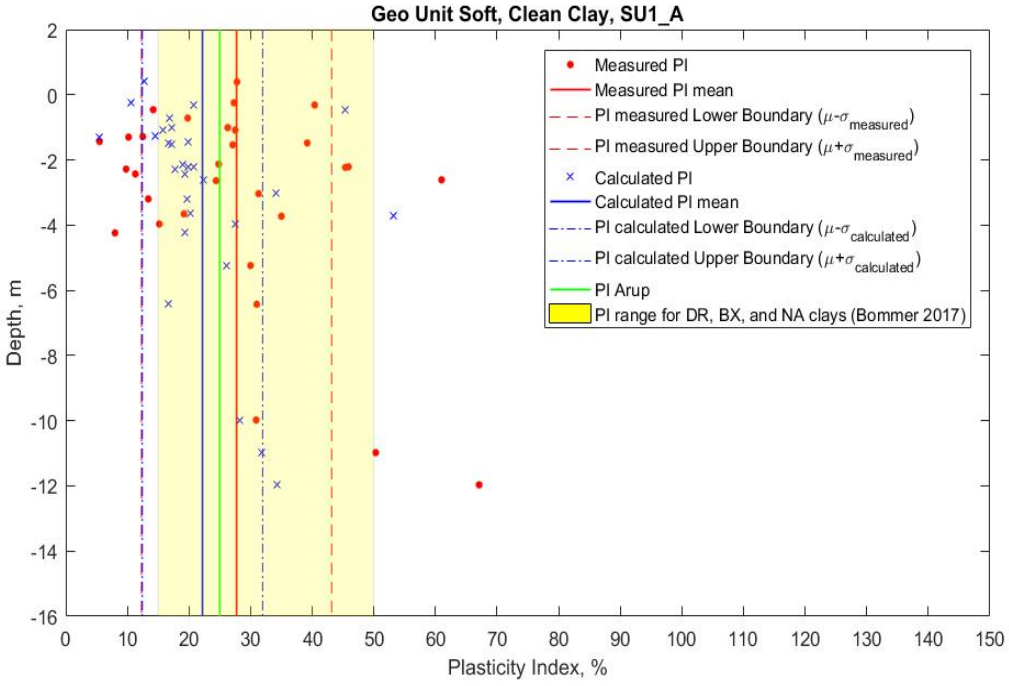

Figure 5.3: PI measurements and calculated values for the soft, clean Clay soil unit.

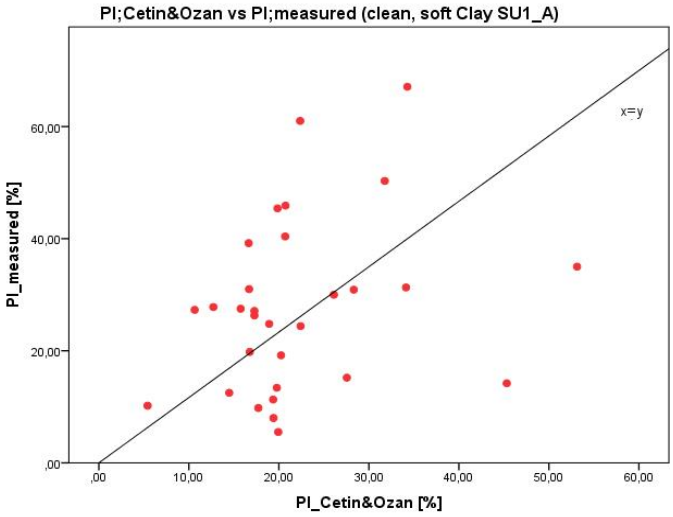

Figure 5.4: Scatter plot with equality line of PI data pairs from the soft, clean Clay soil unit.

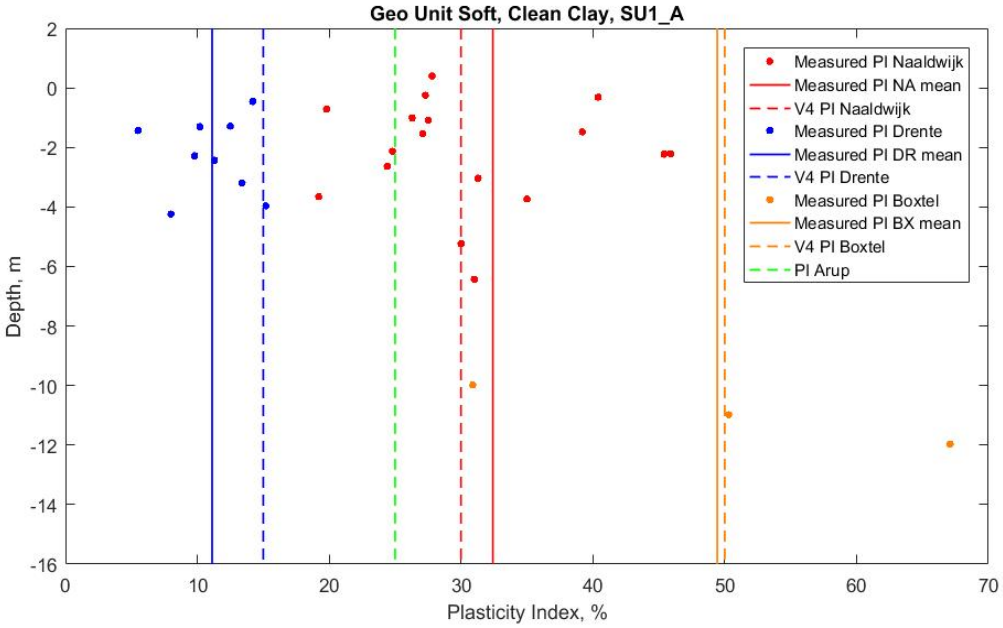

Figure 5.5: PI measurements organised per stratigraphic unit for the soft, clean Clay soil unit.

Figure 5.5 shows the distribution of PI measurements of the SU1_A unit over the depth organised in stratigraphic units after Bommer et al. (2017a), and the comparison between mean values and recommended values from Bommer et al. (2017a) (Table 5.1). The red points represent the measurements that belong to the Naaldwijk formation, the solid red line their mean, and the dashed red line the V4 recommended PI for Naaldwijk clean clays. The blue points represent the measurements belonging to the Drente formation, the solid blue line their mean, and the dashed blue line the V4 recommended PI for Drente clean clays. The orange points represent the measurements from the Boxtel formation, the solid orange line their mean, and the dashed orange line the V4 recommended PI for Boxtel clean clay.
The means of the V4 recommended values are in good agreement with the laboratory PI measurements for this soil unit. Specifically, for the Drente clean clays, a value of 15 % (dashed blue line) is over-predicting the measured mean (11.5 %); for the Naaldwijk formation, a value of 30 % (dashed red line) is under-predicting

the measured mean (32.4 %); and for the Boxtel formation, a value of 50% (dashed orange line) is almost identical to the measured mean (49.4 %).
Table 5.3 shows the exploratory statistics for the three stratigraphic units: NA, DR, and BX.

Table 5.3: Statistical characterisation of NA, DR, and BX formations in SU1_A.

Stratigraphic Unit		**Statistical parameters**						
		N	min	max	μ	σ	COV	median
		[-]	[%]	[%]	[%]	[%]	[-]	[%]
NA	PI measured	18	19.2	61.0	32.4	10.5	0.37	28.9
DR	PI measured	9	5.5	15.2	11.1	3.1	0.28	11.3
BX	PI measured	3	30.9	67.1	49.4	18.1	0.37	50.3

Data Distribution

The data-sets for the SU1_A unit are approximately normally distributed or slightly positively skewed (Figures 5.6a and 5.6b). Considering the randomness of PI measurements in figure 5.6a and the coefficient of variation of the PI data-sets larger than 30 % (5.5), the data-sets distribution may be better described by a log-normal distribution, in agreement to the fact that the plasticity index is a non-negative soil property (with most of the samples characterised by low PI values, ranging from 0 to 50 %). In figures 5.7a and 5.7b, showing the distribution of logarithmic measured and calculated PI values, the data are approximately normally distributed and the coefficient of variation is smaller than 30 %.

Figure 5.6: Histograms of calculated and measured PI values and underlying normal distributions for the soft, clean Clay soil unit.

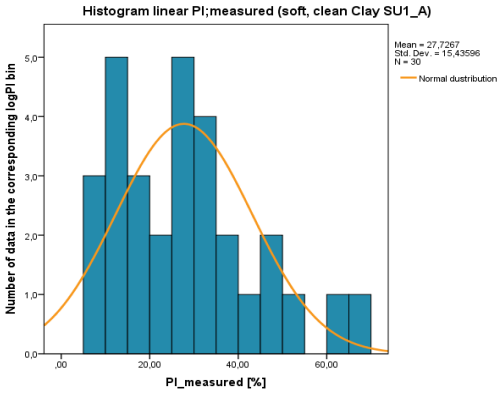

(a) Histogram of linear PI measured for the soft, clean Clay soil unit.

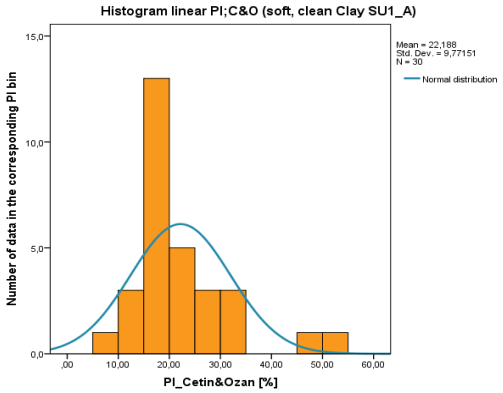

(b) Histogram of linear PI Cetin&Ozan (2009) for the soft, clean Clay soil unit.

Figure 5.7: Histograms of logarithmic calculated and measured PI values and underlying normal distributions for the soft, clean Clay soil unit.

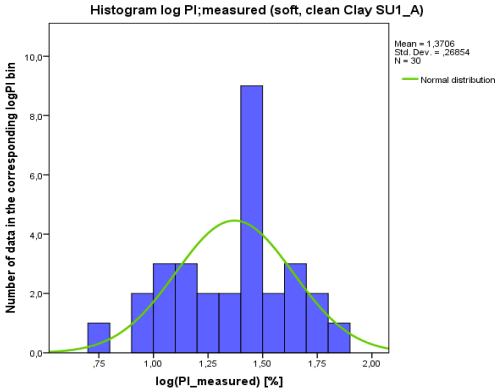

(a) Histogram of logarithmic PI measured for the soft, clean Clay soil unit.

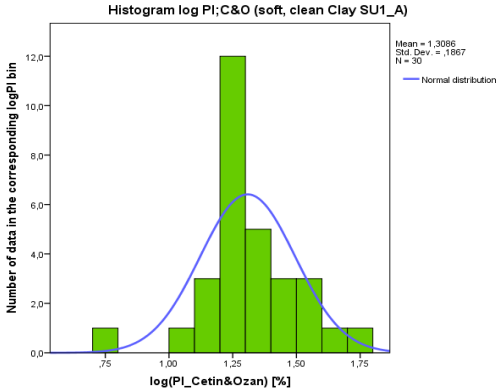

(b) Histogram of logarithmic PI Cetin&Ozan (2009) for the soft, clean Clay soil unit.

In order to display the data-set variability, Box-plots (or Box-and-Whiskers-Diagrams) are created in SPSS. Box-plots give the general image and trend of an entire group of numerical data, by mean of their quartiles, instead of considering individual points. In this "non-parametric" way, variation in samples of a statistical population (PI data-sets) is investigated without making any assumption about the underlying statistical distribution (Laerd-Statistics, 2015).
The bottom and the top of each box represent the first and third quartiles (Q1, Q3), respectively, and the band inside the box represents the median or second quartile (Q2), as explained in table 5.4. The vertical lines, named whiskers, indicate the variability outside the upper and lower quartiles. The ends of the whiskers indicate the maximum and minimum value of the entire data-set, respectively. The points above and below the whiskers represent the unusual points (or outliers) of the data-set, automatically individuated by the software.

Table 5.4: Definition of quartiles (after Laerd-Statistics, 2015)

Symbol	Name	Definition
Q1	First Quartile	Splits off the lowest 25% of the data from the highest 75%
Q2	Second Quartile, Median	Cuts data-set in half
Q3	Third Quartile	Splits off the highest 25% of the data from the lowest 75%

The box-plots from comparison between measured and calculated PI from unit SU1_A are illustrated in figures 5.8a and 5.8b. As shown in figure 5.8a and table 5.5 ("All classes" data-set), the median of the PI measured data-set (27.2 %) is higher than the median of the PI predicted (19.8 %) using the Cetin and Ozan (2009) CPT-based correlation.
Furthermore, as it is visible from the linear histograms (Figures 5.6a and 5.6b), the scatter plot (Figure 5.3), and the linear box-plots (Figure 5.8a), the range of PI values measured in laboratory is wider than the predicted values.
With the purpose to obtain a more detailed indication of the data-sets characteristics and correspondence, the samples were divided into three classes, according to table B.3 (Appendix B). The general descriptive statistical parameters from the re-classified data are given in table 5.5 and their box-plots in figure 5.9.

Figure 5.8: Box-and-Whiskers-Diagram from measured and calculated PI values of the linear and logarithmic PI data-sets for the soft, clean Clay soil unit.

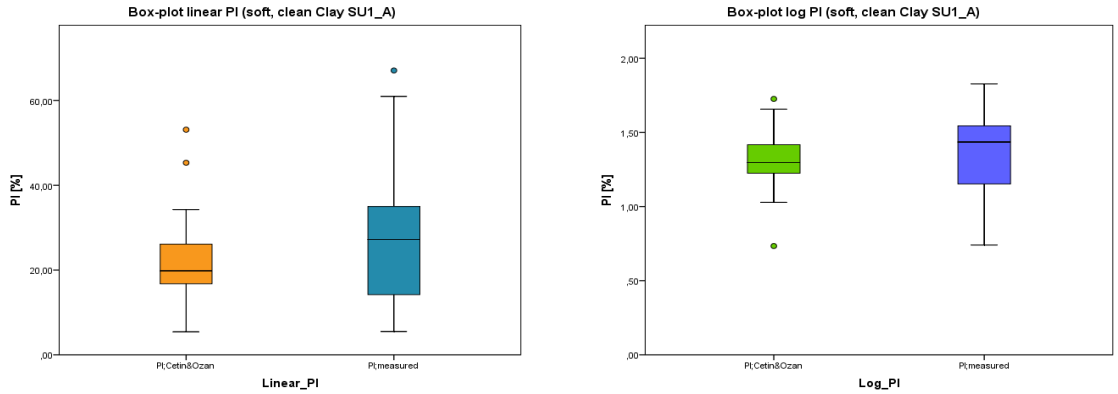

(a) Box-and-Whiskers-Diagram from linear measured and calculated PI values for the soft, clean Clay soil unit.

(b) Box-and-Whiskers-Diagram from logarithmic measured and calculated PI values for the soft, clean Clay soil unit.

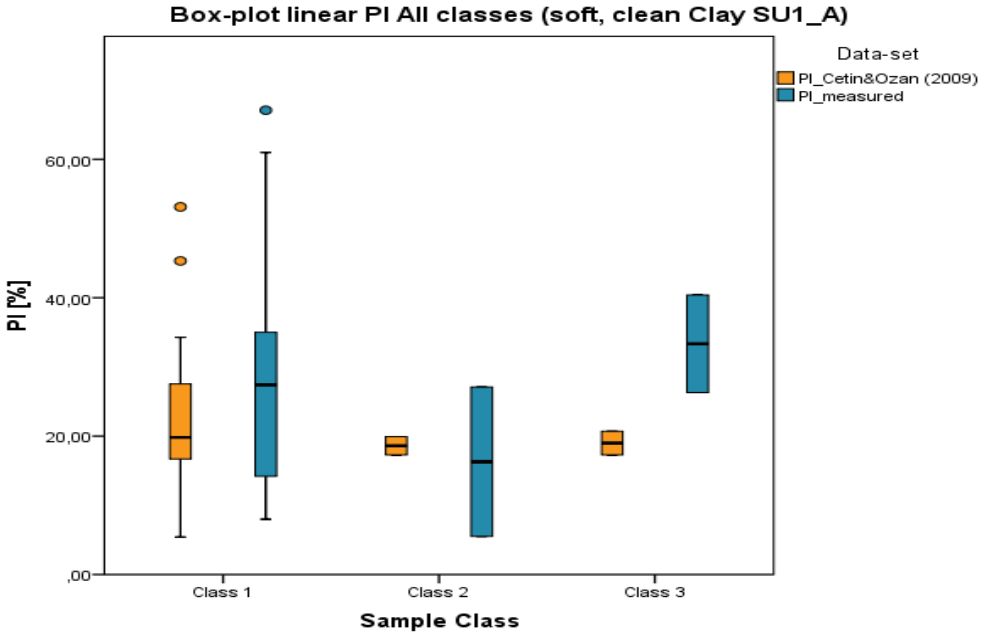

Figure 5.9: Box-and-Whiskers-Diagram from measured and calculated PI values of the three samples classes for the soft, clean Clay soil unit.

Table 5.5: Statistical characterisation of SU1_A unit.

Class		**Statistical parameters**						
		N	min	max	μ	σ	COV	median
		[-]	[%]	[%]	[%]	[%]	[-]	[%]
All classes	PI measured	30	5.5	67.1	27.7	15.4	0.56	27.2
	PI calculated	30	5.4	53.1	22.2	9.8	0.44	19.8
1	PI measured	26	8.0	67.1	28.2	15.8	0.56	27.4
	PI calculated	26	5.4	53.1	22.7	10.4	0.46	19.8
2	PI measured	2	5.5	27.1	16.3	15.3	0.94	16.3
	PI calculated	2	17.3	19.9	18.6	1.9	0.10	18.6
3	PI measured	2	26.3	40.4	33.4	10.0	0.30	33.4
	PI calculated	2	17.3	20.7	19.0	2.4	0.13	19.0

5.3. Undrained Shear Strength Data Analysis

There are 161 Su measurements in total from the Groningen region compiled in the database.
Figure 5.10 depicts the frequency distribution based on undrained shear strength measurements, without differentiating the test types. The most consistent part of the data falls in the ranges from 0 to 60 kPa, precisely, 43 measurements in the <20 kPa bin, 80 measurements in the 21-40 kPa bin and 24 in the 41-60 kPa bin. The remaining values are distributed within the ranges from 60 to 180 kPa.

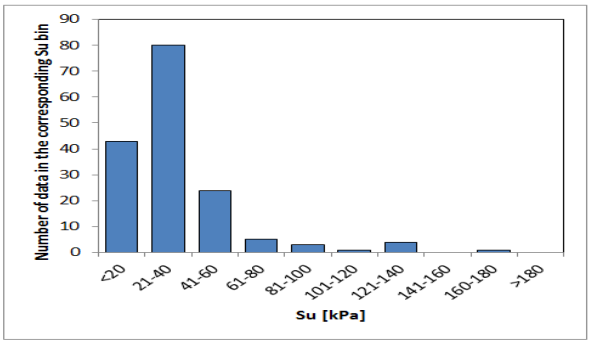

Figure 5.10: Data frequency of Su measurements, without differentiating various test types.

Undrained shear strength measurements are grouped per geotechnical unit, according to the laboratory description reports and engineering judgement (based on the criteria shown in Table B.1, Appendix B). Of the 161 measurements, 141 are classified as Clay (SU1_A, SU1_B and SU1_E), 9 as overconsolidated Clay (SU2), and 11 as Sand (mostly silty and clayey sand, SU3).
As shown in table 5.6 and figure 5.11, the most recurrent clay type is the Sandy Clay (SU1_B) with 79 measurements, followed by Silty Clay (SU1_E) with 55 measurements, soft clean Clay (SU1_A) with 9 measurements.

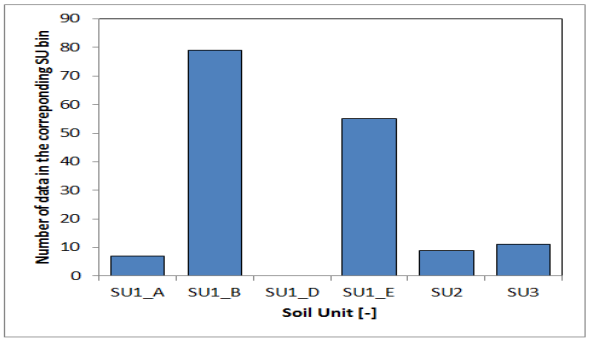

Figure 5.11: Data frequency of Su measurements organised in soil units.

Table 5.6: Summary of soil unit codes, primary and secondary soil type definition (in Dutch and English), amount of measured Su values and data pairs for every geotechnical unit, and stratigraphic units (according to table 5.1) (see tables E.2 and E.1 for soil and stratigraphic units codes).

Soil Unit [SU]	**Soil Type** Primary	**Soil Type** Secondary	**Soil Type** English	**Amount of Samples** [-]	**Amount of Data Pairs** [-]	**Stratigraphic Unit** [-]
SU1_A	Klei	Schoon, slap	Clay, clean, soft	7	3	NA
SU1_B	Klei	Zandig	Clay, sandy	79	67	NA,DR
SU1_D	Klei	Organisch	Clay, organic	0	0	NI
SU1_E	Klei	Siltig	Clay, silty	55	23	NA,NI,DR, AAOP
SU2	Potklei	Potklei	overconsolidated Clay	9	9	PE
SU3	Zand	Kleig/siltig	clayey/silty Sand	11	11	BX
SU4	Veen	Niet voorbelast	Peat, not preloaded	0	0	NI
SU5	Leem	Zandig	Loam, sandy	0	0	PE

5.3.1. Interpretation of Su per Test Type

Different test methods were used to determine the undrained shear strength of the specimens. Out of the 161 Su measurements in the database, 77 were obtained using the Torvane test, 47 with the triaxial apparatus in a consolidated undrained way (CU), and 36 with unconsolidated undrained (UU) triaxial tests.

Torvane test

The Torvane test is a hand-held vane shear device that allows for a prompt measurement of shear strength either in laboratory or directly in-situ, giving a rough picture of the large spatial variability of the uppermost soil layers. Being this test relatively easy and quick, several may be the drawbacks connected to its usage. For instance, rate of loading, progressive failure, degree of saturation, pore water dissipation, etc. are not fully taken into account by the test itself (DGSI, 2017).
The Torvane tests may be characterised by values of Su generally overestimating the actual soil conditions, due to several factors that affect the shear strength of soil materials (e.g. partially or unsaturated saturated soils, lowering of groundwater table and soil desiccation, previous compaction of soils during construction of roads or buildings). In this study, thus, the Torvane measurements are reduced of 20%.
Figure 5.12 contains a histogram of measured values by means of Torvane test. Of 77 data pairs, 2 measurements are contained in the <20 kPa bin, 51 measurements in the 21-40 kPa bin, 18 measurements in the 41-60 kPa bin, and 6 measurements in the remaining four bins.

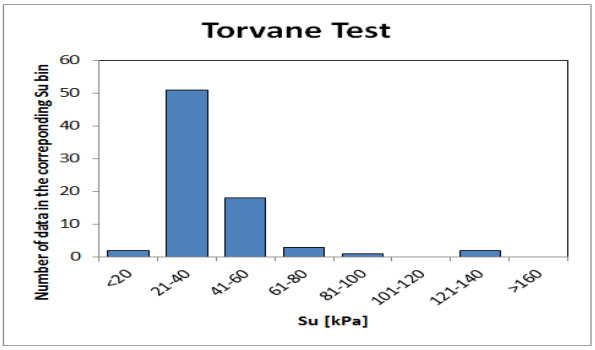

Figure 5.12: Data frequency of Su measurements obtained from Torvane test.

Triaxial CU test

Of the 47 Su measurements obtained from isotropically consolidated undrained triaxial tests 8 values fall within the <10 kPa bin, 25 in the 11-20 kPa bin, 13 in the 21-30 kPa bin, and 2 in the 31-40 kPa bin (Figure 5.13).
In most of the cases, the specimens were tested following the SHANSEP procedure, introduced by Ladd and Foott (1974). Bay et al. (2005) paraphrased the basic systematic laboratory procedure as follows:

1. Select samples and define the pre-consolidation pressure, σ'_p (either from one-dimensional consolidation testing or from in-situ measurements).
2. Using specimens from the same sample, consolidate them to 1, 2, 4 and 6 times the established σ'_p.
3. Select the laboratory consolidation pressure (σ'_c) when a constant relationship between shear strength and consolidation pressure is reached. This constant relationship should be true at least for the higher two pressures in the above step.
4. The specimens are consolidated to this pressure and then allowed to swell to the previously fixed over-consolidation ratios.
5. The shearing phase is then initiated and normalised undrained shear strength is finally plotted against OCR and the resulting relationship is compared with existing data to ensure testing validity.

This procedure generates distinct values of undrained shear strength depending on the consolidation pressures used to reach the established OCR. For this reason, the triaxial (CU) data will not be considered further

as in-situ measurements and will be discarded from the following statistical analysis. However, those data are going to be used in Chapter 6 for the calibration of the SHANSEP parameters per different soil types.

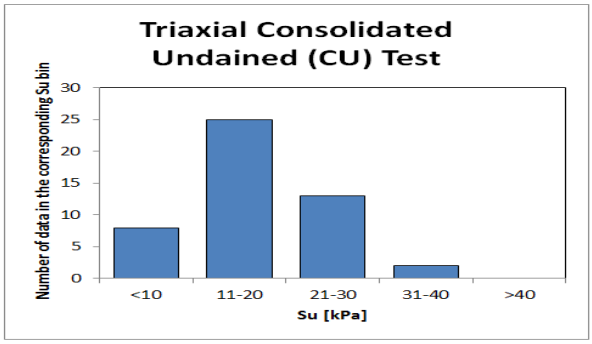

Figure 5.13: Data frequency of Su measurements obtained from triaxial consolidated undrained test.

Triaxial UU test

Of 36 samples tested with the UU triaxial system, 8 measurements have undrained shear strength values lower than 20 kPa, 14 range between 21 and 40 kPa, 6 between 41 and 60 kPa, and the remaining 8 are almost equally distributed in the left bins (Figure 5.14).

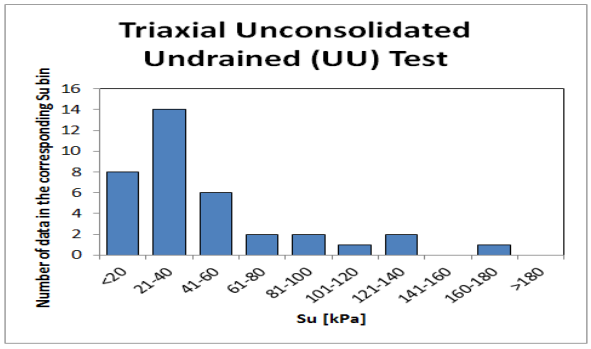

Figure 5.14: Data frequency of Su measurements obtained from Triaxial Unconsolidated Undrained test.

5.3.2. Limitations

The amount of data is limited and may thus not be representative for clays in general. The sites from where the data have been obtained are limited to Groningen region. The hypotheses are tested, results obtained and conclusion are drawn for the specific samples.

The tests methods considered in this statistical characterisation are triaxial UU and Torvane. The triaxial tests were performed on samples collected from few deep boreholes at various locations, which did not necessarily correspond to the locations where the Torvane tests were carried out. This makes more difficult the comparison between laboratory and in-situ data.

The analysis conducted in this study is limited to a restricted number of variables: Su_{UU}, $Su_{Torvane}$, σ'_v, σ'_p, σ'_c, OCR, m, S, and γ. The data have been sorted into data-sets by categorising them with respect to different characteristics (mainly soil type). Other parameters and sorting data may be relevant to analyse, however it has not been within the scope of this study.

The parameters have been evaluated per borehole. The value of a parameter at a certain depth has been evaluated in combination with another (or more) parameter at the same depth in the same borehole. A qualitative approach, analysing for example σ'_p as a site average rather than a single value, would be preferable. However, given the limited amount of boreholes and CPTs per location, this was not possible to execute. Rather than performing qualitative analyses at the locations, a more quantitative and singular approach, utilising all data points, was determined to be more relevant in relation to the aim and purpose of the thesis.

Clays with silty content and silts, are not considered as separate soil units, but are grouped within other units (e.g. Silty Clay, SU1_E).
This study is limited to normally consolidated to slightly overconsolidated clays (maximum OCR=6), where the consolidation process is fully proceeded in laboratory. However, the site information has, at some locations, been limited. This makes the evaluation of the stress history of the site difficult or not possible. The laboratory data lacking of pre-consolidation information have been therefore discarded (e.g. CU data from objects Y2, Y16, and Y17, Table B.2, Appendix B).

5.3.3. Data and Approach

In the following sections only the results and conclusions from the clean Clay and sandy Clay units are reported. The results from the silty Clay (23 measurements) unit and the descriptive statistical parameters for the overconsolidated Clay (9 measurements) and Sand (11 measurements) units can be found in Appendix C (Section C.3).
The models considered for the comparison with Su measurements are listed below (more details can be found in Section 3.6.2):

- SHANSEP (Ladd and Foott, 1974) with $S = 0.25$ and $m = 0.7 - 0.99$ (single calibration, after Arup 2015)
- Robertson, 2015 (with $N_{kt} = 15$)
- Bommer et al., 2017 (for different stratigraphic units)

Firstly, the data are presented all together in order to investigate the suitability of the CPT-based correlations with respect to the in-situ data, successively, the data-sets are divided in sample classes (i.e. classes 1,2, and 3 described in Appendix B, Table B.3) to account for depth mismatch between laboratory and CPT measurements, and exploratory statistic are given for the three classes.
The statistical characterisation presented in the next sections consists of:

1. Scatter plots (Su versus depth, stratigraphic units versus depth, and Su calculated versus Su measured).
2. Data exploration with box-plots (for different correlations, test types and sample classes)
3. Summary tables with descriptive exploratory statistical values from the different data-sets.

In the present chapter, the statistical characterisation of the soil units is carried out considering only the in-situ measurements (Torvane and lab-UU) in comparison to the Su values obtained from the Ladd and Foott (1974) model with single calibration (after Arup, 2015), Robertson and Cabal (2015) correlation, and Bommer et al. (2017a) equations.

5.3.4. Soil Unit: Soft, clean Clay (SU1_A)

For the 7 Su measurements compiled in the database as soft, clean Clay unit it was always possible to find CPT data to be compared with. The 7 data pairs are classified as Class 1 (following the classification presented in Appendix B, Table B.3). However, of the 7 measurements, 4 are obtained with triaxial consolidated undrained tests and 3 are obtained with triaxial unconsolidated undrained test. Given that the Su values obtained from CU tests depend upon the consolidation pressure applied during the test (see Section 5.3.1), they cannot be considered as representative of the in-situ conditions and, thus, are discarded from the following statistical characterisation.
Soft, clean clay samples are assumed to belong to the Naaldwijk formation (Table 5.1).

Su versus Depth

The plot in figure 5.15 illustrates the distribution over the depth of Su measurements and predicted Su values (calculated using the correlations suggested by Ladd and Foott, 1974, Robertson and Cabal, 2015, and Bommer et al., 2017a) and their ranges (± 1 standard deviation).
The points in green represent the Su values measured with UU triaxial tests (Su;measured (UU)), and the vertical green line represents their mean value. The blue points (crosses) represent the calculated values using the Ladd and Foott (1974) correlation with single calibration (hereafter indicated as $Su_{SHANSEP}$), and the vertical blue line represents their mean value. The magenta triangles denote the values calculated with the Robertson and Cabal (2015) correlation (hereafter indicated as $Su_{Robertson}$). The light blue circles describe the Su values obtained using the NA clean clays equation recommended by Bommer et al. (2017a) (hereafter indicated as $Su_{NA;clays}$). The coloured areas (in green and dark blue) display the upper and lower boundaries for the Su;measured (UU) and Su;SHANSEP data-sets, respectively (computed as Su mean ±20%).
As shown in figure 5.15, the Su values calculated with the SHANSEP model (mean = 5.5 kPa, Table 5.7) are lower than the Su measured at the laboratory with UU triaxial tests (mean = 24.8 kPa, Table 5.7).
Furthermore, the SHANSEP predicted values are in poor agreement with both $Su_{NA;clays}$ and $Su_{Robertson}$ calculated values (Figure 5.15) which, in turn, correlate better with the in-situ measurements. The $Su_{Robertson}$ mean (23.2 kPa, Table 5.7) is almost identical to the in-situ measurements mean (24.8, Table 5.7), whilst the $Su_{NA;clays}$ mean is about 7 kPa lower than the in-situ measurements.
The plot in figure 5.16 illustrates the distribution of Su measurements (organised in stratigraphic units after Bommer et al., 2017a) over the depth and the comparison between measured and calculated $Su_{NA;clays}$ mean values. The points in red represent the Su measurements belonging to the Naaldwijk formation ($Su_{NA;clays}$), and the solid red line represents their mean (24.8 kPa, Table 5.7), whilst the red triangles refer to the $Su_{NA;clays}$ values for the Naaldwijk formation, computed using the Bommer et al., 2017a relation for NA clean clays, and the dashed-dotted line in red their mean value (17.9 kPa, Table 5.7). From figure 5.16, the Bommer (2017) correlation shows a fair correspondence with the laboratory data. The predicted mean underestimates the measured Su mean, with a difference of almost 7 kPa.
Nevertheless, due to the scarce amount of in-situ measurements to compare the predicted Su values with, it is difficult to provide an accurate assessment of the correlations' adequacy.

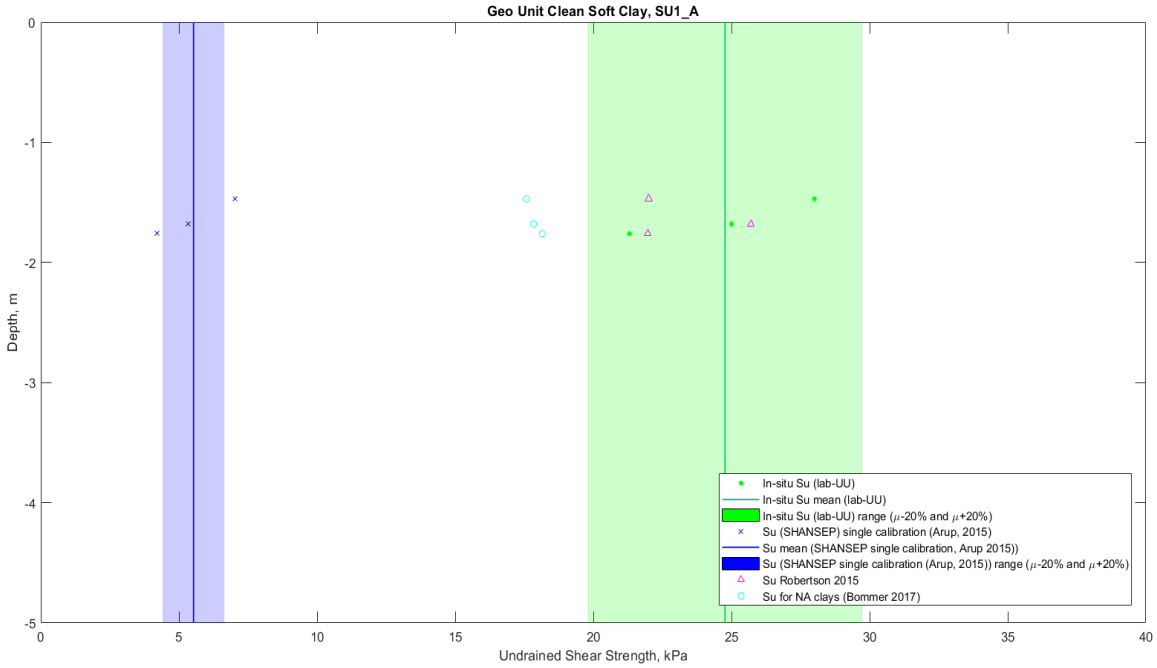

Figure 5.15: Su measurements and calculated values for the soft, clean Clay soil unit.

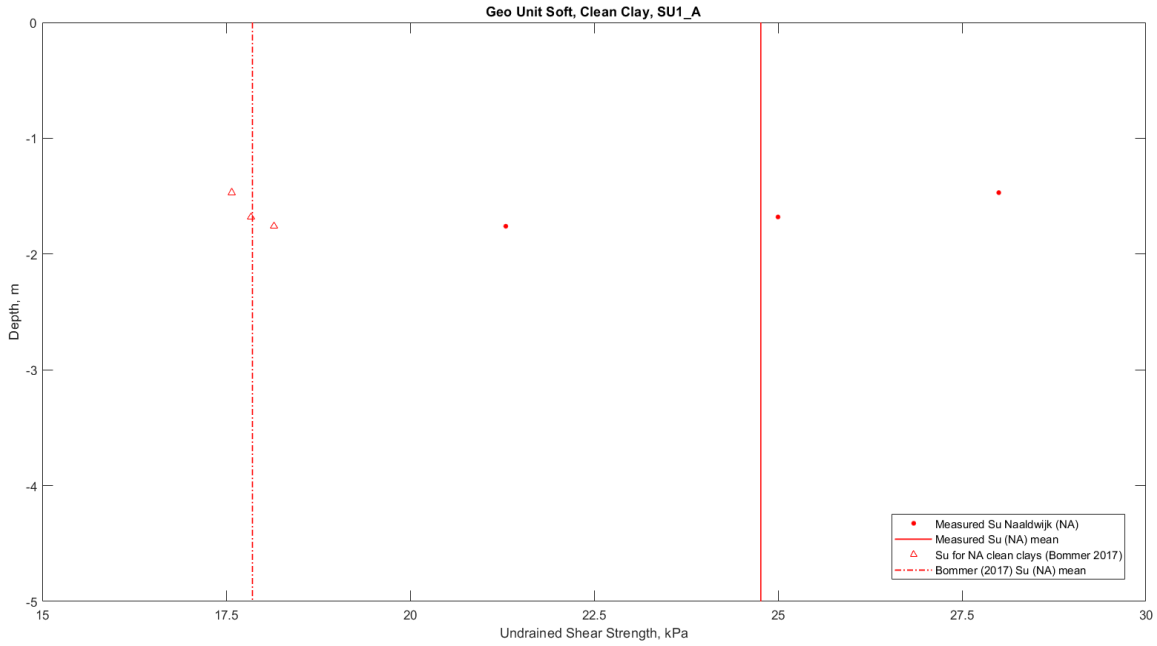

Figure 5.16: Comparison of the in-situ Su measurements and calculated Su value for the soft, clean Clay soil unit organised in stratigraphic units.

In order to obtain a useful visual representation of the correlations fit, the measured values are plotted against the predicted ones in figures 5.17, 5.18a, and 5.18b. The closer the points fall to the equality line the more accurate the fit.
Figure 5.17 shows the poor correlation existing between the in-situ measurements (lab-UU) and Su;SHANSEP (i.e. the three data pairs are located far from the equality line), confirming what illustrated in figure 5.15.
Figures 5.18a and 5.18b show the Robertson and Cabal (2015) and Bommer et al. (2017a) correlations fit, respectively. Figure 5.18a displays an acceptable correlation existing between the in-situ (lab-UU) measurements and the calculated (Robertson, 2015) Su values, whilst figure 5.18b displays that the UU data poorly correlate with calculated (Bommer NA) Su values, being slightly under-predicted.

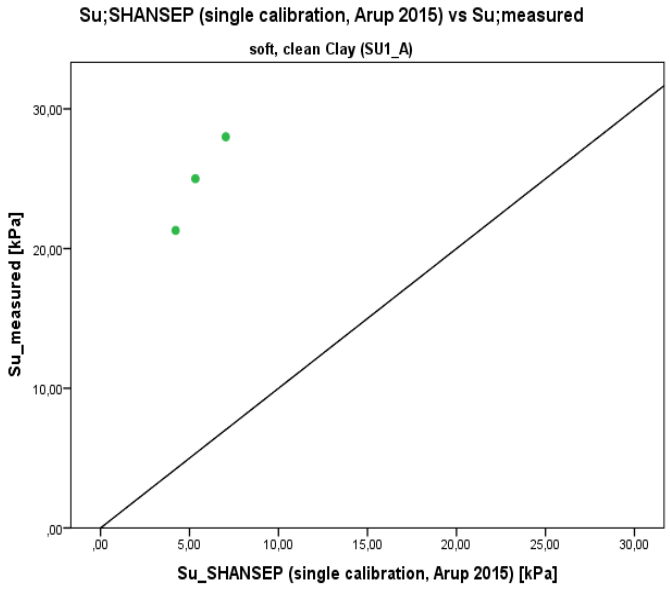

Figure 5.17: Scatter plot with equality line of Su data pairs for the soft, clean Clay soil unit. Green dots: data pairs of in-situ Su measurements (lab-UU) and SHANSEP (single calibration, Arup 2015) calculated values.

Figure 5.18: Scatter plot with equality line of Su data pairs (calculated with the Robertson (2015) and Bommer (2017) correlations) for the soft, clean Clay soil unit.

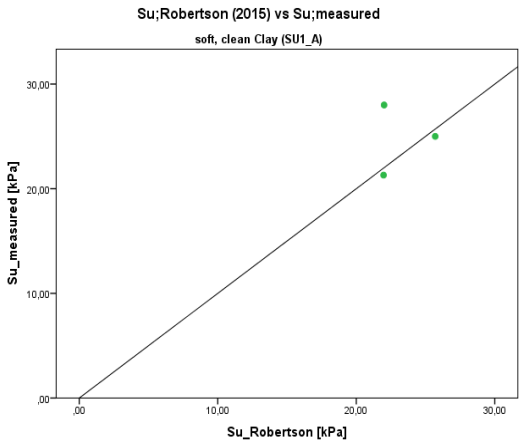

(a) Scatter plot with equality line of Su data pairs for the soft, clean Clay soil unit. Green dots: data pairs of in-situ Su measurements (lab-UU) and Robertson (2015) calculated values.

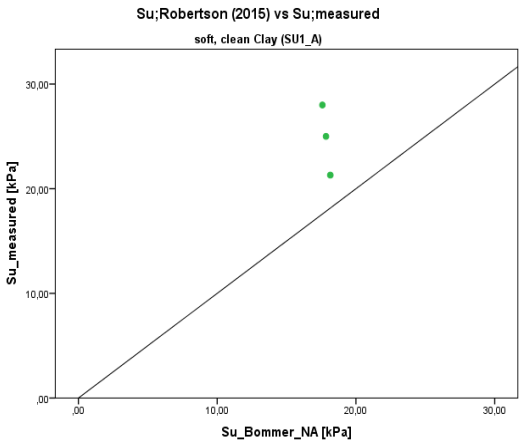

(b) Scatter plot with equality line of Su data pairs for the soft, clean Clay soil unit. Green dots: data pairs of in-situ Su measurements (lab-UU) and Bommer NA (2017) calculated values.

Data Distribution

Figure 5.19 shows the variability of the SU1_A soil unit, illustrating the box-plots from the comparison of the data pairs classified as soft, clean Clay, obtained using the three different correlations.

Figure 5.19 reveals that the SHANSEP correlation with single calibration under-predicts the Su for this soil unit by the most. Its median (5.3 kPa) is visibly lower than the measured median (25.0 kPa), and the range of the calculated values (min = 4.2 kPa and max = 7.0 kPa) is narrower than the measurements' range (min = 21.3 kPa and max = 28.0 kPa) (Table 5.7). The Robertson (2015) correlation estimates a median (22.0 kPa) lower than the measured median but higher than the SHANSEP median. Its range of values (min = 22.0 kPa and max = 25.7 kPa) is narrower than the laboratory measurements range and slightly narrower than the SHANSEP range.

Similarly, the Bommer (2017) correlation yields a median (17.8 kPa) lower than the measured median and greater than the SHANSEP median. However, its range of values (min = 17.6 kPa and max = 18.2 kPa) is visibly narrower than the other data-sets ranges (Table 5.7).

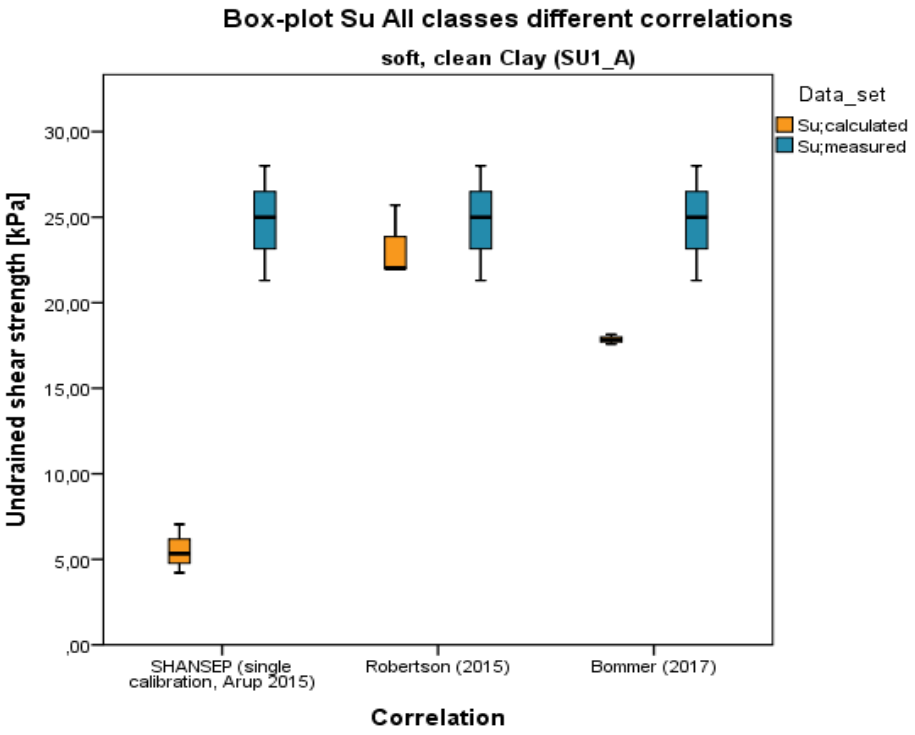

Figure 5.19: Box-and-Whiskers-Diagram from measured and calculated (SHANSEP, 1974, Robertson, 2015, and Bommer, 2017) Su values for the soft, clean Clay soil unit.

Table 5.7: Statistical characterisation of the soft, clean Clay samples (SU1_A).

Correlation	**Statistical parameters all samples**						
	N	min	max	μ	σ	COV	median
	[-]	[kPa]	[kPa]	[kPa]	[kPa]	[-]	[kPa]
Su measured	3	21.3	28.0	24.8	3.4	0.14	25.0
SHANSEP (1974)	3	4.2	7.0	5.5	1.4	0.26	5.3
Robertson (2015)	3	22.0	25.7	23.2	2.1	0.09	22.0
Bommer (2017)	3	17.6	18.2	17.9	0.3	0.02	17.8

5.3.5. Soil Unit: Sandy Clay (SU1_B)

The sandy Clay unit contains the largest amount of Su measurements in the database (79 in total). Of 79 Su measurements, 12 are obtained with triaxial consolidated undrained tests, 18 with triaxial unconsolidated tests, and 49 with Torvane tests. In the following section only the in-situ measurements obtained from Torvane and triaxial (UU) tests are considered. Therefore, a total of 67 measurements will be analysed.
Sandy Clay samples are associated to the Drente, Naaldwijk and Nieuwkoop formations (Table 5.1).
Of the 67 data pairs, 45 are classified as Class 1, 7 as Class 2, and 15 as Class 3 (Table 5.9).

Su versus Depth

The plot in figure 5.20 displays the distribution over the depth of Su data and Su predicted values (calculated using the correlations suggested by Ladd and Foott, 1974, Bommer et al., 2017a, and Robertson and Cabal, 2015) and their ranges (± 1 standard deviation).
As it can be seen in figure 5.20, the Su values calculated with the SHANSEP correlation (All classes mean = 13.5 kPa, Table 5.9) are lower than the in-situ Su measurements, considered all together. Re-organising the data pairs per test type, the divergence between the SHANSEP and Su;measured (Torvane) means is around 27 kPa (Su;SHANSEP (Torvane) mean = 8.5 kPa and Su;measured (Torvane) mean = 35.4 kPa, Table 5.10). Below -4 m NAP, however, a better correspondence between the SHANSEP calculated values and Su measurements is observed, being the difference between the SHANSEP and Su;measured (UU) means less than 1 kPa (Su;SHANSEP (UU) mean = 26.3 kPa and Su;measured (UU) mean = 27.0 kPa, Table 5.10).
The Su;SHANSEP values are in poor agreement with the Robertson (2015) Su calculated values (17.5 kPa lower, on average), as well as poorly correlated with the Bommer (2017) Su values for NA and DR sandy clays (36.5 kPa lower, on average) (Figure 5.20 and table 5.9).
The Su values obtained using the correlations suggested by Bommer et al. (2017a) and Robertson and Cabal (2015), in turn, correlate better with the in-situ data (All classes Su;measured mean = 33.2 kPa, Table 5.9), being the Su;Robertson and the $Su_{NA,DR;sandyclays}$ (All classes) means equal to 33.2 and 49.9 kPa, respectively (Table 5.9).
The plot in figure 5.21 displays the distribution over the depth of the Class 1 Su data and Su predicted values (calculated using the correlations suggested by Ladd and Foott, 1974, Bommer et al., 2017a, and Robertson and Cabal, 2015) and their ranges (± 1 standard deviation).
Figure 5.21 demonstrates that removing the Class 2 and 3 data pairs from the analysis the correlation between in-situ measurements and calculated Su values is slightly improved, even though the large scatter of in-situ measurements between 0 and -2 m NAP is not reduced.
The plot in figure 5.22 illustrates the distribution of Su measurements (organised in stratigraphic units after Bommer et al., 2017a) over the depth and the comparison between measured and calculated mean values. The points in red represent the Su measurements that belong to the Naaldwijk formation ($Su_{NA;sandyclays}$), and the solid red line their mean (34.2 kPa, Table 5.8). The points in green indicate the Su data belonging to the Drente formation ($Su_{DR;sandyclays}$), and the solid green line their mean (30.4 kPa, Table 5.8). The dashed-dotted line in red and the dashed line in green denote the mean value for the Naaldwijk and Drente formations, respectively, using the Bommer (2017) correlations. As shown in figure 5.22, the Bommer (2017) equations show an unsatisfactory correspondence with the laboratory data re-organised in such a way. The predicted mean for NA sandy clays (53.6 kPa, Table 5.8) overestimates the measured Su (NA) mean (34.2 kPa, Table 5.8) with a difference of almost 20 kPa, and the mean for DR sandy clays (40.0 kPa, Table 5.8) over-predicts of about 10 kPa the in-situ (DR) mean (30.4 kPa, Table 5.8).

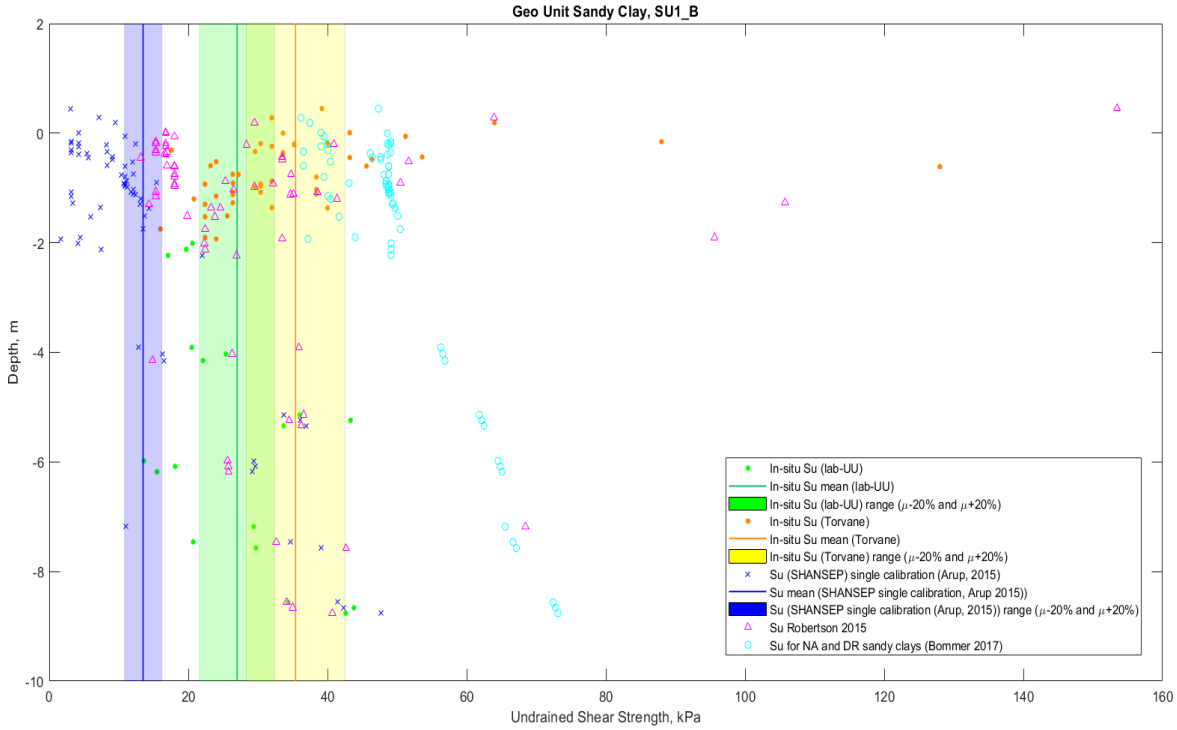

Figure 5.20: Su measurements and calculated values for the sandy Clay soil unit. Green dots: in-situ measurements (lab-UU) values; green solid line: mean; green area: mean ± 20%. Orange dots: in-situ measurements (Torvane) values; orange solid line: mean; yellow area: mean ± 20%. Blue crosses: calculated (SHANSEP, single calibration) values; blue solid line: mean; blue area: mean ± 20%. Magenta triangles: calculated (Robertson) values. Light blue circles: calculated (Bommer) values for NA and DR sandy clays.

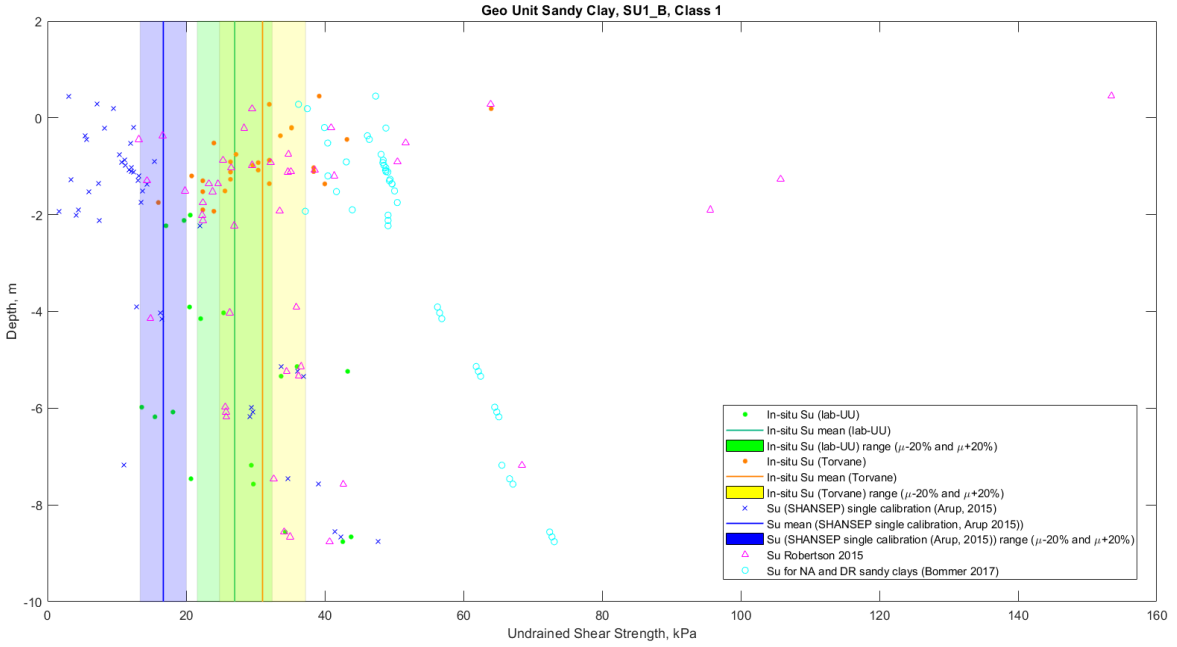

Figure 5.21: Class 1 Su measurements and calculated values for the sandy Clay soil unit. Green dots: Class 1 in-situ measurements (lab-UU) values; green solid line: mean; green area: mean ± 20%. Orange dots: Class 1 in-situ measurements (Torvane) values; orange solid line: mean; yellow area: mean ± 20%. Blue crosses: Class 1 calculated (SHANSEP, single calibration) values; blue solid line: mean; blue area: mean ± 20%. Magenta triangles: Class 1 calculated (Robertson) values. Light blue circles: Class 1 calculated (Bommer) values for NA and DR sandy clays.

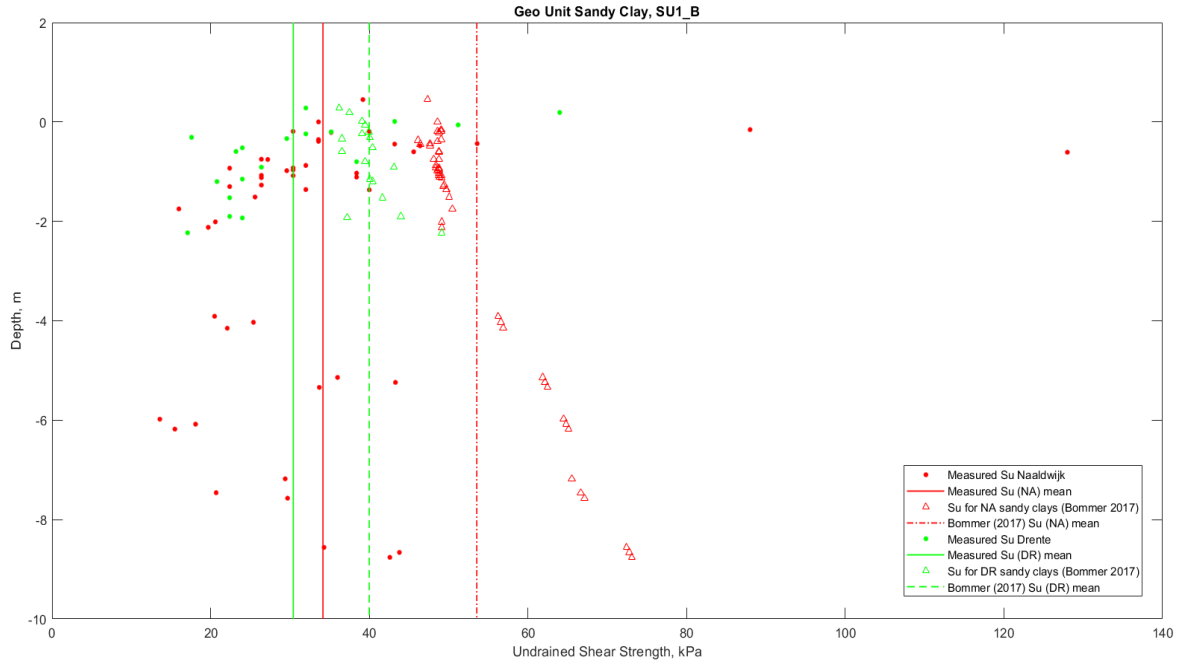

Figure 5.22: Su measurements and calculated mean values for the sandy Clay soil unit organised in stratigraphic units.

Table 5.8: Statistical characterisation of NA and DR formations in SU1_B unit.

Stratigraphic Unit	**Data-set**	**Statistical parameters**						
		N	min	max	μ	σ	COV	median
		[-]	[kPa]	[kPa]	[kPa]	[kPa]	[-]	[kPa]
NA	Su measured	49	13.6	128.0	34.2	18.2	0.53	30.4
	Su SHANSEP (1974)	49	3.0	47.7	15.3	12.3	0.80	11.2
	Su Robertson (2015)	49	13.2	153.5	30.8	23.5	0.76	25.7
	Su Bommer (2017)	49	46.2	73.1	53.6	8.0	0.15	49.1
DR	Su measured	18	17.1	64.0	30.4	12.3	0.41	25.2
	Su SHANSEP (1974)	18	1.7	22.0	8.7	5.2	0.60	8.4
	Su Robertson (2015)	18	15.3	95.6	32.9	21.6	0.66	25.4
	Su Bommer (2017)	18	36.2	49.1	40.0	3.1	0.08	39.7

Consistently with the previous plot (Figure 5.20), figure 5.23 shows an unacceptable performance of the SHANSEP model (single calibration, after Arup, 2015) with respect to the in-situ measurements (Torvane) and, conversely, a fair correlation among the data pairs obtained from the combination of in-situ measurements (lab-UU) and SHANSEP values.
On the other hand, figure 5.24a indicates an overall improved correlation between calculated (Robertson, 2015) Su values and both the in-situ measurements, although the Torvane data-sets are characterised by a larger scatter, which is visible also in figure 5.20.
Differently, figure 5.24b displays a better correspondence between the in-situ measurements (Torvane) and calculated (Bommer NA) Su values, and an over-estimation of the is-situ (lab-UU) data.

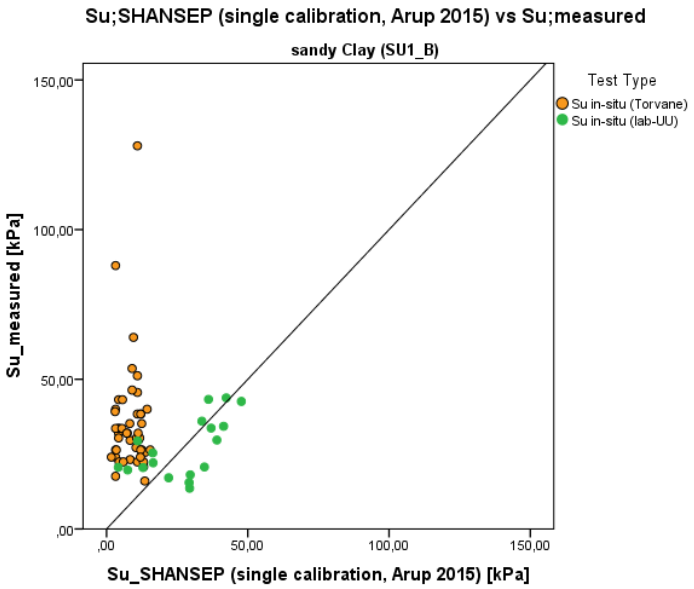

Figure 5.23: Scatter plot with equality line of Su data pairs for the sandy Clay soil unit. Green dots: data pairs of in-situ Su measurements (lab-UU) and SHANSEP calculated values. Orange dots: data pairs of in-situ Su measurements (Torvane) and SHANSEP calculated values.

Figure 5.24: Scatter plot with equality line of Su data pairs (calculated with the Robertson (2015) and Bommer (2017) correlations) for the sandy Clay soil unit.

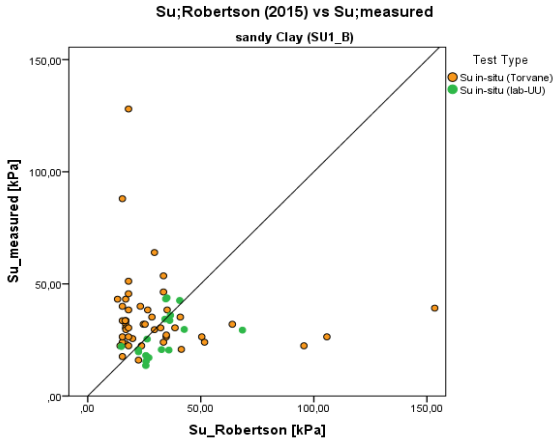

(a) Scatter plot with equality line of Su data pairs for the sandy Clay soil unit. Green dots: data pairs of in-situ Su measurements (lab-UU) and Robertson calculated values. Orange dots: data pairs of in-situ Su measurements (Torvane) and Robertson calculated values.

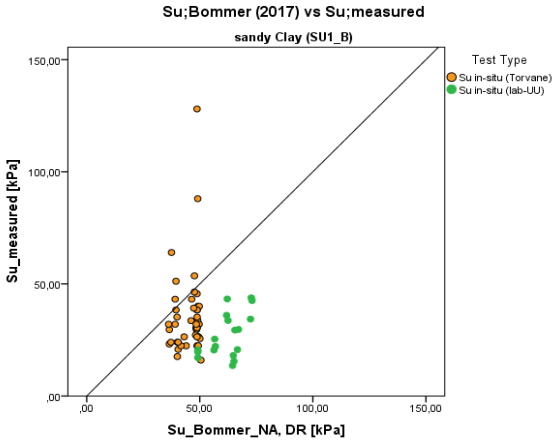

(b) Scatter plot with equality line of Su data pairs for the sandy Clay soil unit. Green dots: data pairs of Su measured (lab-UU) and Bommer NA, DR calculated values. Orange dots: data pairs of Su measured (Torvane) and Bommer NA, DR calculated values.

Data Distribution

Figures 5.25a, 5.26a, 5.26b, and 5.26c present the variability of the SU1_B soil unit, comprehending all the data pairs classified as sandy Clay, without making any consideration about the sample classes, whereas figures 5.25b depicts the variability of the Class 1 data-sets (measured vs calculated Su values with the three different correlations), and 5.25c displays the calculated SHANSEP (single calibration) data organised in classes. Of the 67 data pairs belonging to this unit, 45 are classified as Class 1, 7 as Class 2, and 15 as Class 3 (Table 5.9). Figure 5.25a shows that, among the three correlations considered, the Ladd and Foott (1974) equation, using the S and m parameters suggested by Arup (2015), underestimates the undrained shear strength for the SU1_B unit by the most. The Bommer et al. (2017a), in contrast, overestimates the in-situ measurements.

Comparing figures 5.25a and 5.25b, the correspondence between the calculated and measured Class 1 data-sets is slightly improved, being some of the outliers removed. However, the variability of the data-sets remains almost unvaried, in agreement to figure 5.21.
Figure 5.25c shows that the difference between measured and calculated (SHANSEP, single calibration) medians becomes minimum for the Class 1 data-sets, in which the median of the Su measurements is 29.4 kPa and the median of the Su;SHANSEP is 12.4 kPa (Table 5.9). Conversely, in the Class 3 data-set, composed of samples collected at depths between 0 and -0.75 m, the median of the Su measured data-set is 33.6 kPa and the median of the Su;SHANSEP data-set is 4.3 kPa.
Figures 5.26a, 5.26b, and 5.26c illustrate the distribution of Su data (calculated with SHANSEP single calibration, Robertson (2015), and Bommer (2017), respectively) re-organised based on the type of test.
The SHANSEP correlation underestimates the Torvane in-situ data, and slightly overestimates the UU measurements (Figure 5.26a). Similarly, the Robertson (2015) equation underestimates the Torvane in-situ data, while overestimating the UU measurements (Figure 5.26b). Diversely, the Bommer (2017) overestimates both the Torvane and UU in-situ measurements. Their exploratory statistics can be found in table 5.10.

Table 5.9: Statistical characterisation of the SU1_B unit organised in sample classes for the three correlations considered (SHANSEP, 1974, Robertson, 2015, Bommer, 2017) and the in-situ measurements.

Class	**Data-set**	**Statistical parameters**						
		N	min	max	μ	σ	COV	median
		[-]	[kPa]	[kPa]	[kPa]	[kPa]	[-]	[kPa]
All classes	Su measured	67	13.6	128.0	33.2	16.8	0.51	30.4
	Su SHANSEP (1974)	67	1.7	47.7	13.5	11.2	0.83	10.9
	Su Robertson (2015)	67	13.2	153.5	31.1	22.9	0.74	25.7
	Su Bommer (2017)	67	36.2	73.1	49.9	9.3	0.19	48.8
1	Su measured	45	13.6	64.0	29.4	9.7	0.33	29.4
	Su SHANSEP (1974)	45	1.7	47.7	16.7	12.3	0.74	12.4
	Su Robertson (2015)	45	13.2	153.5	37.7	25.4	0.67	32.6
	Su Bommer (2017)	45	36.2	73.1	52.3	10.0	0.20	49.1
2	Su measured	7	22.4	53.6	34.5	12.0	0.35	30.4
	Su SHANSEP (1974)	7	3.2	10.9	8.2	3.5	0.43	9.0
	Su Robertson (2015)	7	15.3	33.5	21.7	8.2	0.38	18.0
	Su Bommer (2017)	7	39.5	49.1	45.9	4.2	0.09	47.6
3	Su measured	15	17.6	128.0	43.7	28.5	0.65	33.6
	Su SHANSEP (1974)	15	3.2	12.1	6.4	3.4	0.53	4.3
	Su Robertson (2015)	15	15.3	18.0	16.7	1.0	0.06	16.8
	Su Bommer (2017)	15	36.5	49.1	44.7	5.3	0.12	48.6

Figure 5.25: Box-and-Whiskers-Diagram from measured and calculated (SHANSEP, 1974, Robertson, 2015, and Bommer, 2017) Su values for the sandy Clay soil unit.

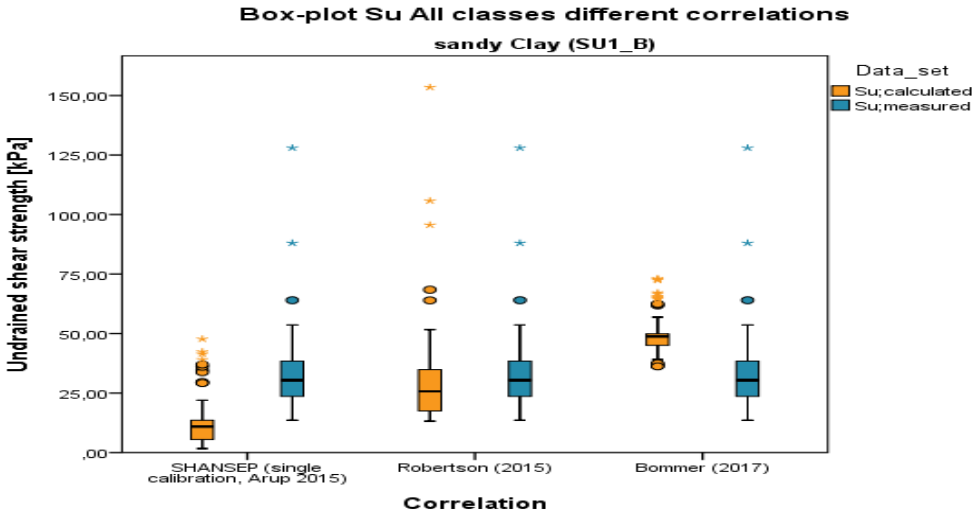

(a) Box-and-Whiskers-Diagram from measured and calculated (SHANSEP, 1974, Robertson, 2015, and Bommer, 2017) Su values for the sandy Clay soil unit.

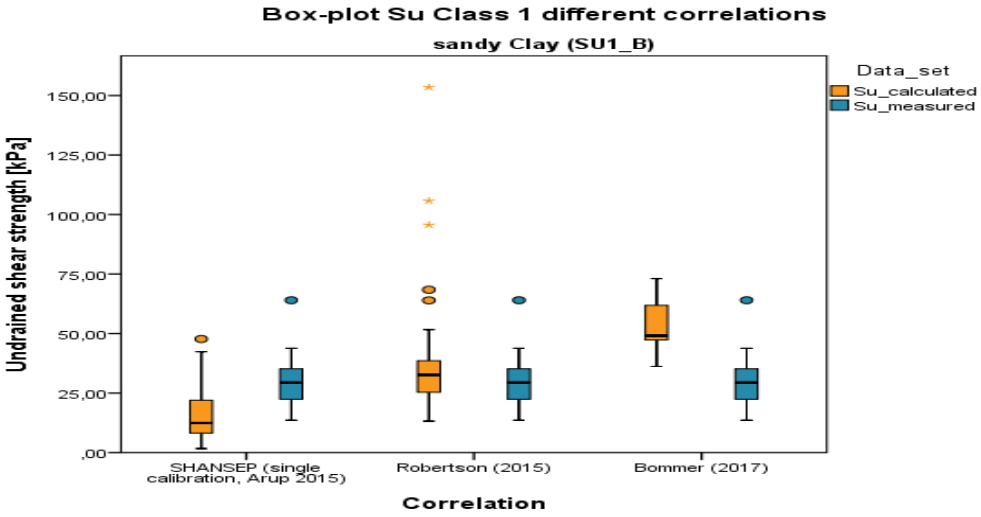

(b) Box-and-Whiskers-Diagram from measured and calculated (SHANSEP, 1974, Robertson, 2015, and Bommer, 2017) Class 1 Su values for the sandy Clay soil unit.

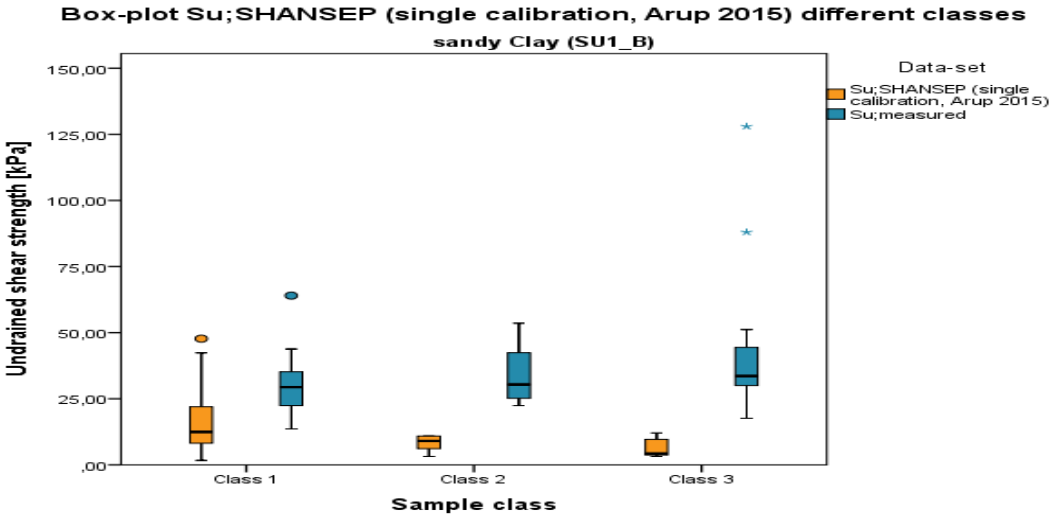

(c) Box-and-Whiskers-Diagram from measured and calculated (SHANSEP, 1947) Su values for the sandy Clay soil unit.

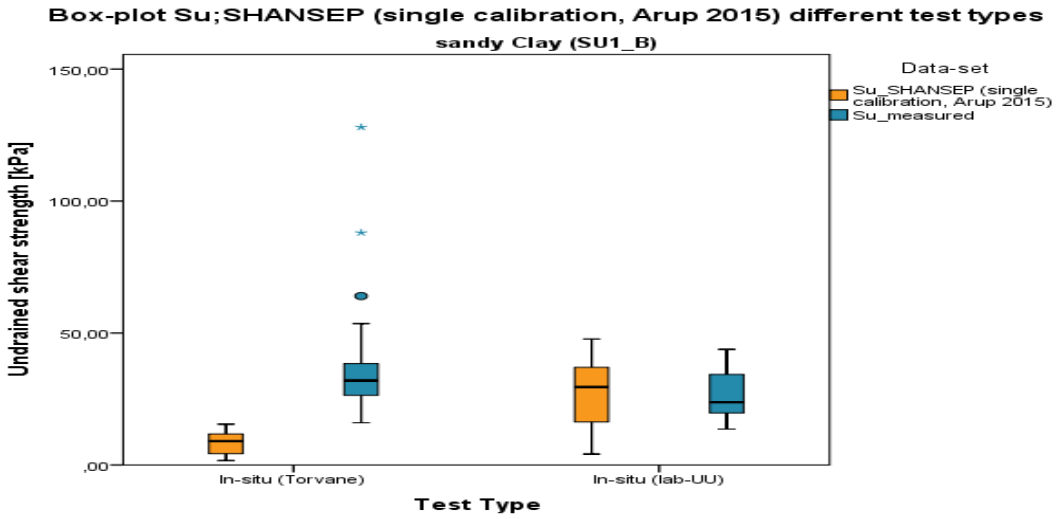

(a) Box-and-Whiskers-Diagram from measured and calculated (SHANSEP, 1947) Su values for the sandy Clay soil unit.

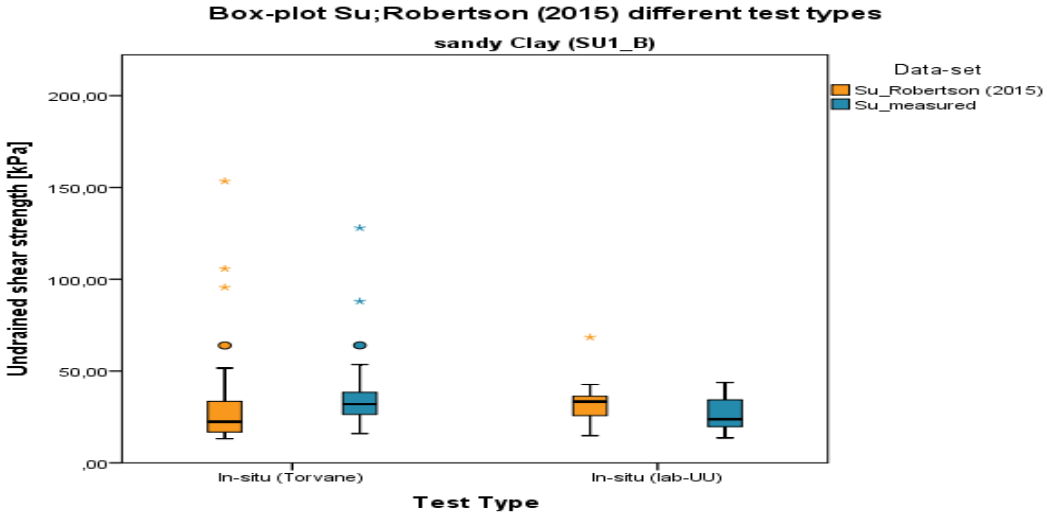

(b) Box-and-Whiskers-Diagram from measured and calculated (Robertson, 2015) Su values for the sandy Clay soil unit.

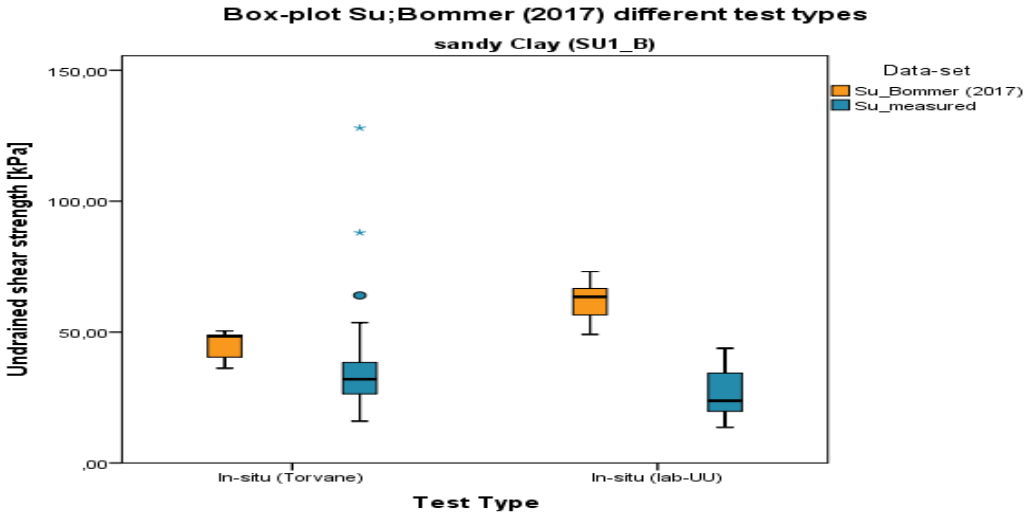

(c) Box-and-Whiskers-Diagram from measured and calculated (Bommer, 2017) Su values for the sandy Clay soil unit.

Table 5.10: Statistical characterisation of the SU1_B unit's data-sets (all classes) organised in types of test for the three correlations considered (SHANSEP, 1974, Robertson, 2015, Bommer, 2017) and the in-situ measurements.

Test Type	**Data-set**	**Statistical parameters**						
		N	min	max	μ	σ	COV	median
		[-]	[kPa]	[kPa]	[kPa]	[kPa]	[-]	[kPa]
UU	Su measured	18	13.6	43.8	27.0	9.9	0.37	23.8
	Su SHANSEP (1974)	18	4.1	47.7	26.3	13.1	0.50	29.5
	Su Robertson (2015)	18	14.9	68.4	32.6	11.5	0.35	33.4
	Su Bommer (2017)	18	49.1	73.1	62.0	7.7	0.12	63.5
Torvane	Su measured	49	16.0	128.0	35.4	18.3	0.52	32.0
	Su SHANSEP (1974)	49	1.7	15.5	8.5	3.9	0.46	9.0
	Su Robertson (2015)	49	13.2	153.5	30.9	25.9	0.84	22.4
	Su Bommer (2017)	49	36.2	50.5	45.5	4.7	0.10	48.4

5.4. Summary and Conclusions

The present chapter provides exploratory statistical analysis carried out on the data compiled in the GI database. The available data were grouped per geotechnical unit in order to compare the laboratory measurements with the values obtained by using different CPT-based correlations. The PI measured at the laboratory are compared with values calculated with the Cetin and Ozan (2009) correlation and the values suggested by Bommer et al. (2017a). Whilst, Su measurements are compared with values calculated with the Ladd and Foott (1974) (single calibration), Robertson and Cabal (2015) and Bommer et al. (2017a) correlations.
In this chapter, the predominant soil units (i.e. clean Clay for PI and clean and sandy Clay for Su) are analysed in detail, presenting several plots and tables containing descriptive statistics for each unit. The remaining soil units are reported in Appendix C. Nonetheless, the results regarding all the units investigated in this research are herein reported.

5.4.1. PI Data

The majority of the samples provided with PI measurements are classified as Clay, namely 376 out 413. The predominant units are sandy Clay, silty Clay, soft, clean Clay, and organic Clay, with 208, 110, 32 and 26 samples, respectively. The remaining 37 samples are defined as Sand (20 measurements), Peat (11 measurements), overconsolidated Clay (4 measurements), and Loam (2 measurements) (Table 5.2).
It was not always possible to find suitable CPTs to compare the PI measurements with, in fact, only 378 out of 413 PI measurements are paired with PI calculated values (Table 5.2).
Following the comparison of the laboratory PI measurements with the predicted PI using the Cetin and Ozan (2009) correlation and the suggested PI values from Arup (2015) and Bommer et al. (2017a), table 5.11 lists the individuated geotechnical units proposed in this research and gives a qualitative indication of the measured-predicted values correspondence.

Table 5.11: Summary table of general trends of predicted PI mean values with respect to their corresponding measured mean values for every geotechnical soil unit, representing the overall assessment of the Cetin and Ozan (2009) correlation adequacy.

Soil Unit [SU]	**Soil Type** [-]	**General Trend of Cetin& Ozan (2009) Mean Value** [-]
SU1_A	Clay, clean, soft	In good agreement/slightly under-predicted
SU1_B	Clay, sandy	In good agreement
SU1_D	Clay, organic	Under-predicted
SU1_E	Clay, silty	Under-predicted
SU2	OC Clay	Under-predicted
SU3	Sand	Under-predicted
SU4	Peat	Under-predicted
SU5	Loam	In good agreement

Soft, clean Clay (SU1_A)

The soil unit SU1_A contains 24 (out of 30 data pairs) samples that were collected at shallow depths (approximately from 0.4 to -4 m NAP, figure 5.3). Results revealed that:

- The laboratory measurements were in fair agreement (slightly overestimated) with the PI values derived with the empirical model from Cetin and Ozan (2009) (especially above -4 m NAP).
- Both PI measured and $PI_{C\&O}$ values were contained within the boundaries for clean clays belonging to the Drente, Naaldwijk, and Boxtel formations, suggested by Bommer et al. (2017a), and were located close to the PI value recommended by Arup (2015) (Figure 5.5).
  From the direct comparison with the geological units, the factual data correlated well to the values recommended by Bommer et al. (2017a), e.g. the measurements from the NA, BX units. Only the measurements from the DR unit were under-predicting the corresponding V4 suggested PI (Table 5.3.
- The factual data mean was in fair agreement with the PI suggested by Arup (2015), whilst the $PI_{C\&O}$ resulted slightly lower.
- The PI values of this soil unit appeared to be described by normal or slightly positively skewed distributions. Log-normal distributions may have been used to account for positive skewness of linear data,

confirming the fact that PI is a non-negative soil property.

Sandy Clay (SU1_B)

The soil unit SU1_B contains 208 PI measurements and 202 data pairs. The vast majority of the samples were collected at a depth ranging from 1 to -2.5 m NAP, where a large scatter of PI values is observed. Results revealed that:

- The PI measurements were under-predicted by the Cetin and Ozan (2009) CPT-based correlation (Figure C.1 and table C.2).
- The Bommer et al. (2017a) PI for NI sandy clays was overestimating the PI;measured. The PI for NA and PE sandy clays were in fair agreement with the PI;measured, whilst and the PI for DR sandy clays was underestimating the PI;measured (Figure C.1).
  However, from the direct comparison with the geological units, the Bommer et al. (2017a) recommended values showed a fair correspondence with the NI, NA, and DR measured means, except for the PI for DR sandy clays which was lower than the PE;measured Su (Table C.1).
- The PI suggested by Arup (2015) gave a good approximation of the PI for this soil unit, whilst it was higher than the $PI_{C\&O}$.
- Similarly to the SU1_A unit, the distribution of PI values was described by approximately normal or slightly positively skewed distributions. Transformation of the data-sets into logarithmic data-sets showed that the positive skeweness could be reduced.

Silty Clay (SU1_E)

The soil unit SU1_E comprehends 110 Su measurements and 98 data pairs. Out of 98 samples, 95 are collected at shallow depths (from 0.92 to -2 m NAP, figure C.8). Results reveal that:

- The factual data were underestimated by the Cetin and Ozan (2009) empirical correlation (Table C.4).
- The PI for NI sandy clays overestimated the PI;measured, the PI for NA sandy clays was in line with the PI;measured, and the PI for DR sandy clays underestimated the PI;measurements (Table C.3).
  However, from the direct comparison with the geological units, the Bommer et al. (2017a) recommended values showed a fair correspondence with the NI, NA, and DR measured means, except for the PI for AAOP sandy clays which is significanty higher than the corresponding AAOP;measured.
- The factual data, as well as the $PI_{C\&O}$ were underestimated by the PI suggested by Arup (2015).
- The distribution of PI values can be approximated to normal or slightly positively skewed distributions.

Other soil units

From the analysis presented in Appendix C, (Section C.2.3), it was observed that the laboratory tests are not necessarily accurate in the estimation of plasticity index of soils such as Peat (SU4) and Sand (SU3) (e.g. measured PI mean for sands is equal to 55.7 % and for Peat is 173.2 %). Consequently, it was difficult to assess the adequacy of the CPT based correlations for these soil units. On the other hand, for the unit OC Clay (SU2) and Loam (SU5) it was difficult to evaluate the correlation proficiency due to the scarce of available laboratory data (i.e. 4 measurements in the SU2 unit and 2 PI measurements for the SU5 unit).
Results revealed that:

- The PI measurements from the OC Clays unit (4 measurements) were underestimated by the Cetin and Ozan (2009) model. However, they were in good agreement with the PI for NI clean and/or sandy clays, but higher than the PI for DR clays recommended by Bommer et al. (2017a).
- The PI data from the Sand unit (20 measurements) were higher than the values derived from the Cetin and Ozan (2009) model, but they showed good correspondnce with the values suggested by Bommer et al. (2017a) for NA, BX and AAOP clayey sands.

- The PI data for Peat (7 measurements) were extremely high in comparison with the values derived from the Cetin and Ozan (2009) model. Similarly, the factual data largely over-predicted the PI for the NIHO and NIBA soil units from Bommer et al. (2017a).
- The laboratory measurements from the Loam unit (2 measurements) resulted to be in good agreement with the predicted values from Cetin and Ozan (2009). In contrast, the factual data were found to be higher than the V4;PI for Peelo materials.

General Conclusions

- The depth mismatch between specimens and CPT measurements depth affected negatively the results. Box-plots (Figures 5.9, C.7, C.14) revealed that the difference between measured and predicted PI mean values for the Class 2 and Class 3 data-sets was higher than the Class 1 data-set.
- Comparing one-to-one the geological units, the laboratory measurements matched well the V4 recommended values. In particular the NA, DR, NI, BX and PE units provided an adequate indication of the plasticity index of such materials. On the other hand, comparing the soil units as used in this research (e.g. SU1_A, SU_B), which comprehend more geological units, with the suggested V4 values, the difference between means increased significantly. Such "generalised" soil classification, however, created outcomes overall in fair agreement with Arup (2015) and the V4 ranges (e.g. yellow area in figure 5.3).
- In general, it can be concluded that the Cetin and Ozan (2009) correlation describes relatively well the plasticity index of the clean Clay, sandy Clay and Loam soil units. Conversely, the model under-predicts the PI of the other soil units (Table 5.11).
  Therefore, the Cetin and Ozan (2009) correlation cannot be generalised for all clayey materials present in Groningen, and other approaches are recommended (i.e. Bommer et al., 2017a PI values).

5.4.2. Su Data

The majority of the samples provided with Su measurements are classified as Clay, namely 141 out 161. The most consistent units are sandy Clay (SU1_B), silty Clay (SU1_E), and soft, clean Clay (SU1_A), with 79, 55, and 7 samples, respectively. The remaining 20 samples are organised in the overconsolidated Clay (SU2) (9 measurements) and Sand (SU3) (11 measurements) units. Of the 161 Su measurements, however, only 113 have were used in the statistical analysis, consisting of in-situ Torvane and laboratory (UU) triaxial tests. Precisely, 67 measurements in the sandy Clay unit, 23 in the silty Clay unit, 3 in the soft, clean Clay unit, 9 in the overconsolidated Clay unit, and 11 in the Sand unit (Table 5.6).
For the in-situ Su measurements it was always possible to find suitable CPTs to compare the factual data with. Following the comparison of the in-situ data with the predicted Su using the Ladd and Foott (1974), Robertson and Cabal (2015) and Bommer et al. (2017a) empirical models, table 5.12 lists the individuated geotechnical units and gives a qualitative indication of the measured-predicted (SHANSEP) values correspondence.

Table 5.12: Summary table of general trends of predicted Su mean values with respect to their corresponding measured mean values for every geotechnical soil unit, representing the overall picture of the SHANSEP (Ladd and Foott, 1974) (with single calibration) model adequacy.

Soil Unit	**Soil Type**	**General Trend of SHANSEP (1974) Mean Value**	
[SU]	[-]	Torvane	lab-UU
SU1_A	Clay, clean, soft	-	Under-predicted
SU1_B	Clay, sandy	Under-predicted	Under-predicted
SU1_E	Clay, silty	Under-predicted	Over-predicted
SU2	OC Clay	-	Over-predicted
SU3	Sand	Under-predicted	Over-predicted

Soft, clean Clay (SU1_A)

The soil unit SU1_A contains 7 samples in total of which only 3 (i.e. the lab-UU measurements) are considered to representative of the in-situ conditions. These were collected at depths ranging from approximately from -1 to -2 m NAP.

- The in-situ measurements (lab-UU) were largely underestimated (20 kPa lower on average) by the SHANSEP correlation (with single calibration, after Arup (2015)) (Table 5.7).

- The in-situ measurements were underestimated as well by using the Bommer et al. (2017a) and Robertson and Cabal (2015) equations (7 kPa and 3 kPa lower on average, respectively, Table 5.7).

- Due to the scarce amount of in-situ measurements it was difficult to quantitatively assess the correlations' adequacy.

Sandy Clay (SU1_B)

The soil unit SU1_B contains 79 data pairs, of which 12 were tested with triaxial (CU) tests, 18 with triaxial (UU) tests, and 49 with Torvane tests (Table 5.10). Only the in-situ measurements obtained from Torvane and triaxial (UU) tests were considered, therefore, a total of 67 measurements were analysed in this chapter. The in-situ measurements (Torvane) were collected at a depth range between 0 and -2 m NAP, whilst the triaxial UU Su value were collected from apporximately -2 to -9 m NAP. In order to account for difference between samples and CPT measurements depths, the 67 data pairs were re-organised in sample classes, precisely 45 were classified as Class 1, 7 as Class 2, and 15 as Class 3 (Table 5.9).

- Both the in-situ measurements were under-predicted by Ladd and Foott (1974) correlation (with single calibration, after Arup, 2015) (Table 5.10).

- In contrast, the Bommer et al. (2017a) equations for DR and NA sandy clays overestimated both the in-situ measurements. Precisely, the stratigraphic unit-based equations produced Su values which were 10 kPa (on average) larger than the Torvane measurements (Table 5.10) and around 35 kPa (on average) larger than the laboratory (UU) data.

- The Robertson and Cabal (2015) correlation, differently, produced Su values in fair agreement with both the in-situ measurements. The difference between the Su;Robertson means and the Su;measured means was around 5 kPa, in both cases (Table 5.10). Moreover, at shallow depths (between 0 and -2 m NAP), the large scatter of the in-situ measurements obtained with Torvane tests was reasonably well reproduced by the Robertson and Cabal (2015) correlation.

- Comparing figures 5.25a and 5.25b, the correspondence between the calculated and measured Class 1 data-sets was slightly improved, being some of the outliers removed. However, the variability of the data-sets remained almost unvaried, in agreement to figure 5.21.

Silty Clay (SU1_E)

The soil unit SU1_E (silty Clay) is composed of 55 measurements (collected at depths between 1 and -9 m NAP), of which 20 were tested with Torvane tests, 32 with triaxial (CU) tests, and 3 with triaxial (UU) tests (Table C.8). Only the in-situ measurements obtained from Torvane and triaxial (UU) tests were analysed in this chapter (23 measurements in total). In order to account for the difference between samples and CPT measurements depths, the 23 data pairs were re-organised in sample classes, precisely 15 are classified as Class 1, and 8 as Class 3 (Table C.7).

- Comparing the results of both types of tests (Torvane and UU) with the values obtained using the SHANSEP correlation (with single calibration, after Arup (2015)) a poor correspondence was observed. The Ladd and Foott (1974) correlation under-predicted the in-situ (Torvane) measurements, while overestimating the in-situ (UU) measurements (Table C.8).

- Similarly, the Robertson and Cabal (2015) correlation over-predicted the in-situ measurements (lab-UU), however, it matched almost perfectly the Torvane data, being able to satisfactorily reproduce the large spatial variability of the uppermost soil layers (Table C.8 and figure 5.20).

- The empirical equations for DR, NA, AAOP, and NI sandy clays, predicted Su values in fair agreement with the Torvane data (slightly over-predicted), however, the in-situ measurements (lab-UU) were largely underestimated, with a difference between the means of more than 55 kPa (Table C.8).

- Comparing figures C.20a and C.20b, the correspondence between the calculated and measured Class 1 data-sets remained almost unvaried, consistently with figures 5.20 and 5.21.

Other soil units

From the analysis of the other soil units (Appendix C, Section C.3.2), it is possible to conclude that:

- The factual data (9 measurements) from the SU2 unit resulted to be lower than the predicted Su values using the Ladd and Foott (1974), Robertson and Cabal (2015) and Bommer et al. (2017a) empirical models.
- From the analysis of the SU3 soil unit (11 measurements), the SHANSEP correlation underestimated the in-situ measurements. In contrast, the Robertson and Cabal (2015) and Bommer et al. (2017a) empirical models predicted values higher than the laboratory data. The in-situ data were significantly overestimated in particular when only the Class 1 were considered.
- Considering that clean sands are cohesionless materials, it is very unlikely to observe, in reality, an undrained behaviour. However, at large level of strains also a sand can exhibit undrained conditions (see Chapter 2, Section 2.5.2). Furthermore, the undrained behaviour observed in-situ and at the laboratory can be explained by the presence of fine materials, such as clay and silt, within the sandy samples.
  This theoretical observation suggests that the above CPT-based correlations can be utilised only for the estimation of Su for silty and/or clayey material, whilst they are observed to be partially inappropriate to describe the shear strength of clean sands. In this case, correlations based on the internal friction angle (e.g. critical state theory, after Schofield and Wroth, 1968) should be considered for a more accurate estimation of the shear strength.

General Conclusions

- In general, it can be concluded that the SHANSEP (Ladd and Foott, 1974) model (with single calibration, after Arup (2015)) consistently under-predicts the undrained shear strength of the majority of the clayey soil materials analysed in this thesis, particularly at shallow depths (e.g. 1 to -3 m NAP).
  The main reason behind this poor predicted-measured correspondence is the fact that the effective soil stresses below the ground surface (used in the CPT-based correlations for the estimation of Su) account for a relatively small amount of soil material proportional to the depth. This results in low σ'_v values, which may not be truly representative of the actual in-situ conditions.
  Furthermore, the SHANSEP correlation is a function of the OCR, which is a difficult soil parameters to determine with high accuracy from CPT profiles. Especially at shallow depths, the in-situ OCR can be affected, for instance, by different consolidation states due to human activity and partially saturated soil behaviour as a consequence of desiccation and fluctuation of the groundwater table. Such conditions are not always adequately captured by common CPT testing techniques, leading to an unsatisfactory correlation's performance.
  Moreover, large amounts of uncertainty are associated to the laboratory data, which are not necessarily representative of the actual in-situ conditions. With triaxial tests, for example, the obtained stress paths and the applied pre-consolidation pressures may be different from the stress states which the soil samples were subjected to in reality. Similarly, the Torvane tests can yield Su values higher than the actual undrained shear strength of shallow clay deposits, given that several factors, such as pore water pressure development, rate of loading etc., are not fully taken into account.

6

Correlation Improvement and Validation

6.1. Introduction

The purpose of this chapter is to illustrate the derivation of new site-specific correlations for the estimation of the undrained shear strength of Holocene Clay soils in Groningen.
Both analytical approaches and regression analyses are performed in order to calibrate the SHANSEP parameters, S and m, based on the available laboratory (CU) measurements provided with pre-consolidation data. The Su values obtained using the SHANSEP model adjusted with the best estimate of these parameters are then compared with the in-situ measurements (Torvane and lab-UU).

6.2. Analytical Calibration of SHANSEP Model

As already mentioned in Chapter 3, according to the SHANSEP procedure, the undrained shear strength of normally consolidated clays, normalised with respect to the current effective vertical stress σ'_v, is unique and constant for each soil type. The importance of this statement relies on the fact that if the undrained shear strength of a clay can be measured or evaluated for a normally consolidated sample, then its value can be determined for other specimens of the same clay, provided that the overconsolidation state is known. Based on the available laboratory (CU) tests (29 in total), different approaches were considered with the aim of calibrating the SHANSEP parameters S and, subsequently, m for different soil types. Hereafter, only one approach is reported. The reader is asked to refer to Appendix D (Section D.1.1 for information about the second analytical approach.

6.2.1. Estimation of S and m - Approach 1

The first approach follows directly the Ladd and Foott (1974) framework.
If the soil has experienced only isotropic stress through laboratory (CU) testing, the normalised undrained shear strength for normally consolidated clays (S) can be obtained by normalising the Su of NC samples with respect to the initial confinement stress applied to the specimen before undrained shear to failure (Wood, 1990).
Following, the m parameter is calibrated by using the SHANSEP equation to fit the data grouped per different overconsolidation ratios, plotted in the $t_{15\%strain} - s'_0$ space.
The calibration of the S and m parameters is executed as an iterative process, aimed to obtain an average coefficient of determination (R^2) as close as possible to 1. R^2=1 indicates a perfect linear association (more details in Appendix D, Section D.3).
The values of S and m obtained with such a procedure (Table 6.1) are consistent with the range of values published by Mayne (1980) and Mayne (1988) for various clay types, and the average coefficient of determinations (calculated according to Equation D.6, Appendix D) are acceptably high (Table 6.1).
Figures 6.1a, 6.1b and 6.1c illustrate an example of the SHANSEP calibration procedure for the three types of soil provided with NC data. The orange points refer to the normally consolidated measurements and the orange soil line their SHANSEP fit. The blue points denote the measurements with OCR=2 and the solid blue line their SHANSEP fit. The red points represent the measurements with OCR=4 and the solid red line their SHANSEP fit. The green points refer to the measurements with OCR=6 and the solid green line their

SHANSEP fit. Note that the SHANSEP fit lines shown in these figures are created using the best parameters S and m, indicated in table 6.1.

Table 6.1: SHANSEP parameters S and m for the SU1_A, SU1_B, and SU1_E soil units, obtained from the analysis of 9 NC and 30 OC measurements, following Approach 1.

Soil Unit	**Stratigraphic Unit**	**SHANSEP parameters**		**Best SHANSEP parameters**		**R^2**
		S	**m**	**S**	**m**	
[SU]	[-]	[-]	[-]	[-]	[-]	[-]
SU1_A (n=8)	Clay, clean, soft	0.40 - 0.49	0.55 - 0.70	0.42	0.67	0.992
SU1_B (n=13)	Clay, sandy	0.36 - 0.61	0.65 - 0.70	0.47	0.57	0.966
SU1_E (n=18)	Clay, silty or Silt, clayey	0.32 - 0.59	0.55 - 1.00	0.39	1.00	0.854

Figure 6.1: Calibration of the SHANSEP model parameters for the SU1_A, SU1_B, and SU1_E soil units following Approach 1.

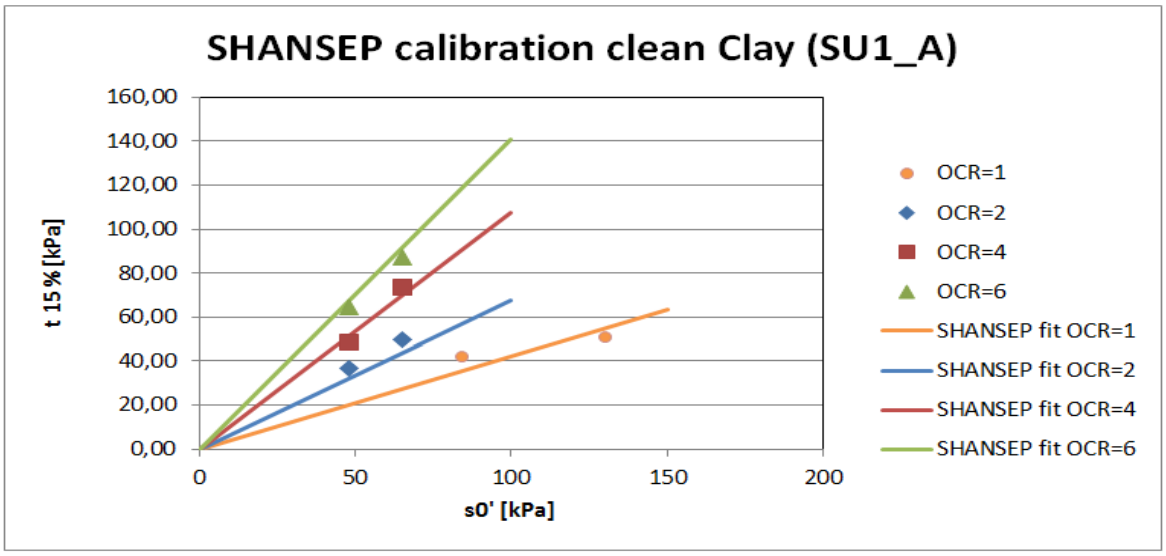

(a) SHANSEP fit of NC and OC laboratory (CU) data from the SU1_A soil unit

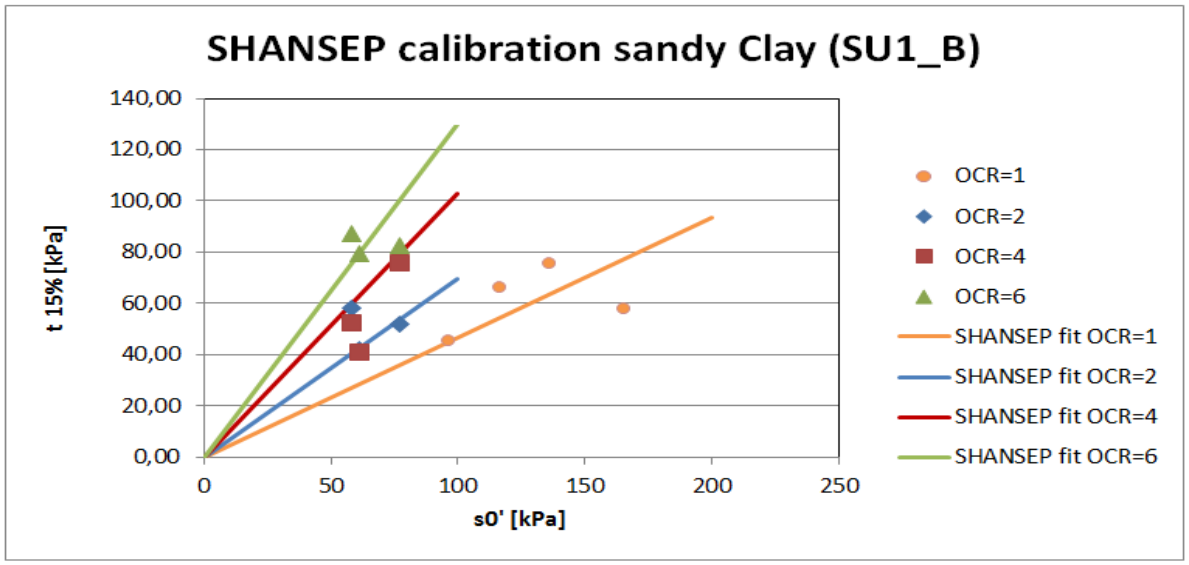

(b) SHANSEP fit of NC and OC laboratory (CU) data from the SU1_B soil unit

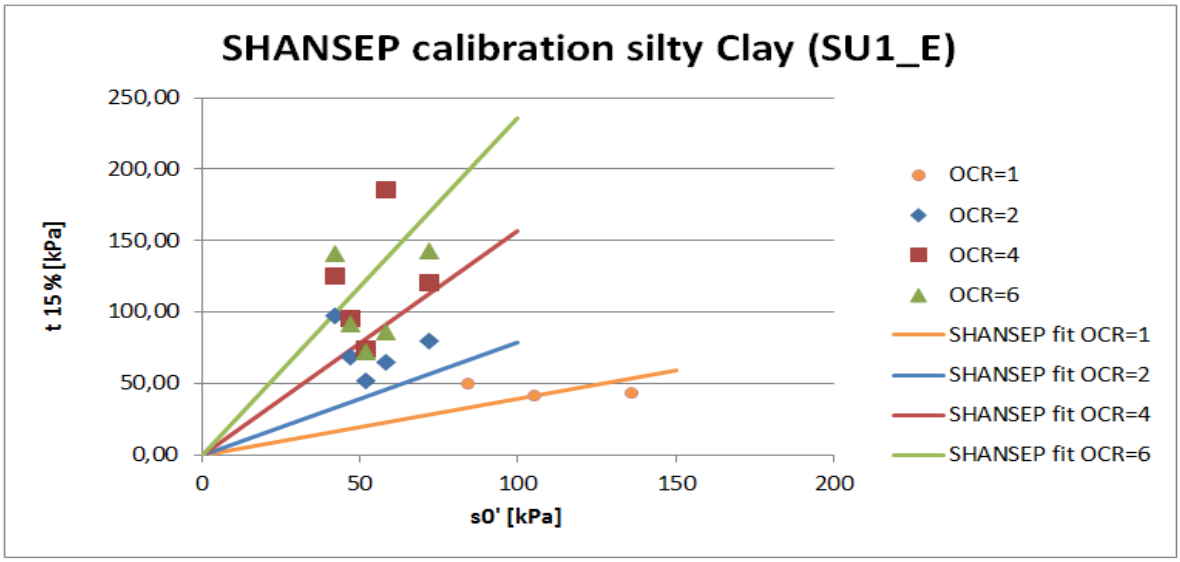

(c) SHANSEP fit of NC and OC laboratory (CU) data from the SU1_E soil unit

6.3. Regression Analysis

In order to validate the SHANSEP parameters presented in the previous section (Section 6.2), linear and non-linear regression analyses in SPSS are conducted between the normalised undrained shear strength for over-consolidated clays and the logarithm of OCR, in order to determine the value of S and m for each soil considering the OC data all together.
The normalised strength is generally presented by various authors (e.g. Ladd and Foott, 1974, Mayne, 1980) as (Su/σ'_{v0}), where σ'_{v0} represents the initial vertical stress. In the following sections, however, the normalised strength is expressed as (Su/σ'_c) given that σ'_c is the mean stress to which the samples are subjected prior the shearing phase, thus, the initial vertical stress.
In the following section only the results of the non-linear regression analysis are reported. The outcomes of the linear regression analysis can be found in Appendix D (Section D.2).

6.3.1. Soil Unit: Soft, clean Clay (SU1_A)

The non-linear regression analysis was performed on the soft, clean Clay unit, using a total amount of 3 triaxial (CU) measurements provided with pre-consolidation and confinement pressures data.
The results of the non-linear regression analysis are shown in figure 6.2. Visual inspection of the scatterplot of normalised undrained shear strength against OCR (in logarithmic scale) indicates a power relationship between the variables.
The prediction equation results: $Su/\sigma'_c = 0.543 * OCR^{0.521}$. The estimated S coefficient (0.543) is statistically significant, $p(S) = 0.036 < 0.05$, accounting for 99.4% of the variation in normalised undrained shear strength with $R^2 = 0.994$. However, there is insufficient evidence to conclude that there is a significant relationship between the dependent variable and the OCR exponent, since the coefficient m is not significantly different from zero ($p(m) = 0.051 > 0.05$).
Nevertheless, the resulting coefficients S and m fall within the range of S and m values obtained from the procedure presented in the previous section (Section 6.2, Table 6.1).

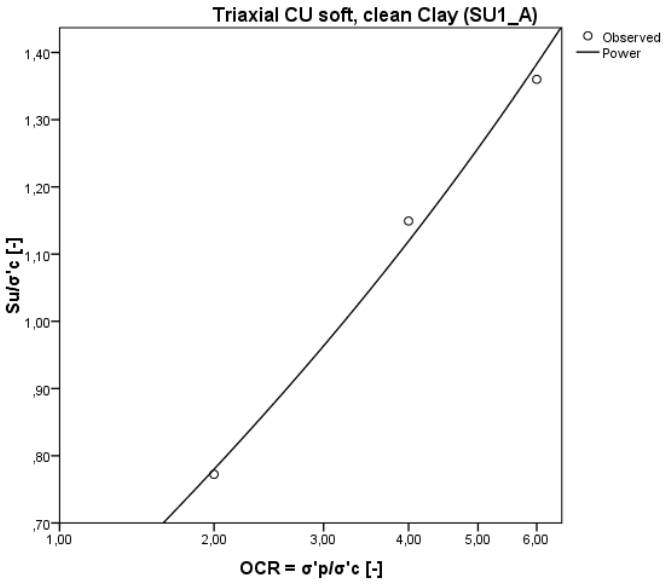

Figure 6.2: Non-linear regression analysis for 3 triaxial CU measurements from the SU1_A soil unit.

6.3.2. Soil Unit: Sandy Clay (SU1_B)

For the sandy Clay unit, a total amount of 9 triaxial (CU) measurements, provided with pre-consolidation and confinement pressures data, was used in the non-linear regression analysis.
Similarly to the SU1_A unit, figure 6.3 confirms the existence of a power relationship between the variables.
The prediction equation results: $Su/\sigma'_c = 0.501 * OCR^{0.536}$, in which the estimated S and m coefficients (0.501 and 0.536, respectively) are both statistically significant, $p(S) = 0.000 < 0.05$ and $p(m) = 0.000 < 0.05$, ac-

counting for 89.2% of the variation in normalised undrained shear strength with $R^2 = 0.892$.
Also in this case, the resulting coefficient S are contained within the range of S values obtained from the procedure presented in the previous section (Section 6.2, table 6.1), but the m is smaller.

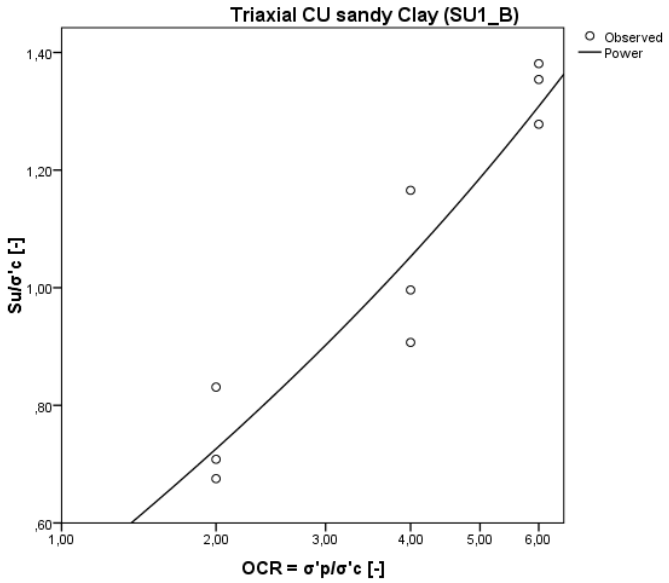

Figure 6.3: Non-linear regression analysis for 9 triaxial CU measurements from the SU1_B soil unit.

6.3.3. Soil Unit: Silty Clay (SU1_E)

The non-linear regression analysis performed for the silty Clay unit is based on a total amount of 9 triaxial (CU) measurements provided with pre-consolidation and confinement pressures data.
Figure 6.4 depicts a power relationship in the form of: $Su/\sigma'_c = 0.682 * OCR^{0.503}$, where the estimated S and m coefficients (0.682 and 0.503, respectively) are statistically significant, $p(S) = 0.003 < 0.05$ and $p(m) = 0.016 < 0.05$, accounting for 58.5% of the variation in normalised undrained shear strength with $R^2 = 0.585$.
The resulting coefficient S, however, is significantly larger than the S value obtained from the procedure presented in the previous section, whilst the m is smaller (Table 6.1).

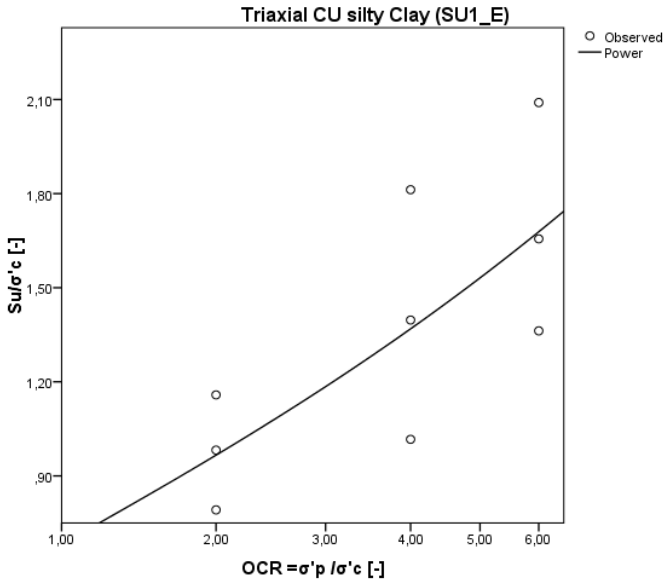

Figure 6.4: Non-linear regression analysis for 9 triaxial CU measurements from the SU1_E soil unit.

The values of S and m obtained from the regression analyses, listed in table 6.2, are in poor agreement with the results of the study conducted by Mayne (1980). The S values appear to be generally greater than those reported by Mayne (1980) and, in contrast, the m values are smaller. Especially for the SU1_E unit, the $(Su/\sigma'_c)_{NC} = 0.68$ and $m = 0.50$ are significantly different from the $(Su/\sigma'_{v0})_{NC} = 0.335$ and $m = 0.714$ for plastic Holocene clay suggested by Koutsoftas and Fisher (1976) (in Mayne, 1980).

Table 6.2: SHANSEP best parameters S and m for the SU1_A, SU1_B, and SU1_E soil units, obtained from linear and non-linear regression analyses of 21 OC measurements.

Soil Unit	**Soil Type**	**SHANSEP parameter**		**R^2**
		S	**m**	
[SU]	[-]	[-]	[-]	[-]
SU1_A (n=3)	Clay, clean, soft	0.543	0.521	0.994
SU1_B (n=9)	Clay, sandy	0.501	0.536	0.892
SU1_E (n=9)	Clay, silty or Silt, clayey	0.682	0.503	0.585

6.4. Validation of Improved SHANSEP Model

In the present section, the SHANSEP model with single calibration (Arup, 2015) and the SHANSEP model with calibration per soil type are compared with the in-situ measurements (Torvane and lab-UU).
The adjusted SHANSEP models (calibration per soil type), chosen for the following comparison, utilise the S and m parameters obtained from the analytical calibration (best parameters from Table 6.1, Section 6.2.1) and from the regression analysis (Table 6.2, Section 6.3).

6.4.1. Soil Unit: Soft, clean Clay (SU1_A)

The plot in figure 6.5 displays the distribution over the depth of in-situ Su measurements and Su predicted values.
As shown in figure 6.5, the in-situ measurements (lab-UU) are underestimated by the Su values calculated using the SHANSEP model with calibration per soil type (both Su;SHANSEP new and Su; SHANSEP regression). However, it is visible that the improved SHANSEP models produce Su values that are greater than those obtained using the SHANSEP correlation with single calibration, creating a slight improvement of the calculated-measured Su values correspondence.
Furthermore, from the comparison of the Su;SHANSEP;new and Su;SHANSEP;regression values, the latter are comparably larger than the former. Nevertheless, both combinations of S and m parameters yield similar results which are both greater than Su values obtained using the old SHANSEP equation, but smaller than the laboratory measurements.
In figure 6.6, the in-situ measurements (lab-UU) are plotted against the Su values computed using both SHANSEP correlations (with single calibration (Arup, 2015) and with calibration per soil type (Su;SHANSEP;new). The closer the points fall to the equality line the more accurate the fit.
For the SU1_A unit, a poor correspondence between measured and calculated Su values is observed. The data-pairs are located far from the equality line. However, the Su:SHANSEP;new data correlate slightly better with the in-situ measurements than the Su;SHANSEP (single calibration), confirming what illustrated in figure 6.5.

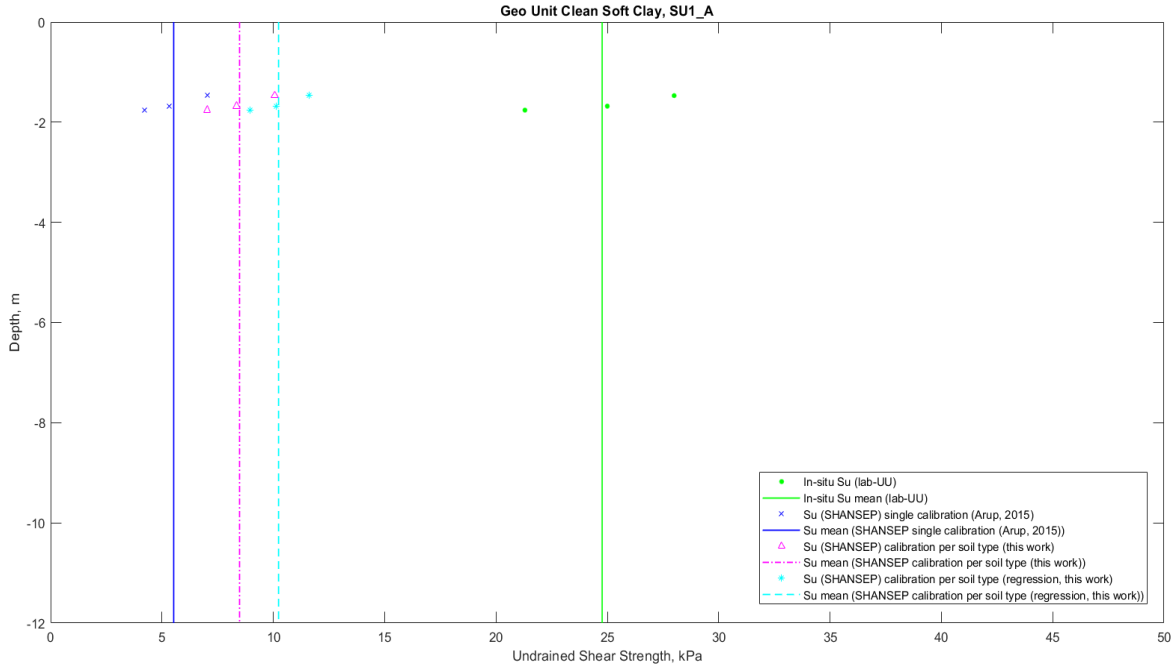

Figure 6.5: Su measurements and calculated values for the clean, soft Clay soil unit. Green dots: in-situ measurements (lab-UU) values; green solid line: mean. Blue crosses: calculated (SHANSEP, single calibration) values; blue solid line: mean. Magenta triangles: calculated (SHANSEP, calibration per soil type) values; magenta dash-dotted line: mean. Light blue circles: calculated (SHANSEP, calibration per soil type from the regression analysis) values; light blue dashed line: mean.

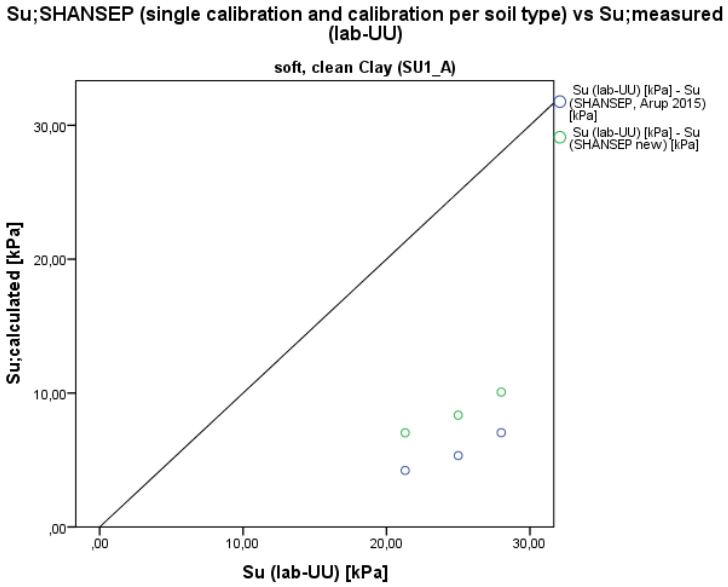

Figure 6.6: Su measurements and calculated values for the clean, soft Clay soil unit. Green dots: data-pairs of in-situ measurements (lab-UU) and Su values with calculated the SHANSEP (single calibration) model. Blue dots: data-pairs of in-situ measurements (lab-UU) and Su values calculated with the SHANSEP (calibration per soil type) model. Black solid line: equality line (x=y).

6.4.2. Soil Unit: Sandy Clay (SU1_B)

The plot in figure 6.7 displays the distribution over the depth of the Class 1 in-situ Su measurements and the Class 1 Su predicted values using the correlation suggested by (Ladd and Foott, 1974) with single calibration (Arup, 2015) and with calibration per soil type (this study).
As shown in figure 6.7, the in-situ measurements (lab-UU) are overestimated by the Su values calculated using the SHANSEP model with calibration per soil type (both Su;SHANSEP new and Su; SHANSEP regression). The improved SHANSEP models produce Su values that are greater than those obtained using the old model, leading to a worse calculated-measured (lab-UU) Su values correspondence.
On the other hand, the in-situ measurements (Torvane) are underestimated by the three SHANSEP models considered. Although the improved SHANSEP models produce Su values slightly larger than those obtained using the old correlation, the correspondence is still not satisfactory.
Furthermore, from the comparison of the Su;SHANSEP;new and Su;SHANSEP;regression values, the data points appear to be similar to each other. Also for this unit, both combinations of S and m coefficient yield almost identical results. In figures 6.8 and 6.9, the in-situ measurements (lab-UU and Torvane, respectively) are plotted against the Su values computed using both SHANSEP correlations (with single calibration (Arup, 2015) and with calibration per soil type (Su;SHANSEP;new)).
Confirming the observation made looking at figure 6.7, a worse correspondence between measured (UU) and the new calculated Su values (in green) is predicted in figure 6.8. Differently, from figure 6.9, the in-situ measurements (Torvane) are almost equally underestimated by both the SHANSEP correlations considered, hence, it is difficult to draw any conclusion about the performance of the improved model for this specific soil unit.

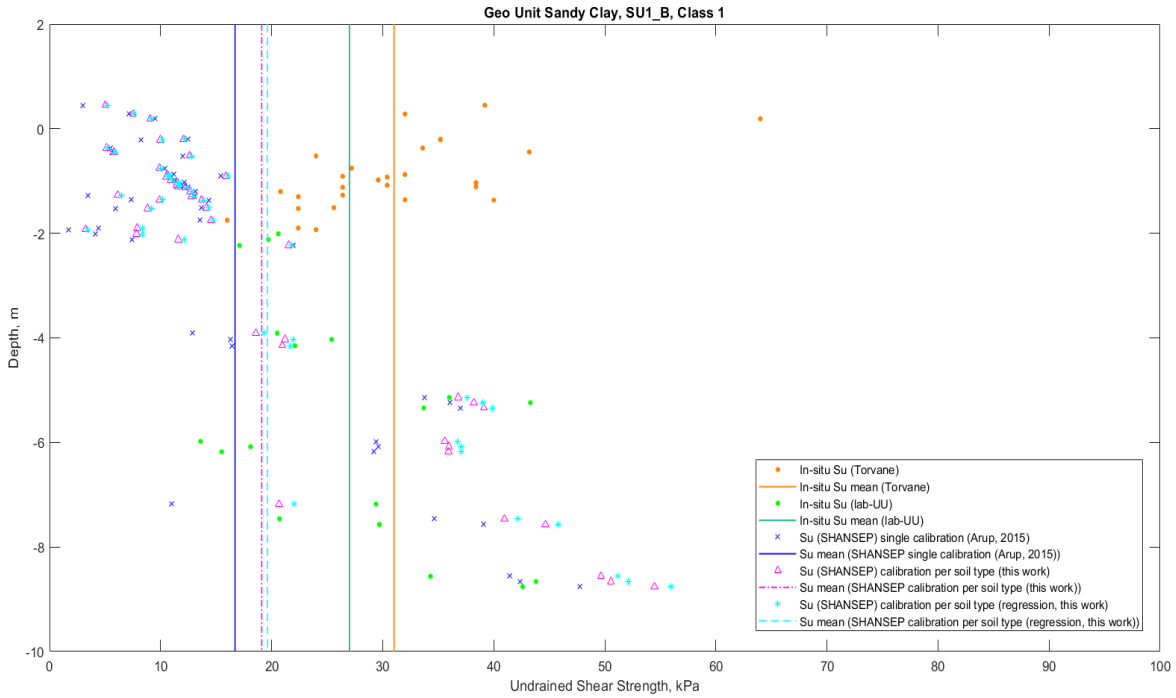

Figure 6.7: Su measurements and calculated Class 1 values for the sandy Clay soil unit. Green dots: in-situ measurements (lab-UU) values; green solid line: mean. Orange dots: in-situ measurements (Torvane); orange solid line: mean. Blue crosses: calculated (SHANSEP, single calibration) values; blue solid line: mean. Magenta triangles: calculated (SHANSEP, calibration per soil type) values; magenta dash-dotted line: mean. Light blue circles: calculated (SHANSEP, calibration per soil type from the regression analysis) values; light blue dashed line: mean.

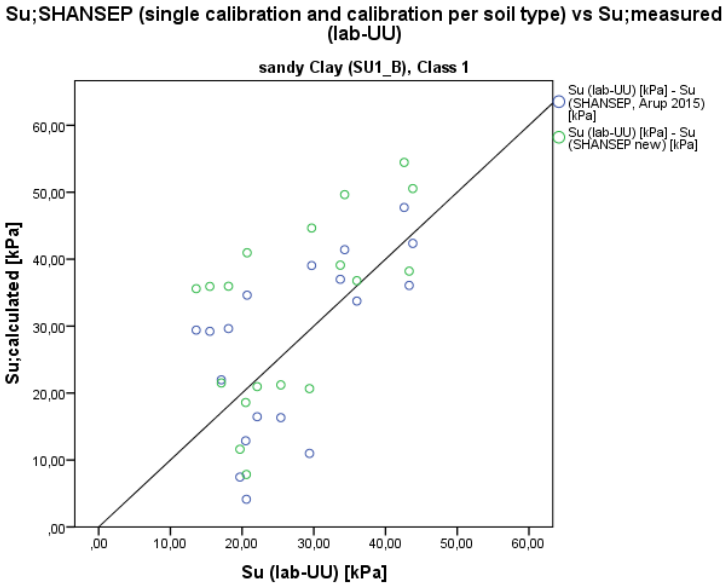

Figure 6.8: Su measurements and calculated values for the sandy Clay soil unit. Green dots: data-pairs of in-situ measurements (lab-UU) and Su values with calculated the SHANSEP (single calibration) model. Blue dots: data-pairs of in-situ measurements (lab-UU) and Su values calculated with the SHANSEP (calibration per soil type) model. Black solid line: equality line (x=y).

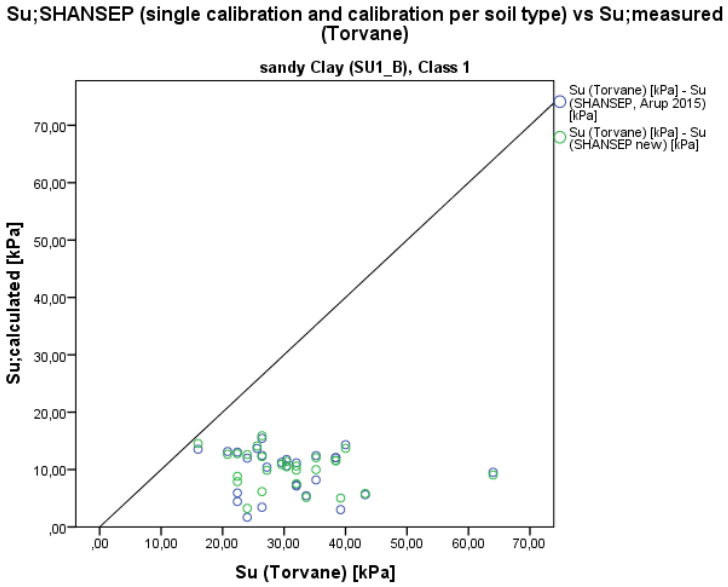

Figure 6.9: Su measurements and calculated values for the sandy Clay soil unit. Green dots: data-pairs of in-situ measurements (Torvane) and Su values with calculated the SHANSEP (single calibration) model. Blue dots: data-pairs of in-situ measurements (Torvane) and Su values calculated with the SHANSEP (calibration per soil type) model. Black solid line: equality line (x=y).

6.4.3. Soil Unit: Silty Clay (SU1_E)

The plot in figure 6.10 displays the distribution over the depth of the Class 1 in-situ Su measurements and Class 1 Su predicted values using the correlation suggested by (Ladd and Foott, 1974), with both single calibration (Arup, 2015) and calibration per soil type.
As shown in figure 6.10, the in-situ measurements (lab-UU) are underestimated by the Su values calculated using the SHANSEP model with calibration per soil type (both Su;SHANSEP new and Su; SHANSEP regression). The improved SHANSEP models produce a worse calculated-measured (lab-UU) Su values correspondence, with greater Su values.
On the other hand, although the in-situ measurements (Torvane) are underestimated by the three SHANSEP models considered, the improved SHANSEP models show a slightly better correspondence with the Torvane data, predicting Su values larger than those obtained using the original SHANSEP correlation.
Similarly to the SU1_B unit, however, it is hard to notice any difference between the Su;SHANSEP,new and SU;SHANSEP values at shallow depths. In contrast, it is clear that the Su;SHANSEP;regression values are larger than the Su;SHANSEP;new at greater depths. Also in this case, both combinations of S and m parameters generate results consistently greater than the Su;SHANSEP values.
In figure 6.11 the in-situ measurements (lab-UU) are plotted against the Su values computed using both SHANSEP correlations (with single calibration (Arup, 2015) and with calibration per soil type (Su;SHANSEP;new)). Confirming the previous observations, a poor correspondence between measured and calculated Su values is observed (Figure 6.11). The laboratory measurements are overestimated by both the correlations, however, the adjusted SHANSEP model (calibration per soil type, this work) over-predicts the factual data by the most, as also shown in figure 6.10.
Differently, in figure 6.12 it is clear that the adjusted SHANSEP equation yields Su values which are in a slightly better agreement with the Torvane measurements than those computed with the single-calibrated SHANSEP model.

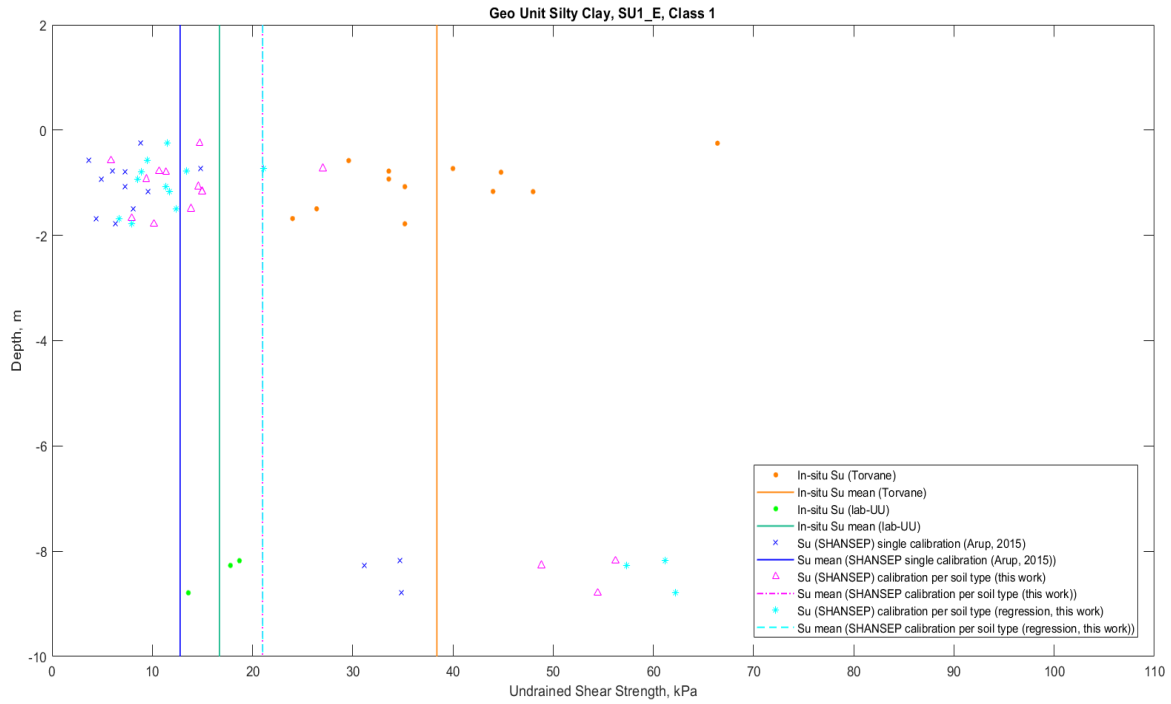

Figure 6.10: Su measurements and calculated Class 1 values for the silty Clay soil unit. Green dots: in-situ measurements (lab-UU) values; green solid line: mean. Orange dots: in-situ measurements (Torvane); orange solid line: mean. Blue crosses: calculated (SHANSEP, single calibration) values; blue solid line: mean. Magenta triangles: calculated (SHANSEP, calibration per soil type) values; magenta dash-dotted line: mean. Light blue circles: calculated (SHANSEP, calibration per soil type from the regression analysis) values; light blue dashed line:mean.

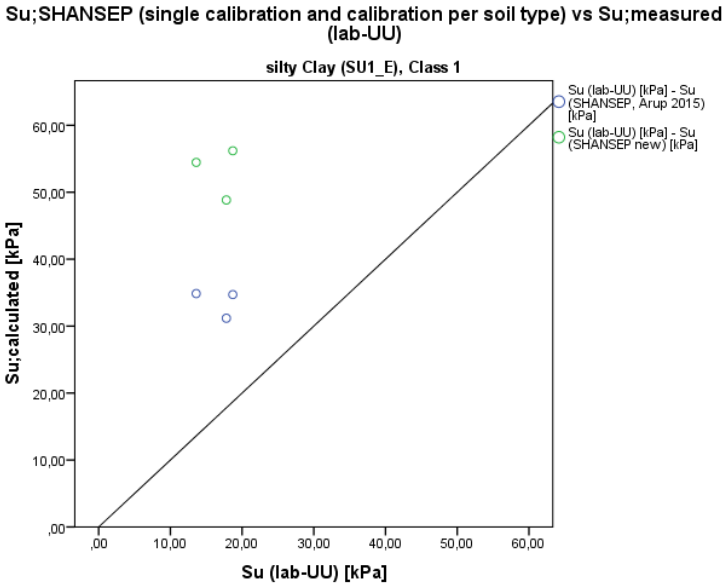

Figure 6.11: Su measurements and calculated values for the silty Clay soil unit. Green dots: data-pairs of in-situ measurements (lab-UU) and Su values with calculated the SHANSEP (single calibration) model. Blue dots: data-pairs of in-situ measurements (lab-UU) and Su values calculated with the SHANSEP (calibration per soil type) model. Black solid line: equality line (x=y).

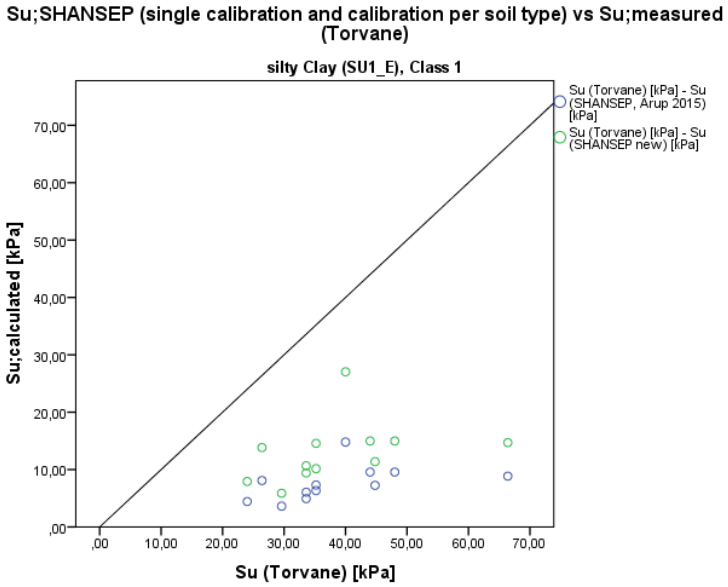

Figure 6.12: Su measurements and calculated values for the silty Clay soil unit. Green dots: data-pairs of in-situ measurements (Torvane) and Su values with calculated the SHANSEP (single calibration) model. Blue dots: data-pairs of in-situ measurements (Torvane) and Su values calculated with the SHANSEP (calibration per soil type) model. Black solid line: equality line (x=y).

6.5. OCR Influence

Despite the overall good agreement between the adjusted SHANSEP models and the triaxial CU tests, illustrated in section 6.2, the correspondence between Torvane and lab-UU and predicted Su values is unsatisfactory. The reason of this mismatch is believed to be primarily related to the overconsolidation ratio values obtained from the CPT measurements.
In the present thesis, the estimation of OCR from CPT measurements is carried out according to the following procedure suggested by Mayne (2014):

$$OCR = \sigma'_p / \sigma'_{v0} \tag{6.1}$$

The pre-consolidation (or yield) stress is calculated as:

$$\sigma'_p = 0.33 \cdot (q_t - \sigma_{v0})^{m'} \cdot (\sigma_{v0;atm}/100)^{1-m'} \tag{6.2}$$

where the exponent of the yield stress, m', is computed as a function of the soil behaviour type index, $I_{c;def}$, (after Robertson and Wride (1998), in Robertson and Cabal (2015)) according to the following relation:

$$m' = 1 - \frac{0.28}{1 + (I_{c;def}/2.65)^{25}} \tag{6.3}$$

The exponent m' decreases with mean grain size (Mayne 2013, in Mayne, 2014) and its range of values goes from 0.72 (in quartz to silica sands) to 1.0 (in intact clays).

However, the OCR values evaluated with such procedure are found to be not appropriate for the SHANSEP framework. The fact that the above procedure yields low OCR at shallow depths and high OCR at great depths is believed to be the principal cause of the unacceptable performance of the improved SHANSEP model.

In lieu of the observed poor correspondence among in-situ measurements and calculated Su values, new empirical correlations are hereafter proposed. These are based on the OCR equation suggested by Bommer et al. (2017a):

- From 0 to -2 m NAP:

$$OCR = 4.5 + 0.005 \cdot \sigma'_{v0} \tag{6.4}$$

- From -2 to -6 m NAP:

$$OCR = 2.5 + 0.005 \cdot \sigma'_{v0} \tag{6.5}$$

- From -6 to -25 m NAP:

$$OCR = 1.0 + 0.005 \cdot \sigma'_{v0} \tag{6.6}$$

As an example, figure 6.13 illustrates the OCR estimates for the samples tested in laboratory (triaxial UU). As shown in figure 6.13, the orange dots are characterised by a large scatter, thus no clear trend can be identified. On the other hand, using the above empirical relations, a decreasing OCR profile over the depth is achieved (R^2 = 0.87). Moreover, the resulting OCR values implemented in the improved SHANSEP model yield Su value in better agreement with the in-situ measurements (both lab-UU and Torvane), as it is shown in figures 6.14 and 6.15. Nevertheless, these relations constitute only a quick first-order estimate of the over consolidation ratio (Bommer et al., 2017a) and cannot be considered totally reliable. The resulting OCR, hence, need to be supported by further data (e.g. oedometer and consolidometer tests).

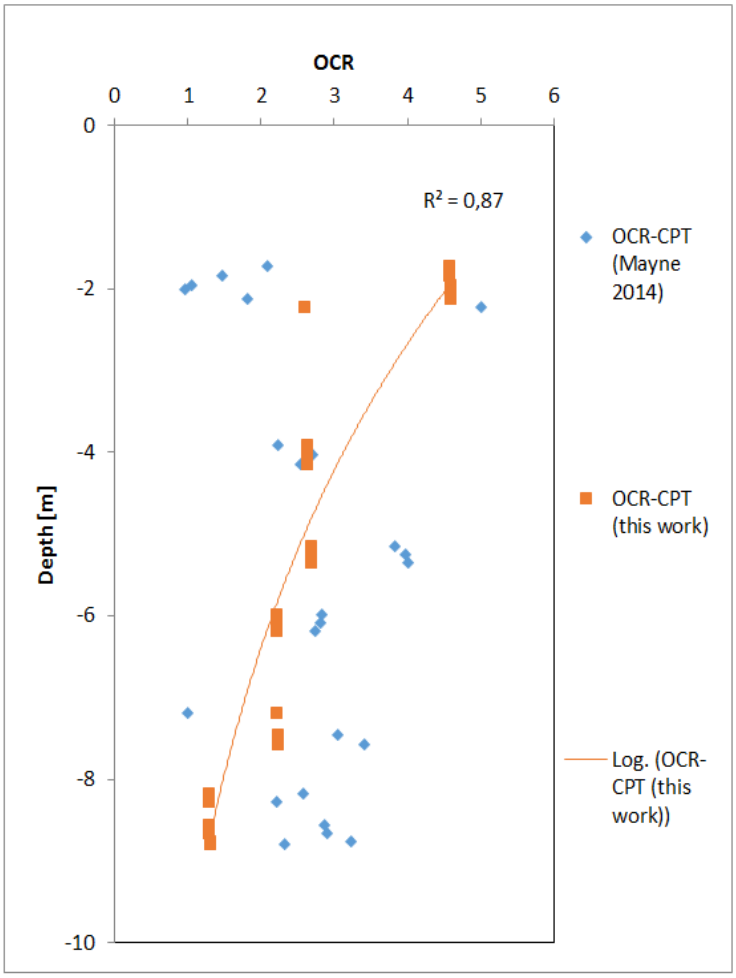

Figure 6.13: OCR over the depth for Su measurements (lab-UU). Blue dots: OCR calculated from CPT measurements (following the Mayne 2014 procedure). Orange dots: OCR calculated from CPT measurements using linear relations with the effective vertical stress in-situ (this work); solid orange line: logarithmic regression line.

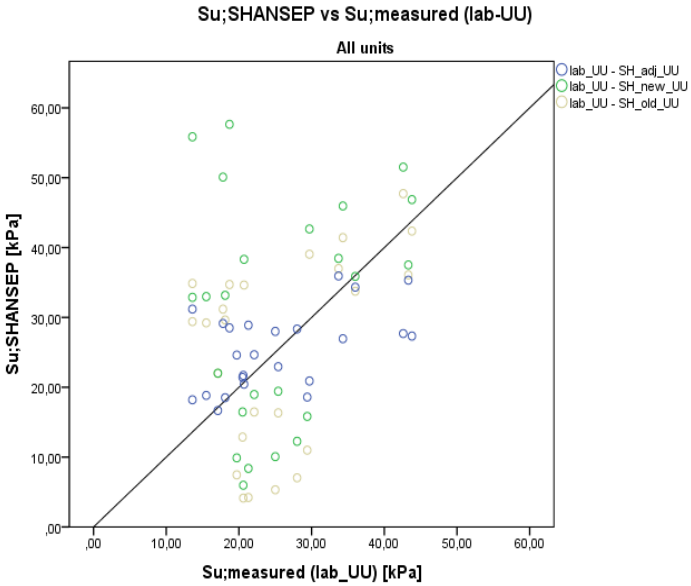

Figure 6.14: Su (lab-UU) measurements and calculated values for the SU1_A, SU1_B and SU1_E soil units. Blue dots: data-pairs of laboratory measurements (lab-UU) and Su values calculated with the SHANSEP (calibration per soil type) model with adjusted OCR. Green dots: data-pairs of laboratory measurements (lab-UU) and Su values calculated with the SHANSEP (calibration per soil type) model with OCR from Mayne (2014). Yellow dots: data-pairs of laboratory measurements (lab-UU) and Su values calculated with the SHANSEP (single calibration) model with OCR from Mayne (2014). Black solid line: equality line (x=y).

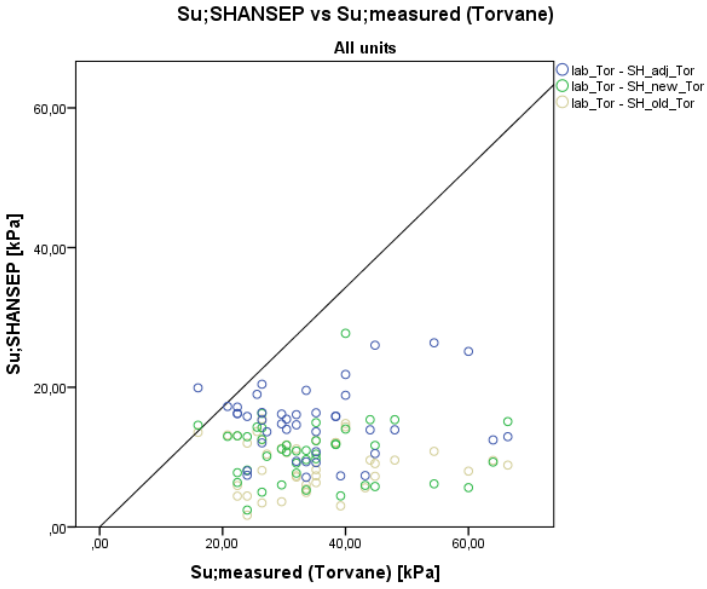

Figure 6.15: Su (Torvane) measurements and calculated values for the SU1_A, SU1_B and SU1_E soil units. Blue dots: data-pairs of in-situ measurements (Torvane) and Su values calculated with the SHANSEP (calibration per soil type) model with adjusted OCR. Green dots: data-pairs of in-situ measurements (Torvane) and Su values calculated with the SHANSEP (calibration per soil type) model with OCR from Mayne (2014). Yellow dots: data-pairs of in-situ measurements (Torvane)) and Su values calculated with the SHANSEP (single calibration) model with OCR from Mayne (2014). Black solid line: equality line (x=y).

6.6. Summary and Conclusions

The present chapter provides the outcomes of different procedures carried out on the laboratory (CU) data compiled in the GI database, in order to improve the Ladd and Foott (1974) correlation with single calibration (Arup, 2015). The main goal of the analyses presented in this chapter is to calibrate the SHANSEP S and m coefficients per different soils types (i.e. soft, clean Clay, sandy Clay and silty Clay).
The most relevant topics discussed are summarised as follows:

- Firstly, an analytical procedure (see Section 6.2 and Appendix D) consisting of two approaches was performed using the triaxial (CU) data, organised per soil unit, to study the influence of the OCR on the undrained shear strength. From the first approach, following the Ladd and Foott (1974) framework, the best estimate of S and m were obtained.

- Secondly, linear and non-linear regression analyses in SPSS were conducted on triaxial (CU) data, organised per soil unit, to validate the analytical procedure, comparing the S and m parameters with each other and with literature (see Section 6.2 and Appendix D).

- Finally, the Su values obtained using the improved SHANSEP correlations (calibration per soil type from analytical procedure and from regression analysis), together with the data predicted by the SHANSEP model with single calibration, were compared to the in-situ measurements (Torvane and lab-UU), in order to qualitatively investigate whether improvements in the calculated-measured Su values correspondence were achieved.

The main findings resulting from the analyses mentioned above are:

- The analysis of 39 isotropically consolidated undrained triaxial tests revealed that the overconsolidation ratio creates the most significant impact on the undrained shear strength of natural clay deposits.

- Considering the data provided with pre-consolidation pressures, it is clear that the relationship between undrained shear strength and OCR can be well described by the power law function, following the SHANSEP framework. Only for the silty Clay unit, a linear relationship between Su and OCR was observed, being the exponent m equal to 1.
  In this context, it was observed that the SHANSEP parameters S and m are soil constants.
  By calculating the normalised undrained shear strength as Su/σ'_c (following approach 1, Section 6.2.1) for the normally consolidated specimens characterised by the same soil type but collected at different locations, small changes in S and m were detected. Therefore, for each soil unit the best combination of SHANSEP parameters was chosen (Table 6.1). These were found to be in fair agreement with the values indicated by Mayne (1980) for natural Holocene clays.
  Subsequently, fitting the CU data with the SHANSEP model implemented with the best coefficients, it was shown that an almost a satisfactory fit of the data with OCR=1 was obtained, as well as of the overconsolidated specimens, was achieved with reasonably high coefficient of determination (see Section 6.2).

- The outcomes of the regression analysis, presented in section 6.3, confirmed that the normalised undrained shear strength is strongly dependent on the overconsolidaton ratio, rising with increasing OCR. For OCR greater than 1, the relation $\frac{(Su/\sigma'_c)_{OC}}{(Su/\sigma'_c)_{NC}} - OCR$ resulted to be non-linear, as the exponent m was found to be consistently lower than 1. The calculated S and m coefficients, however, were different from those obtained with the analytical procedure, and in poor agreement with the values reported by Mayne (1980) and Ladd and Foott (1974). Although the high correlation coefficients (e.g. R^2=0.994 and 0.892 for the SU1_A and SU1_B units, respectively), indicating a good fit of the data, the S values appear to be consistently larger than those suggested by Mayne (1980) and, in contrast, the m values too low.

- The comparison of the Su values predicted using the SHANSEP relations (with calibration per soil type and single calibration) with the in-situ measurements (Torvane and lab-UU) revealed that higher values of undrained shear strength were obtained with the adjusted SHANSEP equations.
  The general trend presented in section 6.4 suggested that a slightly improved correspondence with the Torvane measurements was achieved, but a larger overestimation of the laboratory measurements occurred (especially at greater depths). However, for the soft, clean Clay unit, which consists of only 3

measurements (lab-UU) at relatively shallow depths (between -1 and -2 m NAP), the opposite trend was noted. In this case, the adjusted SHANSEP correlations produced Su values closer to the laboratory data with respect to those calculated with the single-calibrated model.
In general, results from the above analyses showed that, by using the SHANSEP parameters estimated with the analytical procedure rather than the regression analysis, a better correspondence with the in-situ measurements was observable. In addition, the best estimate parameters obtained with the former procedure are in better agreement with the values suggested by Mayne (1980) and Ladd and Foott (1974).

- Taking into account the poor correspondence existing between in-situ measurements and calculated Su values, it was decided to investigate the OCR trend over the depth. Calcualting the OCR from CPTs, using the Mayne (2014) approach, the OCR profile was characterised by a large scatter, and no clear trend was identifiable. Precisely, it was found that low values of OCR were predicted at shallow depths (i.e. $OCR = 1-2$), whereas OCR from 2 to 4 were assigned to samples at greater depths.
Consequently, new empirical relations were proposed, following the equation suggested by Bommer et al. (2017a), which produced OCR values more appropriate for the SHANSEP model (decreasing trend with increasing depth). However, these equations need to be supported with laboratory data, such as oedometer and consolidometer tests, to further validate their adequacy.

7

Conclusions and Recommendations

In the present chapter the collective conclusions drawn throughout this research project are listed and commented.
The present thesis investigates the applicability of a number of CPT-based correlations used for the PI and Su interpretation in the Groningen region. A literature review (Chapter 2 and 3, and Appendix A), comprehending an extensive study of both natural and man-induced earthquakes, the principles and the main correlations used in site response analysis, is meant to introduce the reader to the VIIA project, which is the framework of the present research. In chapter 4 a sensitivity analysis is performed for three soil properties in order to investigate their influence on SRA results. Subsequently, in chapter 5, a statistical analysis is carried out to analyse the suitability of a number of CPT-based mathematical equations in relation to the factual data. Based on the outcomes of the statistical analysis, chapter 6 focuses on the study and the improvement of one of the CPT-based correlations used to estimate the undrained shear strength of soft clays: the SHANSEP model (after Ladd and Foott (1974)).
The primary and secondary research questions that were identified in the beginning of the report were listed as follows:

1. How accurately do the plasticity index and undrained shear strength correlations describe the actual soil properties?
    - Do the PI and Su estimations match the factual in-situ and laboratory data?
    - What is their adequacy with respect to the different soil type and units present in Groningen?
    - Are the individuated soil units in agreement with the stratigraphic units proposed by Bommer et al. (2017a)?
2. How precise can the PI and Su predictions be, based on cone penetration tests?
    - Which are the main parameters affecting the correlations performance?
3. Is the current factual data-set of adequate quality to carry out statistical and regression analyses to calibrate the models' parameters?
    - Which test type is more reliable? Why?
4. Does the adjusted SHANSEP model (calibration per soil type) yield Su predictions in better agreement with the in-situ data?
    - What are the limitations?
5. What is the influences of the parameters PI, Su, and Vs on seismic ground response?
    - Is there any clear depth trend?

The first two key research questions were answered in Chapter 5, where a statistical analysis was performed on the data re-organised per soil type. Furthermore, the statistical analysis, in combination with the result from the analytical and the regression analyses performed on triaxial (CU) data in Chapter 6, provided an answer to questions 3 and 4. An answer to the last research question, was found in Chapter 4 through a sensitivity analysis carried out as a case study on an existing soil column in the region.
The conclusions related to the two soil properties which the thesis focused on, namely plasticity index and undrained shear strength, are described in sections 7.1.1 and 7.1.2, whilst the main findings from the sensitivity analysis are explained in section 7.1.4. Finally, the recommended additions and adjustments for further research are presented in section 7.2.

7.1. Conclusions and Discussion

7.1.1. Plasticity Index

A large database (n=413) of factual data from the laboratory was made available covering most of the soil units from Groningen. Of 413 data, 378 measurements were compared to predicted values with a commonly used semi-empirical CPT-based correlation from Cetin and Ozan (2009), as well as the PI models from Bommer et al. (2017a) implemented in the latest NPR 9998 (2017).
From the analyses carried out in this report, the following conclusions were drawn:

1. Given that the majority of the in-situ PI measurements (approximately 90 %) were obtained at relatively shallow depths (between +1 and -4 m NAP), it was not always possible to find CPT measurements to compare the factual data with. A depth mismatch between specimens and CPT measurements (see Appendix B) was found to negatively influence the results in proximity to the surface, enhancing the poor correspondence among the data. Therefore, the data pairs were re-organised in sample classes to reduce the effect of the depth mismatch (see Appendix B, Table B.3).

2. The Cetin and Ozan (2009) correlation was ascertained to produce an acceptable approximation of the plasticity index for some of the soil materials considered (i.e. sandy Clay and Loam; SU1_B and SU5 in this thesis). Conversely, the model underestimated other soil units, such as clean Clay, silty Clay, OC Clay (Table 7.1).

3. From the comparison of the laboratory data per stratigraphic units the PI values recommended by Bommer et al. (2017a), a fair correspondence between most the data pairs was observed. The factual data from this thesis verifies most of the proposed PI from Bommer et al. (2017a), such as the NA, DR (sandy clay), and BX (clay). Conversely, the values for PE and AAOP (sandy clay) showed to require adjustments. The peat from NI resulted in a high mean measured PI of 95% confirming the assumption by Bommer et al. (2017b) of PI=100% (Table 7.1).

4. Comparing the geotechnical units used in this research (e.g. SU1_A, SU1_B) with the recommended V4 values, the difference between mean values increased significantly given the large spatial variability (Table 7.1). The outcomes of such soil classification, in turn, resulted in rough agreement with the Arup (2015) suggested PI value of 25 %.

5. The distribution of the various PI data-sets was found to be fairly described by approximately normal or positively skewed distributions. Moreover, it was demonstrated that log-normal distributions could be used to account for the positive skew of the linear measurements, confirming the fact the PI is a non-negative soil property.

6. The positive skewed distribution of the PI data-sets is related to the fact that the deterministic depth trends of data were not removed. If data were normalised with respect to the residual standard deviation (σ_{res}) of the de-trended data-set, a standard normal field of data ($\mu = 0$ and $\sigma = 1$) can be achieved (Lloret-Cabot et al., 2014).

7. The standard deviation and the coefficient of variation of the PI data-sets (e.g. SU1_A, SU1_B) were, in some cases, exaggeratedly high. Such high values can be attributed to the large spatial variability of the uppermost layers, as well as sampling technique, testing technique, and interpretational error.

Table 7.1: Comparison from different approaches for PI interpretation (see tables E.2 and E.1 for soil and stratigraphic units codes).

Soil Unit	**Stratigraphic Unit**	**Unit Code**	**Unit Weight Wet**	**PI Laboratory**	**PI Bommer et al. 2017**	**PI Cetin & Ozan 2009**
[SU]	[-]	[-]	[kN/m^3]	[%]	[%]	[%]
SU1_A (n=30)	Naaldwijk	NA	12.9	32.4	30	23 (σ=9.8%)
	Drente	DR	14.7	11.1	15	
	Boxtel	BX	14.4	49.4	50	
SU1_B (n=202)	Naaldwijk	NA	16.2	31.7	30	20 (σ=10.2%)
	Nieuwkoop	NI	17.0	57.1	50	
	Drente	DR	16.7	10.4	10	
	Peelo	PE	18.1	19.5	30	
SU1_D (n=15)	Nieuwkoop	NI	14.1	47.4	50	18-22 (σ=12.3%)
SU1_E (n=98)	Naaldwijk	NA	16.2	29.6	30	19 (σ=7.1%)
	Nieuwkoop	NI	17.0	41.9	50	
	Drente	DR	16.7	12.5	15	
	Antrophogenic	AAOP	16.8	5.0	50	
SU2 (n=4)	Peelo	PE	17.8	44.0	30-50	23 (σ=10.1%)
SU3 (n=20)	Naaldwijk	NA	16.2	28.0	30	6 (σ=3.75%)
	Drente	DR	16.7	8.1	15	
SU4 (n=7)	Nieuwkoop	NI	14.1	95.0	50*	24 (σ=5.5%)
SU5 (n=2)	Peelo	PE	18.1	12.5	30	11 (σ=10.7%)

* Bommer et al. (2017a), in the V4 ground motion model, prescribes PI=100 % to be used in the damping curves for Peat.

7.1.2. Undrained Shear Strength

A database (n=161) from factual data was compiled covering most of the soil units from Groningen. The in-situ and laboratory measurements were compared to predicted values with the SHANSEP framework proposed by Ladd and Foott (1974), as well as the Su correlation proposed by Robertson and Cabal (2015), and the empirical equations from Bommer et al. (2017a) implemented in the latest NPR 9998 (2017).
From the multiple investigations carried throughout the report, the following conclusions can be drawn:

1. The SHANSEP model with single calibration after (Arup, 2015) showed poor correlation with the in-situ Su measurements. While it consistently underestimated the Su of clayey soils at shallow depths (Torvane measurements), the model did not provide clear indication about its performance with respect to the Su measurements at greater depths (lab-UU).

2. The calibration of the SHANSEP parameters through the analytical procedure shown in Chapter 6 produced high coefficients of determination (see Table 6.1) and S and m values consistent with Mayne (1980).

3. The outcomes of Chapter 6 revealed that the overconsolidation ratio creates the most significant impact on the undrained shear strength of clay deposits, confirming the findings of several authors (e.g. Ladd and Foott, 1974, Mayne, 1980 Jamiolkowski et al., 1985, D'Ignazio, 2016).

4. The match between the improved SHANSEP model and the triaxial CU test data was qualitatively accurate (Figures 6.1a to 6.1c, section 6.2). The normalised undrained shear strength of different inorganic clays was observed to correlate satisfactorily with OCR, and the fit of all the available data overall was acceptable.

5. The SHANSEP model is an adequate method to estimate the undrained shear strength of clays, after calibrating coefficients S and m per soil type with triaxial CU data.

6. The comparison of the Su values computed by using the SHANSEP model (with single calibration) and the improved SHANSEP relations (calibration per soil type) with respect to the in-situ measurements (lab-UU and Torvane) resulted in higher values of undrained shear strength with the latter equations (Section 6.4, Chapter 6), however the new model's performance remained unsatisfactory:

    - With respect to the Torvane measurements, it was not possible to determine whether any improvement was achieved (Figures 6.7 and 6.10).
    - With respect to the in-situ (lab-UU) measurements, overestimation of the laboratory data was enhanced (Figures 6.7 and 6.10), except for the SU1_A unit, where the correspondence between in-situ measurements (lab-UU) and the predicted Su values was slightly better (Figure 6.5).

7. The Robertson and Cabal (2015) empirical relation gave an overall good approximation of both Torvane and lab-UU data.

    - This correlation was able to capture, to some extent, the large spatial variability of the first 5 m of soil (e.g. Figures 5.20 and C.15), in fair agreement with the Torvane measurements. On the other hand, the Robertson and Cabal (2015) correlation estimated Su values in poor agreement with the in-situ measurements (lab-UU). There was not a clear trend when considering the different soil types.

8. The Bommer et al. (2017a) empirical equations produced a fair approximation to the in-situ measurements, for both lab-UU and Torvane.

    - The overall trend suggested that the soil-specific relations over-predict the in-situ data from the SU1_B and SU1_E soil units, while underestimating the SU1_A data.
    - The large scatter of the Torvane measurements at shallow depths was fairly reflected by the predicted Su (e.g. Figure C.15). However, at greater depths, the Bommer et al. (2017a) Su estimates consistently over-predicted the laboratory data (e.g. Figures 5.20 and C.15).
    - By re-organising the in-situ measurements per stratigraphic unit, it was observed that the NA data were generally overestimated, whilst the DR and NI data were slightly underestimated. Conversely, a fair agreement was found among the AAOP pairs (see Table E.3).

7.1.3. Overconsolidation Ratio

1. The poor performance of the original and improved SHANSEP models is directly related to the current OCR interpretations.

2. Although the OCR values computed with the Mayne, 2014 procedure appear to be in agreement with considerations regarding the regional geology (i.e. young clays at shallow depths that have not been subjected to previous loading, such as the presence of ice sheets during glaciation periods, cannot be heavily overconsolidated), they resulted to be inappropriate for the SHANSEP framework.

3. High values of OCR at shallow depths can be associated to the generation of negative pore water pressure (suction) experienced by unsaturated or partially saturated soils, due to variation in water content, lowering of groundwater table, soil desiccation, etc.

4. For a quick first-order estimate of the in-situ OCR to be used within the new site-specific SHANSEP models, new empirical CPT-based correlations were proposed in section 6.5. By implementing the resulting OCR values, a satisfactory correspondence among measured and predicted Su values was achieved.

7.1.4. Sensitivity of PI, Su, and Vs effect on SRA

The main outcomes resulting from the sensitivity analysis are:

1. From the analysis of the PGA and MSS profiles, the shear wave velocity is the parameter that influences SRA results the most. However, in closer proximity to the surface, where softer soils are found, the undrained shear strength is a crucial parameter with large effects on the PGA and MSS. For instance, low values of Su produce drastic reduction of PGA and large strains development. For the soil profile assessed from Groningen, PI variations resulted in a negligible or small effect. PI becomes important at extremely large values, out of the range measured and expected for Groningen soils.

2. From the analysis of the response spectra, it was observed that PSA is similarly sensitive to the decrease of the three properties in analysis. However it is somewhat more sensitive to larger PI values rather than Su and Vs increase.

3. The sensitivity analysis outcomes reveal that, in general, PGA and PSA are more sensitive to the reduction of the mean value of these soil properties than the increase in mean value. Whereas, the MSS resulted to be more sensitive to the increase of mean values in closer proximity to the surface and to mean values decrease below 6 m NAP.

7.2. Recommendations

7.2.1. Plasticity Index

1. In order to obtain a more telling indication of the Cetin and Ozan (2009) correlation's adequacy with respect to the soil units that in this thesis showed poor correspondence (e.g. Peelo), it is firmly recommended to perform a more intensive ground investigation in terms of cone penetration tests and laboratory tests for the sites in analysis.
   The addition of extra data can be used to further support or reject the conclusions drawn from the comparison between laboratory and numerical determined properties, and possibly enhance the quality of the prediction relations.

2. The Atterberg's limits determination performed at the laboratory should be consistently executed on samples collected at variable depths. Since depth is a crucial factor that affects soil properties and behaviour, it is strongly suggested to perform a more diverse sample-depth selection.

3. In order to avoid large standard deviation and coefficient of variation from statistical characterisation of data it is advised to de-trend the CPT measurements.

4. A look-up table for PI, after the one from Bommer et al. (2017a), is recommended (see Table 7.1).

7.2.2. Undrained Shear Strength

1. It is recommended to execute Torvane tests at greater depths, to better understand whether the large scatter is connected to the soil spatial variability or to the test technique. Alternatively, it is suggested to perform laboratory (triaxial) tests at shallow depths.

2. With the aim of avoiding unrealistically low values of undrained shear strength at shallow depths, it is suggested to assume a minimum value of $Su = 20kPa$ for the inorganic clay materials near the ground surface, independently from the calculated values of σ'_v and OCR (consistently with Arup, 2015 recommendations).

3. Laboratory triaxial (CU) tests produce valuable data, provided that the consolidation phase is realised with pressures similar to in-situ overburden stresses. It is thus recommended to consistently specify the pre-consolidation used during the test for an accurate determination of the OCR.

4. A look-up table for Su, after the one from Bommer et al. (2017a), is recommended (see Appendix E, Table E.3).

5. In order to avoid large standard deviation and coefficient of variation from statistical characterisation of data it is advised to de-trend the CPT measurements.

7.2.3. Overconsolidation Ratio

1. Following the observation of the crucial effect of OCR on the undrained shear strength, it is firmly recommended to perform additional research on this topic.

2. To develop a full profile of OCR with depth, a series of undisturbed samples should be collected at various depths and subjected to laboratory consolidation testing (e.g. oedometer tests), using pre-consolidation stresses similar to the in-situ overburden pressures.
   The combination of a sufficient amount of laboratory testing with a detailed background and the understanding of the geomorphological origins can be crucial in creating a more accurate indication of the stress history of a certain formation (Mayne et al., 2009) and, thus, improving the SHANSEP model's performance.

3. The proposed empirical correlation for the estimation of OCR from CPT measurements need to be supported by further factual data.

7.2.4. Site Response Analysis

1. In order to assess the performance of the 1D Site Response Analysis model, the effect of other soil parameters should be taken into account (OCR, damping ratio, shear modulus, etc.).

2. It is recommended to implement the PI and Su values from this research.

3. For SRA purposes and during setting of NLTH models, very low values of undrained shear strength should be reviewed and taken with care in order to avoid misinterpretations.

4. It is advised review the OCR interpretation and validate it with factual laboratory data.

7.2.5. General

The statistical approach and the regression analysis can be continued further in more depth. The possible parameter combinations have not been studied to their maximum extent because of the lack of experience in the early stages. For this reason, more combinations can be tested in order to possibly enhance the quality of the analysis, or even to reach the conclusion that the problem lies in the lack and the quality of data.

References

Akkar, S. and Özen, Ö. (2005). Effect of Peak Ground Velocity on Deformation Demands for SDOF Systems. *Earthquake engineering & structural dynamics*, 34(13):1551–1571.

Ansal, A. and Erken, A. (1989). Undrained Behavior of Clay Under Cyclic Shear Stresses. 115(7):968–983.

Arup (2015). Groningen Earthquakes Structural Upgrading - Site Response Analysis. Technical Report Rev.0.01.

Bay, J. A., Anderson, L. R., Colocino, T. M., Budge, A. S., James, A., Loren, R., and Todd, M. (2005). Evaluation of SHANSEP Parameters for Soft Bonneville Clays. Technical Report September, Department of Civil and Environmental Engineering Utah State University Logan, UT 84322-4110, Salt Lake City, Utah, USA.

Bazzurro, P. and Cornell, C. A. (2004). Ground-Motion Amplification in Nonlinear Soil Sites with Uncertain Properties. *Bulletin of the Seismological Society of America*, 94(6):2090–2109.

Benz, T., Schwab, R., and Vermeer, P. (2009). Small-strain stiffness in geotechnical analyses. *Bautechnik - Geotechnical Engineering*, 86(SUPPL. 1):16–27.

Bolt, B. (1999). *Earthquakes*. Freeman, W.H., New York, New York, USA, 4th edition edition.

Bommer., J. J. and Alarcón, J. (2006). The Prediction and use of Peak Ground Velocity. *Journal of Earthquake Engineering*, 10(01):1–31.

Bommer, J. J., Crowley, H., and Pinho, R. (2015a). A Risk-mitigation Approach to the Management of Induced Seismicity. *Journal of Seismology*, 19(2):623–646.

Bommer, J. J., Dost, B., Edwards, B., Kruiver, P., Meijers, P., Ntinalexis, M., Rodriguez-Marek, A., Ruigrok, E., jasper Spetzler, and Stafford, P. J. (2017a). V4 Ground-Motion Model (GMM) for Response Spectral Accelerations, Peak Ground Velocity, and Significant Durations in the Groningen Field. *Earthquake Spectra*, 33(2):481–498.

Bommer, J. J., Dost, B., Edwards, B., Rodriguez, A., Kruiver, P. P., Meijers, P., Ntinalexis, M., and Stafford, P. J. (2015b). Development of Version 2 GMPEs for Response Spectral Accelerations and Significant Durations from Induced Earthquakes in the Groningen Field. Technical Report November.

Bommer, J. J., Edwards, B., Kruiver, P. P., Stafford, P. J., Dost, B., and Ntinalexis, M. (2017b). V5 Ground-Motion Model (GMM) for the Groningen Field. Technical Report October, Nederlandse Aardolie Maatschappij (NAM).

Bommer, J. J., Stafford, P. J., Edwards, B., Dost, B., van Dedem, E., Rodriguez-Marek, A., Kruiver, P., van Elk, J., Doornhof, D., and Ntinalexis, M. (2017c). Framework for a ground-motion model for induced seismic hazard and risk analysis in the groningen gas field, the netherlands. Technical Report June, Nederlandse Aardolie Maatschappij (NAM).

Bommer, J. J., Stafford, P. J., and Ntinalexis, M. (2016). Empirical Ground-Motion Prediction Equations for Peak Ground Velocity from Small-Magnitude Earthquakes in the Groningen Field Using Multiple Definitions of the Horizontal Component of Motion. Technical Report November, Nederlandse Aardolie Maatschappij (NAM).

Booth, E. (2007). The Estimation of Peak Ground-motion Parameters from Spectral Ordinates. *Journal of Earthquake Engineering*, 11(1):13–32.

Bourne, S. J., Oates, S. J., Van Elk, J., and Doornhof, D. (2014). A seismological model for earthquakes induced by fluid extraction from a subsurface reservoir. *Journal of Geophysical Research: Solid Earth*, 119(12):8991–9015.

Braile, L. (2010). Seismic Wave Demonstrations and Animations. Access date: 2017-05-10, url: http://web.ics.purdue.edu/ braile/edumod/ waves/WaveDemo.htm.

Brinkgreve, R. (2015). Behaviour of Soil and Rocks. Lecture slides. TU Delft.

Carlton, B. (2014). *An Improved Description of the Seismic Response of Sites with High Plasticity Soils , Organic Clays, and Deep Soft Soil Deposits*. Phd dissertation, University of California at Berkeley, USA.

Cetin, K. O. and Ozan, C. (2009). CPT - Based Probabilistic Soil Characterization and Classification. *Journal of Geotechnical and Geoenvironmental Engineering*. 10.1061/(ASCE)1090-0241(2009)135:1(84).

Darendeli, M. (2001). *Development of a New Family of Normalized Modulus Reduction and Material Damping Curves*. Phd dissertation, University of Texas at Austin, USA.

Day, R. (2002). *Geotechnical Earthquake Engineering Handbook*. McGraw-Hill, New York, New York, USA.

DGSI (2017). Field Testing - Torvane. Durham Geo Slope Indicator. Access date: 2017-09-26, url: http://www.durhamgeo.com/testing/soils/field-testing-torvane.html.

D'Ignazio, M. (2016). *Undrained Shear Strength of Finnish Clays for Stability Analyses of Embankments*. Phd dissertation, Tampere University of Technology, Tampere, Finland.

Dobry, R. and Vucetic, M. (1987). Dynamic Properties and Seismic Response of Soft Clay Deposits. In Mendoza, M. and Montanez, L., editors, *Proceedings of the International Symposium on Geotechnical Engineering of Soft Soils*, page 37, Mexico City, Mexico.

DvhN (2013). Longread Aardbevingen. Access date: 2017-05-15, url: http://redactie.dvhn.nl/aardbevingen/.

Elnashai, A. and Di Sarno, L. (2008). *Fundamentals of Earthquake Engineering*. Wiley & Sons Ltd., Chichester, United Kingdom.

Foulger, G. R., Wilson, M., Gluyas, J., and Davies, R. (2015). Human-Induced Earthquakes on the Rise. Access date: 2017-08-20, url: https://www.ecowatch.com/human-induced-earthquakes-2211992752/.

Foulger, G. R., Wilson, M., Gluyas, J., and Davies, R. (2016). Human-induced Earthquakes. Technical Report June 2016, Nederlandse Aardolie Maatschappij (NAM).

Google (2017). Google Maps indication of Multiple Locations. Online. Access date: 2017-09-06, url: https://www.google.nl/maps/@53.3491079,6.5036033,10.74z/data=!4m2!6m1!1s1ykGu4Ybp2boCGhwutqubB54T00c.

Groholski, D. and Hashash, Y. (2015). Evaluation of 1-D Non-linear Site Response Analysis using a General Quadratic / Hyperbolic Strength-Controlled Constitutive Model. In *6th International Conference on Earthquake Geotechnical Engineering*, number November, Christchurch, New Zealand.

Gutenberg, B. and Richter, C. (1954). *The Seismicity of the Earth*. Princeton University Press, Princeton, New Jersey, USA.

Gutierrez, A. (2006). Determination of Atterberg limits: Uncertainty and Implications. *Journal of Geotechnical and Geoenvironmental Engineering*, 132(3):420–424.

Hardin, B. and Black, W. (1969). Vibration Modulus of Normally Consolidated Clay (closure). *Journal of the Soil Mechanics and Foundation Division. ASCE 95:6, 1531-1537*.

Hashash, Y., Musgrove, M., Harmon, J., Groholski, D., Phillips, C., and Park, D. (2016). DEEPSOIL 6.1, User Manual. Technical report, University of Illinois at Urbana-Champaign, USA.

He, H., Doeksen, J., van Es, J., Ringers, R., and van Viegen, B. (2016). Inspecties en Versterkingsadvies Aardbevingsbestendigheid Objecten - NLTH-analyse Geotechniek met DIANA. Technical Report november, VIIA, Groningen.

Ishihara, K. (1996). *Soil Behaviour in Earthquake Geotechnics*. Clearendon Press, Oxford, United Kingdom.

Jamiolkowski, M., Ladd, C., Germain, J., and Lancellotta, R. (1985). New developments in field and laboratory testing of soils. In *Proceedings of the 11th International Conference on Soil Mechanics and Foundation Engineering*, volume 1, pages 57–153, San Francisco, USA.

Junfeng, C. and Weidong, F. and Fanyue, M. and Shuanglin, D. (2014). Effect of Shear Wave Velocity on the Ground Motion Parameters of Site Surface. *Earthquake Research in China*, 28(2).

Kamp, H. (2013). Gas Extraction in Groningen.

Kanai, K. (1983). *Engineering Seismology*. University of Tokyo Press, Tokyo, Japan.

Koster, H. and van Ommeren, J. (2015). A shaky business: Natural gas extraction, earthquakes and house prices. *European Economic Review*, 80:120–139.

Kramer, S. (1996). *Geotechnical Earthquake Engineering*. Prentice-Hall, Inc., Upper Saddle River, New jersey, USA.

Kruiver, P., de Lange, G., Wiersma, A., Meijers, P., Korff, M., Peeters, J., Stafleu, J., Harting, R., Dambrink, R., Busschers, F., and Gunnink, J. (2015). Geological schematisation of the shallow subsurface of Groningen. For site response to earthquakes for the Groningen gas field. Technical report, Deltares.

Kruiver, P., van Dedem, E., Romijn, R., de Lange, G., Korff, M., Stafleu, J., Gunnink, J., Rodriguez-Marek, A., Bommer, J. J., van Elk, J., and Doornhof, D. (2017). An Integrated Shear-wave Velocity Model for the Groningen Gas Field, The Netherlands. *Bulletin of Earthquake Engineering*, (February 2017). http://link.springer.com/10.1007/s10518-017-0105-y.

Kulhawy, F. H. and Mayne, P. (1990). Manual on Estimating Soil Properties for Foundation Design. Technical report, Eletric Power Research Institute EL-6800, Project 1493-6, Palo Alto, California, USA.

Kumar, S., Arindam, D., and Krishna, A. (2015). Equivalent linear and Nonlinear Ground Response Analysis of Two Typical Sites at Guwahati City. In *Indian Geotechnical Conference*, number June 2015, Kakinada, India.

Kvalseth, T. O. (1985). Cautionary Note about R2. *The American Statistician Association*, 39(4):279–285.

Ladd, C. and Foott, R. (1974). A New Design Procedure for Stability of Soft Clays. *International Journal of Rock Mechanics and Mining Sciences & Geomechanics Abstracts*, 11(11):220.

Laerd-Statistics (2015). Statistical tutorials and software guides. Retrieved from: https://statistics.laerd.com/.

Lloret-Cabot, M., Fenton, G. A., and Hicks, M. A. (2014). On the Estimation of Scale of Fluctuation in Geostatistics. *Georisk: Assessment and Management of Risk for Engineered Systems and Geohazards*, 8(2):129–140.

Lunne, T., Robertson, P., and Powell, J. (1997). *Cone Penetration Testing in Geotechnical Practice*. EF Spon/Routledge Publ., New York, New York, USA.

Matasovic, N. and Hashash, Y. (2012). Practices and Procedures for Site-Specific Evaluations of Earthquake Ground Motions. Technical Report 428, National Cooperative Highway research Program.

Mayne, P. (2007). Cone Penetration Testing - A Synthesis of Highway Practice. Technical report, National Research Council (U.S.). Transportation Research Board and National Cooperative Highway Research Program and American Association of State Highway and Transportation Officials and United States. Federal Highway Administration, Washington, D.C., USA.

Mayne, P. (2012). Quandary in geomaterial characterization: new versus the old. In McCabe, B., Pantazidou, M., and Phillips, D., editors, *Shaking The Foundations of Geo-Engineering Education*, page 330. CRC Press. Taylor & Francis Group.

Mayne, P., Coop, M., Springman, S., Huang, A.-B., and Zornberg, J. (2009). Geomaterial Behaviour and testing Comportment et essai de Geomaterial. In Hamza, M., Shahien, M., and El-Mossallamy, Y., editors, *17th International Conference on Soil Mechanics and Geotechnical Engineering*, volume 4, pages 2777–2872, Alexandria, Egypt. Millpress/IOS Press Rotterdam.

Mayne, P. W. (1980). Cam-Clay predictions of undrained strength. In Journal of the Geotechnical Engineering Division, editor, *Proceedings of the American Society of Civil Engineers*, volume 106, pages 1219–1242.

Mayne, P. W. (1988). Determining OCR in Clays from Laboratory Strength. *Journal of Geotechnical Engineering*, 114(No. 1).

Mayne, P. W. (2014). Interpretation of Geotechnical Parameters from Seismic Piezocone Tests. In Robertson, P. and Cabal, K., editors, *3rd International Symposium on Cone Penetration Testing (CPT'14, Las vegas), ISSMGE Technical Committee TC 102*, pages 47–73.

Mitchell, J. (1976). *Fundamentals of Soil Behaviour*. Wiley, J. and Sons, Upper Saddle River, New jersey, USA.

Mulder, E., Geluk, M., Ritsema, I., Westerhoff, W., and Wong, T. (2003). *De ondergrond van Nederland*. Wolters-Noordhoff, Groningen/Houten.

NAM (2003). Groningen Winningsplan 2003. Technical report, Nederlandse Aardolie Maatschappij (NAM), Den Haag, the Netherlands.

NAM (2016). Study and Data Acquisition Plan Induced Seismicity in Groningen Update Post - Winningsplan 2016. Technical report, Nederlandse Aardolie Maatschappij (NAM).

NEN 9997-1 (2012). Geotechnisch ontwerp van contructies - Deel 1: Algemene Regels. Technical Report april 2012, NEN.

NPR 9998 (2015). Nederlandse praktijkrichtlijn - NPR 9998 - Beoordeling van de constructieve veiligheid van een gebouw bij nieuwbouw, verbouw en afkeuren – Grondslagen voor aardbevingsbelastingen: geïnduceerde aardbevingen. Technical Report december 2015, NEN.

NPR 9998 (2017). Nederlandse praktijkrichtlijn - NPR 9998 - Beoordeling van de constructieve veiligheid van een gebouw bij nieuwbouw, verbouw en afkeuren – Grondslagen voor aardbevingsbelastingen: geïnduceerde aardbevingen. Technical Report juni 2017, NEN.

O'Kelly, B. (2015). Atterberg Limits Are Not Appropriate for Peat Soils. *Geotechnical Research*, 2(3):123–134.

Peck, R., Hanson, W., and Thornburn, T. (1974). *Foundation Engineering*. Wiley, J. and Sons, New York, New York, USA.

Pitilakis, K., editor (2007). *Earthquake Geotechnical Engineering*, volume 6. Springer.

Rathje, E. M., Kottke, A. R., and Trent, W. L. (2010). Influence of input motion and site property variabilities on seismic site response analysis. *Journal of Geotechnical and Geoenvironmental Engineering*, 136(4):607–619.

Richter, C. (1935). An Instrumental Earthquake Scale. *Bulletin of the Seismological Society of America*, 25(1):1–32.

Richter, C. (1958). *Elementary Seismology. A series of books in geology*. Freeman, W.H., San Francisco, California, USA.

Robertson, P. and Cabal, K. (2015). Guide to Cone Penetration Testing for Geotechnical Engineering. Technical report, Gregg Drilling & Testing, Inc.

Robertson, P. K. (2009). Interpretation of cone penetration tests — a unified approach. *Canadian Geotechnical Journal*, 46:1337–1355.

Schnabel, P., Lysmer, J., and Seed, H. (1972). SHAKE: A computer program for Earthquake response analysis of horizontally layered sites. Technical report, University of California, Berkeley, California, USA.

Schofield, A. and Wroth, P. (1968). *Critical State Soil Mechanics*. McGraw-Hill, London, UK.

Seed, B. H. B., Wong, R. T., Idriss, I. M., and Tokimatsu, K. (1986). Moduli and Damping Factors for Dynamic Analyses of Cohesionless Soils. 112(11):1016–1032.

Senthamilkumar, S. and Muthukkumaran, K. (2017). Study on influence of local soil conditions on ground motion amplification study on influence of local soil conditions on ground motion amplification. *Indian Geotechnical Society*, pages 57–61.

Shin, Y. J. and Kim, D. (2011). Assessment of undrained shear strength based on cone penetration test (cpt) for clayey soils. *KSCE Journal of Civil Engineering*, 15(7):1161.

Sorensen, K. and Okkels, N. (2013). Correlation between drained shear strength and plasticity index of undisturbed overconsolidated clays. In *Proceedings of the 18th International Conference on Soil Mechanics and Geotechnical Engineering*, pages 423–428, Paris, France.

Spetzler, J. and Dost, B. (2016). Probabilistic Seismic Hazard Analysis for Induced Earthquakes in Groningen. Technical report, Royal Netherlands Meteorological Institute (KNMI).

Spetzler, J. and Dost, B. (2017). Probabilistic Seismic Hazard Analysis for Induced Earthquakes in Groningen, Update June 2017. Technical report, Royal Netherlands Meteorological Institute (KNMI).

Stewart, J. P., Afshari, K., Hashash, Y. M. A., Shantz, T., Chiou, B. S.-J., Bozorgnia, Y., and Goulet, C. A. (2014). Guidelines for Performing Hazard-Consistent One-Dimensional Ground Response Analysis for Ground Motion Prediction. Technical report, PEER, Berkeley University, California, USA.

Stokoe, K., Darendeli, M., Andrus, R., and Brown, L. (1999). Dynamic Soil Properties: Laboratory, Field and Correlation Studies. In *2nd International Conference on Earthquake Geotechnical Enigineering*, pages Vol. 3, p(811–845).

Sun, D., Zhang, J., Gao, Y., and Sheng, D. (2016). Influence of suction history on hydraulic and stress-strain behavior of unsaturated soils. *International Journal of Geomechanics*, 16(6):D4015001.

TNO (2016). DINOloket - Data en Informatie van de Nederlandse Ondergrond. Online. Access date: 2017-05-23, url: https://www.dinoloket.nl/html.

Towhata, I. (2014). *Geotechnical Earthquake Engineering*. Springer Berlin Heidelberg.

USGS (2016). U.S. Geological Survay,. Online. Access date: 2017-05-19, url: https://earthquake.usgs.gov/learn/glossary/?term=magnitude.

van der Voort, N. and Vanclay, F. (2015). Social impacts of earthquakes caused by gas extraction in the Province of Groningen, The Netherlands. *Environmental Impact Assessment Review*, 50:1–15.

van Eck, T., Goutbeek, F., Haak, H., and Dost, B. (2006). Seismic Hazard due to Small-Magnitude, Shallow-Source, Induced Earthquakes in The Netherlands. Technical report, Royal Netherlands Meteorological Institute (KNMI).

van Elk, J., Doornhof, D., Bourne, S., Oates, S., Bommer, J., and Visser, C. (2013). Technical Addendum to the Winningsplan Groningen 2013 Subsidence, Induced Earthquakes and Seismic Hazard Analysis in the Groningen Field. Technical Report November, Nederlandse Aardolie Maatschappij (NAM).

van Wees, J. D., Buijze, L., Thienen-visser, K. V., Nepveu, M., Wassing, B. B. T., Orlic, B., and Fokker, P. A. (2014). Geomechanics Response and Induced Seismicity During Gas Field Depletion in The Netherlands. *Geothermics*, 52:206–219.

Vasileiadis, M. (2015). Groningen Earthquake Structural Upgrading - Region Specific CPT-Vs Empirical Correlation. Technical report, ARUP, London, United Kingdom.

Vos, P. (2015). *Origin of the Dutch Coastal Landscape. Long-term Landscape Evolution of the Netherlands During the Holocene, Described and Visualized in National, Regional and Local Palaeogeographical Map Series*. Phd dissertation, Utrecht University.

Vucetic, M. and Dobry, R. (1991). Effect of Soil Plasticity on Cyclic Response. *Journal of Geotechnical Engineering*, 117(1):89–107.

Wood, D. M. (1990). *Soil Behaviour and Critical State Soil Mechanics*. Cambridge University Press.

Woodward, P. K. and Griffiths, D. V. (1996). Comparison of the pseudo-static and dynamic behaviour of gravity retaining walls. *Geotechnical & Geological Engineering*, 14(4):269–290.

A

Tectonic Earthquakes

A.1. Introduction

This appendix includes a brief explanation of the Earth's structure, the factors that generate earthquakes, the main parameters and the fundamental terminology used to describe them. More detailed descriptions of these topics can be found in literature, e.g. Bolt (1999), Elnashai and Di Sarno (2008), Gutenberg and Richter (1954), Kramer (1996), etc.

A.2. Seismology and Plates Tectonics

Over the past, one of the most significant achievement of seismology was to understand the origin of the earthquakes by determining the internal structure of the Earth. The energy released by an earthquake causes strong ground shaking that can be measured at different point all around the globe. By analysing the propagation of seismic waves, the refraction and reflection mechanisms, it was possible to deduce the layered structure of the Earth.

As it is generally known, the Earth's crust is the outer rock layer internally characterised by a very complex geological structure and a variable thickness (Elnashai and Di Sarno, 2008). The Earth's crust is lying on top of a layer, called the *mantle*, that is mainly composed of dense silicate rocks, extending from a depth of approximately 60 km up to 2900 km (Elnashai and Di Sarno, 2008). In the upper mantle (at a depth of about 50 km) there is a soft warm layer called *asthenosphere*, on top of which the *lithosphere* moves horizontally due to convection currents present in the mantle with a velocity of approximately 1 to 10 cm per year.

The theory of "plate tectonics", dating back to the beginning of the nineteenth century, consists of the understanding of a large-scale tectonic process which involves a number of large and stable rigid rock slabs (with a thickness of around 100 km) that constantly move and collide between each other (Figure A.1). This theory provides an explanation for 95 % of the worldwide energy release (Elnashai and Di Sarno, 2008).

As described further by Richter (1958), the most important cause of earthquakes is represented by natural single disturbances, such as tectonic shocks. A consequence of the relative movement between the lithosphere and the asthenosphere is that large tectonic forces are generated at the edges of the tectonic plates. These forces provoke not only a number of chemical and physical consequences that affect the geology of plates, but also the generation of fractures.

However, an earthquake may be caused by a wide range of sources, for instance dislocations of the crust (tectonic earthquakes), volcanic eruptions, collapse of underground cavities, and human activities (Kramer, 1996). This can happen at different depth, from shallow (less than 60 km) to deep (between 300 and 700 km).

A.2.1. Rupture of Fault as a Cause of Earthquake

Figure A.2 depicts the most common types of fault movements: *normal fault, reverse fault, left-lateral strike-slip fault and right-lateral strike-slip fault.* The first two types belong to the *dip-slip faults* category and are generated by a relative vertical movement of one block with respect to another. Dip-slip faults are defined as *normal* if the block underlying the fault plane, so-called *footwall*, moves up the dip and away from the other block and tensile forces trigger the shearing failure of the fault. Contrarily, when the block overhanging the fault plane moves upward with respect to the footwall, the faults are reversed and the compressive forces are

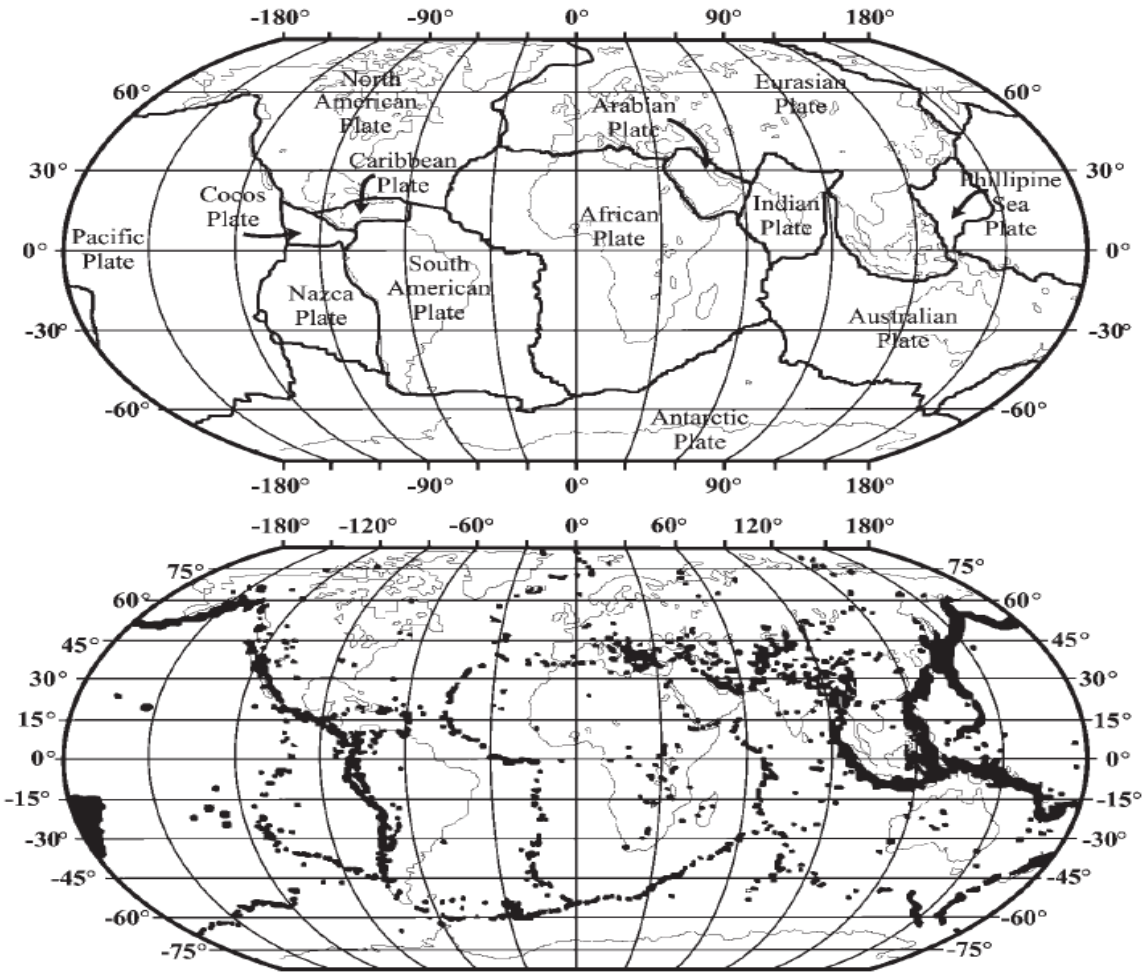

Figure A.1: Overview of tectonic plates (top) and representation of worldwide earthquake distribution (bottom) (source: Elnashai and Di Sarno, 2008).

responsible of the failure.
On the other hand, the strike-slip faults are generated by a horizontal movement between two adjacent blocks. The distinction between left-lateral and right-later is based on the position of the observer (located on one side of the fault line) and on his/her sense of relative motion between the two blocks. In this case, both compressive and tensile forces can be the cause of the relative movement of the two blocks.
There exist other two types of faults, namely *oblique-slip* and *rotational* faults, which are characterised by faults that exhibit a compound of strike-slip and dip-slip movements (oblique-slip) in which one block rotates relatively to the other (Elnashai and Di Sarno, 2008).

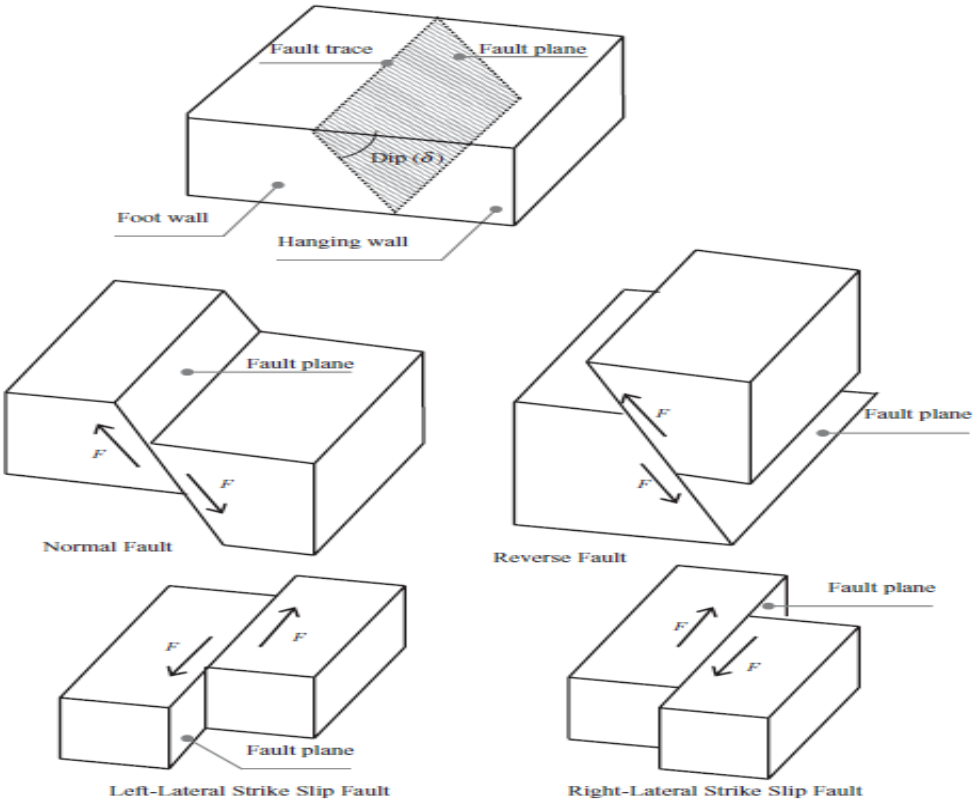

Figure A.2: Principal fault mechanisms of tectonic plates and representation of fault terminology and angle of dip (source: Elnashai and Di Sarno, 2008).

A.2.2. Geometric Considerations

An earthquake occurs when there exist a rupture of the rock along a fault.
In this section the terminology commonly used to describe the fault-based seismic events is presented.

- *Hypocentre* or *focus* is the point where the rupture is considered to have started;
- *Focal depth* is the distance between the hypocentre and the ground surface;
- *Epicentre* is the projection of the focus on the surface;
- *Epicentral distance* represents the distance between the observer and the epicentre.

Figure A.3 shows an illustration of the descriptive terminology accepted in seismology and earthquake engineering practice.
Few difficulties are encountered in characterising earthquake parameters and, especially, in defining the source (focus). Given that an earthquake is not generated at a single point, since the rupture may involve an area of thousands of square kilometres (Kramer, 1996), it may be complex to quantify the focal depth and the epicentral distance for seismology applications. For this purpose, a number of source-site relationships exist, but they should be cautiously used, in particular for large magnitude events and for near-field situations (when the site is very close to the epicentre) (Elnashai and Di Sarno, 2008).

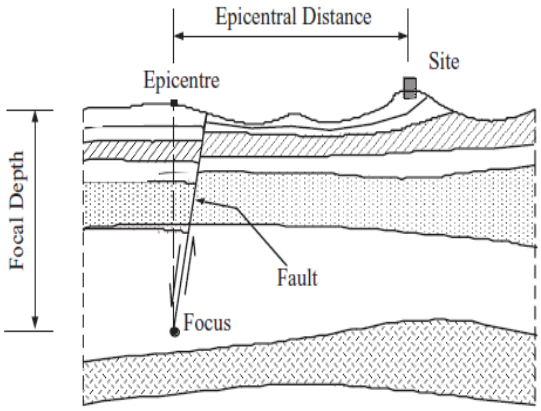

Figure A.3: Descriptive terminology used in common practice for geometric considerations of an earthquake (source: Elnashai and Di Sarno, 2008).

A.2.3. Seismic Waves

During the process of block dislocation, part of the potential energy of accumulated stresses is transformed in kinetic energy scattered around as seismic waves. In general, seismic elastic waves are divided into two types: *body waves* and *surface waves*. P- and S-waves belong to the body waves since they propagate outward from a source in all direction, through the body of the Earth. Whilst Love and Rayleigh waves (respectively L- and R-waves) are part of surface waves, propagating approximately parallel to the surface (Bolt, 1999).
An important difference between the two categories is that P- and S-waves can be reflected and refracted at the boundaries of different layers in the subsurface. When this occurs, part of the energy is transformed into another form of energy, modifying the type of wave as well, e.g. from S- to P-wave. Such reflections may provoke a significant local amplification of the ground shaking at the surface, leading to a high damage potential. Furthermore, the body waves can be also reflected by the "Mohorovicic discontinuity" (located at the interface between the Earth's crust and the mantle), causing the generation of strong motions and severe damage even at large distance from the source (Elnashai and Di Sarno, 2008).
Within the body waves, S-waves are considered the most damaging ones because of their horizontal (SH) and vertical (SV) motions of high amplitude. Contrarily, Primary waves, characterised by small amplitude and short period (similar to sound waves), displace relatively little damage potential.
The surface waves, on the other hand, are considered to have large damage potential due to their long duration and the fact that they propagate at relatively shallow depth where it is more likely to encounter structural systems at ground level (Elnashai and Di Sarno, 2008).
A more detailed description of wave characteristics is given in Table A.1, while in Figure A.6 is shown a schematic representation of the Earth's internal structure.

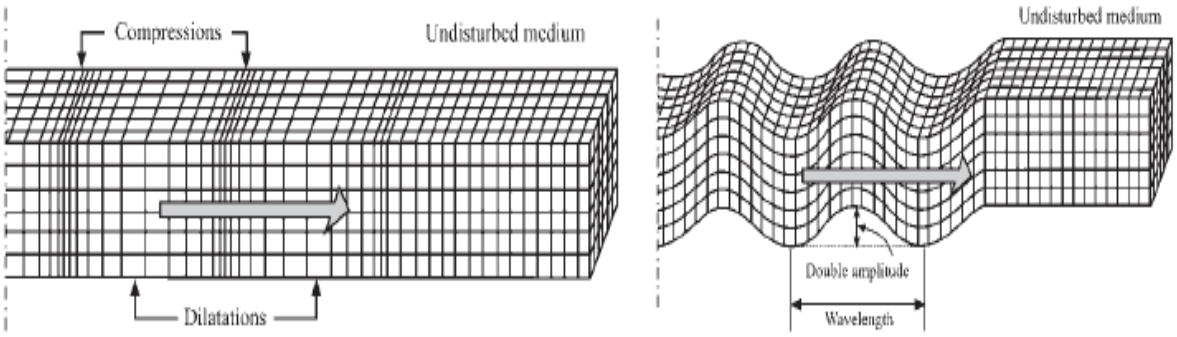

Figure A.4: Representation of travel path of body waves: primary or P-waves (left) and secondary or S-waves (right) (source: Bolt, 1999).

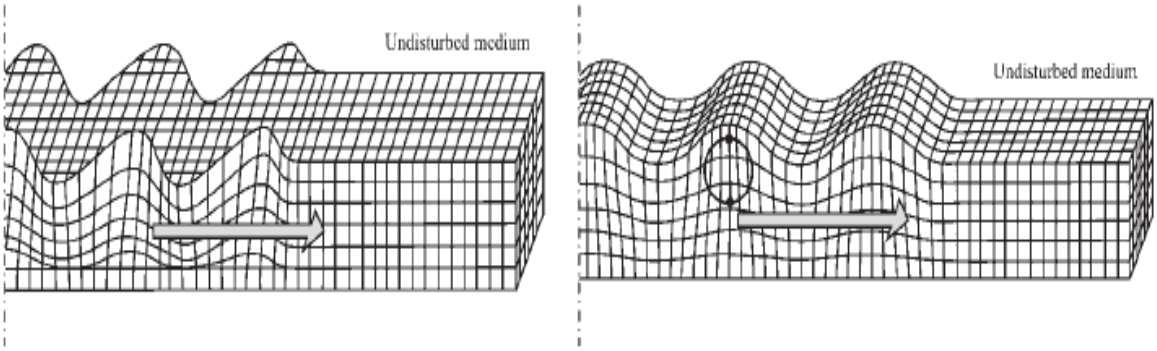

Figure A.5: Representation of travel path of surface waves: Love waves (left) and Rayleigh waves (right) (source: Bolt, 1999).

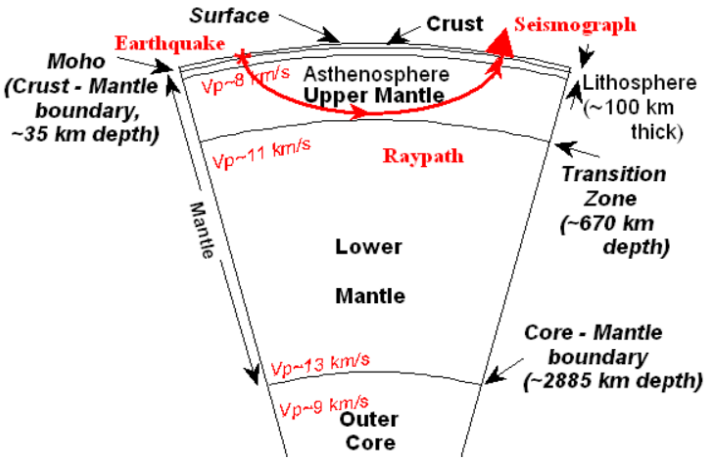

Figure A.6: Conceptual illustration of the internal structure of the Earth with an indication of the most important layer boundaries and approximate layer thicknesses, typical P-wave velocity at different depths, and rough ray path for body waves from a shallow earthquake (with the seismograph $\approx 2000km$ distant from the epicentre) (source: Braile, 2010).

Table A.1: Principal characteristics of seismic waves (adapted from Braile, 2010).

Wave Type (and names)	**Particle Motion**	**Typical velocity**	**Other Characteristics**
P, Compressional, Body waves, Primary, Longitudinal	Alternating push (compression) and pull (tension) directed in the same direction as the wave propagation direction (along the ray path) and perpendicular to the wavefront.	$V_P \approx 5-8km/s$ in Earth's crust, $> 8km/s$ in Earth's mantle and core.	P motion travels fastest in materials, so the P-wave is the first-arriving energy on a seismograph. Generally they show smaller but higher frequency than the S-waves.
S, Shear, Body waves, Secondary, Transverse	Alternating transverse motions (perpendicular to the propagation direction and the ray path) and causing stress generation in the rock along their path (thus also called shear waves).	$V_S \approx 3-4km/s$ in Earth's crust, $> 4.5km/s$ in Earth's mantle and $\approx 2.5-4km/s$ in the solid core.	S-waves travel slower than P-waves in solid materials, in fact, they arrive after the P-wave to a seismograph. S-waves do not travel through fluids.
L, Love, Surface waves, Long waves	Transverse motion, both horizontal and perpendicular to the direction of propagation and generally parallel to the Earth's surface and underlying boundaries.	$V_L \approx 2-4.4km/s$ depending on the frequency of the propagating wave and penetration depth.	Love waves' amplitude is larger at the surface and decreases with depth. The wave velocity is dependent on frequency: generally with low frequencies L-waves propagate at higher velocity. The penetration depth of the Love waves is also dependent on frequency: with lower frequencies they reach greater depth. Cannot travel through liquids
R, Rayleigh, Surface waves, Long waves, Ground roll	Motion is both perpendicular and parallel to the direction of propagation. The motion is generally elliptical (either prograde or retrograde) with the long axis perpendicular to the Earth's surface.	$V_R \approx 2-4.2km/s$ depending on the frequency of the propagating wave and penetration depth. Generally, Rayleigh waves are slightly slower than Love waves.	Rayleigh waves' amplitude is larger at the surface and decreases with depth. The penetration depth of the Rayleigh waves is dependent on frequency: with lower frequencies they reach greater depth.

A.3. Ground Motion Records

The planet vibrates incessantly at intervals that range from few milliseconds to entire days, and with amplitudes that vary significantly from nanometers to meters.
Seismic events with very low amplitudes cannot be perceived by people and sometime cannot be recorded without specialised measurement instruments. According to Kramer (1996), this microseismic activity is of considerable importance for seismologists more than earthquake engineers who, contrarily, are more interested in *strong ground motions*, whose strength can affect people and structures.
Ground motions can be described by rotational (generally neglected), translational and orthogonal components which can be found in a typical ground motion record, such as *acceleration-time histories* (Towhata, 2014).
For engineering purposes, it is not necessary to replicate precisely every time history record, but it results to be more convenient to analyse the records and extract a number of parameters that describe the characteristics of the ground motion. As indicated by Kramer (1996), the main parameters needed in practice are: *amplitude, frequency content* and *duration* of the earthquake.

A.4. Ground Motion Parameters

In this section, the crucial parameters that determine ground motion characteristics are briefly described, namely amplitude and frequency parameters, duration, magnitude and seismic intensity. The techniques and specific equipment used to measure ground motions, such as seismographs and accelerographs, can be found in literature, e.g. Kramer (1996), Towhata (2014).

A.4.1. Amplitude Parameters

The amplitude of ground motion and the response spectrum can be determined through the computation of ground acceleration, velocity and displacement. Generally, only the acceleration is directly measured at different locations (e.g. on a rock outcrop and/or at a certain depth in the subsurface), while the remaining quantities are computed by integration. This produces a sort of frequency filtering effect: the frequency decreases gradually, going from acceleration to displacement (Elnashai and Di Sarno, 2008).

Peak Ground Acceleration

Perhaps, the most frequently used parameter in engineering practice is the *horizontal peak ground acceleration* (HPGA or PGA). This represents the maximum (absolute) horizontal acceleration obtained from an accelerogram, which is identical to the spectral acceleration at zero period (independently of damping level). HPGA is commonly considered to be more important than the vertical acceleration (VPGA) for two main reasons: 1) generally the structures are well designed to resist vertical loads by the counteraction of the static vertical forces, while they can be less resistant to horizontal earthquake loads (Elnashai and Di Sarno, 2008); 2) the vertical component of ground motion has, most of the times, a lower frequency content than the horizontal component (Kramer, 1996).
Generally speaking, motions with high PGAs exhibit a greater damage potential than motions with low peak acceleration, because of their shorter period (Braile, 2010). However, the PGA does not give enough indications about the frequency content and the duration of the ground motion (Elnashai and Di Sarno, 2008).

Peak Ground Velocity

By integrating the acceleration measurements, it is possible to obtain the *peak ground velocity* (PGV). According to Bommer. and Alarcón (2006) (in Booth, 2007), there exists methods to compute PGV directly from spectral values. Also in this case, there is a distinction between horizontal and vertical components of velocity and, as previously, the horizontal component is considered more crucial for determining motion characteristics. Since the velocity is less sensitive to higher-frequency, it is more recommended to describe motion at intermediate-frequency levels. This can be more useful for structures which are affected by intermediate-frequency range of motions (e.g. tall or flexible buildings, bridges) (Kramer, 1996).

Peak Ground Displacement

Accordingly, displacement is obtained by integrating velocity (Akkar and Özen, 2005). Peak displacements are typically associated with lower-frequency ranges of ground motions. Nonetheless, it is considerably an

arduous procedure obtaining accurate values of displacement due to long-period noise and signal processing errors that may occur during the filtering and integration processes. Consequently, this parameter is less popular as a measure of ground motion (Kramer, 1996).

A.4.2. Frequency Parameters

An earthquake can display a wide range of frequencies. The description of the *frequency content*, thus, is important to capture the distribution of the amplitude of a ground motion among different frequencies (Day, 2002).
The frequency content of a strong motion is generally described through the use of Fourier spectra, power spectra and response spectra. The former is the result of a Fourier analysis and is used to decompose a complex loading function of time (e.g. a strong ground motion imposed by an earthquake) into a series of simple harmonic loading functions displayed over a broader range of frequencies (or periods), taking into account source effects (e.g. seismic moment, corner frequency, density of the medium of the seismic bedrock), the effect of propagation path from the source to the seismic bedrock, and site conditions (Hashash et al., 2016). In general, a narrow spectrum indicates that the motion has a dominant frequency, which can produce a smooth (almost sinusoidal) time history, while a broad spectrum implies a motion characterised by a variety of frequencies, leading to a more irregular time history. Fourier spectral amplitudes can be plotted in logarithmic scale versus frequency to illustrate the spectra characteristics in a clearer and more telling manner. As shown in figure A.7, the Fourier amplitude results to be maximum and constant (plateau) between an intermediate range of frequencies, namely the *Corner Frequency,* f_c, and the *Cut-off Frequency,* f_{max}. The corner frequency is inversely proportional to the cubic root of the seismic moment (see Section A.4.4), meaning that larger magnitude earthquakes produce greater low-frequency motions and long period components of motions. Contrarily, the cut-off frequency is assumed to be constant for a given geographic region, being function of near-site effect and/or source effects (Kramer, 1996).
The power spectra, also known as *Power Spectral Density Function*, are employed to study the frequency content of a ground motion by describing a random field in which the statistical quantities are not time-dependent. In general, earthquakes are non-stationary random processes and should be tackled with different approaches (e.g. deterministic intensity function and evolutionary power spectrum). However, considering that the intensity of a seismic event remains approximately constant for a temporal interval of the motion, power spectra can be used for simple interpretations. Precisely, recorded strong motions accelerograms, commonly, show that the largest intensity value occurs in the early part of the motion, while it decreases near the end of the motions, after being constant for a relatively short period of time.
Finally, response spectra are used to describe the response of a single-degree-of-freedom system (SDOF), giving information about the maximum response of a structure and damping ratio of the system (more information in Chapter 2, Section 2.4.4), based on the damping ratio and the natural period of the input motion (Elnashai and Di Sarno, 2008).

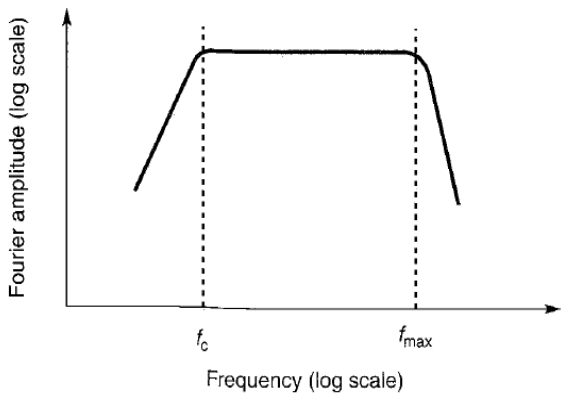

Figure A.7: Theoretical shape of smoothed Fourier amplitude spectrum with representation of corner frequency and cut-off frequency (source: Kramer, 1996).

A.4.3. Duration

A crucial factor in determining the structural damage is the duration of strong ground motion, which is related to the time required for release of the accumulated strain energy (Kramer, 1996), which is way longer than the earthquake duration time (Towhata, 2014). Duration is important also for the activation of a number of physical phenomena that are based not only on the load itself, but also on load and unload cycles and the stress path that is generated. For instance, a motion with a relatively low amplitude but with a long duration can be cause of important damage due to the generation of abundant load reversal.
The duration is also related to the magnitude of the earthquake: the time span of strong motions becomes longer for greater earthquake magnitude. However, in case of a bilateral rupture (rupture that expands in opposite direction from the focus) the duration can be short, independently from the earthquake magnitude. Taking in exam an accelerogram, it is possible to set a threshold acceleration, fixed to ± 0.05 g, and register exceedances. Between the first and the last exceedance lies, generally, the only portion of acceleration that is interesting for engineering purposes: the strong motion (Kramer, 1996).

A.4.4. Magnitude

It is defined *magnitude* a descriptive method of the fault dimension and the size of the seismic event, depending on the peak amplitude of seismic waves.
Different measure scales have been developed in order to quantify the relative size of an earthquake, i.e. in Japan by Wadati in the 1920s, and in California by Richter in the 1930s (Kanai, 1983). Nowadays, the most commonly adopted are those scales which are *frequency-dependent*, meaning that there is a direct relation between the magnitude and the specific waves and their frequency. The most common is the *Richter Magnitude (M_L)*, which measures waves that are of remarkable importance for engineers due to their high damage potential (Richter, 1935). The Richter scale presumes the use of standard Wood-Anderson seismograph that have particular characteristics. Precisely, these seismographs measures the maximum seismic waves amplitude (A) at a distance of 100 km from the source (Elnashai and Di Sarno, 2008). The equation that expresses the dependency between the magnitude and the seismic waves amplitude is:

$$M_L = log(A) - log(A_0) \tag{A.1}$$

where A_0 is a calibration factor founded by Richter (1958).
However, the use of the Richter scale presents some disadvantages related to the fact that the maximum amplitude of seismic waves is recorded. Basically, the Richter scale is based on the vibrations registered at the surface, independently from the depth of the source. In this way, the amplitude of waves of a shallow earthquake with far less energy release would be captured at ground level with the same amplitude as a bigger earthquake at larger depth (Elnashai and Di Sarno, 2008).
In literature, in addition to semi-empirical correlations which consider the focal depth and local geological condition (Kanai, 1983), and scales specifically developed for certain wave types (e.g, Surface wave magnitude, Body wave magnitude etc.), there exists a scale that, rather than estimating the magnitude based on the amplitude of seismic waves, accounts for the released amount of energy (Elnashai and Di Sarno, 2008). This is called *Moment magnitude* (M_w) and was introduced by Hanks and Kanamori in 1979 (in Elnashai and Di Sarno, 2008). The moment magnitude involves consideration about the rock movement in terms of average slip between the two walls of the fault (Δu), the force necessary to overcome the friction between rocks generated by the formation of the rupture expressed in shear modulus (G), and the area of the rupture surface (A). The seismic moment does not depend on the wave length and may be calculated as well using the amplitude spectra of seismic waves (USGS, 2016). Precisely, M_w is related to the moment M_0 (expressed in ergs) that can be calculated as follows:

$$M_0 = G \cdot A \cdot \Delta u \tag{A.2}$$

From which the moment magnitude is computed as:

$$M_w = 0.67 \cdot log(M_0) - 10.70 \tag{A.3}$$

A.4.5. Seismic Intensity

In order to define the size of ground shaking, Mercalli introduced the so-called *seismic intensity* scale (between 1850 and 1914), that involves the analysis of both the damage and the human perception caused by earthquakes. The main difference between intensity and magnitude scales relies on the fact that the former depends on the place of observation, on the population density, on the construction quality of the structures and even on the people familiarity with earthquakes in that specific exposed region (Elnashai and Di Sarno, 2008). For instance, based on this scale, an earthquake of relatively small magnitude that occurs at a shallow depth may be rated as significantly important because of the large vibrations perceived at the surface. In this case, amplification factors, represented by the presence of soil deposits in superficial layers, can affect the ground shaking and the estimated intensity.

A.5. Summary and Conclusions

In this appendix the main features of natural earthquakes are reported as a part of the literature review.
The most relevant topics discussed are summarised as follows:

- Natural (tectonic) earthquakes are triggered mainly by tectonic movements and fault activity (caused by the collision and interaction between different tectonic plates). There exist several types of faults which generate different kinds of forces (shear, compression, and tension), based on the direction of the relative movement between two blocks.
- Seismic waves are divided in body and surface waves. Although body waves are generally faster and stronger in amplitude, surface waves are considered to have the same or even larger damage potential, because of their long duration and shallow depth.
- Earthquakes are also known as the cause of strong ground motions, which can be described by a number of parameters, such as amplitude, frequency content, and duration. All these information can be extrapolated from acceleration-time history records. Nonetheless, the raw data obtained from a seismograph need to be corrected, removing non-seismic noises.
- Amplitude parameters can be divided in: Peak Ground Acceleration (PGA), Peak Ground Velocity (PGV), and Peak Ground Displacement. The process of integration allows the calculation of displacements, starting from the recorded acceleration.
  Generally speaking, motions with high PGA (higher than 0.5 g) exhibit a greater damage potential because of their relatively short period.
- Frequency parameters can be divided in Fourier spectra, Power spectra, and Response spectra. The former category utilises logarithmic scales to plot the frequency (x-axis) versus the Fourier amplitude (y-axis); the Power spectra represent the frequency content through a random field (time independent); the Response spectra are employed to describe the maximum response and damping ratio of a SDOF.
- Duration, magnitude, and seismic intensity are essential for the determination of the damage caused by an earthquake. The duration gives information about the time span of the ground motion: the longer the duration the more damage is expected. The magnitude expresses the fault dimensions and the size of the event. Lastly, the seismic intensity considers also the vulnerability of the place (in terms of structures and people) where the event occurs.

B

Geotechnical Ground Investigation Database

B.1. Introduction

The aim of this appendix is to describe the geotechnical ground investigation database that includes information related to 50 study objects, of which 43 are provided with laboratory data.
The data used for correlation purposes originate from a total of 29 sites. Most of them are situated in the north and east of the city of Groningen (Figure B.1).
In the following sections, it will be described the database structure and the assumptions made throughout the entire compilation process.

Figure B.1: Representation of the location of the 29 municipalities (within the Groningen region) which the study objects belong to (created in Google, 2017).

B.2. Stratigraphy

One of the ultimate goals of creating a comprehensive GI database is to investigate the relation between CPT-based correlations and specific soils units. With this purpose, part of the database is dedicated to the soil classification, individuating the soil type at the depth where the samples were collected.
The soil classification follows the Dutch code (NEN 9997-1, 2012) (Figure B.2), for consistency. The section *Grondsoort* of this table is divided in three columns which indicate: primary soil, secondary soil and consistency, respectively. Whereas, the second part of the table (*Karakteristieke waarden van grondeigenschappen*) displays the characteristic values of a number of soil properties, such as soil unit weight (dry and saturated), cone resistance, consolidation coefficient, internal friction angle, cohesion etc. (Figure B.2).

Tabel 2.b — Karakteristieke waarden van grondeigenschappen

Grondsoort			Karakteristieke waarde[a] van grondeigenschap											
Hoofd-naam	Bijmengsel	Consis-tentie[b]	γ[c] kN/m³	γ_{sat} kN/m³	q_c[d,g] MPa	C'_p[g]	C'_s	$C_p/(1+e_0)$[g] [-]	C_a[f] [-]	$C_{sw}/(1+e_0)$[g] [-]	E_{100}[g,h] MPa	φ'[g] Graden	c' kPa	c_u kPa
Grind	Zwak siltig	Los	17	19	15	500	∞	0,0046	0	0,0015	45	32,5	0	
		Matig	18	20	25	1000	∞	0,0023	0	0,0008	75	35,0	0	n.v.t.
		Vast	19 20	21 22	30	1200 1400	∞	0,0019 0,0016	0	0,0006 0,0005	90 105	37,5 40,0	0	
	Sterk siltig	Los	18	20	10	400	∞	0,0058	0	0,0019	30	30,0	0	
		Matig	19	21	15	600	∞	0,0038	0	0,0013	45	32,5	0	n.v.t.
		Vast	20 21	22 22,5	25	1000 1500	∞	0,0023 0,0015	0	0,0008 0,0005	75 110	35,0 40,0	0	
Zand	Schoon	Los	17	19	5	200	∞	0,0115	0	0,0038	15	30,0	0	
		Matig	18	20	15	600	∞	0,0038	0	0,0013	45	32,5	0	n.v.t.
		Vast	19 20	21 22	25	1000 1500	∞	0,0023 0,0015	0	0,0008 0,0005	75 110	35,0 40,0	0	
	Zwak siltig, kleiig		18 19	20 21	12	450 650	∞	0,0051 0,0035	0	0,0017 0,0012	35 50	27,0 32,5	0	n.v.t.
	Sterk siltig, kleiig		18 19	20 21	8	200 400	∞	0,0115 0,0058	0	0,0038 0,0019	15 30	25,0 30,0	0	n.v.t.
Leem[e]	Zwak zandig	Slap	19	19	1	25	650	0,0920	0,0037	0,0307	2	27,5 30,0	0	50
		Matig	20	20	2	45	1300	0,0511	0,0020	0,0170	3	27,5 32,5	1	100
		Vast	21 22	21 22	3	70 100	1900 2500	0,0329 0,0230	0,0013 0,0009	0,0110 0,0077	5 7	27,5 35,0	2,5 3,8	200 300
	Sterk zandig		19 20	19 20	2	45 70	1300 2000	0,0511 0,0329	0,0020 0,0013	0,0170 0,0110	3 5	27,5 35,0	0 1	50 100
Klei	Schoon	Slap	14	14	0,5	7	80	0,3286	0,0131	0,1095	1	17,5	0	25
		Matig	17	17	1,0	15	160	0,1533	0,0061	0,0511	2	17,5	5	50
		Vast	19 20	19 20	2,0	25 30	320 500	0,0920 0,0767	0,0037 0,0031	0,0307 0,0256	4 10	17,5 25,0	13 15	100 200
	Zwak zandig	Slap	15	15	0,7	10	110	0,2300	0,0092	0,0767	1,5	22,5	0	40
		Matig	18	18	1,5	20	240	0,1150	0,0046	0,0383	3	22,5	5	80
		Vast	20 21	20 21	2,5	30 50	400 600	0,0767 0,0460	0,0031 0,0018	0,0256 0,0153	5 10	22,5 27,5	13 15	120 170
	Sterk zandig	-	18 20	18 20	1,0	25 140	320 1680	0,0920 0,0164	0,0037 0,0007	0,0307 0,0055	2 5	27,5 32,5	0 1	0 10
	Organisch	Slap	13	13	0,2	7,5	30	0,3067	0,0153	0,1022	0,5	15,0	0 1	10
		Matig	15 16	15 16	0,5	10 15	40 60	0,2300 0,1533	0,0115 0,0077	0,0767 0,0511	1,0 2,0	15,0	0 1	25 30
Veen	Niet voorbelast	Slap	10 12	10 12	0,1	5 7,5	20 30	0,4600 0,3067	0,0230 0,0153	0,1533 0,1022	0,2 0,5	15,0	1 2,5	10 20
	Matig voorbelast	Matig	12 13	12 13	0,2	7,5 10	30 40	0,3067 0,2300	0,0153 0,0115	0,1022 0,0767	0,5 1,0	15,0	2,5 5	20 30
Variatiecoëfficiënt v			0,05		–	0,25					0,10		0,20	

Figure B.2: Characteristic values of soil properties (source: NEN 9997-1, 2012).

Table B.1 shows the soil types and the soil units (SU) investigated throughout the present research. To the main soil type it is usually assigned a number: 1 to Clay, 2 to Over Consolidated Clay, 3 to Sand, 4 to Peat, and 5 to Loam. Instead, the secondary soil type is indicated with a letter. For instance, for the soil unit Clay (SU1), the letter A indicates a Clean (Schoon) Clay, B a Sandy (Zandig) Clay, C a Silty (Siltig) Clay, and D an Organic (Organisch) Clay. Furthermore, the second number following the letter points out the soil consistency (e.g. SU1_A is the symbol used for a Soft Clean Clay, while SU1_A1 for a Moderately Stiff Clean Clay, and SU1_A2 for a Stiff Clean Clay) or the amount of fine contents present in the main soil (e.g. SU1_B stands for slightly Sandy Clay, SU1_B2 for moderately Sandy Clay, and SU1_B3 for highly Sandy Clay).

Table B.1: Summary of Soil Unit codes, soil type definition (Dutch + English), and average cone tip resistance and friction ratio ranges compiled in the GI database, after Table 2.b in NEN 9997-1 (2012).

Soil Unit Code	**Soil Type** Primary	**Soil Type** Secondary	**Soil Type** English	**q_c** [MPa]	**FR** [%]
SU1	Klei	-	Clay	0.5 - 2.5	1.4 - 7
SU1_A	Klei	Schoon, slap	Clay, clean, soft	0.2 - 0.7	2 - 4
SU1_A1	Klei	Schoon, matig	Clay, clean, moderately stiff	0.7 - 1.5	2 - 4
SU1_A2	Klei	Schoon, vast	Clay, clean, stiff	1.5 - 2.5	2 - 4
SU1_B	Klei	Zwak zandig	Clay, slightly sandy	0.7 - 2.5	3 - 5
SU1_B2	Klei	Matig zandig	Clay, moderately sandy	0.7 - 2.5	2 - 4
SU1_B3	Klei	Sterk zandig	Clay, highly sandy	0.7 - 2.5	1 - 3
SU1_C	Klei	Zandig/Siltig + Organisch	Clay, sandy/silty + organic	0.7 - 2.5	6 - 8
SU1_D	Klei	Organisch	Clay, organic	0.2 - 0.5	6 - 9
SU1_E	Klei	Zwak siltig	Clay, slightly silty	0.7 - 1.5	4 - 6
SU1_E2	Klei	Matig siltig	Clay, moderately silty	0.7 - 1.5	2 - 5
SU1_E3	Klei	Sterk siltig or Uiterst siltig	Clay, highly silty	0.7 - 1.5	1 - 3
SU2	Potklei	Potklei	Over Consolidated Clay	0.7 - 10	5 - 10
SU3	Zand	-	Sand	5 - 30	0 - 2
SU3_A	Zand	Schoon, los/vast	Sand, clean, loose/dense	5 - 25	0 - 1
SU3_B	Zand	Zwak siltig, kleiig	Sand, slightly silty, clayey	8 - 15	0 - 2
SU3_C	Zand	Sterk siltig, kleiig	Sand, highly silty, clayey	6 - 10	1 - 3
SU4	Veen	Niet voorbelast	Peat, not preloaded	0.1 - 0.2	6 - 8
SU4_A	Veen	Matig voorbelast	Peat, moderately preloaded	0.1 - 0.3	7 - 10
SU5	Leem	Zwak zandig	Loam, slightly sandy	1 - 3	2 - 4
SU5_B	Leem	Sterk zandig	Loam, highly sandy	1 - 3	1 - 3

B.3. Database Structure

One of the ultimate goals of creating this GI database is to investigate the relation between CPT-based correlations and specific soils units. With this purpose, the database is built as Excel spreadsheets that could be easily imported into SPSS and MATLAB, in order to perform the statistical analysis (Chapter 5 and 6). It is structured with the following sheets:

1. Objects Overview
2. Plasticity Index
3. Undrained Shear Strength

B.3.1. Sheet - Overview

The first sheet represents a general overview of the 50 study objects in analysis. As listed below, every bullet point corresponds to an excel sheet's column:

- **Owner DB**: database owner indicating the party which originally provided field and laboratory investigation data
- **DB nr**: number of the database from which the data have been retrieved
- **Objects nr**: object identity as it is named within the project
- **Report ID**: geotechnical report containing field and laboratory data, provided by external contractors (e.g. Fugro, Mos Grondmechanica, and Wiertsema & Partners)
- **Object name**: address of the object location
- **Location**: object location, specifying the municipality which the object belongs to
- **SCPT**: amount of available Seismic Cone Penetration Test (SCPT)

- **CPT**: amount of available Cone Penetration test (CPT)
- **CPT nr**: SCPT and CPT identity
- **Boring**: amount of available boreholes
- **Borehole nr**: borehole identity
- **Borehole adjacent to CPT**: indication of an approximate distance between boreholes and CPTs (and/or SCPTs) expressed in meters
- **Handboring**: amount of available handborings
- **Handboring nr**: handboring identity
- **Reported Atterberg Limits**: Atterberg Limits availability, indicated as *ja* or *nee*
- **Available Atterberg Limits**: amount of Atterberg Limits
- **Particle Size**: amount of samples with particle size distribution
- **Unit Weight**: amount of unit weight measurements
- **Organic Content Test**: amount of organic content tests
- **Loss on Ignition**: amount of loss of ignition tests
- **DSS tests**: amount of Direct Simple Shear tests
- **Triaxial UU**: amount of Undrained Unconsolidated triaxial tests
- **Triaxial CU**: amount of Undrained Consolidated triaxial tests
- **Torvane**: amount of Torvane tests
- **Compression tests (5 steps)**: amount of 5 steps Compression tests
- **Compression tests (7 steps)**: amount of 7 steps Compression tests

The data regarding the 17 objects provided by VIIA were obtained from *Overzicht laboratoriumonderzoek 12-12-2016.XLS*, VIIA project written communication, 12-12-2016.
The 17 objects named as Y are provided with an official ID, however, in the present report they are indicated with fictitious names (e.g. *Y1*, *Y2*, and *Y3*) for confidentiality. Of these 17, the object *Y1*, lacking of laboratory data, has not been processed further (refer to Table B.2).
Similarly, 6 out of the 33 remaining objects, named as X, have been excluded from the analysis (five objects lacking of laboratory data: X6, X14, X16, X17, and X24; one lacking of CPTs: X32) (refer to Table B.2).
All the factual data, related to the 27 objects named as X, have been obtained directly from geotechnical reports. For these objects, the laboratory investigation is generally limited to the Atterberg Limits determination and Torvane tests for undrained shear strength estimation (Table B.2).
This overview revealed that it is essential to keep good traceability of the objects that have been analysed. The object ID are kept as named in the project directories for traceability. As well as, the identity of the geotechnical reports from the corresponding test is specified, since they contain all the laboratory data, CPT profiles, locations, etc.
Table B.2 presents a summary of the objects in analysis with the associated laboratory data used in this study.

Table B.2: Overview of objects' information with Atterberg Limits and undrained shear strength measurements

Object nr	SCPT	CPT	Boreholes	Atterberg Limits	Undrained Shear Strength
X1	1	1	10	26	-
X2	1	2	6	6	6
X3	1	1	6	6	6
X4	1	2	13	12	-
X5	1	1	8	28	-
X6	1	4	1	-	-
X7	1	-	4	3	-
X8	1	3	6	5	5
X9	1	-	5	5	5
X10	1	1	6	9	8
X11	1	2	4	2	4
X12	1	3	10	20	25
X13	1	-	3	-	8
X14	-	-	-	-	-
X15	1	3	11	17	-
X16	1	7	8	-	-
X17	1	1	9	-	-
X18	-	-	9	7	-
X19	-	-		15	-
X20	1	1	3	3	-
X21	1	1	6	12	-
X22	1	4	10	33	-
X23	1	3	9	11	-
X24	1	2	6	-	-
X25	-	-	3	3	3
X26	1	3	12	6	-
X27	1	-	6	16	-
X28	1	1	8	17	-
X29	1	1	7	12	-
X30	-	1	7	20	-
X31	1	3	11	10	-
X32	-	-	9	18	-
X33	1	3	9	4	-
Y1	1	1	1	-	-
Y2	1	8	1	6	24
Y3	-	5	1	8	21
Y4	-	3	2	8	27
Y5	-	1	-	5	-
Y6	-	3	-	5	-
Y7	-	5	-	5	-
Y8	-	11	-	4	-
Y9	-	7	5	4	-
Y10	-	4	4	4	-
Y11	-	5	2	2	-
Y12	-	3	2	5	-
Y13	-	2	3	3	-
Y14	-	1	3	2	-
Y15	-	4	4	3	-
Y16	1	4	1	3	24
Y17	1	4	1	5	24

B.3.2. Sheet - Plasticity Index

The plasticity index sheet contains information on factual (laboratory tests) and predicted PI values (e.g. using the Cetin and Ozan, 2009 correlation), as well as other the parameters (e.g. cone resistance, sleeve friction, pore water pressure, friction ratio, soil unit weight, vertical soil stress, effective vertical soil stress) utilised to calculate PI using CPT-based correlations for every study object (see Section 3.6.1 in Chapter 3). The calculated PI values are associated to the PI measurements in order to form data pairs.
It is organised as:

- **Owner DB**: database owner indicating the party which originally provided field and laboratory investigation data
- **DB nr**: number of the database from which the data have been retrieved
- **Objects nr**: object identity as it is named within the project
- **Report ID**: geotechnical report containing field and laboratory data, provided by external contractors (e.g. Fugro, Mos Grondmechanica and Wiertsema & Partners)
- **Location**: object location, specifying the municipality which the object belongs to
- **Boring**: amount of available boreholes
- **Borehole nr**: borehole identity
- **X coordinates and Y coordinates**: X and Y coordinates with respect to the Rijksdriehoekstelsel (RD) coordinate system in the Netherlands
- **Sample nr**: sample number as specified in the laboratory
- **Core Depth (m t.o.v. mv)**: core depth which indicates the depth, in meters, of the entire sampling core with respect to the local surface level (maaiveld, mv, in Dutch)
- **Middle Core Depth (m t.o.v. mv)**: representing the depth of the point at the middle of the sampling core with respect to the local surface level (mv), chosen as indicative of the specimen depth
- **Ground Level (m NAP)**: indicating the surface ground level with respect to NAP, in meters
- **Core Depth (m NAP)**: representing the depth of the sampling core with respect to NAP, in meters
- **Sample Depth (m NAP)**: sample depth with respect to NAP, obtained either selecting the point in the middle of the sample core (in case the latter was reported already with respect to NAP), or back calculating it using the middle core (with respect to mv) and the ground level depth
- **Closest CPT**: indicating the closest CPT with respect to the specific borehole, established from the *situation drawings* given in the surveys
- **PI;measured**: Plasticity Index obtained from laboratory tests, expressed in %
- **Depth in CPT (m NAP)**: depth at which the predicted value is calculated using the CPT-based correlations
- $\gamma_t; Mayne$ **(**kN/m^3**)**: soil unit weight (wet) calculated with the Mayne (2012) correlation
- $\gamma_d; Mayne$ **(**kN/m^3**)**: soil unit weight (dry) calculated with the Mayne (2012) correlation
- σ_v **(kPa)**: total vertical soil stress
- σ'_v **(kPa)**: effective vertical soil stress
- **Stress-normalised friction ratio FR (%)**: stress-normalised friction ratio according to equation 3.7 from Cetin and Ozan (2009)
- $q_{t;1;net}$ **(kPa)**: normalised net cone tip resistance according to equation 3.3 from Cetin and Ozan (2009)
- $q_{t;1}$ **(kPa)**: corrected cone tip resistance according to equation 3.2 from Cetin and Ozan (2009)

- **c (-)**: power law for $q_{t;1;net}$ estimation according to equation 3.4 from Cetin and Ozan (2009)
- **R (-)**: parameter for the estimation of the power law, c, according to equation 3.6 from Cetin and Ozan (2009)
- **PI;calculated (%)**: Plasticity Index calculated with the CPT-based correlation from Cetin and Ozan (2009)
- **Stratigraphic Unit**: indication of the geological unit according to Kruiver et al. (2015) and Bommer et al. (2017a)
- **Soil Unit (SU)**: indication of the soil unit symbols according to table B.1
- **SU Depth 1 (m NAP)**: top of the individuated geotechnical soil unit (SU) which the sample has been collected from
- **SU Depth 2 (m NAP)**: bottom of the individuated geotechnical soil unit
- **GWT (m NAP)**: groundwater table, expressed in meters NAP, as indicated in the geotechnical reports
- **Stratigraphy**: soil classification, indicating the primary soil type (e.g. klei, zand, etc.), the secondary soil type (zwak zandig, matig siltig, etc.), and the consistency (e.g. matig, stevig, los, etc.)
- **Comments**: additional notes on the soil classification
- **PI;Arup (%)**: Plasticity Index used in SRA calculations by Arup
- **PI;Bommer2017 (%)**: Plasticity Index as recommended by Bommer et al. (2017a)

For every object PI was calculated with the Cetin and Ozan (2009) correlation to have a complete overview of measured and predicted values of PI. In order to do so, a CPT was associated to every borehole, and calculated PI values were taken from the closest CPT.
In most of the cases, samples were collected within the first 5 m of soil (often from hand-boring), and only in few cases (e.g. objects X30, Y2, and Y17) samples' depths extend up to about 12 m, 25 m and 13 m NAP, respectively. Hence, it was not always possible to associate a CPT measurement to very shallow samples. Such specimens were paired to the first available CPT measurement.

B.3.3. Sheet - Undrained Shear Strength

As for the plasticity index sheet, the undrained shear strength sheet consists of factual data (Su measured in-situ and in laboratory) and Su values calculated with the SHANSEP and other CPT-based predictive models (i.e. Robertson and Cabal, 2015 and Bommer et al., 2017a). In Table B.2 are listed the 14 objects provided with Su measurements.
The structure from this excel sheet is:

- **Owner DB**: database owner indicating the party which originally provided field and laboratory investigation data
- **DB nr**: number of the database from which the data have been retrieved
- **Objects nr**: object identity as it is named within the project
- **Report ID**: geotechnical report containing field and laboratory data, provided by external contractors (e.g. Fugro, Mos Grondmechanica and Wiertsema & Partners)
- **Location**: object location, specifying the municipality which the object belongs to
- **Boring**: amount of available boreholes
- **Borehole nr**): borehole identity
- **X coordinates and Y coordinates**: X and Y coordinates with respect to the Rijksdriehoekstelsel (RD) coordinate system in the Netherlands

- **X coordinates and Y coordinates**: sample number as specified in the laboratory
- **Monster nr**: sample number as specified in the laboratory
- **Depth (m t.o.v. mv)**: sample depth expressed, in meters, with respect to the local surface level (maaiveld, mv, in Dutch)
- **depth (m NAP)**: sample depth expressed, in meters, with respect to NAP
- **Closest CPT**: indicating the closest CPT with respect to the specific borehole, established from the *situation drawings* given in the surveys
- Su**;measured (kPa)**: undrained shear strength measured in laboratory
- **lab test Type**: laboratory test type, indicating the name of the test performed in laboratory (i.e. Torvane, Triaxial CU, triaxial UU)
- **sig'c (kPa)**: stress level (or confining stress) measured in the triaxial apparatus at which the Su value is obtained
- **Consolidation Pressure (kPa)**: consolidation pressure applied in the triaxial apparatus (UU tests)
- **Strain rate (%/h)**: strain rate applied in the triaxial apparatus
- **Depth in CPT (m NAP)**: depth at which the predicted value is calculated using the CPT-based correlations
- $\gamma_t; Mayne$ **(**kN/m^3**)**: soil unit weight (wet) calculated with the Mayne (2012) correlation
- σ'_v **(kPa)**: effective vertical soil stress
- **m'(-)**: dimensionless empirical parameter according to equation 3.16 from Robertson and Cabal (2015)
- σ_v **(atm)**: total vertical soil stress
- σ'_p **(kPa)**: pre-consolidation stress
- **OCR (-)**: over consolidation ratio calculated as σ'_p/σ'_{v0}
- **OCR;adjusted (-)**: over consolidation ratio adjusted manually for uppermost layers
- Su**;SHANSEP (kPa)**: undrained shear strength extrapolated from the SRA-tool, calculated using the SHANSHEP correlation from Ladd and Foott (1974)
- q_t **(kPa)**: normalised cone tip resistance
- σ_v **(kPa)**: total vertical soil stress
- **Soil Unit (SU)**: indication of the soil unit symbols according to table B.1
- **SU Depth 1 (m NAP)**: top of the individuated geotechnical soil unit (SU) which the sample has been collected from
- **SU Depth 2 (m NAP)**: bottom of the individuated geotechnical soil unit
- **GWT (m NAP)**: groundwater table, expressed in meters NAP, as indicated in the geotechnical reports
- **Stratigraphic Unit**: indication of the geological unit according to Kruiver et al. (2015) and Bommer et al. (2017a)
- **Stratigraphy**: soil classification, indicating the primary soil type (e.g. klei, zand, etc.), the secondary soil type (zwak zandig, matig siltig, etc.), and the consistency (e.g. matig, stevig, los, etc.)
- **Su;Robertson (kPa)**: Su calculated using equation 3.19 with $N_{kt} = 15$

- **Su;V4 LB (kPa)**: Su calculated using the equations recommended by Bommer et al. (2017a) for clean clays
- **Su;V4 UB (kPa)**: Su calculated using the equations recommended by Bommer et al. (2017a) for sandy clays and clayey sands
- **Comments**: additional notes on the used Bommer et al. (2017a) correlations

CPT-based Su calculation with SHANSEP produces a value of Su is computed every 1 or 2 cm. However, due to the fact that CPT measurements often start at a certain depth, it was not always possible to associate a calculated Su value to those samples collected at very shallow depths (e.g. from 1 to -1 m NAP).
Analyses will be carried out with the aim of comparing different existing correlations in Chapter 5. Hence, a number of parameters (e.g. m', vertical total and effective soil stress, OCR, N_{kt}) are included as well in the database.

B.4. Factual Data Limitations

Generally speaking, classification of soils is a complicated task which presumes the use not only of different sources (e.g. CPTs, borehole logs, DINOloket stratigraphy, Soil Behaviour Type (SBT) charts, existing soil classification from existing SRAs, the official Dutch code), but also of engineering judgement, together with some experience and knowledge about the typical Groningen soil conditions and geology. With the purpose of analysing the in-situ measurements statistically (see Chapter 5), the data are provided with a qualitative indicator (e.g. sample class 1,2, and 3).
The following sections describe the main limitation encountered during the compilation process, such as pre-drilling, partially saturated soils, and depth mismatch between factual data and CPT measurements.

B.4.1. Pre-drilling

For penetration in man-made fills or hard soils a pre-drill is often realised with the purpose of avoiding that the drilling cone is damaged (Mayne, 2014). Pre-drilling is generally performed with a solid steel probe with a diameter larger than the cone. The measurements obtained from this phase may constitute an important source of error. More precisely, the uppermost part of the CPT profile (the first meter, generally) is found to contain higher friction ration than usual, as well as the measured cone resistance may be slightly higher than expected.
As an example, figure B.3 shows the first 11.5 meters of a CPT and figure B.4 represents the borehole log associated to this specific CPT (the closest). From the surface level (0.78 m NAP) up to approximately 5 m depth, the soil has been classified as sandy Clay. However, in the first 1.5 m of soil the friction ratio reaches a peak of about 6 %, suggesting that this clay contains peat or organic materials, while from -1.5 m to -5 m NAP the soil is characterised by a friction ratio between 3 and 4 %. Clearly, the difference in friction ratio indicates that these two soils are not identical. Nevertheless, considering that higher friction ratio may result from pre-drilling operations, it is relatively safe to classify the uppermost 5 m of soil as: slightly sandy Clay, soft (SU1_B).
In order to account for pre-drilling effects, soil classification has been carried out firstly comparing the CPT profile with the borehole log, and secondly comparing the profile with other CPTs in that specific area, double checking the conclusions previously drawn.

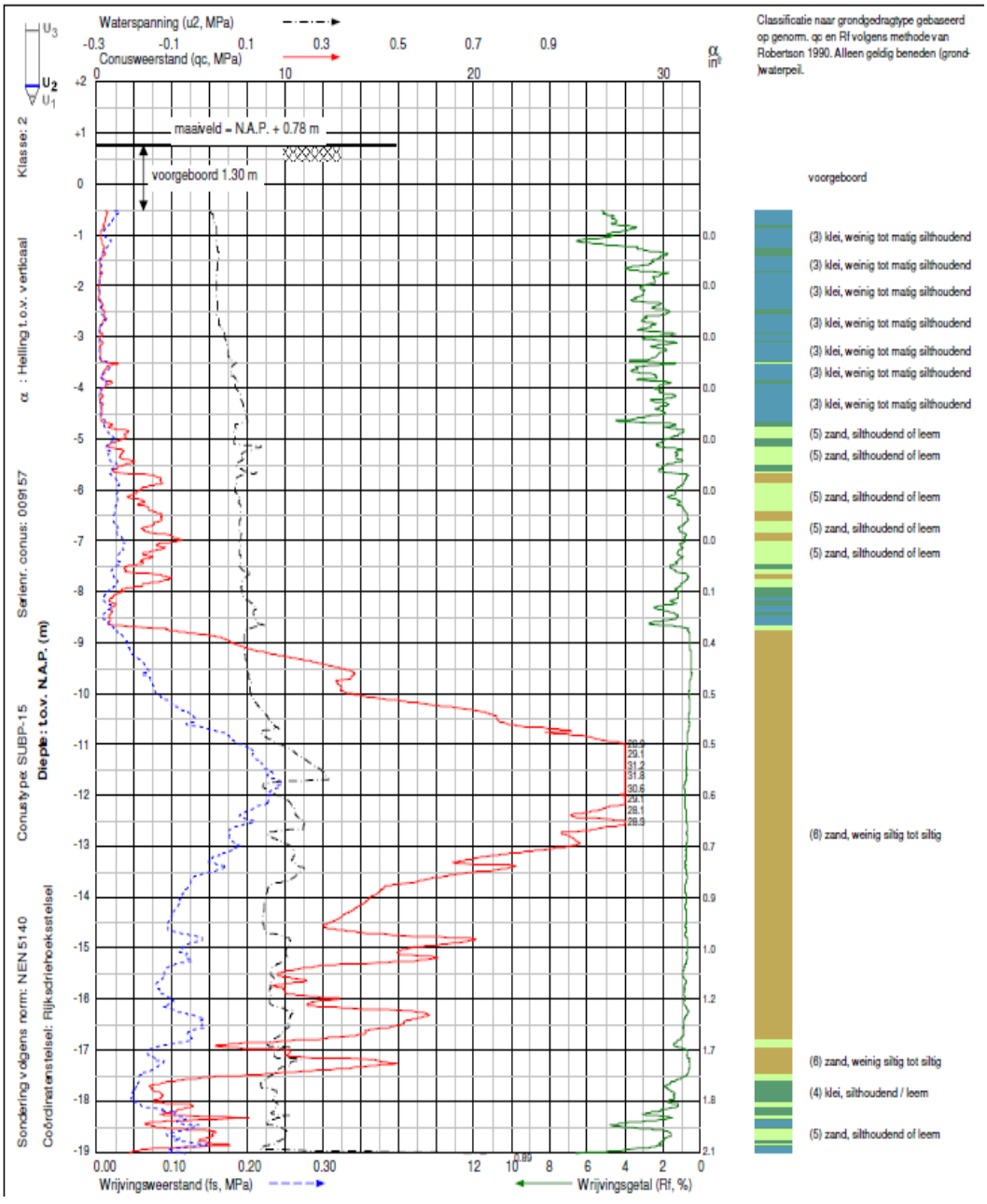

Figure B.3: First 11.5 m of a CPT from the object X1, showing in red the cone resistance profile, in blue the sleeve friction, and in green the friction ratio (source: Geotechnisch Onderzoek, report nr. XXX, Wiertsema & Partners BV).

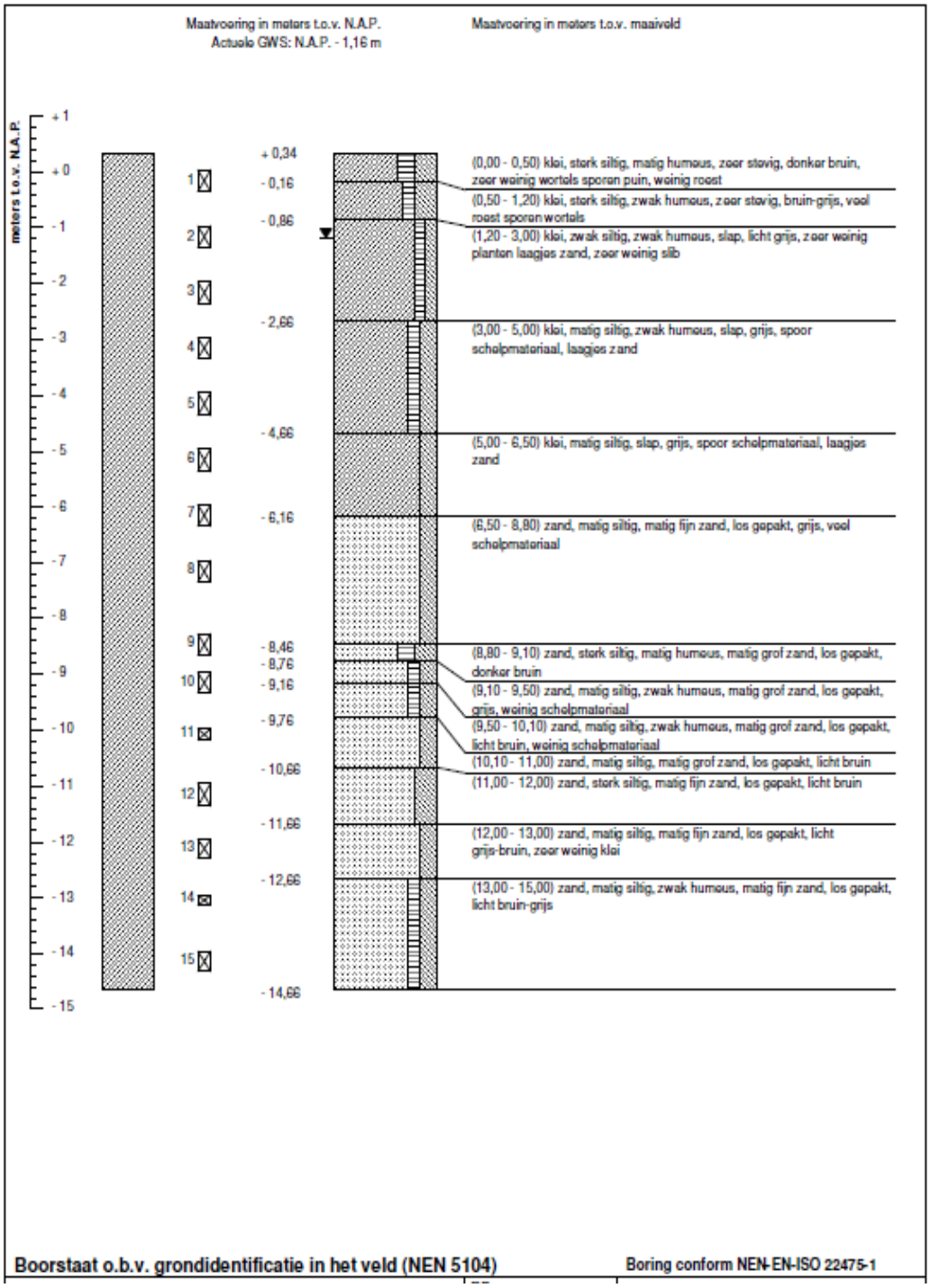

Figure B.4: Borehole representation, object X1, showing the depth in m NAP, the location of the samples (numbered, in this case, from 1 to 15) and the soil description with an indication of the depth of the top and the bottom of every individuated layer (source: Geotechnisch Onderzoek, report nr. XXX, Wiertsema & Partners BV).

B.4.2. Groundwater Table

An other important aspect to be taken into account during classification of soils is the ground water table. It is largely accepted that cone penetration test measurements above ground water table are not entirely reliable. Using the words of Mayne (2007):

> *[...]. At test depths above the ground water table, pore water pressure, as well as sleeve friction and cone resistance readings may vary with capillarity, moisture, degree of saturation, and other factors and should therefore be considered tentative.*

Unsaturated zones are of significant importance in geotechnical engineering, because of the complex soil behaviours that are observed above the groundwater table. Soils above the preathic surface can influence the effective stress calculations, given that the effective stress is directly related to the soil structure and the degree of saturation (Hilf, 1956, Bishop, 1960, etc., in Sun et al. (2016)).
Clayey soil deposits, formed in various climatic environments and different geological eras, are naturally characterised by complicated behaviours due to their stress history, resulting in different overconsolidation states. For instance, partially saturated soils such as silts and clays (modelled as a multi-phase system composed mainly of a water phase filling most of the voids and a discontinuous air phase), characterised by continuous void spaces and variable degree of saturation, are normally affected by a number of events such as capillarity (rise of the water within the capillary tubes), rainfall infiltration ans subsequent evaporation, which can lead to the modification of some of their soil properties (e.g. degradation of soil due to imposed wetting and drying cycles).
The variation in water content during the soil history is connected to the generation of negative pore water pressure (also known as suction) that may influence the stress-strain behaviour of soils. According to Sun et al. (2016), the samples that have undergone a higher suction throughout their history, such that the maximum skeleton average stress experienced in the past is higher than the current skeleton average stress, can be considered to be overconsolidated, and thus, higher values of shear strength can be expected.
The influence of suction history on the hydraulic and stress-strain behaviour of unsaturated soils (especially clayey soils) should be considered in constitutive models, and taken into account when empirical correlations are used in dynamic calculations.
Soil near the ground surface, where unsaturated or partially saturated soil are present, are often defined as "problematic" soils, and must be considered as such in assessing the quality of samples (Sun et al., 2016).
However, in this study, every sample is assumed to be fully saturated. This is possible considering that in Groningen the ground water table is relatively shallow (see Table B.4).

B.4.3. Correspondence among Laboratory and CPT Measurements Depth

Every sample tested in laboratory has an associated predicted value, obtained using CPT-based correlations, both for PI and Su. However, the majority of the samples are collected at relatively shallow depths (i.e. uppermost 2 m), whereas most of the CPT measurements begin after the pre-drilling phase (usually around 1.5 m below the surface level). Therefore, it was not always possible to associate to the laboratory samples CPT values (e.g. cone tip resistance and sleeve friction) at exactly the same depth. In these cases, the first available CPT measurement is used (i.e. at greater depths).
The step followed for the creation of data pairs are listed below:

1. Determination of the sample depth (m NAP)
2. Selection of the closest CPT to the sample's borehole
3. Individuation of the CPT measurements to be paired with the laboratory sample
   (a) Selection of CPT measurements at the same depth as the sample, if available
   (b) If not, selection of the first available CPT measurements (i.e. the closest)
4. Application of CPT-based correlations on the selected CPT measurements
5. Creation of data pair
6. Definition of sample class

To account for correspondence among laboratory and CPT measurements depth (i.e. point 3(b) in the above list), three sample classes are used to filter out the data pairs (Table B.3). Division in classes allows for more accurate statistical exploratory (see Chapter 5).
As an example, one of the samples from the object X1, collected at -0.87 m NAP, is paired to measurements from the CPT closest to the borehole. In this case, the CPT readings start at -0.52 m NAP, therefore, it is possible to create a data pair of measurements collected at identical depths. Consequently, this data pair is classified as Class 1 (Table B.3).
Oppositely, another sample, collected at a depth of 0.02 m NAP (from the same object: X1) is paired with the first available measurement from the closest CPT, which is at a depth of -74 m NAP, resulting in a depth mismatch of around 0.76 m. Hence, this data pair is classified as class 3, as the difference between sample and CPT measurement depth is larger than 20 cm (Table B.3).

Table B.3: Overview of soil classes created to account for depth mismatch between measured and calculated values

Sample Class	Description
1	Sample depth is identical to CPT measurements depth
2	Difference between sample and CPT measurements depths from 15 to 20 cm
3	Difference between sample and CPT measurements depths larger than 20 cm

Table B.4: Summary of sample depths, CPTs starting depth, and groundwater table (GWT) for all objects provided with laboratory data

Object nr -	**Samples depth range** [m NAP]	**CPTs starting depth** [m NAP]	**GWT depth range** [m NAP]
X1	0.02 to -1.45	-0.52, -0.74	-0.83 to -1.16
X2	-1.00 to -1.80	-1.39, -1.49, -1.49	-1.1 to -1.23
X3	-0.83 to -1.49	-0.62, -0.21	-0.58 to -1.2
X4	0.13 to -0.74	-0.44, -0.32	-0.19 to -1.03
X5	-0.14 to -2.10	-1.13, -1.59	-1.03 to -1.38
X7	0.25 to -0.38	-0.34	0.07 to 0.57
X8	0.88 to -0.38	-0.04	0.29 to -0.66
X9	0.01 to -0.38	-0.69	-0.14
X10	-0.15 to -1.18	-0.91, -1.29	-0.56 to -1
X11	-0.37 to to -1.12	-0.38, 0.26	-1.04
X12	-0.05 to -1.66	-0.57, -1.01, -0.52	-1.23 to -1.85
X13	-0.58 to -1.28	-1.14	-1.95 to -2.03
X15	-0.06 to -2.61	-1, -0.53, -0.80, -0.76	-0.75 to -1.52
X18	-1.99 to -3.74	-3, -2.58, -1.99	-2.24 to -3.37
X20	0.84 to -0.07	0.26, -0.16	0.74 to -0.07
X21	0.39 to -0.84	1.04	0.36 to -0.26
X22	-0.21 to -2.00	-0.40, -1.21, -1.54, -1.54, -1.31	-1.22 to -1.84
X23	0.35 to -1.42	-0.70, -0.36	-0.11 to -0.54
X25	-0.56 to -0.79	-0.13, -0.13	-0.36 to -0.38
X26	0.51 to -0.29	0.44, 0.13, 1.11	0.81 to -0.05
X27	-0.40 to -1.75	-0.97	-0.88 to -1.5
X28	-0.76 to -2.30	-1.52, -0.13	-1.07 to -1.9
X29	0.79 to -0.44	-0.51, -0.39	-0.35 to -0.78
X30	-0.01 to -11.98	-0.49, 0.61	-0.28 to -0.93
X31	0.04 to -0.50	-0.33, -0.24, -0.19, -0.35	10.29 to -0.08
X33	0.71 to -0.91	-0.54, 1.14, 0.48, 0.57	-0.55 -1.47
Y2	-3.46 - 29.29	-0.88	-5.1
Y3	-1.08 to -5.78	-0.79	-0.90
Y4	-0.16 to -4.44	-0.78	-1.4
Y5	-0.25 to -4.24	0.46	-0.87
Y6	0.69 to -3.04	1.36	0.13 to -0.03
Y7	0.40 to -3.56	0.98	-0.46
Y8	-2.80 to -3.03	-0.56, -0.66, -0.34, -0.55	-1.21 to -1.59
Y9	-4.14 to -5.05	-0.43, -0.40	-1.35 to -1.41
Y10	-3.31 to -4.04	0.31, 0.28	-0.89 to -0.99
Y11	-1.3 to -2.23	-0.11	-0.96 to -1.85
Y12	-1.6 to -3.69	-0.75, -0.81	-1.20 to -1.67
Y13	0.30 to -2.13	1.92, 2.01	0.48 to -0.07
Y15	-1.01 to -3.66	-1.71	0.54 to -0.72
Y16	-0.88 to -24.98	-0.63	-0.45
Y17	-1.72 to -14.69	-0.77	-0.42

B.5. Summary and Conclusions

The GI database developed for this research is reported in the present appendix. Table B.4 displays an overview, for every object, of the depth range of the collected samples, the range of the starting depth of CTP, and the ground water depth range. In addition, the main points of attention individuated in the present chapter are herein highlighted:

- An Overview database gives a general outlook of the object in analysis, including the location, the geotechnical report associated, the amount of data available per object, etc.
- Plasticity Index and Undrained Shear Strength measurements are divided in two different sheets named after the soil property in analysis. Predicted values (obtained by using CPT-based correlations) are associated to each measured value.
- The soil type of each sample is classified according to the Dutch national code (NEN 9997-1, 2012), considering a number of different sources such as laboratory soil classification (borehole logs), CPT reading (q_c and F_R profiles), DINOloket soil classification, and engineering judgement.
- In the geotechnical reports the sample depths are mostly expressed in meters with respect to the local surface level (t.o.v. maaiveld, or mv). In this case, a simple calculation is performed in order to express consistently the depths in meters with respect to NAP (Normaal Amsterdams Peil). When only the entire core depth is reported, the sample depth is assumed at the middle of the core.
- The most significant limitations encountered in the soil classification process are: depth mismatch, soil classification of uppermost soil layers, and the presence of high ground water table. The depth mismatch is due to the very shallow depth of the majority of the samples (usually the uppermost 2 m) in contrast to the relatively large depth at which the CPT measurements start (mostly from -1 m downwards). Secondly, the soil classification of the uppermost soil layers may be not totally exact, due to the uncertainty deriving from CPT measurements. Thirdly, in this study, every sample is assumed to be fully saturated, neglecting the possibility to encounter partially saturated samples within the uppermost soil layers. Lastly, considering that the geotechnical reports are protected by a confidentiality agreement (locked PDF), every single number has been manually reported into the database. This created potential sources of mistakes.

C

Statistical Characterisation

C.1. Introduction

The present appendix is divided in two main sections which present the results and the discussion of the statistical characterisation of a number of soil units with respect to PI and Su. In section C.2, the descriptive statistical parameters of PI for the SU1_B, SU1_E, SU1_D, SU2, SU3, SU4, and SU5 soil units are reported and discussed, whilst in section 2.5.2 the descriptive statistical parameters of Su for the SU1_E, SU1_D, SU2, SU3 soil units are illustrated and commented. The procedure followed to obtain these results is presented in Chapter 5.

C.2. Plasticity Index Data Analysis

In the following two sections (Sections C.2.1 and C.2.2), it is reported in detail the statistical analysis executed for the sandy Clay and silty Clay soil units, similarly to the analysis carried out for the soft, clean Clay unit (Chapter 5, Section 5.2). On the other hand, in section C.2.3, only an overview of the descriptive statistics from the remaining soil units (organic Clay, overconsolidated Clay, Peat, and Loam) is given. These units will not be presented in detail as the previous ones due to their relatively limited amount of samples (Table 5.2). In addition, few considerations about the soil unit Sand (SU3) will be made, considering that sands are in general non-plastic materials. Likewise, some aspect regarding the applicability of Attemberg limits to peat (SU4) will be discussed.

C.2.1. Soil Unit: Sandy Clay (SU1_B)

The geotechnical unit sandy Clay (SU1_B), contains the largest number of samples in the PI database (208 measurements and 202 data pairs). Sandy Clays are assumed to belong to the Naaldwijk, Nieuwkoop, and Drente formations (hereafter indicated as NA, NI, and DR, respectively, according to table 5.1).

PI versus Depth

The plot in figure C.1 shows the distribution of PI data-pairs and PI values recommended by Bommer et al. (2017a) and Arup (2015), as a generalised range to cover all the stratigraphic units implied, over the depth. The points in red represent the measured values (PI;measured), and the vertical red line indicates the mean value of the data-set (24.7 %). The blue crosses denote the calculated values (using the Cetin and Ozan, 2009 correlation) and the vertical blue line their mean ($PI_{C\&O}$ mean = 19.7 %). The dashed red and blue lines display the calculated and measured PI means ± 1 time the standard deviation ($\sigma_{PI;measured}$ = ±15.3% and $\sigma_{PI;C\&O}$ = ±10.2%, respectively). The solid green line represents the PI as suggested by Arup (2015) (PI_{Arup} = 25% for all clays), whilst the coloured area (in yellow) defines the range of PI values recommended by Bommer et al. (2017a), hereafter PI_{V4}. The lower boundary of this area depicts the average PI value for Drente sandy clays ($PI_{DR;sandyclays}$ = 10 %), whilst the upper boundary the PI for Nieuwkoop sandy clays ($PI_{NI;sandyclays}$ = 50 %). The PI for Naaldwijk sandy clays lies almost in the middle of the range, being $PI_{NA;sandyclays}$ = 30 %.
Most of the samples of this soil unit were collected at relatively shallow depths (between 1 and -2.5 m NAP, Figure C.1). The PI measurements range from 0 to 87.2 %, and the PI calculated with the model from Cetin

and Ozan (2009) vary between 3.8 and 49.7 % (Figure C.1 and Table C.2).
As shown in figure C.1, the measured PI (24.7 %, Table C.2) is in line with the assumption from Arup (2015) (25 %, Table C.2), and it is higher than the PI mean calculated with Cetin and Ozan (2009) (19.7, table C.2). Since this data-set comprises different stratigraphic units, it is more difficult to make a comparison with the Bommer et al. (2017a) recommended values. The measured mean PI is located near the PI from NA, below the NI and above the DR limits (30%, 50% and 15% respectively, Tables C.2 and 5.1).
Figure C.2 depicts the correspondence between measured and calculated PI, with indication of the equality line (x=y), providing another visual representation of the results shown in figure C.2 and table C.2).

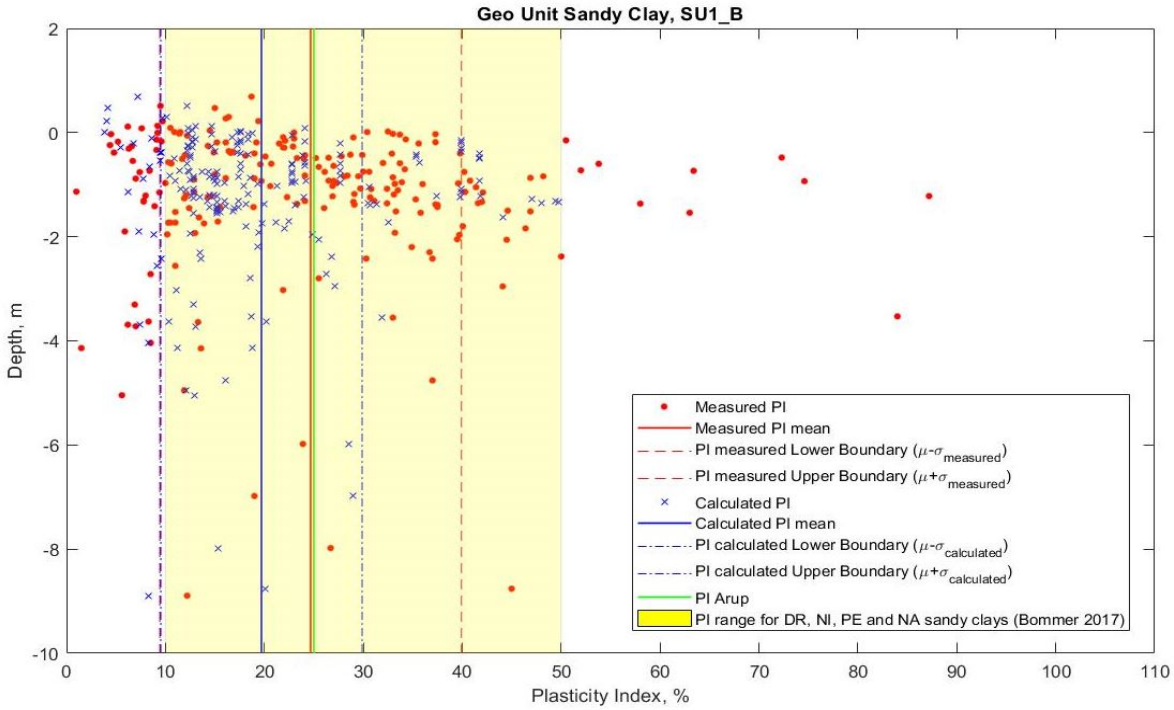

Figure C.1: PI measurements and calculated values for the sandy Clay soil unit. Red dots: measured values; red solid line: mean; red dashed lines: ±1 standard deviation. Blue x: calculated PI with Cetin & Ozan (2015); blue solid line: mean; blue dashed lines: ±1 standard deviation. Green solid line: proposed PI after Arup (2015). Yellow area: PI range for Drente, Nieuwkoop, Peelo, and Naaldwijk sandy clays (after Bommer et al., 2017a)

.

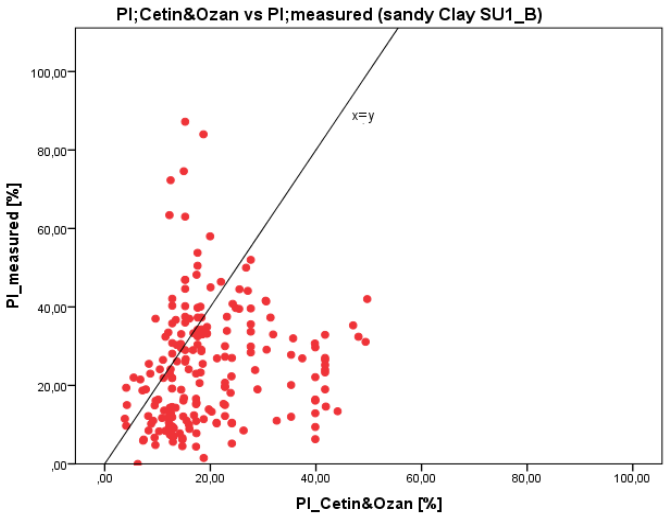

Figure C.2: Scatter plot with equality line of PI data pairs from the sandy Clay soil unit.

Figure C.3 shows the distribution of PI measurements of the SU1_B unit in depth organised in stratigraphic units after Bommer et al. (2017a), and the comparison between measured mean values and recommended PI from Bommer et al. (2017a). The red points represent the measurements considered to belong to the Naaldwijk formation, the solid red line their mean, and the dashed red line the V4 recommended PI for Naaldwijk sandy clays. The blue points represent the measurements belonging to the Drente formation, the solid blue line their mean, and the dashed blue line the V4 recommended PI for Drente sandy clays. The ochre points represent the measurements from the Peelo formation, the solid ochre line their mean, and the dashed ochre line the V4 recommended PI for Peelo sandy clay.
The V4 recommended values are in good agreement with the laboratory PI measurements for most cases (Figure C.3 and Table C.1). For the Drente and Naaldwijk formations, the measured PI mean is almost identical to the recommended PI values (10.4 and 10 %, respectively, for the Drente formation, and 31.2 and 30 %, respectively, for the Naaldwijk formation); for the Peelo formation, a suggested value of 30 % (dashed ochre line, coinciding with the red dashed line in figure C.3) over-predicts the measured mean (19.5 %); and, for Nieuwekoop sandy clays, the suggested value (50 %) is lower than the measured PI mean, which is 57.1 %.
Table C.1 shows the exploratory statistics for the three stratigraphic units: NA, DR, NI and PE.

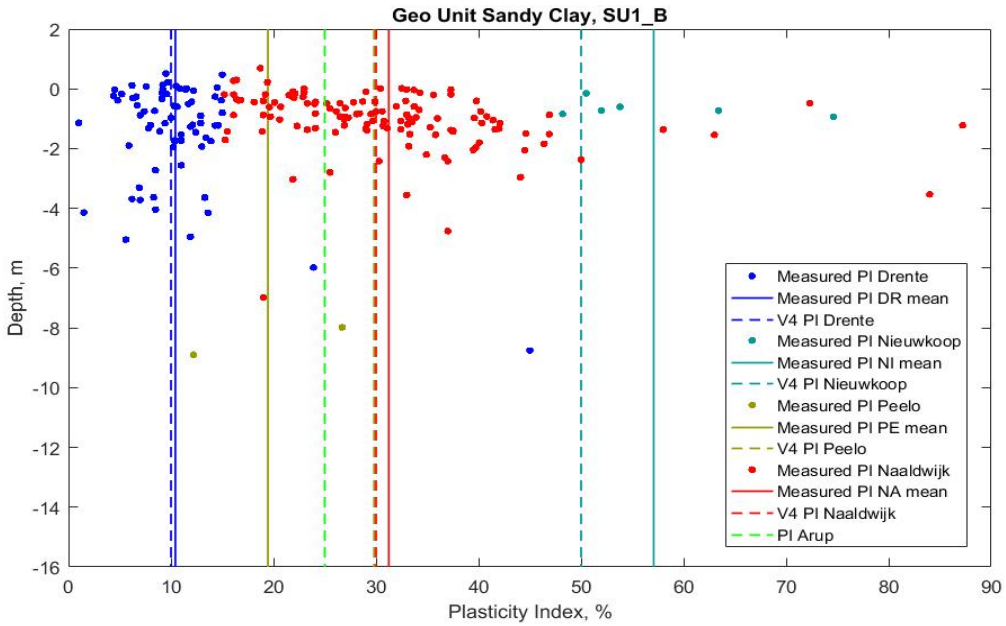

Figure C.3: PI measurements organised per stratigraphic unit for the sandy Clay soil unit.

Table C.1: Statistical characterisation of NA, DR, NI, and PE formations in SU1_B.

Stratigraphic Unit		**Statistical parameters**						
		N	min	max	μ	σ	COV	median
		[-]	[%]	[%]	[%]	[%]	[-]	[%]
DR	PI measured	70	1.0	45.0	10.4	5.5	0.53	10.1
NI	PI measured	6	48.2	74.6	57.1	10.1	0.18	52.9
PE	PI measured	2	12.2	26.7	19.5	10.3	0.53	19.5
NA	PI measured	124	15.2	87.2	31.2	12.1	0.39	30.0

Data Distribution

By visual inspection of figures C.4a and C.4a, the distribution of the linear PI;measured data-set is assessed to be positively skewed, while the PI;C&O data-set is approximately normally distributed (or slightly positively skewed). From figures C.5a and C.5a, the logarithmic data-sets appear to be better approximating normal distributions (or slightly negatively skewed).

Figures C.6a and C.6b show box-plots from the comparison between measured and calculated PI from unit SU1_B. The median of the measured values is higher than the predicted median (23.0 and 17.3 %, respectively, from the "All classes" data-set in table C.2).

Furthermore, the range of PI values measured in laboratory is larger than the one predicted using the Cetin and Ozan (2009) CPT-based correlation, as it is visible from the linear histograms (Figures C.4a and C.4a), the scatter plot (Figure C.1), and the linear box-plots (Figure C.6a). The maximum value of the measured PI data-set (87.2 %) is almost twice as high as the maximum predicted value (49.7 %), confirming the greater variability of the measured PI data-set.

Considering the logarithmic PI data-sets (Figure C.6b), the data variability is reduced, and the medians become more similar to each other (comprised in the range from 1 to 1.5 %).

Figure C.4: Histograms of calculated and measured PI values and underlying normal distributions for the sandy Clay soil unit.

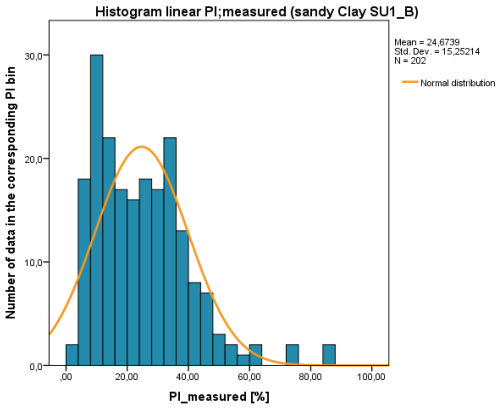

(a) Histogram of linear PI measured for the sandy Clay soil unit.

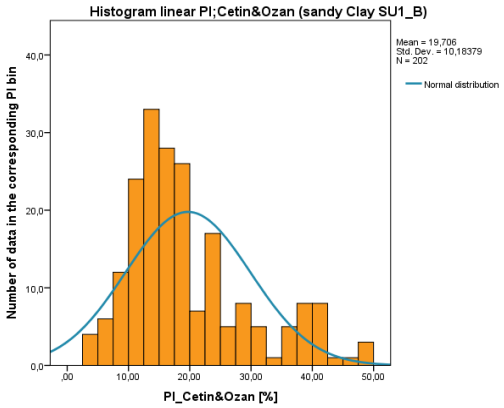

(b) Histogram of linear PI Cetin&Ozan (2009) for the sandy Clay soil unit.

Figure C.5: Histograms of logarithmic calculated and measured PI values and underlying normal distributions for the sandy Clay soil unit.

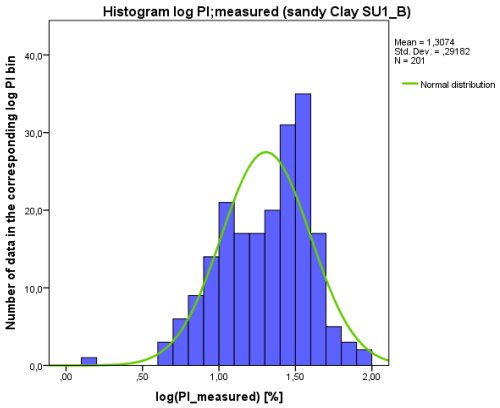

(a) Histogram of logarithmic PI measured for the sandy Clay soil unit.

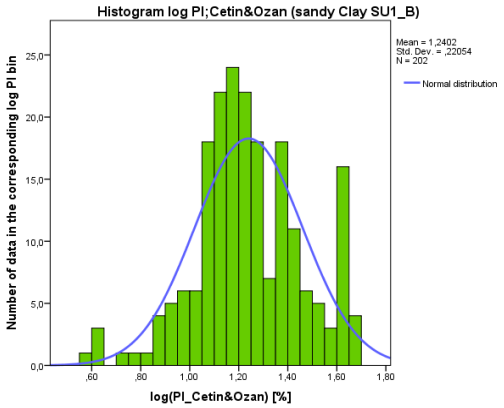

(b) Histogram of logarithmic PI Cetin&Ozan (2009) for the sandy Clay soil unit.

Figure C.6: Box-and-Whiskers-Diagram from measured and calculated PI values of the linear and logarithmic PI data-sets for the sandy Clay soil unit.

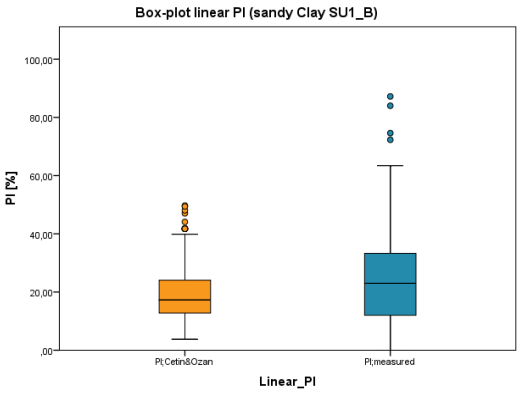

(a) Box-and-Whiskers-Diagram from linear measured and calculated PI values for the sandy Clay soil unit.

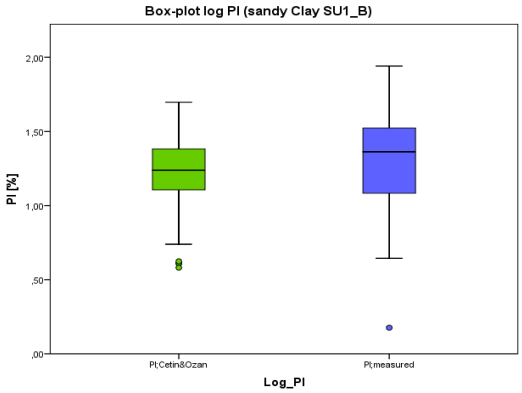

(b) Box-and-Whiskers-Diagram from logarithmic measured and calculated PI values for the sandy Clay soil unit.

With the purpose to obtain a more detailed indication of the data-sets characteristics and correspondence, the samples were divided into three classes (according to table B.3, Appendix B). The general descriptive statistical parameters from the re-classified data are given in table C.2 and their box-plots are shown in figure C.7. In this way, the data pairs' depth mismatch between laboratory and CPT measurements (for instance, the maximum measured PI of the data-set prior to re-classification, equal to 87.2 %) are discarded (see Appendix B, Section B.4.3). The medians of the measured and calculated Class 1 data-sets become 21.3 and 16.0 %, respectively.

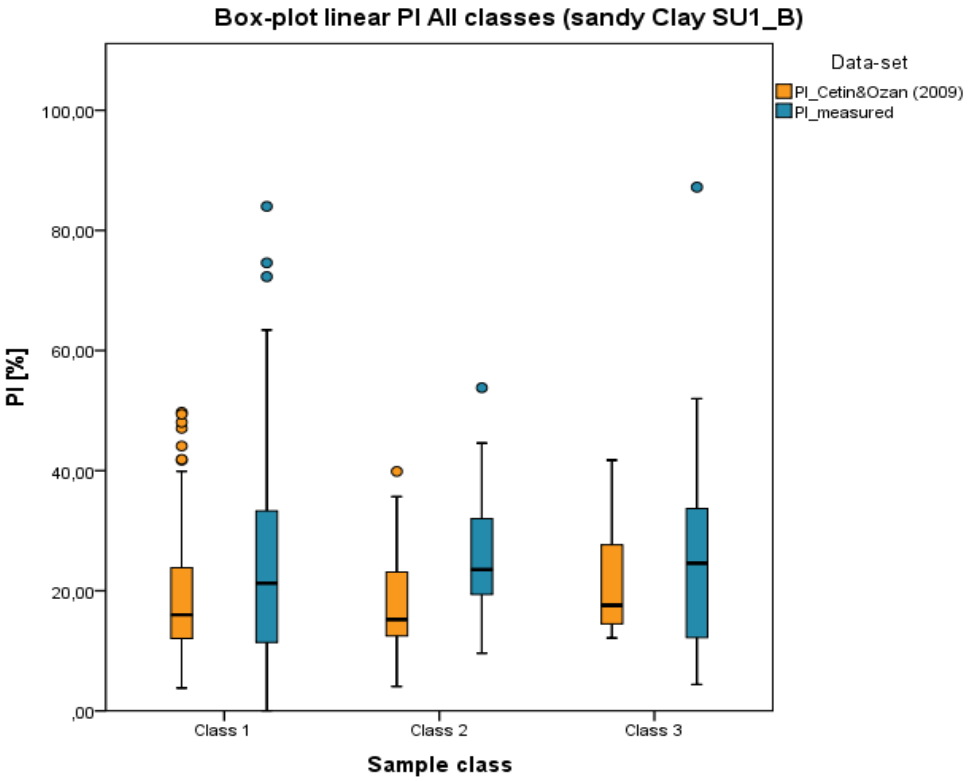

Figure C.7: Box-and-Whiskers-Diagram from measured and calculated PI values of the three samples classes for the sandy Clay soil unit.

Table C.2: Statistical characterisation of SU1_B unit.

Class		**Statistical parameters**						
		N	min	max	μ	σ	COV	median
		[-]	[%]	[%]	[%]	[%]	[-]	[%]
All classes	PI measured	202	0.0	87.2	24.7	15.3	0.62	23.0
	PI calculated	202	3.8	49.7	19.7	10.2	0.52	17.3
1	PI measured	114	0.0	84.0	24.3	16.4	0.68	21.3
	PI calculated	114	3.8	49.7	18.9	10.4	0.55	16.0
2	PI measured	26	9.6	53.8	25.4	10.8	0.42	23.6
	PI calculated	26	4.1	39.9	18.7	10.2	0.54	15.2
3	PI measured	62	4.4	87.2	25.0	14.8	0.59	24.6
	PI calculated	62	12.1	41.7	21.5	9.8	0.45	17.6

C.2.2. Soil Unit: Silty Clay (SU1_E)

The geotechnical unit silty Clay (SU1_E), contains 110 laboratory measurements and 98 data pairs.
Silty Clays are assumed to belong to the Naaldwijk, Nieuwkoop, Drente, and Anthropogenic formations (hereafter indicated as NA, NI, DR, and AAOP respectively, Table 5.1). The AAOP formation in the present research may be different from Bommer et al. (2017a). Herein, AAOP is utilised for indicating mostly man-made sandy (or sandy and silty clay) superficial layers.

PI versus Depth

The plot figure C.8 displays the distribution of PI data pairs and PI values recommended by Bommer et al. (2017a), as a generalised range to cover all the stratigraphic units implied, over the depth.
Most of the samples of this soil unit (95 out of 98) were collected at relatively shallow depths (between 0.92 and -2 m NAP). The measured PI range from 1.0 to 103.0 %, and the PI calculated with the model from Cetin and Ozan (2009) vary between 5.7 and 36.9 % (Figure C.8 and Table C.4). The mean PI calculated with Cetin and Ozan (2009) (19 %) is lower than the mean PI measured at the laboratory (30.2 %), indicating that the Cetin and Ozan (2009) correlation is under-predicting PI values from this soil unit (Table C.4).
The measured and calculated values below -4 m NAP do not deviate significantly from each other, showing a stronger correlation than at shallow depths where, conversely, the divergence between points is more enhanced due to a greater spatial variability.
Since this data-set comprises different stratigraphic units, it is more difficult to make a comparison with the Bommer et al. (2017a) recommended values. The measured mean PI (30.2%) is almost identical to the PI from NA, lower than NI and higher than DR (30%, 50% and 10% respectively, Table 5.1). However, the majority of the PI calculated fall within the PI_{V4} range considering the different stratigraphic units.
Figure C.9 depicts the correspondence between measured and calculated PI, with indication of the equality line (x=y). This graph confirms that the Cetin and Ozan (2009) under-predicts the laboratory measurements.

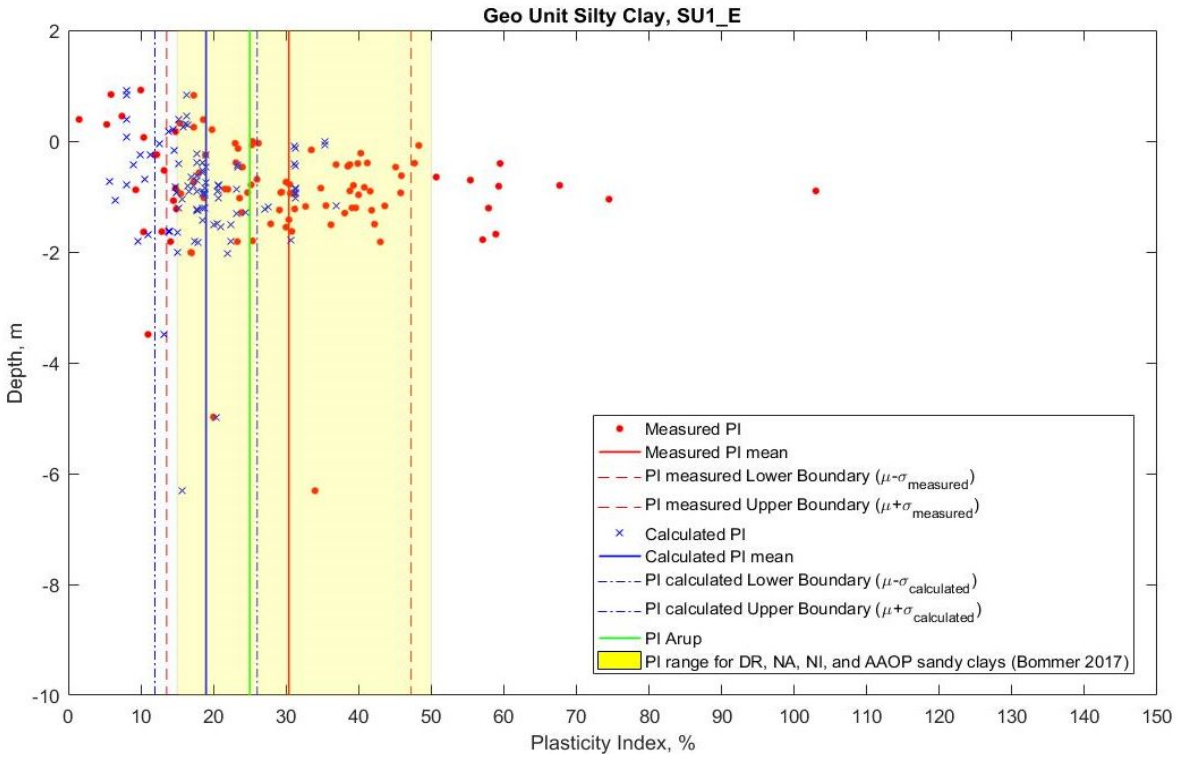

Figure C.8: PI measurements and calculated values for the sandy Clay soil unit. Red dots: measured values; red solid line: mean; red dashed lines: ±1 standard deviation. Blue x: calculated with Cetin & Ozan; blue solid line: mean; blue dashed lines: ±1 standard deviation. Green solid line: proposed PI after Arup (2015). Yellow area: PI range for Drente, Naaldwijk, Nieuwkoop, and Anthropogenic sandy clays (after Bommer et al., 2017a).

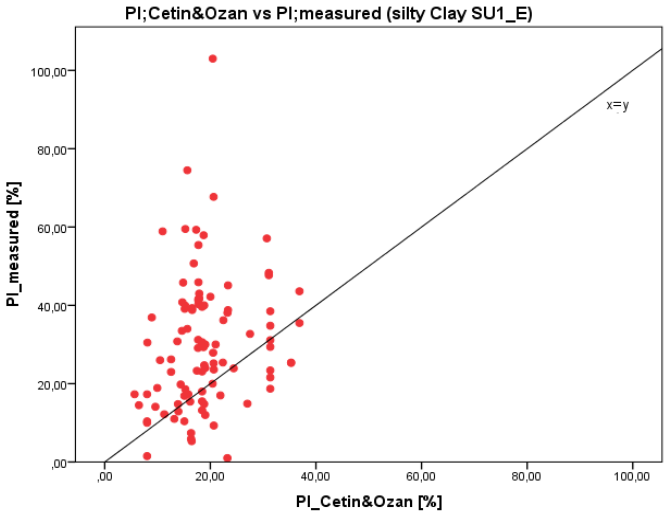

Figure C.9: Scatter plot with equality line of PI data pairs from the silty Clay soil unit.

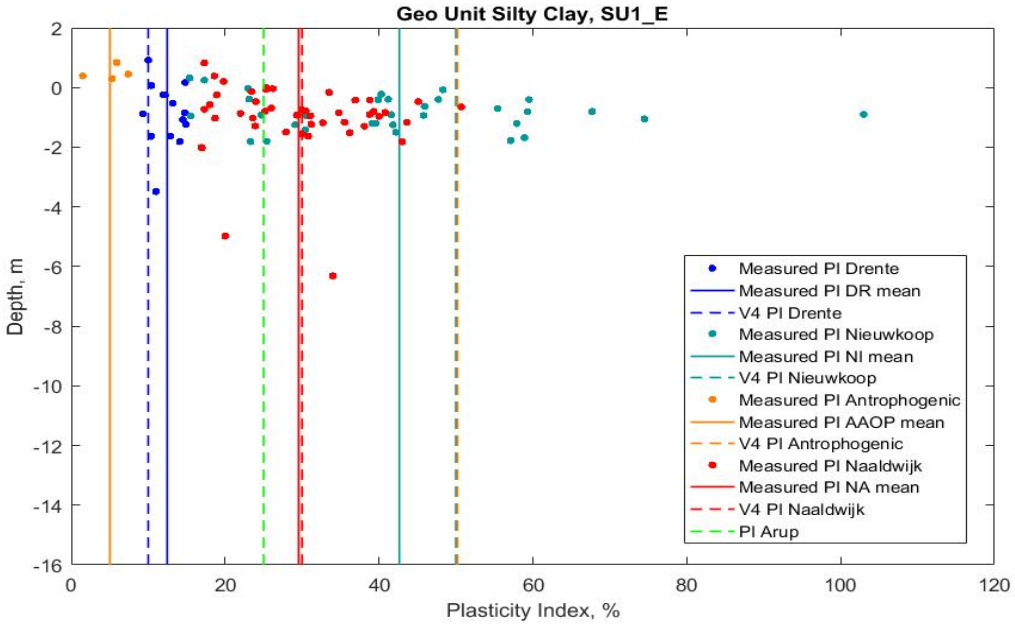

Figure C.10: PI measurements for the sandy Clay soil unit. Blue dots: Drente measured PI values; blue solid line: Drente measured PI mean; blue dashed line: V4 recommended PI value for Drente sandy clays. Light blue dots: Nieuwkoop measured PI values; light blue solid line: NI measured PI mean; light blue dashed line: V4 recommended PI value for Nieuwkoop sandy clays. Orange dots: Anthropogenic measured PI values; orange solid line: AAOP measured PI mean; orange dashed lines: V4 recommended PI value for Anthropogenic sandy clays. Red dots: Naaldwijk measured PI values; red solid line: Naaldwijk measured PI mean; red dashed line: V4 recommended PI value for Naaldwijk sandy clays. Green dashed line: proposed PI after Arup (2015).

Most of the V4 recommended values are in good agreement with the laboratory PI measurements (Figure C.10). For the Drente and Naaldwijk formations, the measured PI mean is almost identical to the recommended PI values (12.5 and 15 %, respectively, for the Drente fromation, and 29.6 and 30 %, respectively, for the Naaldwijk formation); for the Nieuwkoop formation, a suggested value of 50 % (light blue dashed line, coinciding with the orange dashed line in figure C.10) over-predicts the measured mean (41.9 %). For Anthropogenic sandy clays, the suggested value (50 %) over-predicts the measured PI mean, which is 5.0 %. The AAOP formation, in the present research, is referred to mainly man-made sandy layers characterised by low PI value (i.e. 1.5, 5.9, 7.4, and 5.3 %).
Table C.3 shows the exploratory statistics for the three stratigraphic units: NA, DR, NI and AAOP.

Table C.3: Statistical characterisation of NA, DR, NI, and PE formations in SU1_E.

Stratigraphic Unit		**Statistical parameters**						
		N	min	max	μ	σ	COV	median
		[-]	[%]	[%]	[%]	[%]	[-]	[%]
DR	PI measured	14	9.3	14.9	12.5	2.0	0.16	12.6
NI	PI measured	34	15.4	103.0	41.9	18.8	0.45	40.8
AAOP	PI measured	4	1.5	7.4	5.0	2.5	0.50	5.6
NA	PI measured	46	16.9	50.7	29.6	8.7	0.29	29.7

Data Distribution

The data-sets for the SU1_E unit are normally distributed (Figure C.11b) or slightly positively skewed (FigureC.11a). As well as, in figures C.12a and C.12b, showing the distribution of logarithmic measured and calculated PI values, the data are approximately normally distributed.
Figures C.13a and C.13b show box-plots from the comparison between measured and calculated PI values from unit SU1_E (from both linear and logarithmic data-sets). From the linear box-plots (Figure C.13a) it can be observed that the median of the measured data-set is higher than the predicted PI median (29.2 and 17.9 %, respectively), and the range of PI values measured at the laboratory is wider than the one obtained using the Cetin and Ozan (2009) CPT-based correlation. The measured PI values range from 1.0 to 103.0 %, whilst the PI calculated vary between 5.7 and 36.9 % (also visible in figure C.8 and Table C.4). In figure C.13b, after the transformation of PI measured and calculated values in logarithmic data-sets, the variability of both data-sets is reduced.
With the purpose to obtain a more detailed indication of the data-sets characteristics and correspondence, the samples were divided into three classes (according to table B.3, Apppendix B). The general descriptive statistical parameters from the re-classified data are given in table C.4 and their box-plots are shown in figure C.14.

Figure C.11: Histograms of calculated and measured PI values and underlying normal distributions for the silty Clay soil unit.

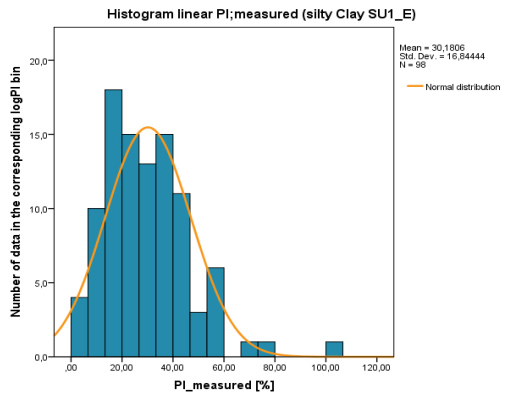

(a) Histogram of linear PI measured for the silty Clay soil unit.

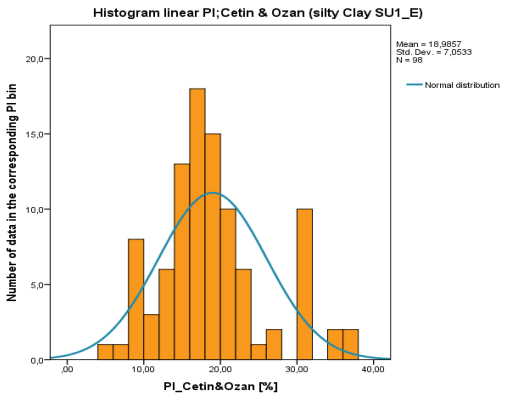

(b) Histogram of linear PI Cetin&Ozan (2009) for the silty Clay soil unit.

Figure C.12: Histograms of logarithmic calculated and measured PI values and underlying normal distributions for the soft, clean Clay soil unit.

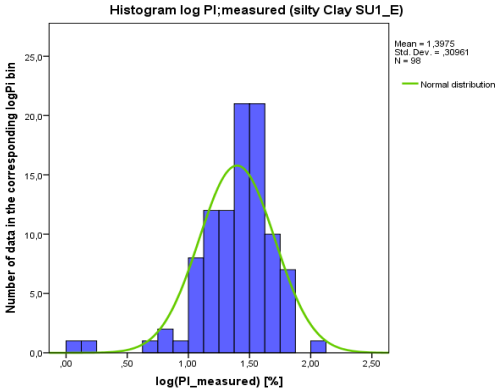

(a) Histogram of logarithmic PI measured for the silty Clay soil unit.

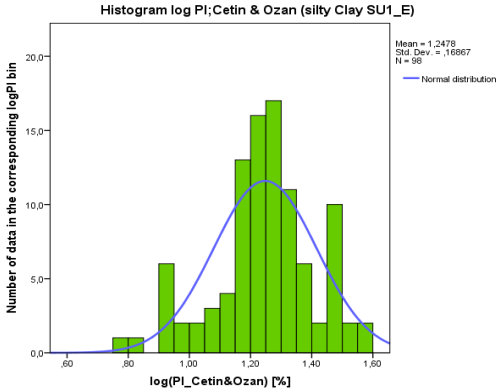

(b) Histogram of logarithmic PI Cetin&Ozan (2009) for the silty Clay soil unit.

Figure C.13: Box-and-Whiskers-Diagram from measured and calculated PI values of linear and logarithmic data-sets for the silty Clay soil unit.

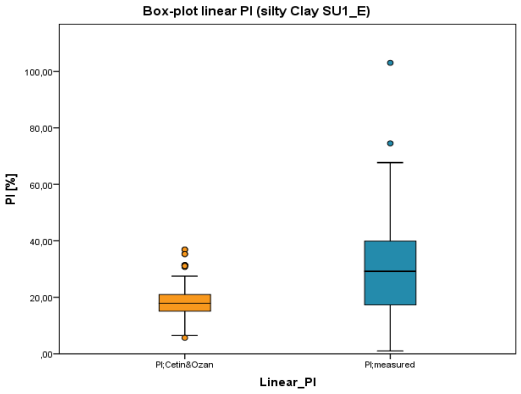

(a) Box-and-Whiskers-Diagram from linear measured and calculated PI values for the silty Clay soil unit.

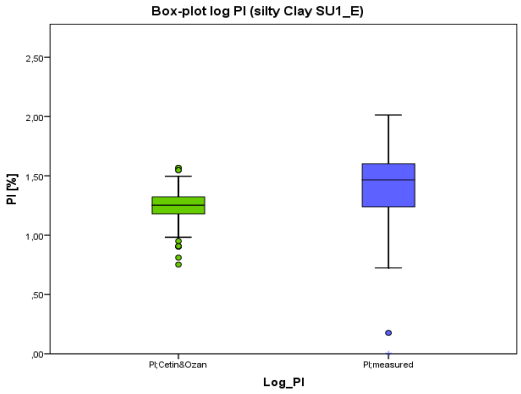

(b) Box-and-Whiskers-Diagram from logarithmic measured and calculated PI values for the silty Clay soil unit.

Table C.4: Statistical characterisation of SU1_E unit.

Class		**Statistical parameters**						
		N	min	max	μ	σ	COV	median
		[-]	[%]	[%]	[%]	[%]	[-]	[%]
All classes	PI measured	98	1.0	103.0	30.2	16.8	0.56	29.2
	PI calculated	98	5.7	36.9	19.0	7.1	0.37	17.9
1	PI measured	56	1	103.0	31.2	18.4	0.59	28.5
	PI calculated	56	5.7	36.9	17.5	6.3	0.36	16.6
2	PI measured	9	7.4	50.7	30.0	15.5	0.51	30.4
	PI calculated	9	8	31.4	19.3	17.5	0.39	17.7
3	PI measured	33	1.5	59.6	28.6	14.6	0.51	25.4
	PI calculated	33	8	35.3	21.4	7.6	0.36	18.8

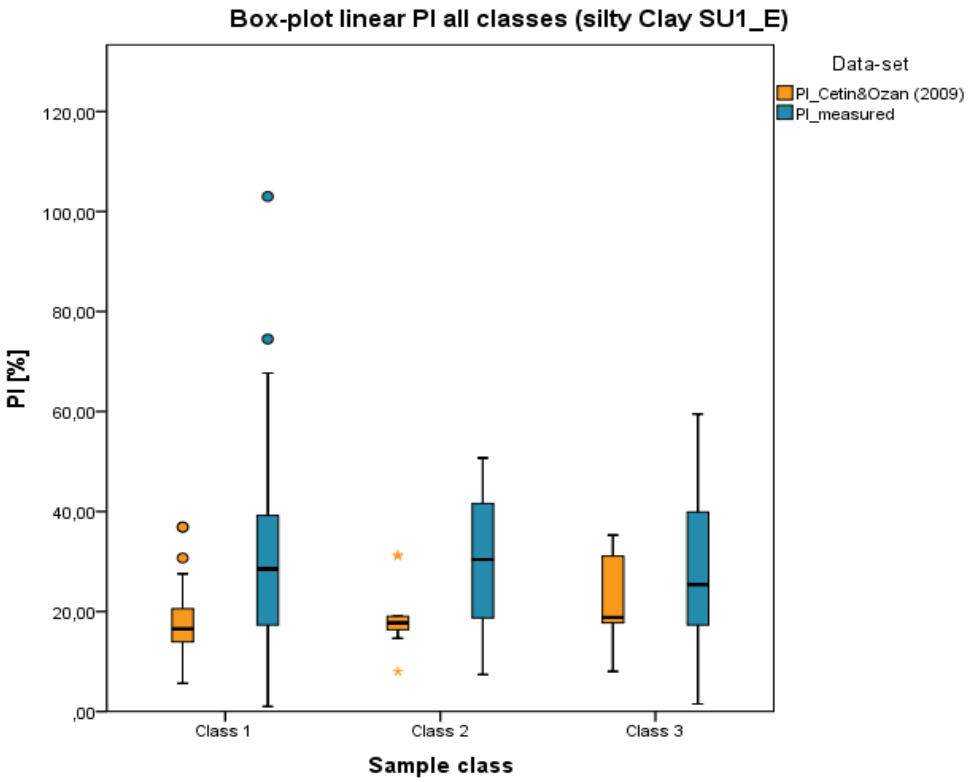

Figure C.14: Box-and-Whiskers-Diagram illustrating the comparison between measured and calculated PI values of the three samples classes for the silty Clay soil unit.

C.2.3. Other Soil Units

The soil units sandy Clay, silty Clay, organic Clay, overconsolidated Clay, Sand, Peat, and Loam are characterised by a limited amount of available measurements (i.e. SU1_D with 26 samples and 15 data pairs, SU2 with 4 samples and 4 data pairs, SU3 with 20 samples and 20 data pairs, SU4 with 11 samples and 7 data pairs, and SU5 with 2 samples and 2 data pairs, Tables 5.2 and C.5).

Table C.5: Statistical characterisation of $SU1\_D$, $SU2$, $SU3$, $SU4$, and $SU5$ soil units.

Soil Unit	Class	Data-set	Statistical parameters						
			N	min	max	μ	σ	COV	median
			[-]	[%]	[%]	[%]	[%]	[-]	[%]
SU1_D	all classes	PI measured	15	12.0	78.1	47.4	18.2	0.38	47.4
		PI calculated	15	11.8	60.2	21.4	12.3	0.57	17.0
	1	PI measured	14	12.0	78.1	47.2	18.9	0.40	46.1
		PI calculated	14	11.8	60.2	21.6	12.7	0.59	16.4
	3	PI measured	1	50.0	50.0	50.0	-	0.0	50.0
		PI calculated	1	18.4	18.4	18.4	-	0.0	18.4
SU2	1	PI measured	4	8.0	61.0	44.0	24.3	0.55	53.5
		PI calculated	4	10.2	33.8	23.3	10.1	0.43	24.7
SU3	all classes	PI measured	20	2.7	55.7	15.0	14.3	0.95	8.3
		PI calculated	20	2.7	15.3	5.9	3.75	0.64	5.1
	1	PI measured	6	3.6	55.7	24.7	21.0	0.85	21.9
		PI calculated	6	6.7	15.3	10.2	3.6	0.35	9.1
	2	PI measured	3	6.0	33.7	20.7	13.9	0.67	22.3
		PI calculated	3	2.7	7.4	4.2	2.7	0.64	2.7
	3	PI measured	11	4.9	14.2	8.7	3.2	0.37	7.3
		PI calculated	11	2.7	5.1	3.6	1.2	0.34	2.7
SU4	all classes	PI measured	7	42.9	173.2	95.0	51.9	0.55	66.9
		PI calculated	7	19.9	35.2	24.6	5.5	0.22	24.2
	1	PI measured	4	42.9	173.2	100.9	58.1	0.58	93.8
		PI calculated	4	20.5	26.2	24.2	2.7	0.11	25.1
	2	PI measured	3	47.2	147.5	87.1	53.2	0.61	66.5
		PI calculated	3	19.9	35.2	25.0	8.8	0.35	19.9
SU5	1	PI measured	2	8.9	16.1	12.5	5.1	0.41	12.5
		PI calculated	2	3.4	18.6	11.0	10.7	0.98	11.0

Organic Clay (SU1_D)

This soil unit contains 26 samples, associated to Nieuwkoop and Drente formations (see Table 5.1), of which 15 have calculated values to be compared with. Of the 15 data pairs, 14 are classified as Class 1, and only 1 sample as Class 3. For the latter, thus, it is not possible to estimate the standard deviation and the coefficient of variation.

In table C.5 it can be found the descriptive statistics from the data belonging to the Organic Clay unit. The Cetin and Ozan (2009) correlation is underestimating the PI for this soil unit (measured PI mean = 47.4 %), yielding a calculated PI mean equal to 21.4 % (Table C.5).

The $PI_{C\&O}$ values are in agreement with the PI suggested by Arup (2015) and the PI for DR clays ($PI_{DR;clays}$ = 15%) from Bommer (2017), but lower than the average PI for NI clays and sandy clays ($PI_{NI;clays,sandyclays}$ = 50%) from Bommer (2017) which, in turn, shows a good correlation with the mean of the laboratory measure-

ments.
The samples from the SU1_D unit were collected at shallow depths (between -0.87 and -3.25 m NAP). CPT measurements, at the very beginning of the penetration process, may exhibit high values of cone resistance and friction ratio, not necessarily representative of the actual soil conditions. High values of F_R (typical of peat of organic clay deposits) may lead, for example, to classify soil samples as organic Clay, rather than other clay types. This uncertainty in CPT measurements can influence the classification of samples and, consequently, the correspondence between measured and calculated PI values.

Overconsolidated Clay (SU2)
Data pairs for the OC clay unit are very scarce in the PI database (4 data pairs, Tables 5.2 and C.5). The first reason is that the OC clays are soil deposits typically encountered at great depths (e.g. below -5 m NAP, due to their geological history, see Section 3.7 in Chapter 3), while laboratory measurements are often realised on specimens collected at shallow depths.
In total, 4 samples belong to this unit (all them considered as Class 1, Table C.5), whose depth range varies between -10.44 and -13.56 m NAP.
Table C.5 shows the exploratory statistics for the SU2 unit. The Cetin and Ozan (2009) correlation is underestimating the PI of the SU2 unit, predicting a mean equal to 23.3 %, while the measured PI mean is equal to 44.0 % (Table C.5).
For the comparison between $PI_{C\&O}$ mean and the suggested PI values from Bommer et al. (2017a), both the PI for clean and sandy clays from the Peelo stratigraphic unit are considered. The $PI_{C\&O}$ mean is closer to the PI suggested value for PE clean clays ($PI_{PE;clays}$ = 30%), rather than the $PI_{PE;sandyclays}$ (equal to 50 %). Oppositely, from the comparison between laboratory and Bommer (2017) PI values, the measured PI mean (44.0 %) is better correlated to the $PI_{PE;sandyclays}$ boundary than the $PI_{PE;clays}$ limit.

Sand (SU3)
Although sand is a non-plastic material which should be considered with a PI = 0 %, in the database there are 20 data measurements from the laboratory that exhibit PI values different from zero. The majority of these samples are classified as silty and/or clayey Sands, meaning that their plastic behaviour is connected to the presence of some clay and/or silty material within the specimens.
Table C.5 shows the exploratory statistics for the SU3 unit. The mean PI measured at the laboratory is higher than the mean PI calculated with the Cetin and Ozan (2009) correlation, being $PI_{C\&O}$ equal to 5.9 % and measured PI mean equal to 15.0 %. Moreover, most of the measurements (1 out 20) are lower than the recommended PI values from Bommer et al. (2017a) ($PI_{NA;clayeysands}$ = 30% and $PI_{BX,AAOP;clayeysands}$ = 50%). After the re-classification of the 20 samples from this unit, 6 samples are in Class 1, 4 in Class 2, and 11 in Class 3 (Table C.5). From the analysis of the Class 1 data-set, the divergence between measured and calculated PI means is larger than what observed in the data-set prior re-classification ($PI_{C\&O;class1}$ = 15.3% and $PI_{measured;class1}$ = 24.7%).
For clayey sands, Bommer et al. (2017a) suggests $PI_{NA;clayeysands}$ equal to 30 % and $PI_{BX,AAOP;clayeysands}$ equal to 50 %, which are greater than both the calculated $PI_{C\&O}$ mean and the measured PI mean. Moreover, only 3 out 20 samples are contained within the Bommer (2017) range.

Peat (SU4)
First of all, it is crucial to mention the limited applicability of Atterberg Limits determination on peat. According to O'Kelly (2015), there are fundamental issues making these tests not appropriate for peat. The determination of both Plastic Limit (PL) and Liquid Limit (LL) is drastically affected by scale and reinforcement effects connected to the peat fibres (that account for microstructure, stress history, and remoulding of samples), in combination with the degree of humidity of the tested sample. Furthermore, the sample preparation method, which itself is operator-dependent, produces great difference in LL and PL and, therefore, in PI values.
Taking into account these limitations, it is difficult to assess the adequacy of the CPT-based correlations.
In table C.5 are illustrated the descriptive statistical parameters for the 7 samples of peat from the database. Results reveal that the Cetin and Ozan (2009) correlation is underestimating the PI for this soil unit, producing a PI mean equal to 24.2 %, while the measured PI mean is equal to 100.9 %.

For Holocene Formations with peat lithology, such as peat and peaty clays, Bommer et al. (2017a) suggest PI values from the Nieuwkoop Holland peat (NIHO) (50 %) and, for older peats, from the Nieuwkoop Basal peat (NIBA) formations (50 %).
The Cetin and Ozan (2009) correlation predicts a PI mean 24.2 %) which is almost half the $PI_{NIHO;NIBA}$. Oppositely, the measured PI mean is almost twice as high as the $PI_{NIHO;NIBA}$.

Loam (SU5)
The samples classified as Loam are only 2, whose statistical parameters are reported in table C.5.
The predicted and measured values are overall in good agreement with each other, being the mean equal to 11.0 and 12.5 %, respectively. The standard deviation of the calculated data-set is 10.74 %, indicating that for the same soil type two significantly different values have been estimated (3.4 and 18.6 %). Conversely, the standard deviation of the measured data-set is lower (5.1 %), being the PI of the two samples 8.9 and 16.1 %.

C.3. Undrained Shear Strength Data Analysis

Section C.3.1 illustrates the statistical analysis executed for the silty Clay soil unit, similarly to the analysis carried out for the soft, clean Clay and sandy Clay units (Chapter 5, Section 5.3). Differently, in section C.3.2, only an overview of the descriptive statistics from the remaining soil units (overconsolidated Clay and Sand) is given. These units will not be presented in detail as the previous ones due to their relatively limited amount of samples (Table 5.6).

C.3.1. Soil Unit: Silty Clay (SU1_E)

The silty Clay unit contains 55 measurements for which it was possible to find CPTs to compare with. Of the 55 Su measurements, 20 samples were tested with the Torvane machine, 32 with the triaxial apparatus, by means of isotropically consolidated undrained tests, and 3 with triaxial unconsolidated undrained tests. In the following statistical characterisation only the in-situ data obtained from Torvane and triaxial (UU) will be considered (23 measurements in total).
To account for correspondence between samples and CPT measurements depth (following the classification presented in section B.4.3), Table B.3), the 23 data pairs are re-organised in sample classes (15 pairs as Class 1 and 8 pairs as Class 3, Table C.7).
Silty Clay samples are considered to belong to the Drente, Naaldwijk, Anthropogenic, and Nieuwkoop formations (Table 5.1).

Su versus Depth

The plot in figure C.15 illustrates the distribution over the depth of Su data and Su predicted values (calculated using the correlations suggested by Ladd and Foott, 1974, Bommer et al., 2017a, and Robertson and Cabal, 2015) and their ranges (± 1 standard deviation).
The red dots represent the Su values obtained from the SHANSEP model calibrated upon the results of CU triaxial tests (Su;measured (CU)), and the vertical solid red line their mean (81.6 kPa, Table C.8). The green dots denote the Su values measured with UU triaxial tests, and the vertical solid green line their mean value (16.7 kPa, Table C.8). The orange dots indicate the in-situ measurements from Torvane tests, and the vertical solid orange line their mean (38.6 kPa, Table C.8). The blue points (crosses) represent the calculated values (using the Ladd and Foott, 1974 correlation with single calibration, after Arup, 2015), and the vertical blue line their mean (10.0 kPa, Table C.7). The magenta points (triangles) denote the values calculated with the Robertson and Cabal (2015) CPT-based correlation, and the light blue points (circles) describe the Su values obtained using the NA, DR, AAOP, and NI equations for sandy clays recommended by Bommer et al. (2017a) (hereafter indicated as $Su_{NA,DR,AAOP,NI;sandyclays}$). The coloured areas (in green, yellow, and dark blue) display the upper and lower boundaries for the Su;measured (UU), Su;measured (Torvane), and Su;SHANSEP data-sets, respectively (computed as Su mean ±20%).
As shown in figure C.15, the Su values calculated with the SHANSEP correlation with single calibration (All classes mean = 10.0 kPa, Table C.7) are lower than the in-situ Su measurements at shallow depths. Precisely, the divergence between the SHANSEP and Su;measured (Torvane) means is around 32 kPa (Su;measured (Torvane) mean = 38.6 kPa and Su;SHANSEP (Torvane) mean = 6.5 kPa, Table C.8). However, below -8 m NAP, the SHANSEP correlation correlates better (or slightly overestimates) with the in-situ measurements (lab-UU) and the difference between their means is about 7 kPa (Su;measured (UU) mean = 16.7 kPa and Su;SHANSEP (UU) mean = 33.6 kPa, Table C.8).
The SHANSEP Su values are in poor agreement with the Robertson (2015) Su calculated values (27.8 kPa lower, on average), as well as with the Bommer (2017) Su values (37.5 kPa lower, on average, figure C.15 and table C.7).
The Su values obtained using the correlations suggested by Bommer et al. (2017a) show, in general, a fair correspondence with the mean of the in-situ data (about 12 kPa higher), being the "All classes $Su_{NA,DR,AAOP,NI;sandyclays}$" mean equal to 51.6 kPa and the "All classes Su measured" mean equal to 35.7 kPa (Table C.7). The majority of the Su;Bommer values fall within the Torvane measurements range (yellow area) at shallow depths, demonstrating that the Bommer et al. (2017a) relationships are able to partially reflect the large spatial variability of the uppermost soil layers (Figure C.15). However, the Su;Bommer values poorly correlate with the in-situ measurements (lab-UU) at greater depths, overestimating the Su;measured (UU) mean of more than 55 kPa (Su;measured (UU) mean = 16.7 kPa and $Su_{NA,DR,AAOP,NI;sandyclays}$ (UU) mean = 72.3 kPa, Table C.8).

The Su values computed with the Robertson (2015) correlation show the best agreement with both the in-situ measurements. Their mean (All classes Su;Robertson = 37.8 kPa, Table C.7) is around 2 kPa larger than the measurements mean (All classes Su;measured mean = 35.7 kPa, Table C.7). However, the Su;Robertson values are characterised by a large standard deviation (28.5 kPa, Table C.7) and a large coefficient of variation (0.75, Table C.7).

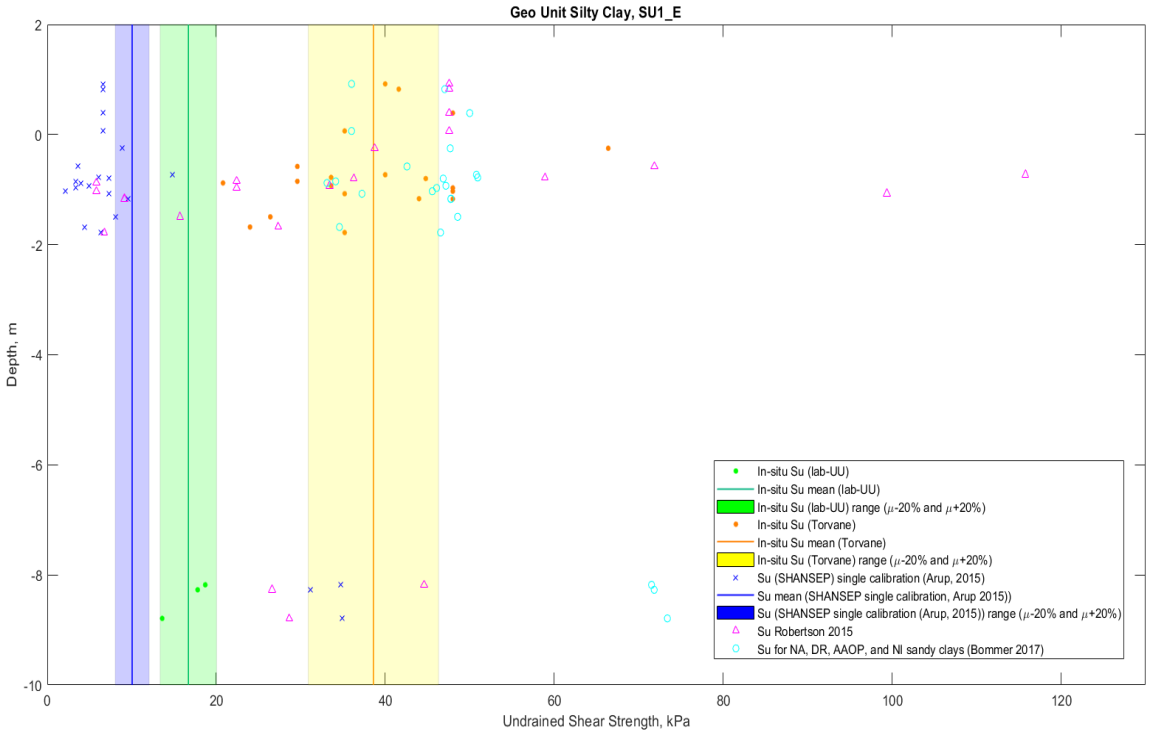

Figure C.15: Su measurements and calculated values for the sandy Clay soil unit.

The plot in figure C.16 displays the distribution over the depth of the Class 1 Su measurements and Su predicted values (calculated using the correlations suggested by Ladd and Foott, 1974, Bommer et al., 2017a, and Robertson and Cabal, 2015) and their ranges (± 1 standard deviation).
Figure C.16 demonstrates that removing the Class 3 data-pairs from the analysis the correlation between in-situ measurements and calculated Su values remain almost unvaried and the large scatter of in-situ measurements in the uppermost layers (between 0 and -2 m NAP) is still significant.

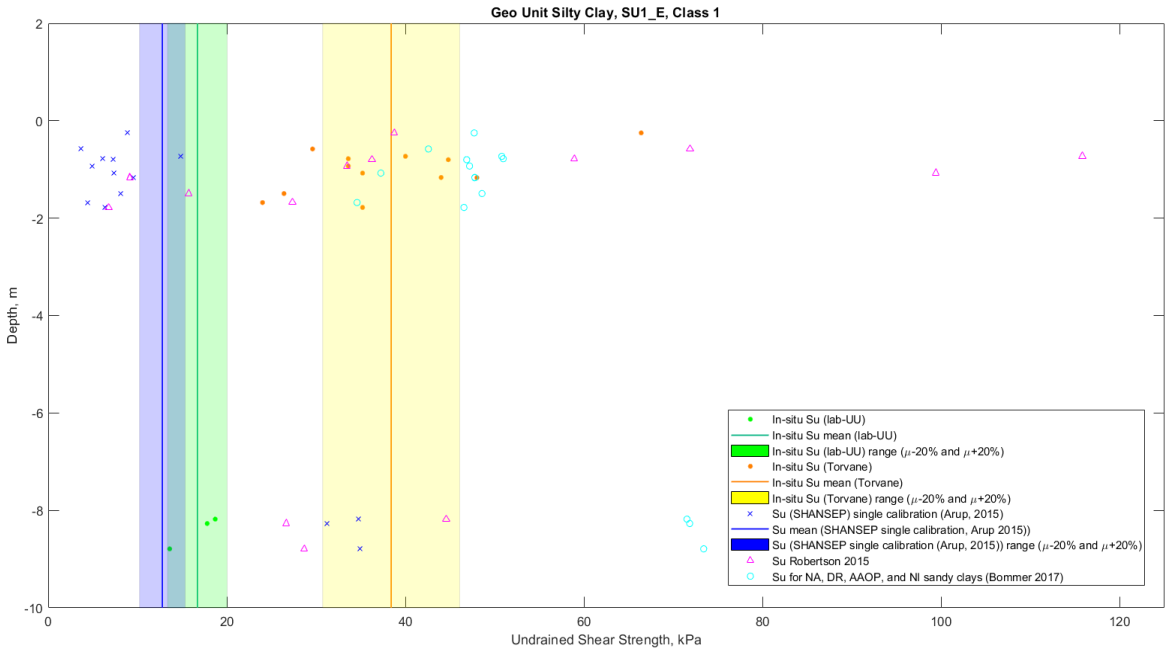

Figure C.16: Class 1 Su measurements and calculated values for the sandy Clay soil unit. Green dots: Class 1 in-situ measurements (lab-UU) values; green solid line: mean; green area: mean ± 20%. Orange dots: Class 1 in-situ measurements (Torvane) values; orange solid line: mean; yellow area: mean ± 20%. Blue crosses: calculated (SHANSEP, single calibration) values; blue solid line: mean; blue area: mean ± 20%. Magenta triangles: Class 1 calculated (Robertson) values. Light blue circles: Class 1 calculated (Bommer) values for NA, DR, AAOP, and NI sandy clays.

The plot in figure C.17 illustrates the distribution of Su measurements (organised in stratigraphic units after Bommer et al., 2017a) over the depth and the comparison between measured and (Bommer) calculated mean values. The points in red denote the Su measurements considered to belong to the Naaldwijk formation ($Su_{NA;sandyclays}$), and the solid red line represents their mean (37.5 kPa, Table C.6). The points in green indicate the Su data belonging to the Drente formation, and the solid green line their mean (31.7 kPa, Table C.6). The point in black and the solid black line indicate the only measurement belonging to the Anthropogenic formation (60.0 kPa, Table C.6). The points in orange refer to the Su data belonging to the Nieuwkoop formation, and the solid orange line their mean (7.9 kPa, Table C.6). The triangles in red, green, black, and orange denote Bommer (2017) calculated Su values for the Naaldwijk, Drente, Anthropogenic, and Nieuwkoop formation, respectively. The dash-dotted line in red indicate the mean value for the Naaldwijk data pairs using the Bommer (2017) correlation for NA sandy clays (Table C.6). The dashed line in green depicts the mean value for the Drente data pairs using the Bommer (2017) correlation for DR sandy clays (Table C.6). The dotted line in black denotes the mean value for the Anthropogenic data pairs using Bommer (2017) correlation for AAOP sandy clays (Table C.6). Finally, the star-dotted line in orange refers to the mean values for the Nieuwkoop data pairs using the Bommer (2017) correlation for NI sandy clays (Table C.6).
Since the SU1_E data-set comprises four different stratigraphic units, it is more difficult to make a comparison between estimated Su and Bommer et al. (2017a) units.
From figure C.17, the Bommer (2017) correlations show an overall good correspondence with the laboratory data (53.1 kPa for NA, 36.5 kPa for DR, 54.0 kPa for AAOP, and 40.6 kPa for NI, Table C.6), with a difference of 15.6, 4.8, 6.0 and 11.0 kPa, respectively.

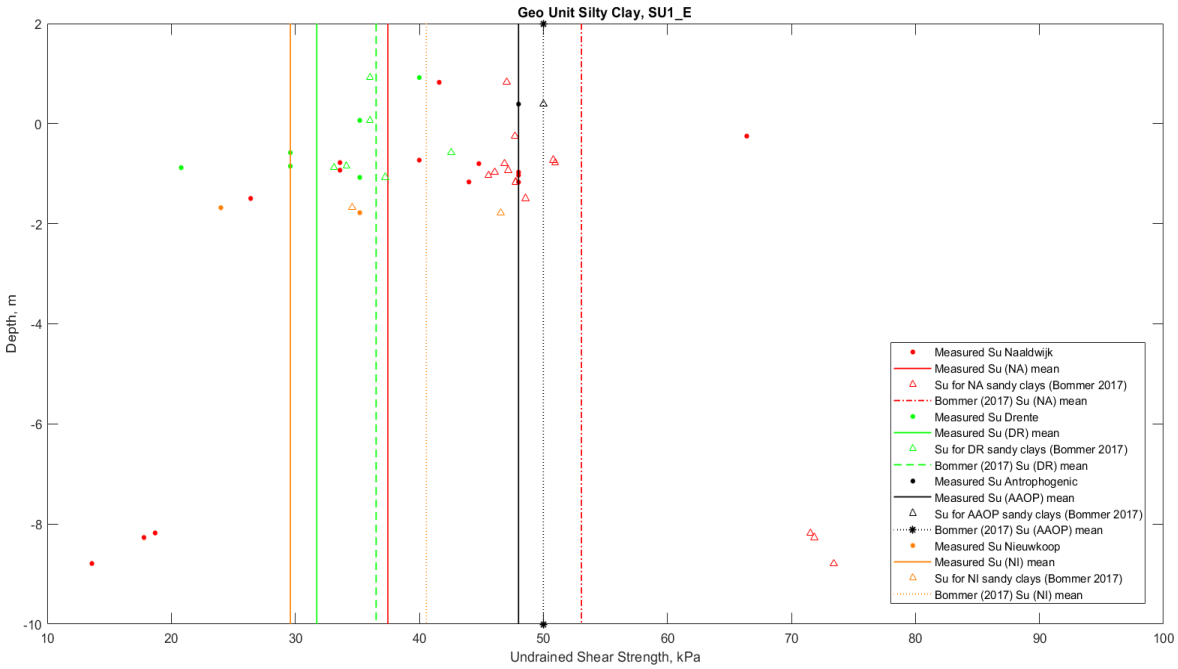

Figure C.17: Su measurements and calculated mean values for the silty Clay soil unit organised in stratigraphic units.

Table C.6: Statistical characterisation of DR, NA, NI, and AAOP formations in the SU1_E unit.

Stratigraphic Unit	**Data-set**	**Statistical parameters**						
		N	min	max	μ	σ	COV	median
		[-]	[kPa]	[kPa]	[kPa]	[kPa]	[-]	[kPa]
NA	Su measured	14	13.6	66.4	37.5	14.6	0.39	40.8
	Su SHANSEP (1974)	14	2.1	34.9	13.0	11.6	0.89	8.5
	Su Robertson (2015)	14	5.8	115.8	35.2	28.0	0.80	31.0
	Su Bommer (2017)	14	45.6	73.4	53.1	10.5	0.20	47.8
DR	Su measured	6	20.8	40.0	31.7	6.6	0.21	32.4
	Su SHANSEP (1974)	6	3.4	7.3	5.3	1.8	0.34	5.3
	Su Robertson (2015)	6	5.8	99.4	49.1	33.6	0.68	47.6
	Su Bommer (2017)	6	33.1	42.6	36.5	3.3	0.09	36.0
AAOP	Su measured	1	48 .0	48.0	48 .0	-	-	48 .0
	Su SHANSEP (1974)	1	6.6	6.6	6.6	-	-	6.6
	Su Robertson (2015)	1	47.6	47.6	47.6	-	-	47.6
	Su Bommer (2017)	1	50.0	50.0	54.0	-	-	54.0
NI	Su measured	2	24.0	35.2	29.6	7.9	0.27	29.6
	Su SHANSEP (1974)	2	4.4	6.3	5.4	1.4	0.26	5.4
	Su Robertson (2015)	2	6.7	27.3	17.0	14.6	0.86	17.0
	Su Bommer (2017)	2	34.6	46.6	40.6	8.5	0.21	40.6

Figure C.18 displays the poor correlations resulting from the comparison of in-situ and SHANSEP Su data, confirming what illustrated in figure C.15. Almost all the data pairs (3 green (UU) dots and 20 orange (Torvane) dots) are located far from the equality line.
On the other hand, the correspondence between in-situ data and Su values calculated with the Robertson and Cabal (2015) correlation is improved, being the data pairs relatively closer to the equality line (Figure C.19a). Similarly, the Bommer et al. (2017a) equations fairly correlate with the in-situ measurements (Torvane), but they are in poor agreement with the in-situ measurements (lab-UU) (Figure C.19b).

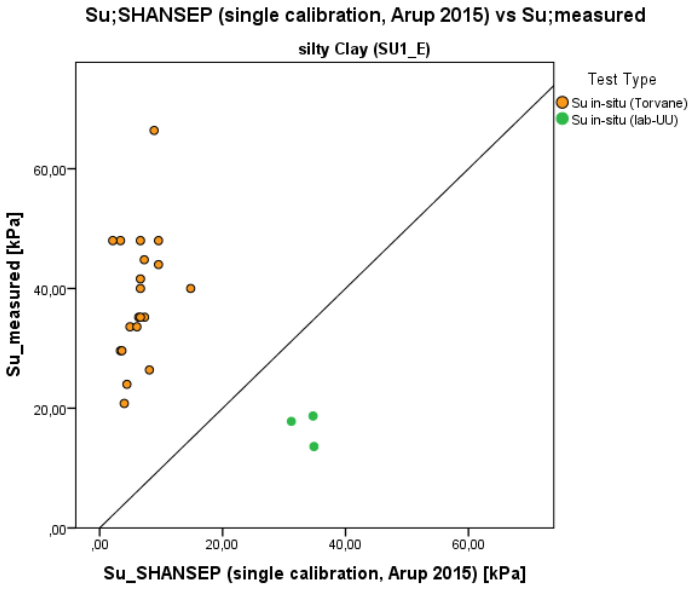

Figure C.18: Scatter plot with equality line of Su data pairs for the silty Clay soil unit. Orange dots: data pairs of in-situ Su measurements (Torvane) and SHANSEP (1974) calculated values. Green dots: data pairs of in-situ Su measurements (lab-UU) and SHANSEP (1974) calculated values.

Figure C.19: Scatter plot with equality line of Su data pairs (calculated with the Robertson (2015) and Bommer (2017) correlations) for the silty Clay soil unit.

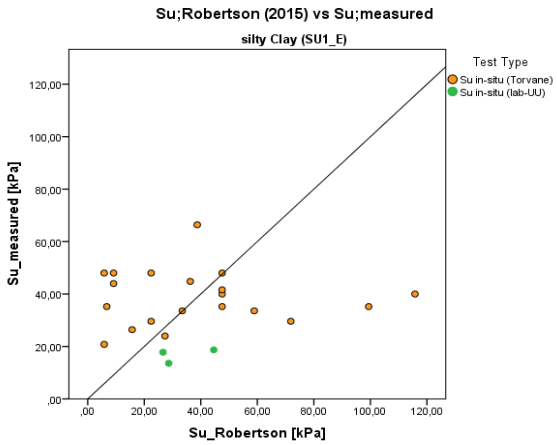

(a) Scatter plot with equality line of Su data pairs for the silty Clay soil unit. Orange dots: data pairs of in-situ Su measurements (Torvane) and Robertson (2015) calculated values. Green dots: data pairs of in-situ Su measurements (lab-UU) and Robertson (2015) calculated values.

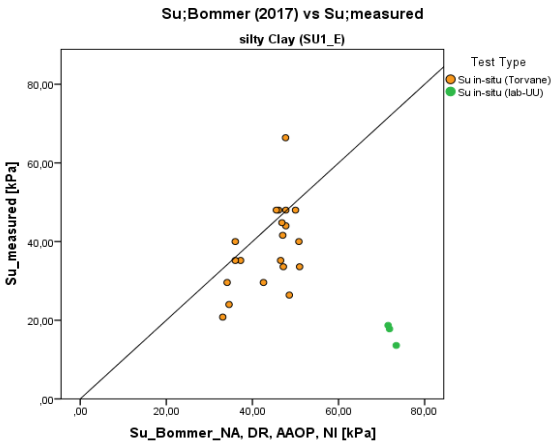

(b) Scatter plot with equality line of Su data pairs for the silty Clay soil unit. Orange dots: data pairs of in-situ Su measurements (Torvane) and Bommer (2017) NA, DR, AAOP, NI calculated values. Green dots: data pairs of in-situ Su measurements (lab-UU) and Bommer (2017) NA, DR, AAOP, NI calculated values.

Data Distribution

Figures C.20a, C.21a, C.21b, and C.21c show the variability of the SU1_E soil unit, including all the samples classified as silty Clay, without making any consideration about the the sample classes. Diversely, figure C.20b illustrates the distribution of the Class 1 data-sets (from the three different correlations) in comparison to the in-situ Class 1 data, and figure C.20c presents the calculated SHANSEP data organised in sample classes.

Figures C.20a confirms the observations made previously from the analysis of figure C.15. The Ladd and Foott (1974) correlation underestimates the laboratory data by the most, with a difference between the medians of 28.6 kPa, followed by the Bommer et al. (2017a) equations with a difference of 11.8 kPa, and the Robertson and Cabal (2015) relation with a difference of almost 2 kPa.

Of the 23 data pairs belonging to this soil unit, 15 are re-classified as Class 1 and 8 as Class 3. After re-organising the data pairs in sample classes, figure C.20b, in agreement with figure C.16, shows that, considering only the Class 1 samples, the data-sets' variability remains almost unvaried (i.e. the medians are almost identical, as well as the the COVs, Table C.7).

Figures C.21a, C.21b, and C.21c illustrate the Su;SHANSEP, Su;Robertson, and Su;Bommer data-sets, respectively, re-organised based on the type of test.

The SHANSEP correlation underestimates the in-situ (Torvane) measurements while over-predicting the in-situ (lab-UU) measurements (Figure C.21a, Table C.8). The Robertson (2015) correlation also overestimates the Su data from UU tests, but it correlates better (almost perfectly) with the Torvane data (Figure C.21b, Table C.8). Differently, the Bommer (2017) equations overestimate the measurements from both test types, and in particular the in-situ (Torvane) measurements (Figure C.21c, Table C.8).

Table C.7: Statistical characterisation of the SU1_E unit organised in sample classes for the three correlations considered (SHANSEP, 1974, Robertson, 2015, Bommer, 2017) and the in-situ measurements.

Class	**Data-set**	**Statistical parameters**						
		N	min	max	μ	σ	COV	median
		[-]	[kPa]	[kPa]	[kPa]	[kPa]	[-]	[kPa]
All classes	Su measured	23	13.6	66.4	35.7	12.4	0.35	35.2
	Su SHANSEP (1974)	23	2.1	34.9	10.0	9.7	0.97	6.6
	Su Robertson (2015)	23	5.8	115.8	37.8	28.5	0.75	33.4
	Su Bommer (2017)	23	33.1	73.4	47.5	11.3	0.24	47.0
1	Su measured	15	13.6	66.4	34.0	13.6	0.40	33.6
	Su SHANSEP (1974)	15	3.6	34.9	12.8	11.1	0.87	8.1
	Su Robertson (2015)	15	6.7	115.8	41.5	32.5	0.78	33.4
	Su Bommer (2017)	15	34.6	73.4	51.0	11.9	0.23	47.8
3	Su measured	8	20.8	48.0	38.9	9.9	0.28	40.8
	Su SHANSEP (1974)	8	2.1	6.6	4.9	1.9	0.39	4.9
	Su Robertson (2015)	8	5.8	47.6	30.8	18.9	0.61	35.0
	Su Bommer (2017)	8	33.1	50.0	41.0	6.8	0.17	40.8

Figure C.20: Box-and-Whiskers-Diagram from measured and calculated (SHANSEP, 1974, Robertson, 2015, and Bommer, 2017) Su values for the silty Clay soil unit.

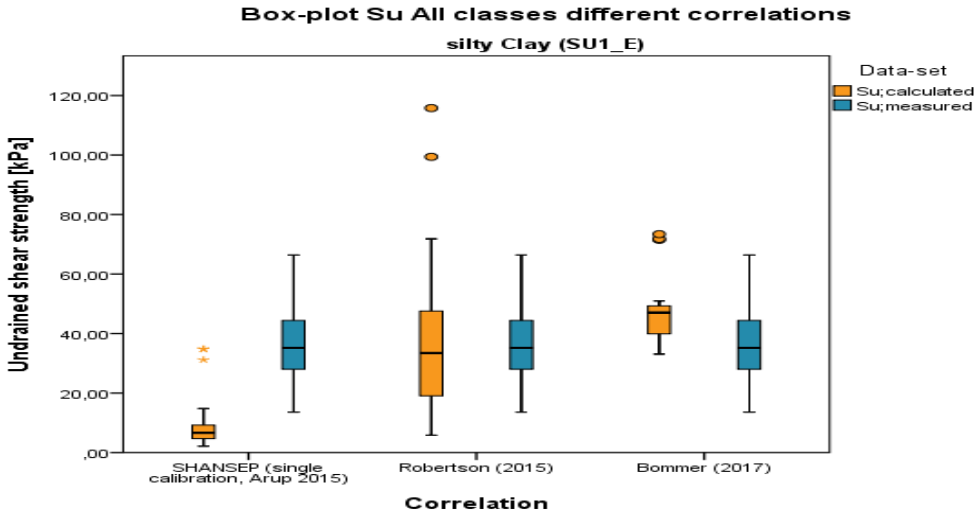

(a) Box-and-Whiskers-Diagram from measured and calculated Su values for the silty Clay soil unit.

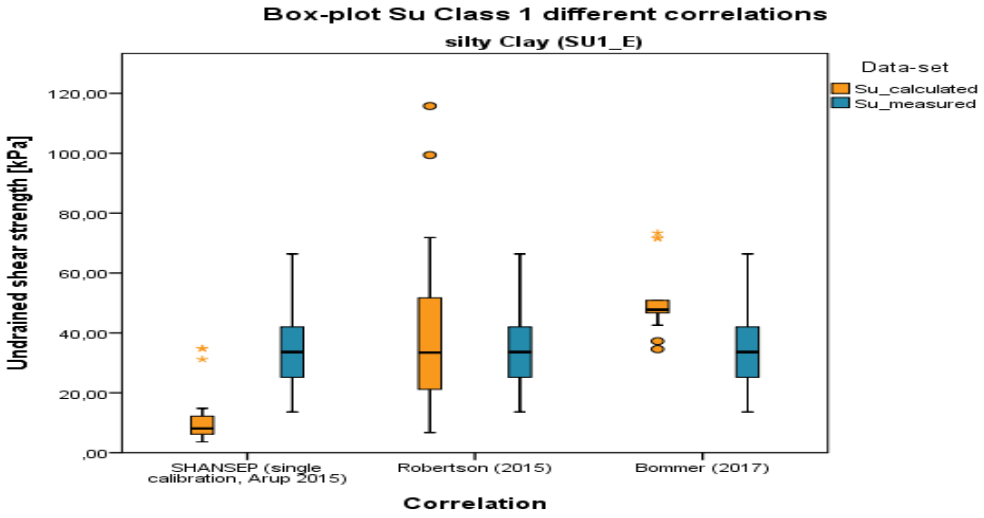

(b) Box-and-Whiskers-Diagram from measured and calculated (Class 1) Su values for the silty Clay soil unit.

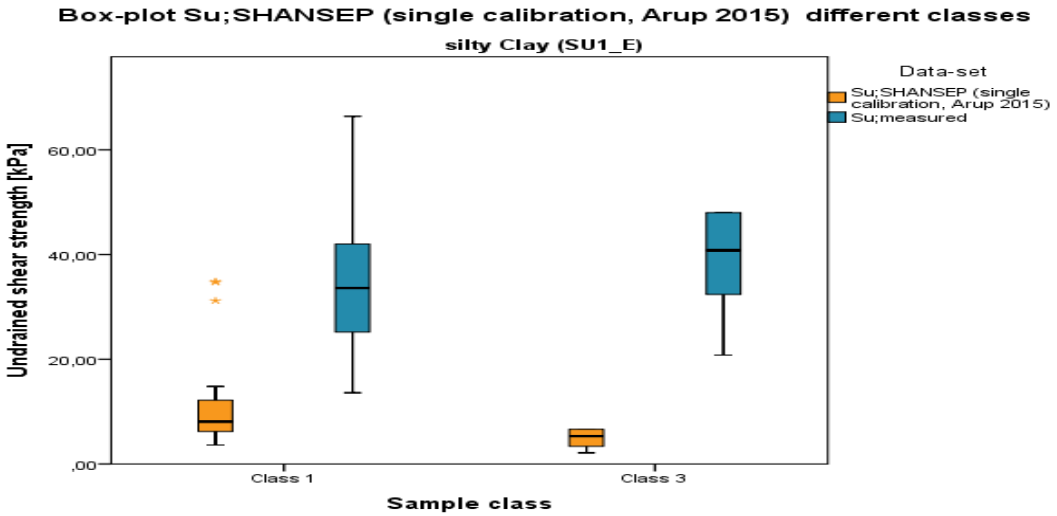

(c) Box-and-Whiskers-Diagram from measured and calculated (SHANSEP with single calibration, after Arup, 2015) Su values for the silty Clay soil unit, organised in sample classes.

Figure C.21: Box-and-Whiskers-Diagram from measured and calculated (SHANSEP, 1974, Robertson, 2015, and Bommer, 2017) Su values for the silty Clay soil unit, organised in test type data-sets.

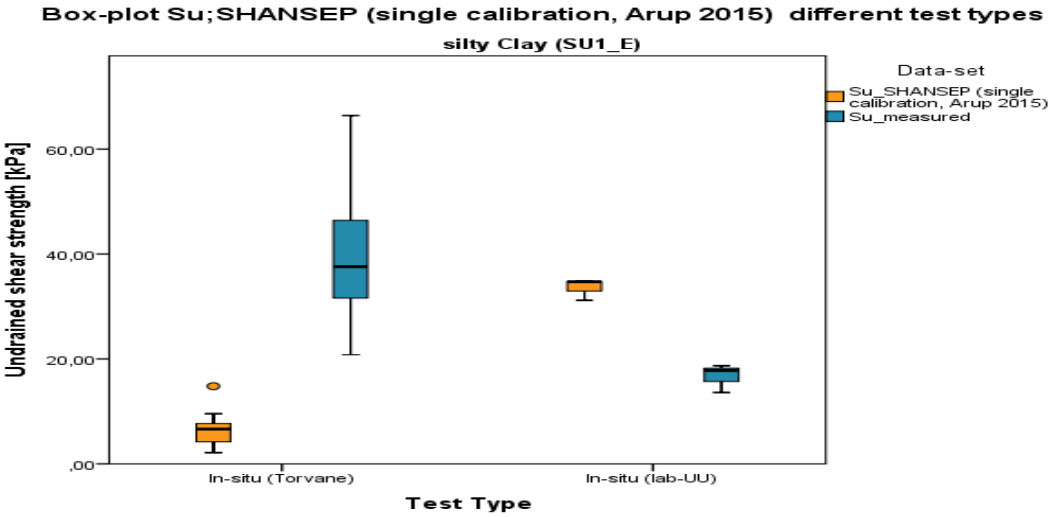

(a) Box-and-Whiskers-Diagram from measured and calculated (SHANSEP with single calibration, after Arup, 2015) Su values for the silty Clay soil unit, organised in test type data-sets.

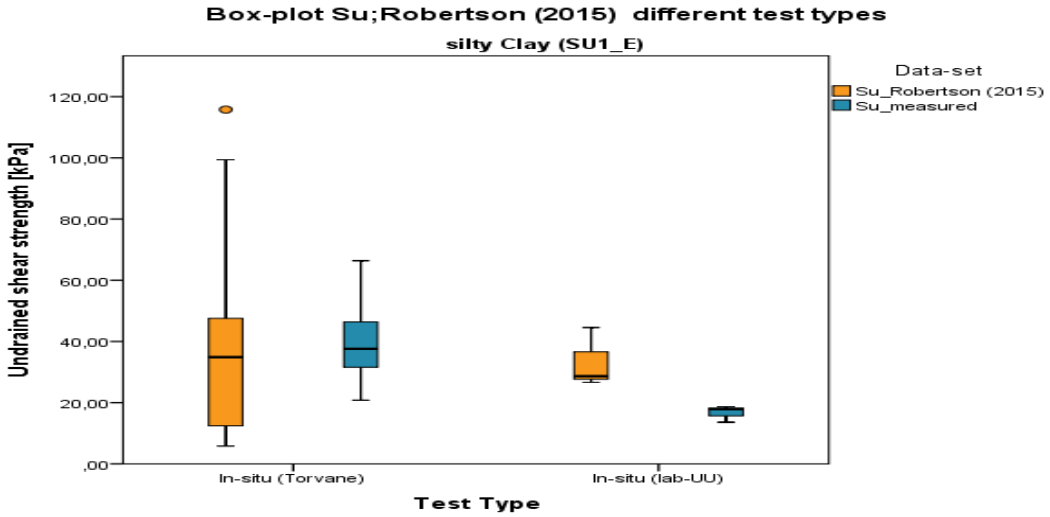

(b) Box-and-Whiskers-Diagram from measured and calculated (Robertson, 2015) Su values for the silty Clay soil unit, organised in test type data-sets.

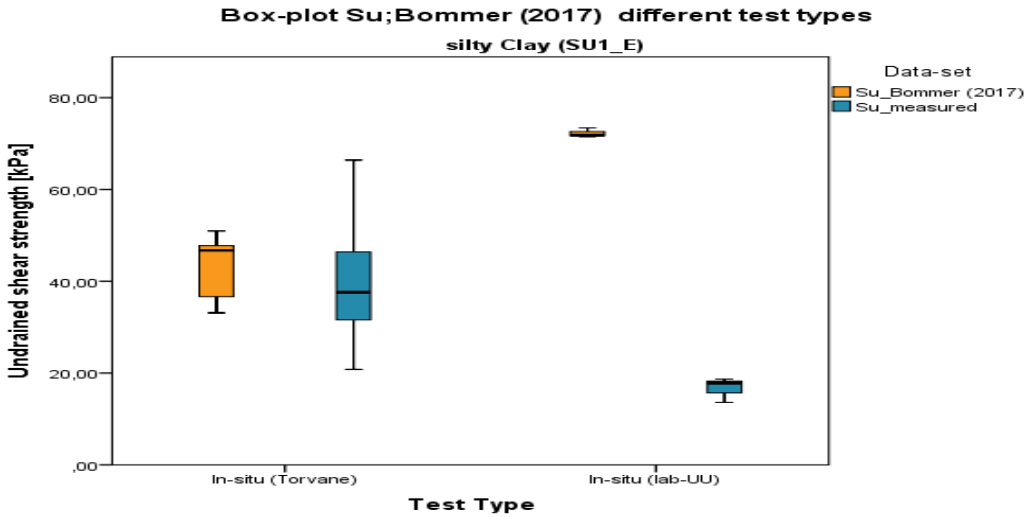

(c) Box-and-Whiskers-Diagram from measured and calculated (Bommer, 2017) Su values for the silty Clay soil unit, organised in test type data-sets.

Table C.8: Statistical characterisation of the SU1_E unit's data-sets (all classes) organised in type of tests for the three correlations considered (SHANSEP, 1974, Robertson, 2015, Bommer, 2017) and the in-situ measurements.

Test Type	**Data-set**	**Statistical parameters**						
		N	min	max	μ	σ	COV	median
		[-]	[kPa]	[kPa]	[kPa]	[kPa]	[-]	[kPa]
Torvane	Su measured	20	20.8	66.4	38.6	10.6	0.28	37.6
	Su SHANSEP (1974)	20	2.1	14.8	6.5	2.9	0.45	6.6
	Su Robertson (2015)	20	5.8	115.8	38.5	30.4	0.79	34.9
	Su Bommer (2017)	20	33.1	51.0	43.8	6.1	0.14	46.7
UU	Su measured	3	13.6	18.7	16.7	2.7	0.16	17.8
	Su SHANSEP (1974)	3	31.2	34.9	33.6	2.1	0.06	34.7
	Su Robertson (2015)	3	26.6	44.6	33.3	9.8	0.29	28.7
	Su Bommer (2017)	3	71.5	73.4	72.3	1.0	0.01	71.8

C.3.2. Other Soil Units

Table C.9 gives an overview of the descriptive statistics from the remaining individuated soil units (overconsolidated clay and Sand).

Table C.9: Statistical characterisation of SU2, and SU3 soil units.

Soil Unit	Class/Test Type	Data-set	Statistical parameters						
			N	min	max	μ	σ	COV	median
			[-]	[kPa]	[kPa]	[kPa]	[kPa]	[-]	[kPa]
SU2	1	Su measured	9	42.0	130.2	76.9	29.7	0.39	78.2
		Su SHANSEP (1974)	9	87.9	266.8	159.5	71.1	0.75	138.5
		Su Robertson (2015)	9	82.8	238.1	145.8	66.6	0.46	121.7
		Su Bommer (2017) clean clays	9	93.2	229.5	146.0	56.1	0.38	124.5
		Su Bommer (2017) sandy clays	9	100.8	193.8	136.8	38.3	0.28	122.2
SU3	All classes	Su measured	11	23.3	164.3	73.7	47.2	0.64	56.0
		Su SHANSEP (1974)	11	6.9	184.0	31.3	53.3	1.70	8.0
		Su Robertson (2015)	11	6.1	924.5	186.4	324.6	1.70	7.4
		Su Bommer (2017)	11	38.0	225.5	87.7	84.8	0.97	38.3
	1	Su measured	6	23.3	164.3	80.2	55.9	0.70	57.2
		Su SHANSEP (1974)	6	8.0	184.0	51.6	67.7	1.31	29.2
		Su Robertson (2015)	6	7.4	924.5	336.7	388.8	1.15	232.3
		Su Bommer (2017)	6	38.3	225.5	129.2	99.2	0.77	126.6
	3	Su measured	5	25.6	131.2	65.9	39.2	0.59	56.0
		Su SHANSEP (1974)	5	6.9	6.9	6.9	-	-	6.9
		Su Robertson (2015)	5	6.1	6.1	6.1	-	-	6.1
		Su Bommer (2017)	5	38.0	38.0	38.0	-	-	38.0
	Torvane	Su measured	8	25.6	131.2	61.1	30.6	0.50	55.2
		Su SHANSEP (1974)	8	6.9	10.8	7.8	1.5	0.19	6.9
		Su Robertson (2015)	8	6.1	15.0	7.6	3.1	0.41	6.1
		Su Bommer (2017)	8	38.0	39.1	38.2	0.4	0.01	38.0
	UU	Su measured	3	23.3	164.3	107.4	74.3	0.69	50.4
		Su SHANSEP (1974)	3	47.5	184.0	94.0	78.0	0.83	50.4
		Su Robertson (2015)	3	449.7	924.5	663.2	241.0	0.36	615.4
		Su Bommer (2017)	3	214.2	225.5	219.7	5.6	0.03	219.4

Overconsolidated Clay (SU2)

Su measurements from the overconsolidated (OC) Clay unit are 9 in total, collected at a depth varying from -11.1 to -27.9 m NAP, and associated to the Peelo formation (table 5.6).

The OC clay measurements are obtained from triaxial (UU) tests and all the 9 measurements are classified as Class 1 (Table C.9).

The Ladd and Foott (1974) correlation (with single calibration after Arup, 2015) is overestimating the Su measured at the laboratory, predicting a Su mean equal to 159.5 kPa, while the measured Su mean is equal to 76.9 kPa.

The Robertson and Cabal (2015) correlation estimates a Su mean (145.8 kPa, Table C.9) higher than the in-situ measurements mean.

For the comparison between Su;measured and Su;Bommer, both the equations for Peelo clean and sandy clays, suggested by Bommer et al. (2017a), are considered. The former predicts a Su mean of 146.0 kPa and the latter a Su mean of 136.8 kPa, which are both overestimating the Su measured at the laboratory (Table

C.9).

Sand (SU3)

The Sand soil unit contains 11 Su measurements, of which 8 were obtained from Torvane tests (at depths between -0.50 and -1.28 m NAP), and 3 from triaxial (UU) tests (at depths between -22.73 and -23.18 m NAP). The 11 Su measurements belong to the Boxtel formation (Table 5.6) and, in order to account for difference between samples and CPT measurements depth, 6 data pairs are classified as Class 1 and 5 as Class 3 (Table C.9). From table C.9, showing the descriptive statistical parameters from the SU3 unit without distinction of the test types, the Ladd and Foott (1974) correlation (with single calibration after Arup (2015)) predicts a Su mean equal to 31.3 kPa (Table C.9), which is underestimating the measured Su mean (73.7 kPa, Table C.9). Similarly, from the Class 1 data-sets (Table C.9), the calculated mean is 51.6 kPa, lower than the measured mean which is 80.2 kPa. A similar trend is observed when considering different data-sets from the re-organisation of data based on test type. Both the in-situ measurements (Torvane and lab-UU) are under-predicted by the Ladd and Foott (1974) correlation by a difference between the means of 53.3 and 13.4 kPa, respectively (Su;measured (Torvane) mean = 61.1 kPa and Su;measured (lab-UU) mean = 107.4 kPa, while Su;SHANSEP (Torvane) mean = 7.8 kPa and Su;SHANSEP (lab-UU) mean = 94.0 kPa, Table C.9).
The Robertson and Cabal (2015) correlation overestimates the in-situ measurements when all the samples are considered (All classes Su;Robertson mean = 186.4 kPa and All classes Su;measured mean = 73.7 kPa, Table C.9), as well as when only the Class 1 data-pairs are analysed (Class 1 Su;Robertson mean = 336.7 kPa and Class 1 Su;measured mean = 80.2 kPa, Table C.9). Considering different data-sets from the re-organisation of data based on test type, the Torvane measurements are under-predicted (Su;Robertson (Torvane) mean = 7.6 kPa and Su;measured (Torvane) mean = 61.1 kPa, Table C.9) but the UU measurements are largely overestimated (Su;Robertson (lab-UU) mean = 663.2 kPa and Su;measured (lab-UU) mean = 107.4 kPa, Table C.9). Similarly, the Bommer et al. (2017a) equations overestimate the undrained shear strength for the SU3 unit when the totality of the data-pairs are considered, predicting Su mean equal to 87.7 kPa (All classes data-set, Table C.9), as well as when only the Class 1 data-pairs are analysed (Class 1 Su;Bommer mean = 129.2 and Class 1 Su;measured median = 80.2, Table C.9). Moreover, the Bommer et al. (2017a) equations under-predict the in-situ (Torvane) measurements (Su;Bommer (Torvane) mean = 38.2 kPa and Su;measured (Torvane) mean = 61.1 kPa, Table C.9) but overestimate the in-situ (lab-UU) data (Su;Bommer (lab-UU) mean = 219.7 kPa and Su;measured (lab-UU) mean = 107.4 kPa, Table C.9).

D

SHANSEP Correlation Improvement

D.1. Introduction

The present appendix comprehends the remaining approaches that have been carried out for the improvement of the SHANSEP model (see Chapter 6 for more details). Furthermore, a brief explanation of the regression coefficients needed to determine the quality of the fit are reported in Section D.3.

D.1.1. Estimation of S and m - Approach 2

The first approach follows the Critical State Soil Mechanics (CSSM) concept, introduced by Schofield and Wroth (1968), which states that the normalised undrained shear strength for normally consolidated clays relates to the critical state line slope, which can be determined when the deviatoric and the mean stresses from a consolidation test are plotted against each other.
Results reveal that acceptable S values can be obtained using the Mohr-Coulomb (M-C) failure criterion on NC data at failure plotted in the plane of shearing ($t-s'$ space). In this context, by plotting values of the mean stress (s, s') against the maximum shear stress (t) at failure, obtained from triaxial (CU) tests, it was noted that the slope of the M-C envelope increased due to the effect of pore water pressure. Furthermore, a little scatter of the strength data was observed. This scatter can be ascribed to the variation in water content of the different samples. A series of specimens collected from a single profile in the ground, or a series of samples which have been unloaded from a single maximum past pressure, can be characterised by quite different water contents and, thus, can exhibit failure points which lie each on a quite different strength line (Wood, 1990). Nevertheless, the variations of water content were not great, and the amount of data scatter was not significant. Hence, for an undrained analysis, it was decided to calculate the NC normalised shear strength, S_0, as the slope of the line of best fit (tangent of the effective friction angle, α') of the failure values in the effective plane of shearing ($t-s'$). With this procedure, the SHANSEP equation resulted in the form of:

$$Su = s'_0 * S_0 * OCR^m \tag{D.1}$$

However, considering that in the SHANSEP model the effective vertical stress is used rather than the mean effective stress ($s'_0 = (\sigma'_v + \sigma'_h)/2 = \sigma'_v * (1+k_0)/2$), the tangent of the friction angle ($S_0 = tan(\alpha')$) was corrected using the following relation:

$$S = tan(\alpha') * (1 + k_0) * 0.5 \tag{D.2}$$

where K_0 is the ratio of horizontal and vertical effective stress during one-dimensional normal compression which is given fairly accurately by the expression $k_0 = 1 - sin(\alpha') * OCR^{sin(\alpha')}$ (after Kulhawy and Mayne, 1990).
The values of S obtained with such procedure (Table D.1) are in fair agreement with the range of values proposed by Mayne (1980) and Mayne (1988) for various clay types.
Following, the m parameter is evaluated as in the previous approach (Section 6.2.1, Chapter 6). Figures D.1a, D.1b and D.1c illustrate the SHANSEP calibration procedure for the three types of soil provided with NC data. The orange points indicate the normally consolidated measurements. The blue points denote the measurements with OCR=2. The red points represent the measurements with OCR=4. The green points refer to the

measurements with OCR=6. The solid lines in orange, blue, red, and green refer to the SHANSEP best fits for the above mentioned NC and OC points, respectively.
The values of m obtained from the above procedures, listed in table D.1, are almost identical to those obtained with Approach 1 (Table 6.1, Chapter 6), and in fair agreement with the result of the study conducted by Mayne (1980).

Table D.1: SHANSEP best parameters S and m for the SU1_A, SU1_B, and SU1_E soil units, obtained from the analysis of 9 NC and 30 OC measurements, following Approach 2.

Soil Unit	**Stratigraphic Unit**	**SHANSEP parameters**		**Best SHANSEP parameters**	
		S	**m**	**S**	**m**
[SU]	[-]	[-]	[-]	[-]	[-]
SU1_A (n=8)	Clay, clean, soft	0.45 - 0.47	0.58 - 0.70	0.45	0.62
SU1_B (n=13)	Clay, sandy	0.43 - 0.44	0.40 - 0.55	0.40	0.65
SU1_E (n=18)	Clay, silty or Silt, clayey	0.42 - 0.46	0.75 - 1.00	0.42	1.00

Figure D.1: Calibration of the SHANSEP model parameters for the SU1_A, SU1_B, and SU1_E soil units following Approach 2.

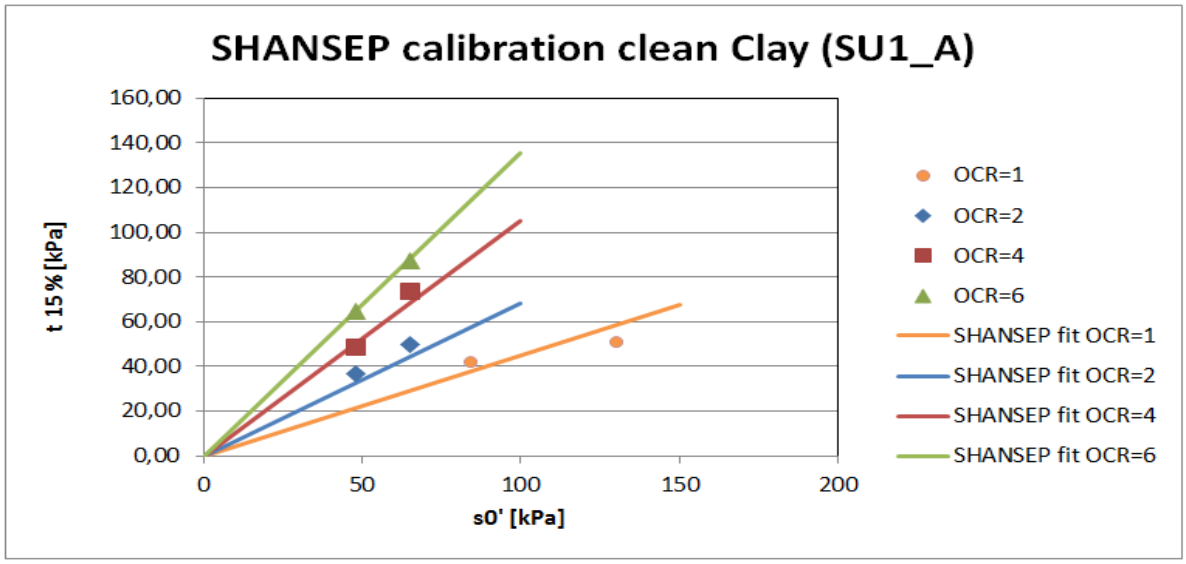

(a) SHANSEP fit of NC and OC laboratory (CU) data from the SU1_A soil unit

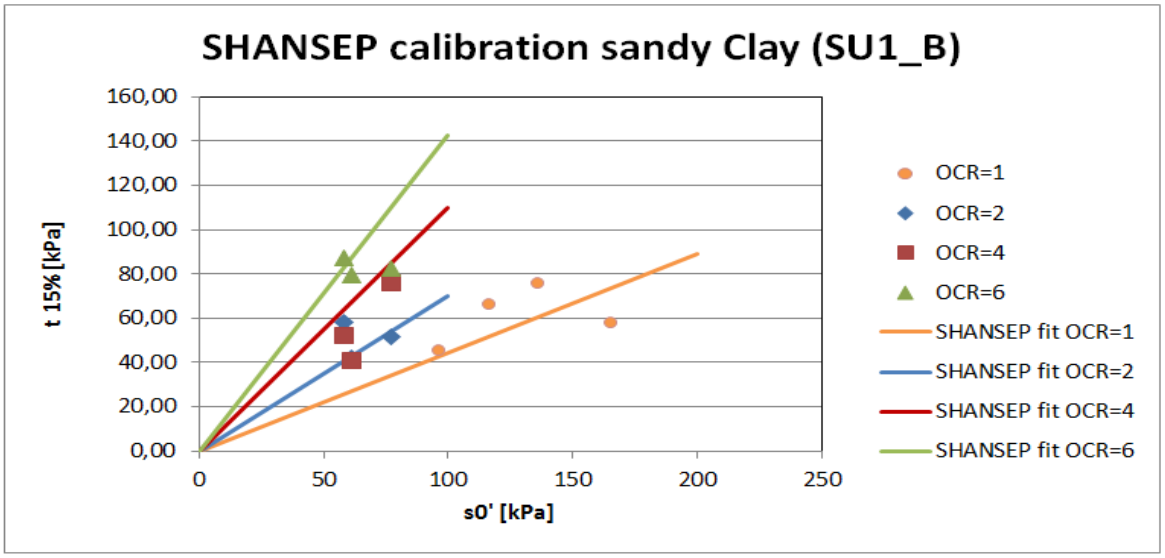

(b) SHANSEP fit of NC and OC laboratory (CU) data from the SU1_B soil unit

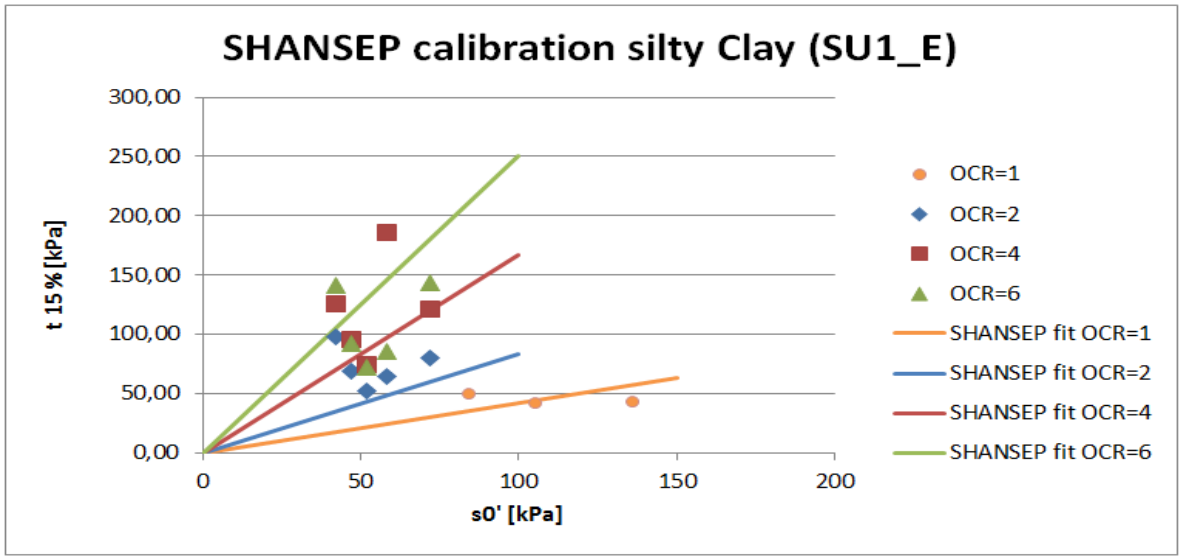

(c) SHANSEP fit of NC and OC laboratory (CU) data from the SU1_E soil unit

D.2. Linear Regression Analysis

Hereafter, the results of the linear regression analysis are illustrated.

Linear regression analysis was carried out between $log(\frac{(Su/\sigma'_c)_{OC}}{(Su/\sigma'_c)_{NC}})$ and $log(OCR)$ to force the linear relationship between (Su/σ'_c) and OCR on a log-log plot, allowing a clearer evaluation of the m parameter. Figures D.2, D.3, and D.4 confirm that there exist linear relationships between the two variables, with high sample correlation coefficients and statistically significant ($p < 0.05$) slope coefficients (Table D.2). The soil unit SU1_E (Figure D.4), is the only one that is characterised by a relatively low correlation coefficient (R^2 = 0.590, Table D.2).

Table D.2: Regression parameters for the SU1_A, SU1_B, and SU1_E soil units, obtained from linear regression analysis of 21 OC measurements

Soil Unit	**Stratigraphic Unit**	**SHANSEP parameter**	**R^2**	**Significance (p)**
		S		
[SU]	[-]	[-]	[-]	[-]
SU1_A (n=3)	Clay, clean, soft	0.522	0.996	0,000
SU1_B (n=9)	Clay, sandy	0.536	0.892	0,000
SU1_E (n=9)	Clay, silty or Silt, clayey	0.503	0.590	0,016

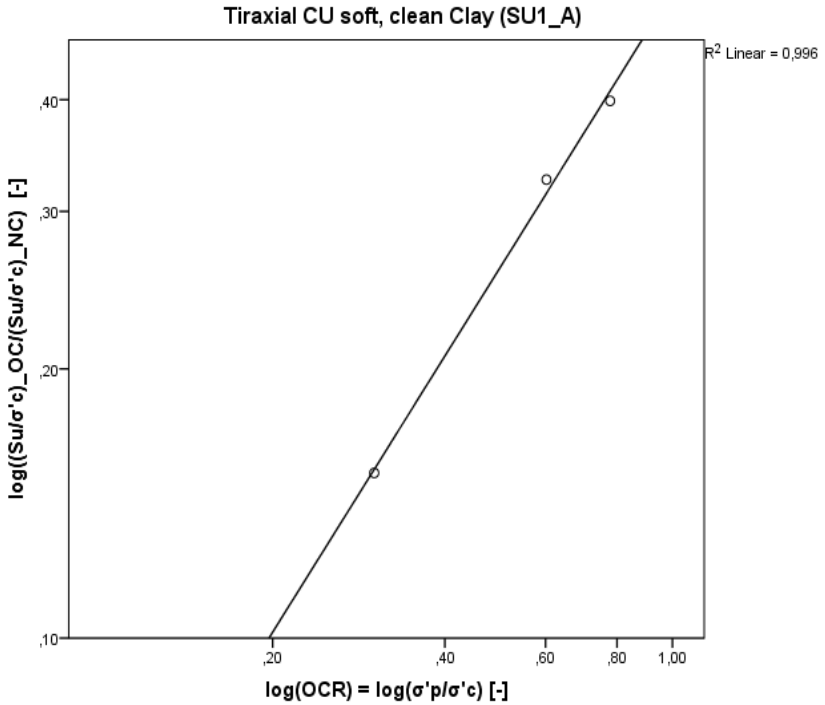

Figure D.2: Linear regression analysis for 3 triaxial CU measurements from the SU1_A soil unit.

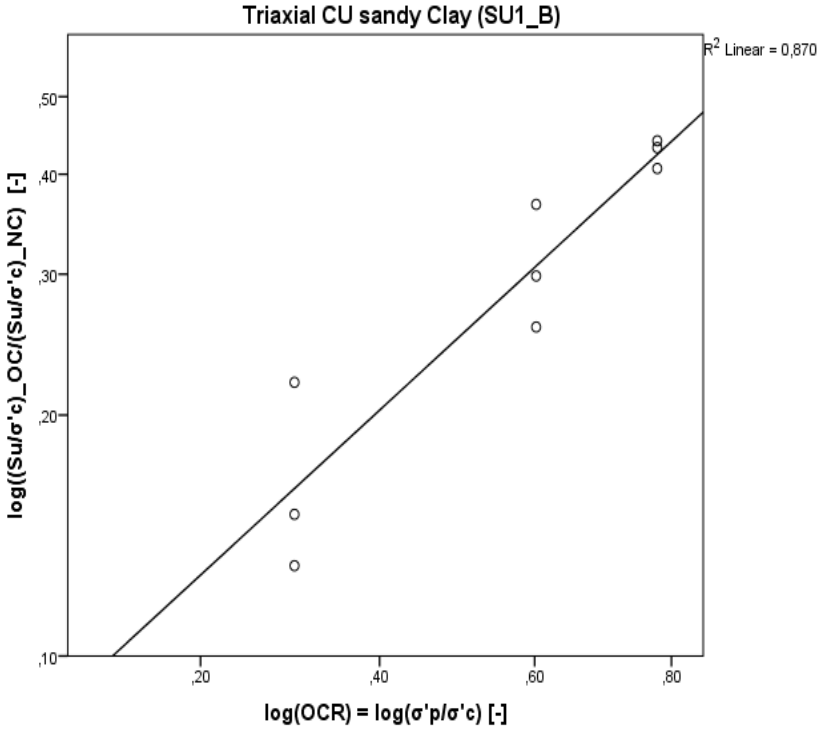

Figure D.3: Linear regression analysis for 9 triaxial CU measurements from the SU1_B soil unit.

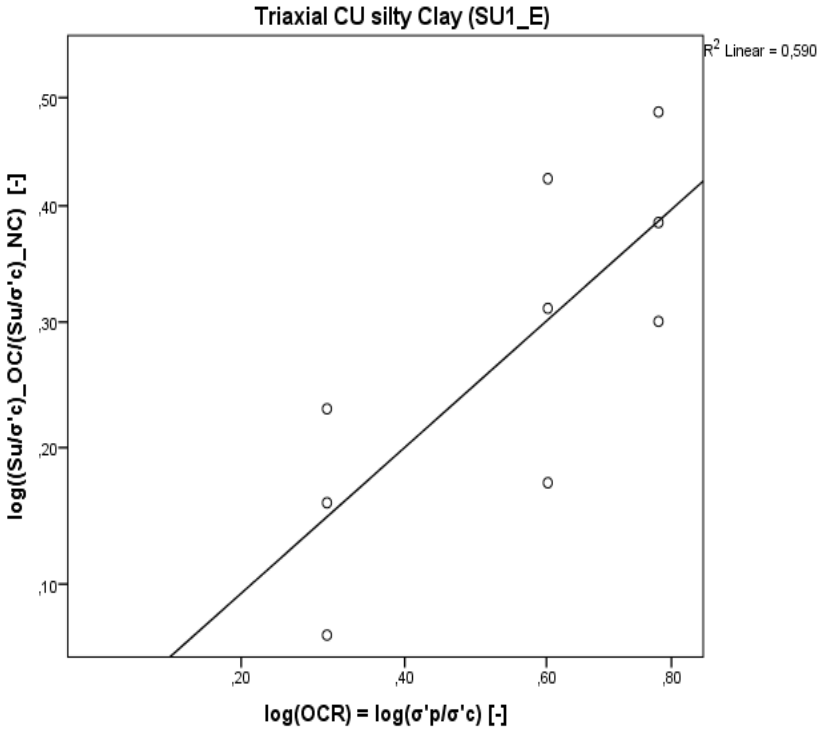

Figure D.4: Linear regression analysis for 9 triaxial CU measurements from the SU1_E soil unit.

D.3. Regression Coefficients

There exist a number of statistics used to determine the quality of the fit, such as (a) multiple correlation coefficient, (b) percentage of the variance explained, (c) statistical significance of the model, and (d) precision of the predictions from the regression model (Laerd-Statistics, 2015).
The multiple correlation coefficient (a), commonly indicated as R, is the (absolute) Pearson correlation coefficient between the dependent variable and the scores predicted by the regression model. This is a representation of the strength of the linear correlation between the variables, giving an indication of the suitability of the fit. It can vary from -1 to 1, with the higher absolute value indicating a stronger linear association. A value of 1 indicates a perfect linear association.
The total variation explained (b) is represented by the coefficient of determination, denoted as R^2, which is a proportion of the variance in the target variable that is explained by the predictor. Having for example an R^2 equal to 0.132 means that 13.2 % of the variability of the the dependent variable is explained by the independent variable in the regression model. R^2 is calculated as:

$$R^2 = 1 - \frac{SS_{res}}{SS_{tot}} \tag{D.3}$$

$$SS_{res} = \sum_i (y_i - f_i)^2 \tag{D.4}$$

$$SS_{tot} = \sum_i (y_i - \bar{y})^2 \tag{D.5}$$

where SS_{res} is the sum of squares of the residuals; SS_{tot} is the total sum of squares (proportional to the variance of the data); y_i is the observed value; $\bar{y}$ is the mean of the observed data; and f_i is the predicted value.
For linear non-intercept models, it has been proposed (e.g. Hahn, 1977, Marquardt and Snee, 1974, Montgomery and Peck, 1982, in Kvalseth, 1985) that Equation D.6 should be used to evaluate R^2.

$$R^2 = 1 - \frac{SS_{res}}{\sum_i (y_i)^2} \tag{D.6}$$

The statistical significance of the model (c) is measured with the p-value. This indicate the probability to have an observed (or more extreme) result assuming the null hypothesis is true. If $p < 0.05$ the result is statistically significant.

E

Look-up Tables

E.1. Introduction

In the present appendix the look-up table for and Su (Table E.3) is reported. The look-up table for PI can be found in Chapter 7 (Table 7.1).
The descriptive statistical parameters are obtained following the procedure explained in Chapter 5. Furthermore, table E.1 presents the stratigraphic units and codes from Bommer et al. (2017a), and table E.2 displays the soil units codes, soil type definition (Dutch + English), and approximate cone tip resistance and friction ratio ranges used in the GI database, after Table 2.b in NEN 9997-1 (2012).

Table E.1: Codes for stratigraphic units, after Bommer et al. (2017a).

Stratigraphic Unit	**Stratigraphic Unit Code**
[-]	[-]
Anthropogenic	AAOP
Boxtel	BX
Drente	DR
Naaldwijk	NA
Nieuwkoop	NI
Peelo	PE

Table E.2: Summary of Soil unit codes, soil type definition, and approximate cone tip resistance and friction ratio ranges used in this report.

Soil Unit Code	**Soil Type** Primary	**Soil Type** Secondary	**Soil Type** English	**q_c** [MPa]	**FR** [%]
SU1	Klei	-	Clay	0.5 - 2.5	1.4 - 7
SU1_A	Klei	Schoon, slap	Clay, clean, soft	0.2 - 0.7	2 - 4
SU1_A1	Klei	Schoon, matig	Clay, clean moderately stiff	0.7 - 1.5	2 - 4
SU1_A2	Klei	Schoon, vast	Clay, clean stiff	1.5 - 2.5	2 - 4
SU1_B	Klei	Zwak zandig	Clay, slightly sandy	0.7 - 2.5	3 - 5
SU1_B2	Klei	Matig zandig	Clay, moderately sandy	0.7 - 2.5	2 - 4
SU1_B3	Klei	Sterk zandig	Clay, highly sandy	0.7 - 2.5	1 - 3
SU1_C	Klei	Zandig/Siltig + Organisch	Clay sandy/silty + organic	0.7 - 2.5	6 - 8
SU1_D	Klei	Organisch	Clay, organic	0.2 - 0.5	6 - 9
SU1_E	Klei	Zwak siltig	Clay, slightly silty	0.7 - 1.5	4 - 6
SU1_E2	Klei	Matig siltig	Clay, moderately silty	0.7 - 1.5	2 - 5
SU1_E3	Klei	Sterk siltig or Uiterst siltig	Clay, highly silty	0.7 - 1.5	1 - 3
SU2	Potklei	Potklei	Over Consolidated Clay	0.7 - 10	5 - 10
SU3	Zand	-	Sand	5 - 30	0 - 2
SU3_A	Zand	Schoon, los/vast	Sand, clean, loose/dense	5 - 25	0 - 1
SU3_B	Zand	Zwak siltig, kleiig	Sand, slightly silty, clayey	8 - 15	0 - 2
SU3_C	Zand	Sterk siltig, kleiig	Sand, highly silty, clayey	6 - 10	1 - 3
SU4	Veen	Niet voorbelast	Peat, not preloaded	0.1 - 0.2	6 - 8
SU4_A	veen	Matig voorbelast	Peat, moderately preloaded	0.1 - 0.3	7 - 10
SU5	Leem	Zwak zandig	Loam, slightly sandy	1 - 3	2 - 4
SU5_B	Leem	Sterk zandig	Loam, highly sandy	1 - 3	1 - 3

E.2. Undrained Shear Strength

Table E.3: Comparison from different approaches for Su interpretation (see tables E.2 and E.1 for soil and stratigraphic units codes).

Soil Unit	**Unit Code**	**Unit Weight Wet**	**Su Torvane**	**Su Triaxial-UU**	**Su Bommer et al. 2017**	**Su Robertson 2015**	**Su SHANSEP 1974**	**Su SHANSEP new*** **
[SU]	[-]	[kN/m^3]	[kPa]	[kPa]	[kPa]	[kPa]	[kPa]	[kPa]
SU1_A (n=3)	NA	12.9	-	24.8 (n=3)	17.9	23.2	5.5	28.4
SU1_B (n=67)	NA	16.2	35.4 (n=32)	27.0 (n=18)	48.7 - 62.0 *	29.6 - 32.6 *	8.7 - 27.3 *	14.1 -28.5 *
	DR	16.7	31.1 (n=17)	-	39.5	33.2	8.0	13.7
SU1_E (n=23)	NA	16.2	43.1 (n=11)	13.6 (n=3)	47.8 - 72.3 *	35.7 - 33.3 *	7.4 - 33.6 *	12.6 - 29.6 *
	NI	17.0	29.6 (n=2)	-	40.6	17.0	5.4	8.3
	DR	16.7	32.2 (n=6)	-	35.3	44.6	5.6	9.7
	AAOP	16.8	48 (n=1)	-	50	47.6	6.6	9.7
SU2 (n=9)	PE	17.8	-	76.9 (n=9)	146.0 - 136.8 **	145.8	159.6	222.3
SU3 (n=11)	BX	16.9	61.1 (n=8)	107.4 (n=3)	38.2 - 219.7 *	7.6 - 663.2 *	7.7 - 94.0 *	24.9 - 225.0 *

* The first value refers to the data-pairs with Torvane measurements, whilst the second indicates the data-pairs with triaxial UU measurements.
** The first value refers to the Bommer et al. (2017a) equation for clay, whilst the second indicates Bommer et al. (2017a) equation for sandy clay and clayey sands.
*** The SHANSEP new model is implemented with the best estimates of S and m coefficients (Table 6.1, Chapter 6) and the OCR calculated using equations 6.4, 6.5, and 6.6 (Section 6.5, Chapter 6)